AD-A077 042 WESTINGHOUSE DEFENSE AND ELECTRONIC SYSTEMS CENTER B--ETC F/6 9/5
DIPOLE BROADSIDE GLIDE SLOPE ARRAY.(U)
MAY 79 R S LITTLEPAGE , R RAJNIC

UNCLASSIFIED FAA-RD-79-69 DOT-FA74WA-3353 NL

1 OF 3
AD-
A077042

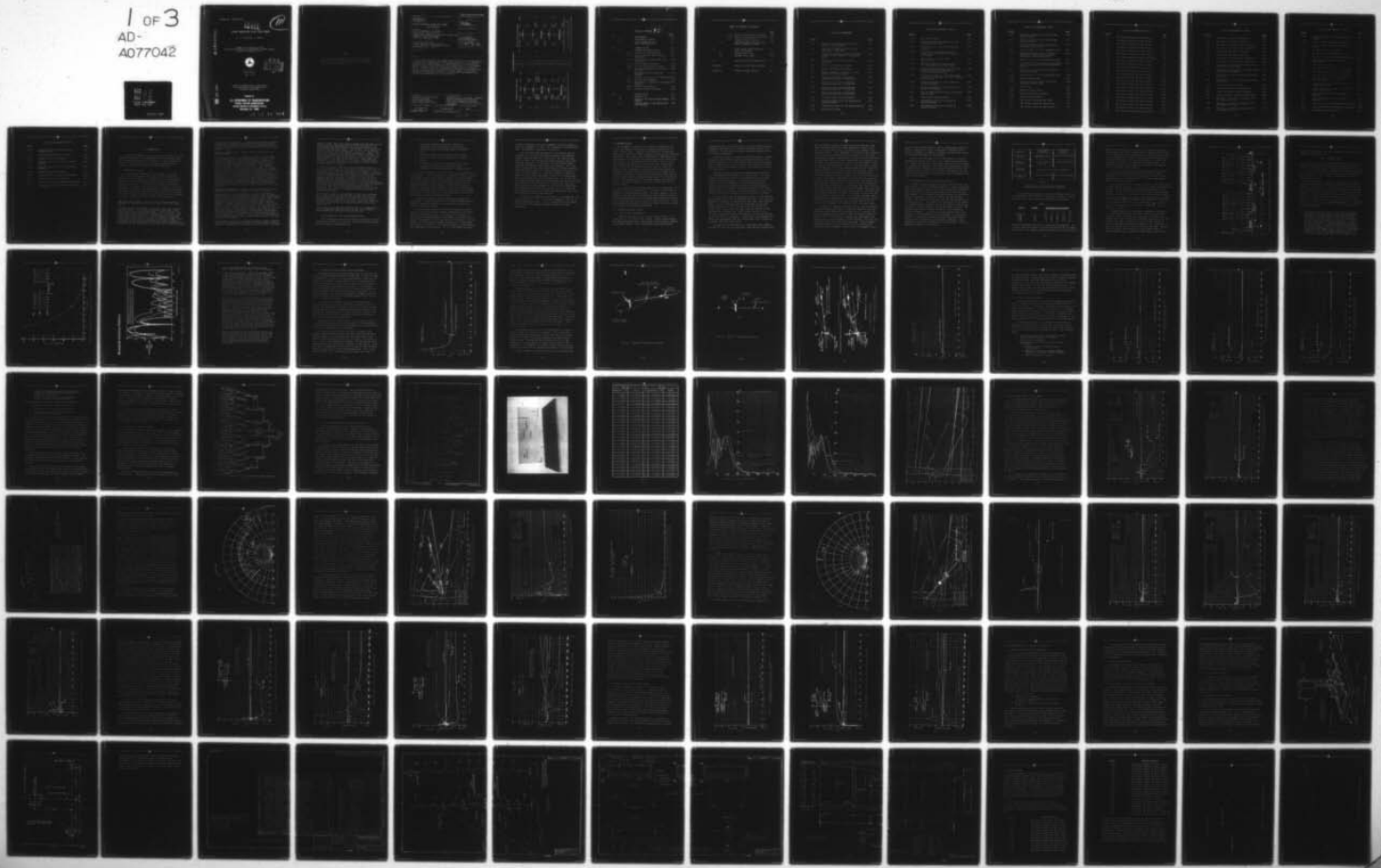

REPORT NO. FAA-RD-79-69

LEVEL II

DIPOLE BROADSIDE GLIDE SLOPE ARRAY

R. S. Littlepage, R. Rajnic

COMMAND AND CONTROL DIVISION
WESTINGHOUSE DEFENSE AND ELECTRONIC SYSTEMS CENTER
BALTIMORE, MARYLAND 21203

FINAL REPORT
MAY, 1979

Prepared for

U.S. DEPARTMENT OF TRANSPORTATION
FEDERAL AVIATION ADMINISTRATION
Systems Research & Development Service
Washington, D.C. 20590

NOTICE

Technical Report Documentation Page

1. Report No.	2. Government Accession No.	3. Recipient's Catalog No.
FAA-RD-79-69		

4. Title and Subtitle	5. Report Date
DIPOLE BROADSIDE GLIDE SLOPE ARRAY Final Report	May 1979
	6. Performing Organization Code
7. Author(s) R. S. Littlepage R. Rajnic	8. Performing Organization Report No.
9. Performing Organization Name and Address Westinghouse Defense & Electronic Systems Ctr. Command & Control Division Baltimore, Maryland 21203	10. Work Unit No. (TRAIS)
	11. Contract or Grant No. DOT-PA74WA-3353
12. Sponsoring Agency Name and Address Federal Aviation Administration Systems Research & Development Service Washington, D.C. 20591	13. Type of Report and Period Covered Final Report, Nov 1973 - May 1979
	14. Sponsoring Agency Code

15. Supplementary Notes

16. Abstract

This report describes the analysis and design, and the fabrication and test of an improved glide slope antenna system. It is capable of providing CAT II performance over level ground, rising ground, and severe broken ground associated with problem sites. It is broadband and can operate at any ILS glide slope frequency with no special tuning. A new monitoring technique was developed which is applicable to any antenna system consisting of a large number of radiators. The report contains the results of antenna range measurements and flight check data taken at a typical site.

17. Key Words	18. Distribution Statement
Instrument Landing Systems Glide Slope Arrays Glide Slope Monitors Glide Slope Flight Check	Availability is unlimited. Document may be released to the National Technical Information Service, Springfield, VA 22151, for sale to the public.

19. Security Classif. (of this report)	20. Security Classif. (of this page)	21. No. of Pages	22. Price
Unclassified	Unclassified	188	

Form DOT F 1700.7 (8-72) Reproduction of completed page authorized

METRIC CONVERSION FACTORS

Approximate Conversions to Metric Measures

Symbol	When You Know	Multiply by	To Find	Symbol
		LENGTH		
in	inches	*2.5	centimeters	cm
ft	feet	30	centimeters	cm
yd	yards	0.9	meters	m
mi	miles	1.6	kilometers	km
		AREA		
in^2	square inches	6.5	square centimeters	cm^2
ft^2	square feet	0.09	square meters	m^2
yd^2	square yards	0.8	square meters	m^2
mi^2	square miles	2.6	square kilometers	km^2
	acres	0.4	hectares	ha
		MASS (weight)		
oz	ounces	28	grams	g
lb	pounds	0.45	kilograms	kg
	short tons (2000 lb)	0.9	tonnes	t
		VOLUME		
tsp	teaspoons	5	milliliters	ml
Tbsp	tablespoons	15	milliliters	ml
fl oz	fluid ounces	30	milliliters	ml
c	cups	0.24	liters	l
pt	pints	0.47	liters	l
qt	quarts	0.95	liters	l
gal	gallons	3.8	liters	l
ft^3	cubic feet	0.03	cubic meters	m^3
yd^3	cubic yards	0.76	cubic meters	m^3
		TEMPERATURE (exact)		
°F	Fahrenheit temperature	5/9 (after subtracting 32)	Celsius temperature	°C

*1 in = 2.54 (exactly). For other exact conversions and more detailed tables, see NBS Misc. Publ. 286, Units of Weights and Measures, Price $2.25, SD Catalog No. C13.10:286.

Approximate Conversions from Metric Measures

Symbol	When You Know	Multiply by	To Find	Symbol
		LENGTH		
mm	millimeters	0.04	inches	in
cm	centimeters	0.4	inches	in
m	meters	3.3	feet	ft
m	meters	1.1	yards	yd
km	kilometers	0.6	miles	mi
		AREA		
cm^2	square centimeters	0.16	square inches	in^2
m^2	square meters	1.2	square yards	yd^2
km^2	square kilometers	0.4	square miles	mi^2
ha	hectares (10,000 m^2)	2.5	acres	
		MASS (weight)		
g	grams	0.035	ounces	oz
kg	kilograms	2.2	pounds	lb
t	tonnes (1000 kg)	1.1	short tons	
		VOLUME		
ml	milliliters	0.03	fluid ounces	fl oz
l	liters	2.1	pints	pt
l	liters	1.06	quarts	qt
l	liters	0.26	gallons	gal
m^3	cubic meters	35	cubic feet	ft^3
m^3	cubic meters	1.3	cubic yards	yd^3
		TEMPERATURE (exact)		
°C	Celsius temperature	9/5 (then add 32)	Fahrenheit temperature	°F

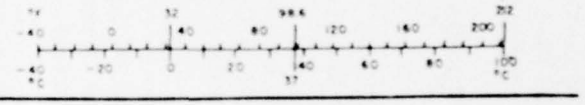

TABLE OF CONTENTS

TABLE OF CONTENTS (Continued)

LIST OF ILLUSTRATIONS

LIST OF ILLUSTRATIONS (CON'T.)

LIST OF ILLUSTRATIONS (CON'T.)

LIST OF ILLUSTRATIONS (CON'T.)

LIST OF ILLUSTRATIONS (CON'T.)

LIST OF ILLUSTRATIONS (CON'T.)

LIST OF ILLUSTRATIONS (CON'T.)

1.0 INTRODUCTION

Contract DOT FA74WA-3353 was a multi-tasked contract. Three mathematical analyses were performed under the contract, and were reported in separate final reports. It was also required to design, develop, and test a glide slope antenna system capable of operating over severe terrain conditions.

1.1 MATHEMATICAL STUDIES

The Westinghouse approach to the problem of siting ILS glide slope antenna systems has been to develop a computer modeling technique capable of determining; (1) the effects on flyability of various antenna parameters leading to improved antenna designs, and (2) the ability to predict how specific antennas will perform in a given terrain environment. Under this contract, the computer modeling was used to study potential improvements to existing image glide slope systems and to evaluate the current grading and siting criteria with a view to upgrading 6750.16A. A synopsis of these reports is included here:

Report No. FAA-RD-78-42, "Study of Rough Ground and Grading Criteria For Instrument Landing System Glide Slope Site Preparation."

The scattering of electromagnetic radiation from rough surfaces has been studied. The diffuse and specular components of the scattered field are treated separately. Current grading of ILS sites requires rather stringent preparation of the ground. The application of this report is to develop grading criteria that reflect the statistical nature of the disturbance in observed signal rather than simply to consider the maximum allowable phase differences as the basis for establishing a grading criteria. The results of this work indicate that the current grading is too stringent and that substantial cost savings can be effected through

a more systematic approach. In specifying the grading criteria, the expressions developed allow for the treatment of several statistically different surfaces with the requirement that the solutions be self-consistent when the roughness of each adjacent surface is equal.

Report No. FAA-RD-78-41, "Capture Effect Array Glide Slope Guidance Study".

The purpose of this study has been to examine the performance of the Capture Effect Glide Slope Array as a function of the quality and quantity of required ground plane. Methods of improvement were also investigated; wherein either a smoothing of the glide path structure or a reduction of the required ground plane was considered an improvement. The study was directed entirely to the structure on glide path. All Capture Effect installations are operated with an additional clearance signal which guarantees sufficient below path fly-up to provide absolute safety. In the conclusions it was shown that some modification of the standard antenna configuration results in a reduction of the phase sensitivity of the glide path structure. This would result in a reduction in the exactness of monitoring presently used on all operational systems. The results of this study have favorably compared to limited experimental data. However, a complete and controlled experimental program would be required to establish the useful range of application of this analysis.

Report No. FAA-RD-78-43, "Analysis Of The Performance Of Image Glide Slope Antenna In The Presence Of Truncated Ground".

Terrain modeling in electromagnetic scattering problems has traditionally involved separating the terrain under consideration into small enough segments so that a Huygens source approximation to the treatment of the scattered field is possible. Use of this technique very often requires an exceedingly large number of segments to properly represent the ground surface. Moreover, numerical integration techniques are often used to calculate the scattered fields from the Hugens sources. This approach can lead to computer programs running times on the order of hours for many applications. This paper is concerned with applying the half-plane scattering solutions of Senior, Woods, and Bromwich to the modeling of a wide variety of terrain conditions using closed form analytic solutions. The use of such a technique can reduce computer running times for many common terrain situations by orders of magnitude.

The motivation for the work presented here was a need to develop more practical techniques (in terms of reduced computer running times) for computing the performance characteristics of instrument

landing systems (ILS) glide slope antennas over non-ideal terrain. Practically all glideslope antennas in use today are of the ground-image type which depend on ground reflections for the formation of the guidance beam. The formation of an ideal glide path in space requires a ground plane in front of the antenna that is infinite, flat, and perfectly conducting. Such a case is readily calculated using simple image theory. However, this ideal condition is never encountered in practice and rarely is the flat ground in front of the antenna of such an extent that image theory can provide an accurate model. Many times the terrain is of such a nature that it can be accurately modeled by half-planes and large (> 2-3 wavelengths) connected strips that are infinite in length.

In order to properly characterize the performance of an ILS glide slope antenna on the glide path one needs to calculate the total fields at a large number of points corresponding to an aircraft's position as it is approaching the runway. In addition, several more approaches above and below the glide path and either side of the runway are needed to complete the glide slope characterization. Thus the scattered fields at a very large number of aircraft positions are needed. In order to have a terrain model that can economically and accurately account for scattering from large segments of terrain, a closed form expression for scattering from these segments that is valid when the segments are in the near field of the radiating antenna system is necessary. Use of the half-plane scattering solution and combining two half-planes to form strips provides the basis for such a terrain model.

Redlich has computed the performance of glide slope antennas over limited ground planes, however, his approach involved a two-dimensional terrain model and allowed evaluation of far field performance characteristics only. The terrain model developed in this paper is a fully three dimensional model and allows for near and far field characterization of the glide slope antenna.

Verification of the approach presented has been accomplished by using experimental data obtained by Lucas. Good agreement between theory and experiment has been achieved.

1.2 DIPOLE BROADSIDE GLIDE SLOPE ANTENNA DESIGN

This contract provides for the analysis and design, and the fabrication and test of an improved glide slope antenna system. The basic antenna requirements are:

1. It must be capable of providing Category II performance over level ground, rising ground, and severe broken ground associated with problem sites.

2. It must be broad band such that it can operate at any ILS glide slope frequency with no special tuning.

3. It must be consistent with FAA construction and installation practices and compatible with transmitters and monitor systems in current usage.

In order to satisfy item one (1) above, a non-image antenna must be used. In this application, "broadside" refers to a class of antennas in which the radiation pattern is entirely formed within the physical extent of the aperture. This is opposed to the "image" systems, which depend on ground adjacent to the antenna in support of the formation of the final radiation pattern. The rough ground condition of item one requires that energy be surpressed over a critical region which would produce scattering into the glide path. This specialized tailoring of the radiation pattern requires an array.

A number of different types of radiating elements were considered. It was decided that, on the basis of manufacturing ease and overall reliability, the dipole would be the most practical radiating element.

The final configuration determined to satisfy the design goals, is an array of dipole elements referred to as the Dipole Broadside Glide Slope Array. The analysis to determine the final desired radiation pattern, the element excitations, and a physical description of the array are given in Section 2 of this Report. As with other ILS arrays consisting of a large number of radiators, monitoring is a difficult problem. A new approach was developed on this program. It is a time shared technique,

in which the monitor function is stepped through the array of radiating elements, in a time short compared to aircraft movement. This system is described in Section 3.

Section 4 describes the results of the antenna testing program. This includes both antenna pattern range data and flight check data taken at a field site. The antenna range data indicates that the desired radiation pattern was almost perfectly achieved. It also shows that the desired planar guidance and broadband performance were achieved. The flight check program was marred by repeated failure of SMA connectors. These have been replaced with type TNC and should provide a high level of reliability. There was, however, a sufficient amount of flight check data taken in the field to demonstrate CAT II performance at a severe terrain site. It is felt that the antenna not only meets all performance goals, but can provide an exceptional quality guidance at virtually any tough site. Path roughness and the linearity of the level run transitions were outstanding over this rough ground test site. They are significantly better than the Compensated Waveguide, which had been initially tested at the same site.

In Section 5 a mechanical modification is recommended. The purpose is two fold: (1) to increase reliability, and (2) to reduce construction costs. This is consistent with the design goal of having an inexpensive antenna designed for mass production.

2.0 ANTENNA DESIGN

The statement of work for this contract provides for the theoretical analysis and design of several versions of a reduced aperture array. Based on this theoretical analysis and design, one version of a reduced aperture array will be fabricated and tested. This effort shall include design, fabrication and factory test of parts and of the assembled array which will provide Category II performance at level ground, rising ground and broken ground types of problem sites. The factory tests shall include pattern range and monitor tests to insure the antenna array is operating as designed before field tests are attempted. The work shall also provide for field tests of the reduced length array at a site where rough ground tests can be conducted such that the complete capabilities of the antenna are tested. The antenna shall be broadband, capable of providing CAT II performance, anywhere in the glide slope band, with no special tuning.

Many different antenna configurations were investigated. Only the final design will be reported. It should be noted that the expression "reduced aperture array" no longer applies. As the analysis progressed and performance estimates based on aperture length became available, more stringent requirements were defined by the FAA Technical Offier, requiring larger apertures. It was decided that the new array could be any length, but not to exceed the length of the compensated waveguide.

2.1 ANTENNA ELECTRICAL DESIGN

2.1.1 Preliminary Considerations

There are two basic types of glide slope antennas; (1) image systems, and (2) non-image arrays. Image systems require the energy reflected from a near perfect ground plane to complete the guidance pattern. This ground must extend over several

thousand feet and, not only be flat, but also, fixed in position. Acceptable performance often requires extensive terrain modifications. For the case of an over tidal water approach, this is virtually impossible.

Broadside arrays are systems from which the desired guidance pattern is formed entirely within the physical extent of the radiating aperture. The ideal site would be one in which there was no ground in front of the antenna. The presence of ground can only degrade performance, since it will scatter energy into the glide path.

Neither of these two perfect situations can be achieved; i.e., the perfect ground plane or no ground plane. For sites from which the existing ground is reasonably flat, the image system is the most feasible. For sites with either rough ground or tides, an adaptation of the broadside antenna is a viable approach. The adaptation consists of suppressing any energy which would scatter into the glide path in such a way as would take the guidance out of specifications. It is to the design of this type of antenna that the program was directed.

The ILS glide slope radiates two signals: (1) the carrier-plus-sideband (CSB), and the sideband-only (SBO). The CSB signal serves as a reference for demodulation and signal level measurements. It has a maximum within the glide path course width (glide path angle $\pm$ 0.35°), and is slowly varying over the course width. The direct CSB signal strength compared to any reflected CSB is always very large, hence, the CSB is not affected by scattered energy, and therefore, no special shaping of the CSB pattern is required. A sufficiently low sidelobe CSB pattern can be achieved with the conventional cosine squared on a pedestal aperture distribution.

The case for the SBO pattern is considerably more complex. The SBO has a null on the glide path, known as the guidance null,

and very rapidly increasing signal above and below the glide path. Reflected energy can cause appreciable shifts in the position of this null, which is equivalent to changes in the glide path angle. The requirement of controlling this scattered energy must be approached from two directions: (1) the lower (below path) guidance lobe must be tailored to provide sufficient guidance signal with a minimum illumination of the ground, and (2) based on a typical siting location (antenna backset, offset, and center height above level ground) a critical angular region must be defined, which would scatter energy into the glide path, and the sidelobes in this region must be suppressed. Each of these considerations presents a particular set of problems. The lower guidance lobe would ideally have a null on the horizon in order to minimize illumination of objects near the horizon. It should also have a peak amplitude which is considerably less than the upper guidance lobe, to further reduce the scattering from objects near the horizon. At the same time, there must be sufficient energy available in the lower guidance lobe to provide the required below path clearance (fly-up signal), and there can be no angle of approach for which an aircraft can get under the fly-up signal (no false course). If the lower guidance lobe is to have a null on the horizon, and the normal glide path angle is 3^{o}, then the width of the lower guidance lobe will be 3^{o}. This is a key parameter in determining over all array length.

The desire to suppress sidelobes over as large an angular region as possible must also be carefully examined. Consider the total energy radiated by an antenna to be a constant, and directly proportional to the area under the antenna radiation pattern curve. If particular sidelobes are suppressed, this energy must go to an increase in other sidelobes, such that the total area under the curve remains the same. These increased sidelobes must occur at angles which do not interfere with achieving quality guidance. For an array of N elements, only N

points on the radiation pattern may be independently specified. Hence, increasing the region of suppressed sidelobes would require increasing the number a radiators and would also result in very large sidelobes at other angles.

Another very important initial consideration is that the radiated SBO field must be real. This means that the SBO must be in phase with the CSB. An extensive analysis of the effects of a quadrature component of SBO phase was performed and reported in FAA-RD-72-139, "Analysis of Instrument Landing System Glide Slope Broadside Antennas". This "real" requirement on the SBO field places limitations on the technique used to synthesize the aperture distribution.

2.1.2 Determination Of Key Radiation Parameters

In order to generate antenna patterns consistent with the above goals, a synthesis technique was used. Several techniques were investigated, including the popular Schelkunoff Polynominal and a very precise discrete-continuous approach developed by Westinghouse. The Schelkunoff Polynominal method is relatively simple to implement but does not assure real SBO radiation fields. Even an error as small as $\pm$ 10° can produce distortion in some receivers. As a result, its application in the design of the Redlich Array required the use of a special feed system in order to achieve broadside CSB and SBO fields in phase. The approach used on this program, referred to as a continuous-discrete synthesis, is based on the low sidelobe Taylor distribution. Its key feature is the development of an integral method for translating the resulting continuous aperture distribution into a distribution of discrete radiators. This technique is described in Appendix B of this report. The two methods are compared in Table 2.1.

Quantity	Schekulnoff Polynomial	Continuous Discrete
Phase of SBO Pattern	Deviates From Zero Up to $\pm$ 10°	Zero Phase Deviation
Placement of Radiators	Rigidly Uniform Spacing	Optimized Spacing
Amplitude Patterns	Essentially Equivalent Capability	
Mathematical Complexity	Relatively Simple	Very Sophisticated

TABLE 2.1

Comparison of Schekulnoff and Continuous Discrete Approaches to Aperture Synthesis

This technique was applied to apertures ranging from 13 to 22 wavelengths. The results are summarized in Table 2.2, which includes a 6dB coned Compensated Waveguide for comparison.

TABLE 2.2

Array	Length	Angle Below The Horizon				
		0°	3°	6°	9°	12°
Comp. W/G	65'	120	7	11	2	36
13 λ	42'	218	<5	<5	<5	21
19 λ	60'	42	<5	<5	<5	7
21 λ	65'	20	<5	<5	<5	<5
22 λ	69'	8	<5	<5	<5	<5

The signal strengths are given in equivalent microamperes. All of these arrays are capable of being sited within 500' of runway center line. The computer modeling technique was used to predict

how each of the above would perform over a variety of terrain. The FAA Technical Officer decided that in order to achieve CAT II over a wide variety of terrains, the new array could be as long as the Compensated Waveguide. Hence, the decision was to fabricate a 21 λ array. The final array design is 21.75 λ long. The number of elements is determined by three factors: (1) minimum for cost, (2) as required to synthesize the pattern, and (3) acceptable mutual coupling.

The mutual coupling factor is somewhat nebulous since the close-in coupling decreases with spacing, distant coupling increases with spacing, and since it is only a factor to the extent that it is not predictable. The pattern approximation places more specific limits.

For an antenna with N elements, N points on the pattern may be independently specified. The rest of the pattern automatically follows. If the pattern has a mainlobe with nulls and is not complex, the pattern can be entirely specified by the peak and N-1 null locations. For length L, the pattern repeats when $\frac{L}{N} \cdot \sin\theta = \lambda$. Therefore, we have N points specified over a region of sin θ that is $\frac{N\lambda}{L}$ wide, averaging one every λ/L. Thus, for a given length array, there are a fixed number $\frac{2L}{\lambda}$ of nulls in real space, independent of the number of elements. This is depicted in Figure 2-1.

Consider what limits the number of elements. Ordinarily, if one allows grating lobes the gain suddenly drops and the impedance jumps. But with many lobes this is not the case. Instead, one finds it harder to synthesize the pattern. As one reduces the number of elements the cycle length reduces in length at the same rate that the number of nulls decreases, so that the average density to work with stays the same. However, the low sidelobe region requires a nearly fixed number of closely spaced nulls so that the average density left to use

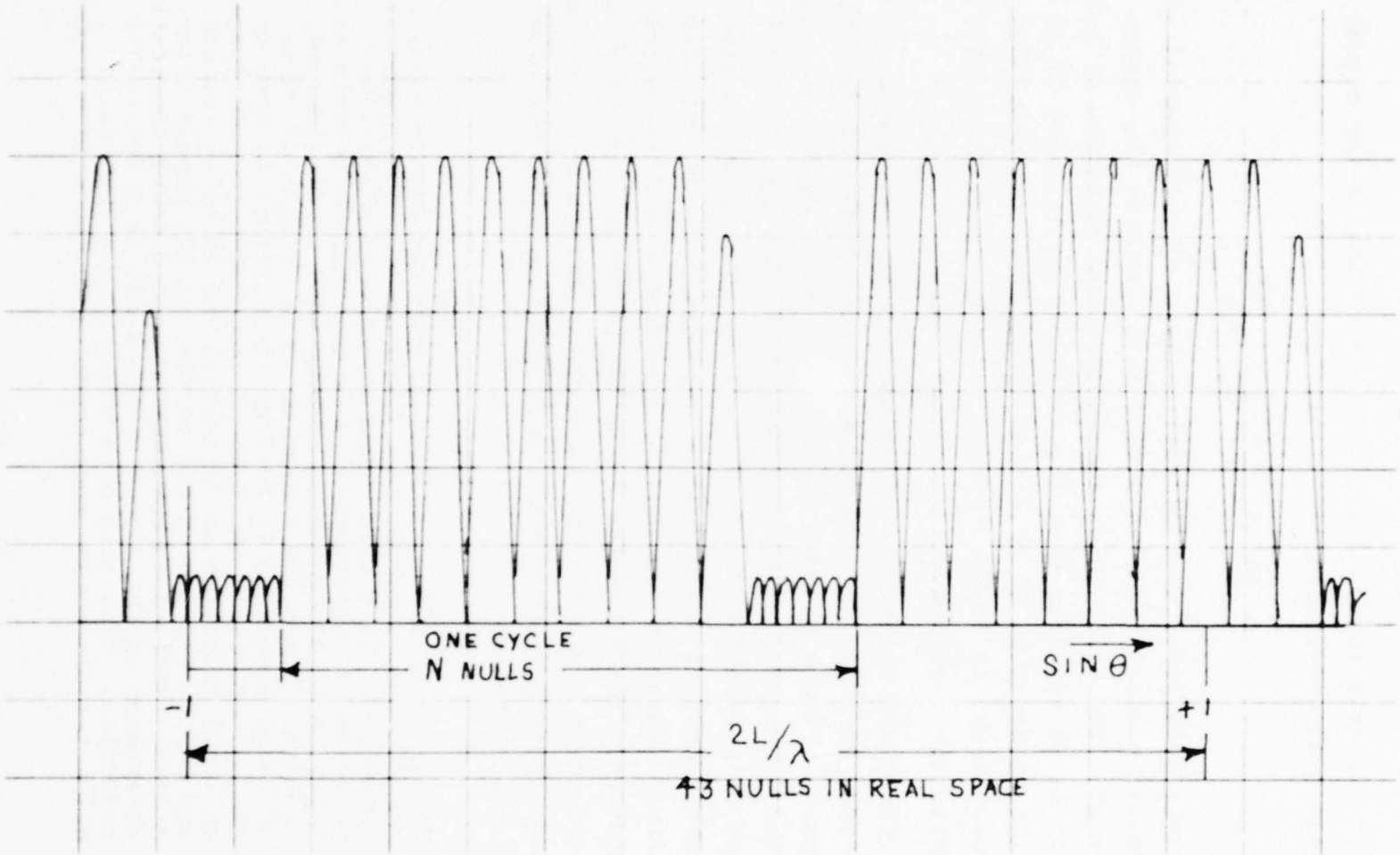

Figure 2-1 Relation Of The Number Of Nulls As A Function Of Array Length

outside of this region falls off. Referring to the figure, the average null spacing is

$$ANS = \frac{N\lambda/L - .276}{N - 10}$$

The lobe peak level varies drastically with null spacing so that increased spacing leads to a high level outside the region of interest. The graph shows the approximate variation of level vs N. If it is required that the sidelobes be at least 24 dB down and the peaks to be no more than 40 dB above the sidelobes, the net peak level is 16 dB. Figure 2-2 shows that at least 27 elements are required.

There are mechanical advantages to building the array in sections, each of which contains the same number of radiating elements. It was decided to build the array in seven sections of four elements each for a total of 28 elements. Dipoles were chosen on the basis of mutual coupling. A continuous-discrete synthesis program was performed for this array to optimize the far field radiation pattern and determine an initial element excitation. These results are given in Figure 2-3, in which a comparison is given for the Compensated Waveguide. A comparison of these patterns and their effect on glide slope performance shows the following:

A.) The width of the lower main lobe of the Dipole Array is considerably narrower than the 9 dB coned, compensated waveguide. What this means in terms of glide slope performance characteristics is that uneven terrain and hilly terrain derogation effects will be considerably reduced. Since the radiation in the region of 2^{o} to 4^{o} below broadside ($\pm$ 1^{o} from the horizon) is down on the average by 15 dB it seems reasonable to anticipate an ideal reduction in derogation due to hilly terrain and uneven terrain of 80% to 85% for the dipole array. A more practical number, taking into account fabrication tolerances of the dipole array, would be a 70% to 75% reduction. Thus at a site where uneven terrain or hilly terrain would cause bends of 30 μa with a 9 dB

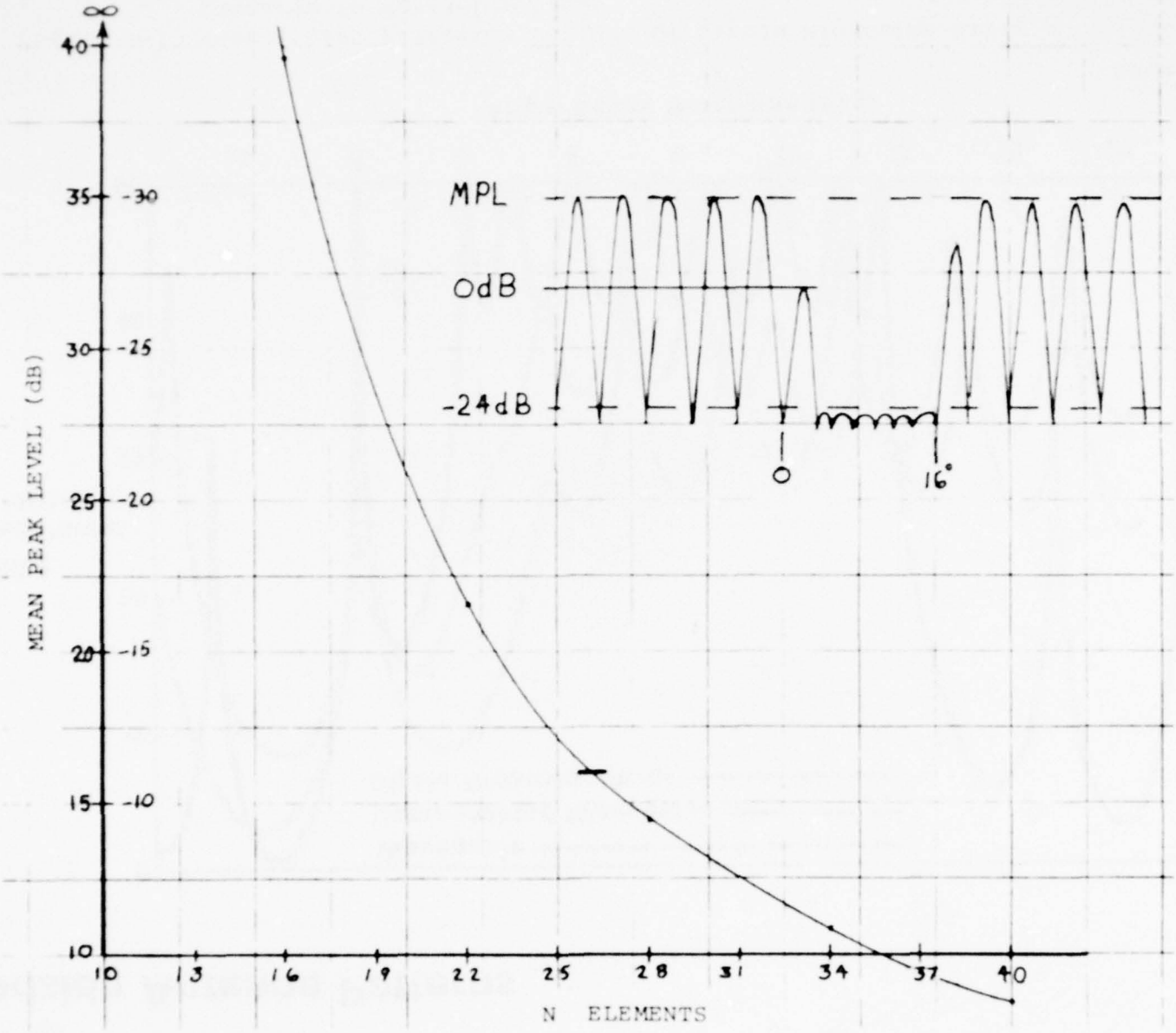

Figure 2-2 Variation Of Lobe Peak Level Versus The Number Of Radiators

Broadside Antenna Patterns

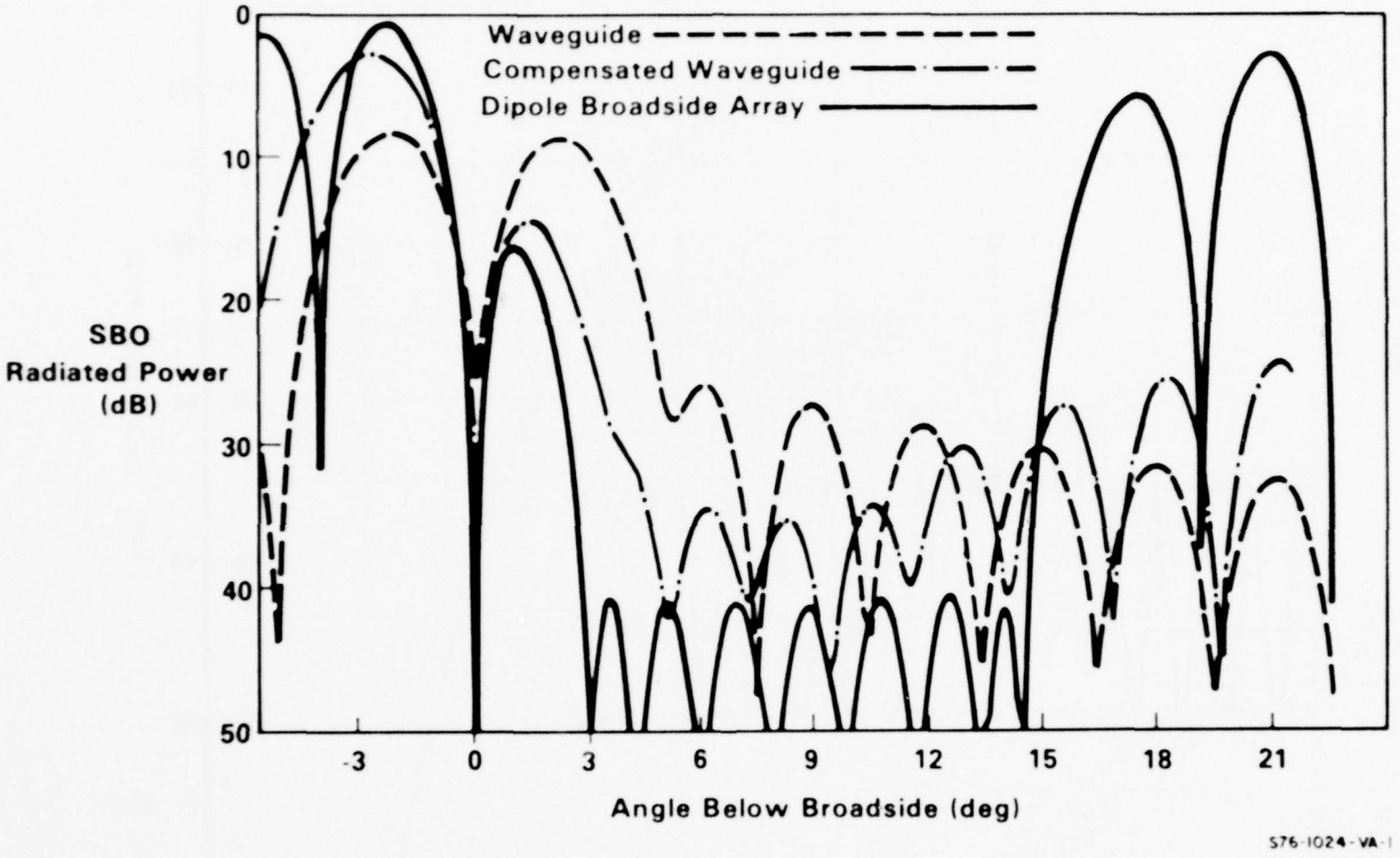

Figure 2-3 Theoretical Radiation Pattern Of Dipole Broadside Array Compared to Waveguide Array

coned, compensated waveguide the Dipole Array should have bends of less than 9 λua (70% reduction).

B.) In the critical sidelobe region the sidelobe levels of the dipole antenna are lower than the 9dB coned, compensated waveguide. What this means in terms of glide slope performance is that at tidal sites or snow accumulation sites the derogation effects due to varying ground height will be less with the dipole array than with the 9dB coned, compensated waveguide. The radiation in the region of sidelobe reduction is down by 7dB ideally and more practically would be at least 4dB down with the dipole array. This means that for a tidal variation of 9 feet (such as LaGuardia RW 22) where the compensated waveguide antenna exhibited an angle change of $\pm$ .035° the dipole array would have a maximum angle change of $\pm$ .02°.

C.) The sidelobe reduction region extends over a greater range for the dipole array than for the compensated waveguide. This means that the dipole array would be less susceptible to derogation due to very rough terrain (such as drainage ditches) close in to the antenna. There has not been very much data on the effect of rough terrain very close to the waveguide although, at Lynchburg, the 6dB and 9dB coned, compensated waveguide antenna performed within CAT II limits except for the flare due to coning with less than 100 feet of flat ground in front of it. It is expected that the dipole array would need about 200 feet of relatively smooth ground in front (or a complete lack of ground) so that the high sidelobes out past the critical region will not cause derogation. It should be mentioned that the terrain need not be flat or graded but rather severe discontinuities such as drainage ditches or man made structures should be avoided within this close-in region.

D.) There is another significant advantage that is not apparent by comparing the antenna patterns and that is the elimination of the flare due to coning. By proper focusing of the dipole broadside array there is virtually no flare that exists while for the coned, compensated waveguide this flare can be significant and many times would preclude CAT II performance.

2.1.3 Focusing For Improved Near Field Performance

The antenna has been computer modeled over an infinite flat ground and fly-ins have been run for this case. Figure 2-4 shows the results for a fly-in at an unfocused antenna. There are two graphs on the figure, the one marked "red" includes the effect of the ground while the other curve includes only the radiation from the antenna itself neglecting the effect of the ground. The difference between the two is due to energy re-radiated from the ground which has been illuminated by the sidelobes of the antenna pattern. The close correspondence ($\sim 5\mu A$) between the two is a direct indication of the effectiveness of the low sidelobes in reducing derogation.

As can be seen from this figure a significant amount of fly-down signal occurs within 2000 feet of threshold. This is due to null defocusing in the near field and is a common problem with arrays that have non-symmetrical SBO antenna patters (the Thomson-CSF array described in a report entitled "Special Glide Path Antenna" has a similar defocusing effect and the Redlich Aerial also had a defocusing problem).

There are two basic methods that could be used to correct for near field defocusing of a linear array: (1) electronically, by modifying the phase of the array elements, and (2) mechanically, by curving or bowing the array structure.

In focusing electronically, typically the phase of the elements from the center to both ends are incremented from their nominal values in such a fashion that the phase front in any plane containing the array is an arc of a circle. The radius of this circle is the focalization distance. The Thomson-CSF array utilized electronic focusing at a distance of 1000 meters. There is a major disadvantage to this kind of focusing: exact focusing occurs at only one point along the approach path. This occurs due to the fact that, with electronic focusing, the locus of

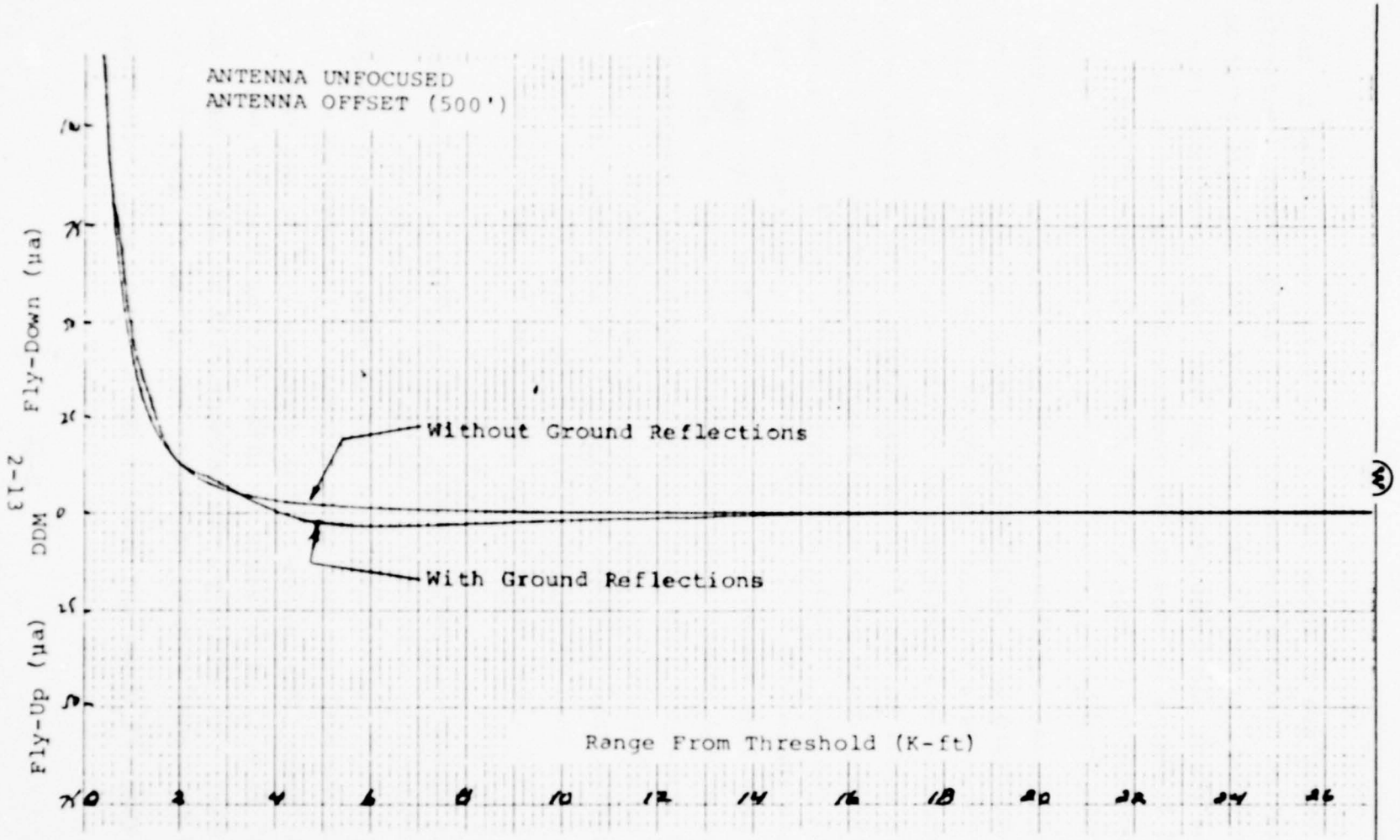

Figure 2-4 Fly-In Over Infinite Flat Ground-Unfocused

points which are in focus is a circle with radius equal to the focalization distance and center at the array center. Referring to Figure 2-5, it can be seen that exact focusing will occur at only one point along the array. As mentioned previously this type of focusing is used on the Thomson-CSF array and it still had a defocusing or loss of null close-in in spite of the electronic focusing.

Mechanical focusing is achieved by curving or bowing the array structure in a circular arc. The locus of points which are in focus is a straight line through the center of the circle, perpendicular to the circle (see Figure 2-6). The focal distance is equal to the radius of the circle. For a linear array, the structure could be curved sideways, forwards or some combination of the two. Figure 2-7 shows the side and forward focused modes and their effect in an ILS glide slope application. As can be seen from Figure 2-7, the only mode that allows for focusing at all points along the approach would be the sideways focused structure. The other modes of mechanical focusing allow only a single point of focus along the approach path. Thus these would suffer from the same deficiency that electronic focusing has, i.e., a loss of guidance null in the near field. Thus sideways mechanical focusing is being used for the Dipole Broadside array.

The mechanical focusing will be accomplished by inserting wedges between each section in the array. This is the same technique that was successfully used to make far field measurements of the modified waveguide antenna at the Westinghouse antenna range. The nominal focal distance will be 500 feet although it will be possible to alter this by changing the wedges only. In addition, the antenna will be able to be side-focused to either side by reversing the wedges in the structure.

Figure 2-8 shows the results for a fly-in with wedges used

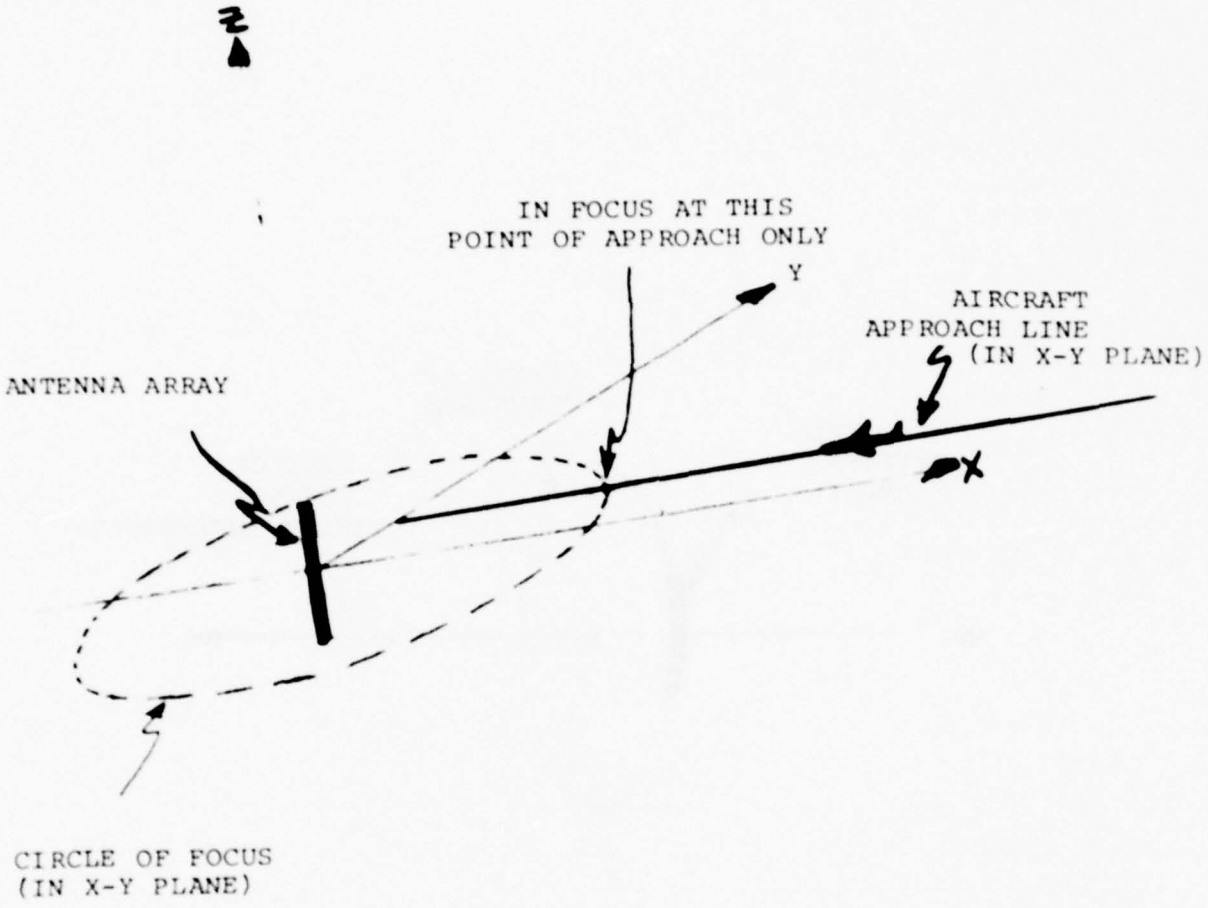

Figure 2-5 Results Of Electronic Focusing

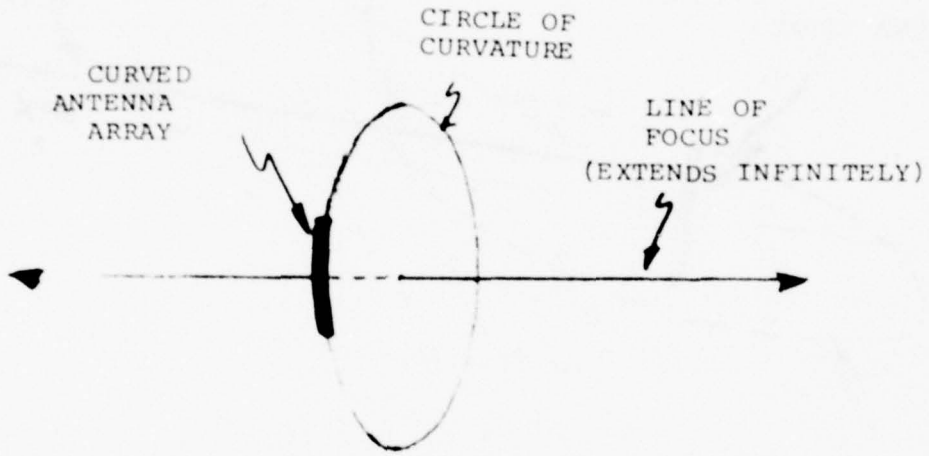

Figure 2-6 Results Of Mechanical Focusing

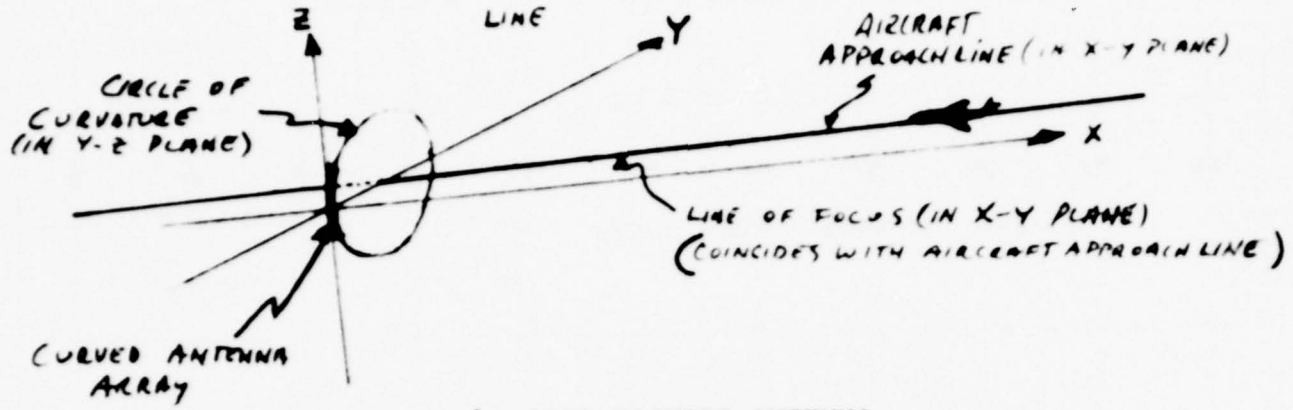

a.) SIDE-FOCUSED ANTENNA

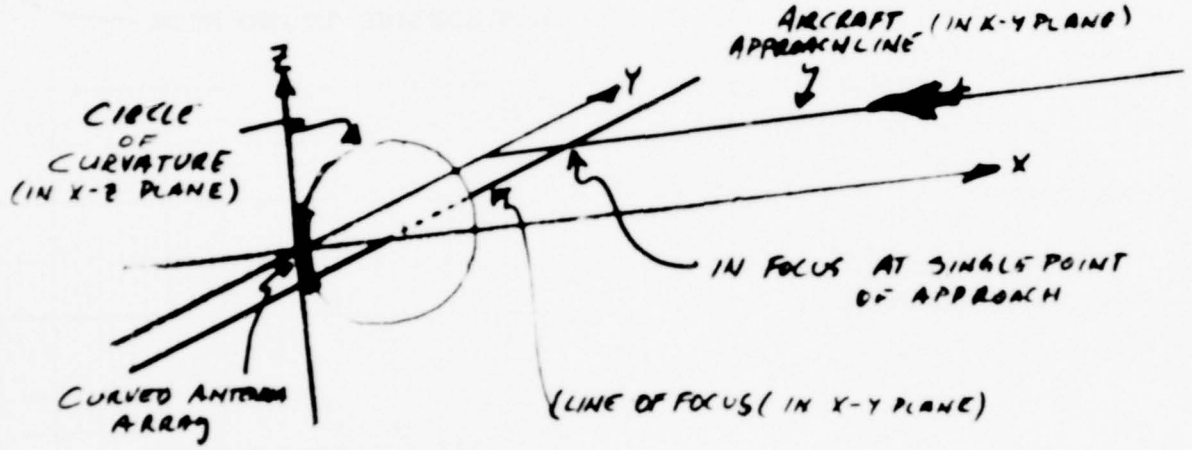

b.) FRONT-FOCUSED ANTENNA

Figure 2-7 Modes Of Mechanical Focusing
(a) Side Focused, (b) Front Focused

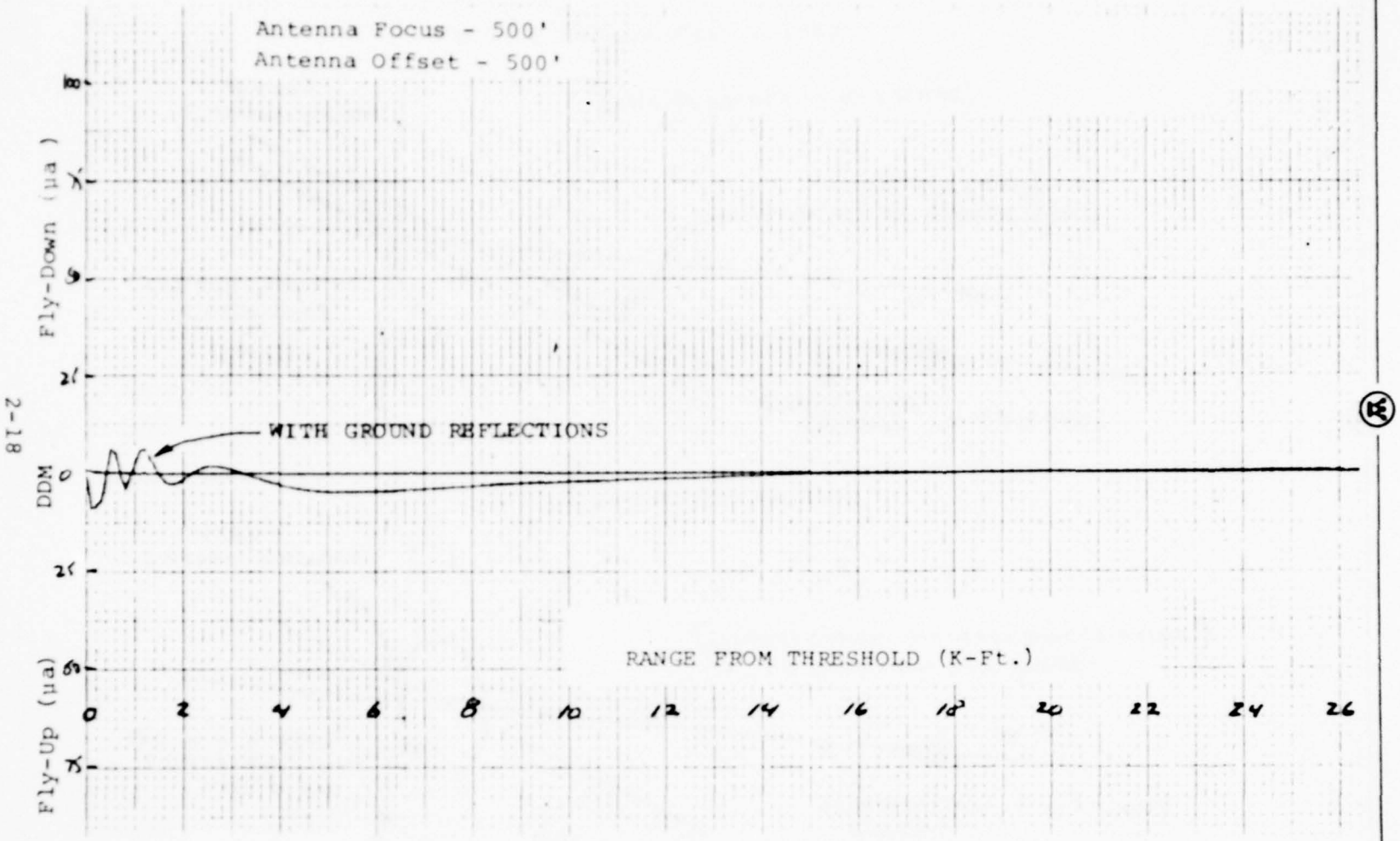

Figure 2-8 Fly-In Over Infinite Flat Ground - Antenna Focused 500' & Offset 500'

to side-focus the antenna. The focal distance and antenna offset are both 500 feet. Comparison with Figure 2-4 shows a complete correction of the near-field defocusing or loss of null. Figures 2-9, 2-10, and 2-11 give similar results but for antenna offsets of 400 feet, 600 feet and 700 feet respectively. It appears that in order to keep the defocusing flare due to offset changes to under 25 ua, the antenna offset whould be within ± 200 feet of the focal distance.

2.1.4 Mutual Coupling Analysis

The controlling factor in the dipole broadside array design was the sidelobe level in the angular region below the main beam. The effects of tolerances, mechanical and electrical, will be discussed elsewhere. To complete the design in a thorough manner requires an accounting of the effects of mutual coupling. Mutual coupling causes changes in the element impedance and pattern that can bring about rather serious disturbances in the array performance if not properly included in the array design.

Because of the nature of the changes caused by mutual coupling, the effects must be found early in an array design and factored with the pattern synthesis. The design procedure used during the dipole array program did this in the following manner:

1. An element was selected that exhibits minimum mutual coupling effects - the dipole.
2. Mutual coupling analysis.
3. Measurements were made on an array of these elements to:
   a. Evaluate means of further reducing intercoupling.
   b. Measure the change in element pattern shape for both center and edge elements.
   c. Match the element to space.

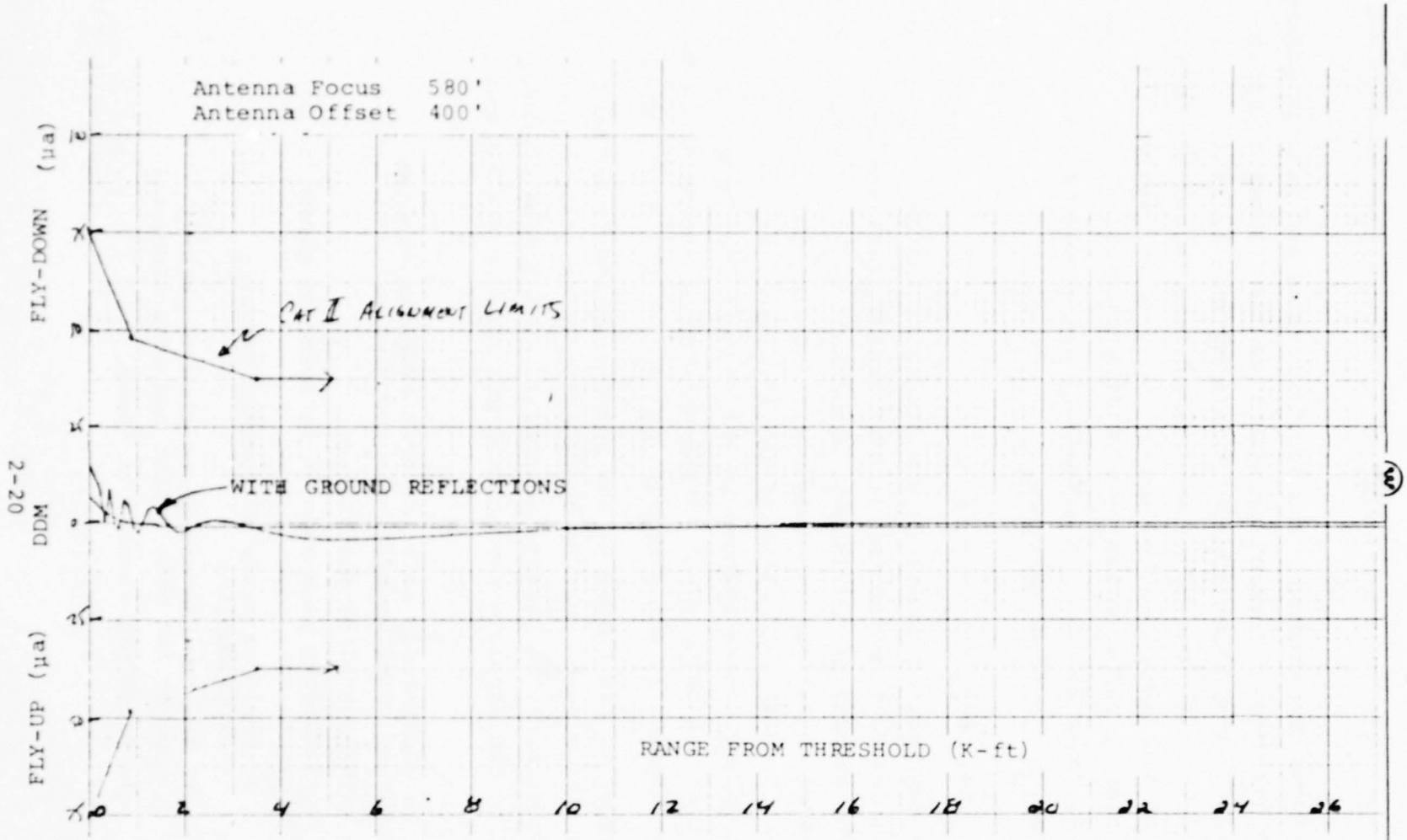

Figure 2-9 Fly-In Over Infinite Flat Ground - Antenna Focused 500' & Offset 400'

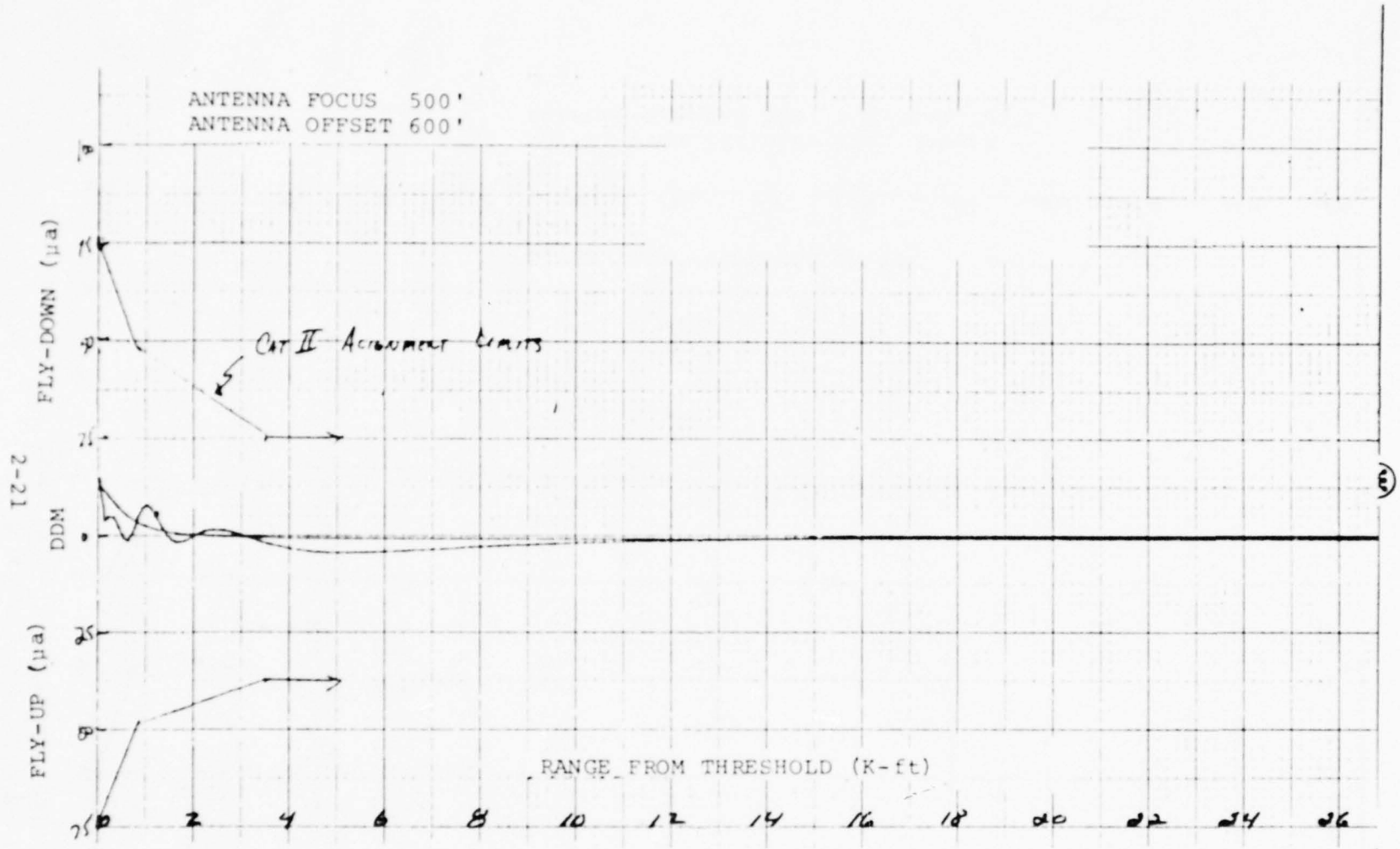

Figure 2-10 Fly-In Over Infinite Flat Ground - Antenna Focused 500' & Offset 600'

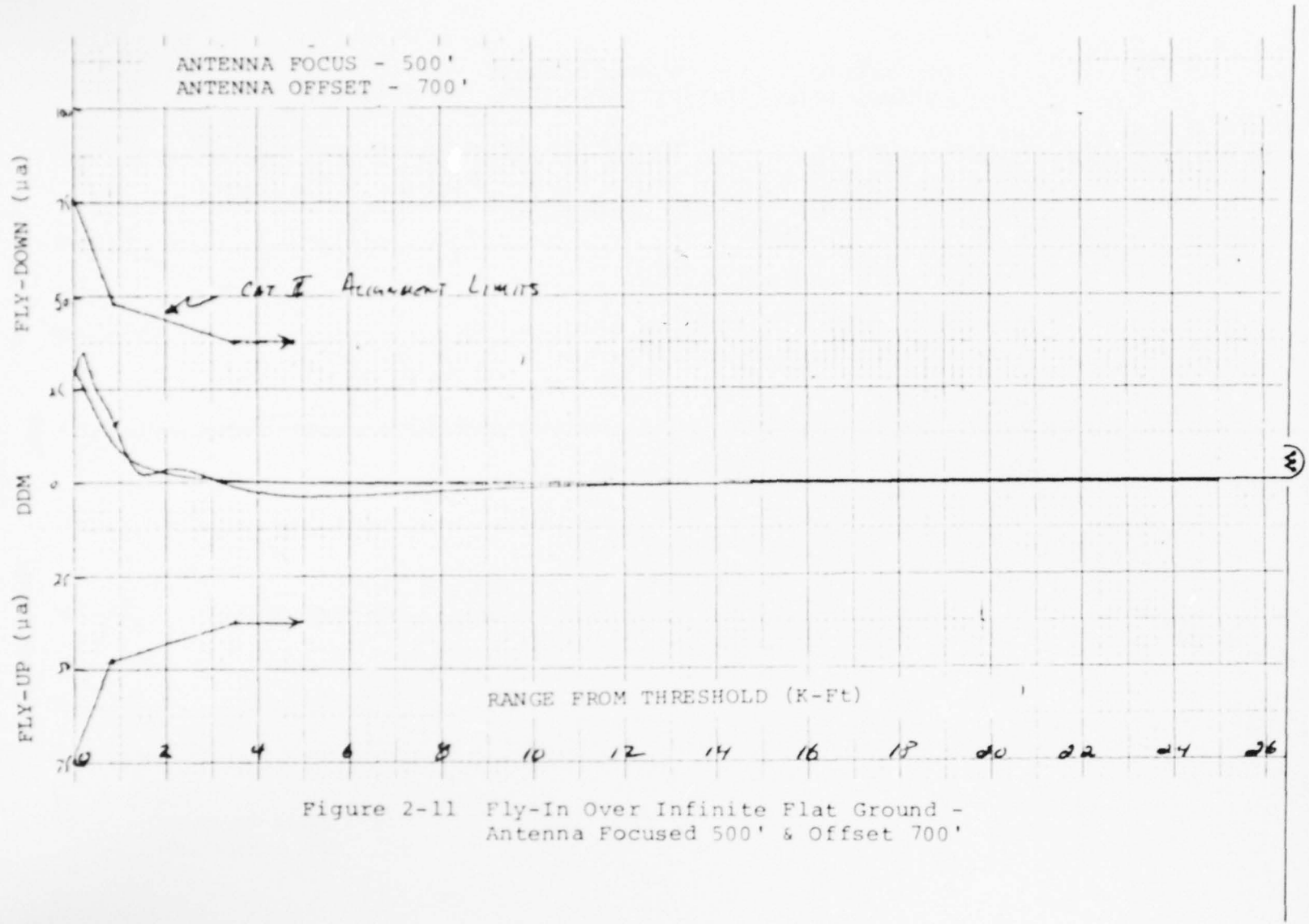

Figure 2-11 Fly-In Over Infinite Flat Ground - Antenna Focused 500' & Offset 700'

4. Factor the element patterns into the pattern synthesis to evaluate changes necessary in the illumination excitation.

5. Design a directive power divider network to produce the required array excitation.

This program was organized to answer three questions:

* What is the effect of mutual coupling?

* What can be done to minimize this effect?

* What should be done to the array design to account for mutual coupling?

Mutual coupling affects the impedance of the array elements and the element patterns. These effects differ depending on the element environment, i.e., is it an edge element or a center element? Both of these effects can be evaluated by measuring the element pattern and element impedance in the presence of other elements. To perform these measurements, an array several wavelengths (> 3 wavelengths) was built. Patterns of edge elements and center elements were measured with all elements terminated in a load except for the element under test. The measured element patterns were then factored into the pattern synthesis program. An analytical effort was performed in conjunction with the element measurements to provide a guide to the measurements and to allow deeper insight into the intercoupling mechanism.

Having obtained and verified the element patterns, this information was then used in the array pattern synthesis. The synthesis now reflects the true pattern shape, and the aperture excitation can now be adjusted to achieve the desired array patterns.

The key to this entire effort is the design of the power divider network that distributes power to the radiating elements. The analysis and the measurements were based on a matched element. Or to put it another way, the energy coupled into an element

from adjacent elements must be absorbed so that it cannot reflect and reradiate. The power divides network uses directive couplers as the means of dividing the power. Thus each element is isolated within the power divider network and reflections or coupled energy is absorbed in the directive coupler loads. None will be reradiated nor will any reach the antenna input and appear as a high VSWR.

The array that was used to measure the effects of mutual coupling was also used to evaluate means of reducing these mutual effects. Various configurations were considered. The most promising were to place a metal divider between elements or to place parasitic strips between the elements. The latter was incorporated into this array.

2.1.5 Feed And Distribution Systems

This antenna system was required to operate, with no special tuning, anywhere in the ILS glide slope band. This represents a total operating bandwidth of 2%, relatively narrow in terms of broadband antennas, but difficult in this application due to the very critical pattern requirements. Several approaches were investigated, with the final choice being an equal line length (or constant time delay) system.

Manufacturing tolerances and frequency characteristics were investigated by perturbing the excitation and plotting radiation patterns. Tolerances of 4° of phase and 0.6 dB were found acceptable. Tests of several units showed that by using conventional microstrip construction, these tolerances could be held with Wilkinson hybrids and Schiffman phase shifters. As discussed in Section 2.1.4, the amplitude distribution is accomplished via directional couplers in order to surpress mutual coupling.

There is a separate equal line length corporate feed for the CSB and SBO. Schematics are given in Figure 2-12 for the

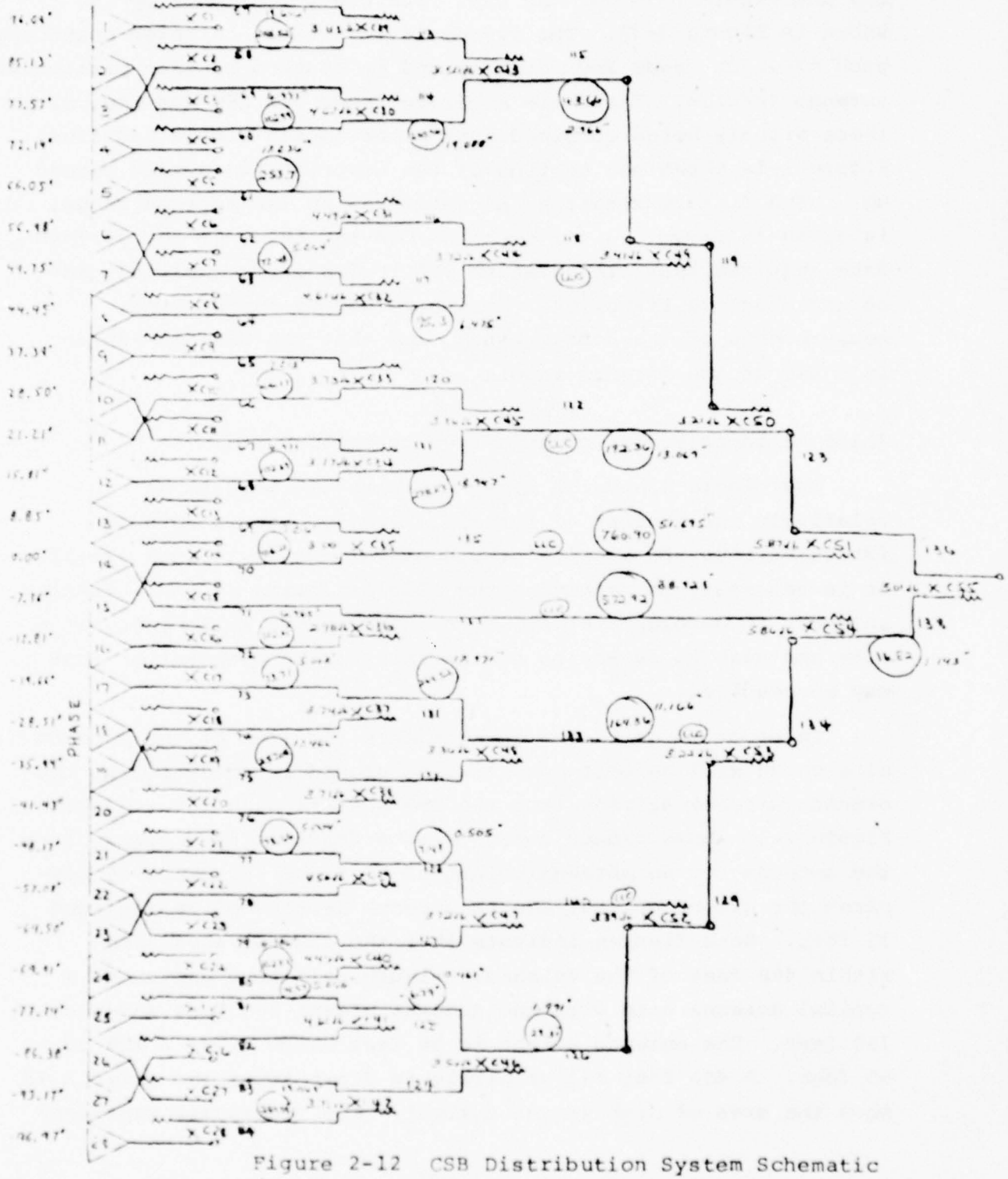

Figure 2-12 CSB Distribution System Schematic

CSB and Figure 2-13 for the SBO. The electrical hook up is shown in Figure 3-39. The system is fabricated in seven sections, each of which feeds four dipoles and is mounted on that particular antenna section. There are separate feeds for CSB and SBO, with these signals being combined just prior to the dipole radiator. Figure 2-14 shows one section of the distribution system opened up. The final excitation, as optimized on the antenna range, is given in Table 2-3 for both the CSB and SBO. Proper performance requires that the relative SBO to CSB input amplitude be adjusted on the transmitter as determined by flight check measurements of the course width, and that the CSB and SBO be in phase at the antenna input.

2.1.6 Antenna Performance As A Function Of Terrain

The Dipole Broadside Array has been designed to be relatively independent of terrain. However, severe ground irregularities and sloping ground can affect it to some extent. It is necessary to determine the allowed limits of these factors in order to develop a criteria for judging the suitability of a site and also to determine the extent of site preparation that may be required.

In order to gain some insight into the area of the antenna site which will be most sensitive to ground irregularities, the ground currents arising from the SBO pattern were investigated. Figure 2-15 shows ground currents as a function of distance from the antenna for an antenna height of 50 feet. Figure 2-16 compares the ground current due to antenna heights of 50 feet and 35 feet. Both figures indicate that the crucial area lies within 400 feet of the antenna. Figure 2-17 is a sketch of a typical antenna site with the antenna offset 500 feet and backset 100 feet. The antenna height is 50 feet which gives a TCH of 55 feet. A 400 foot radius circle is drawn about the antenna to show the area of high ground current. The rectangles represent

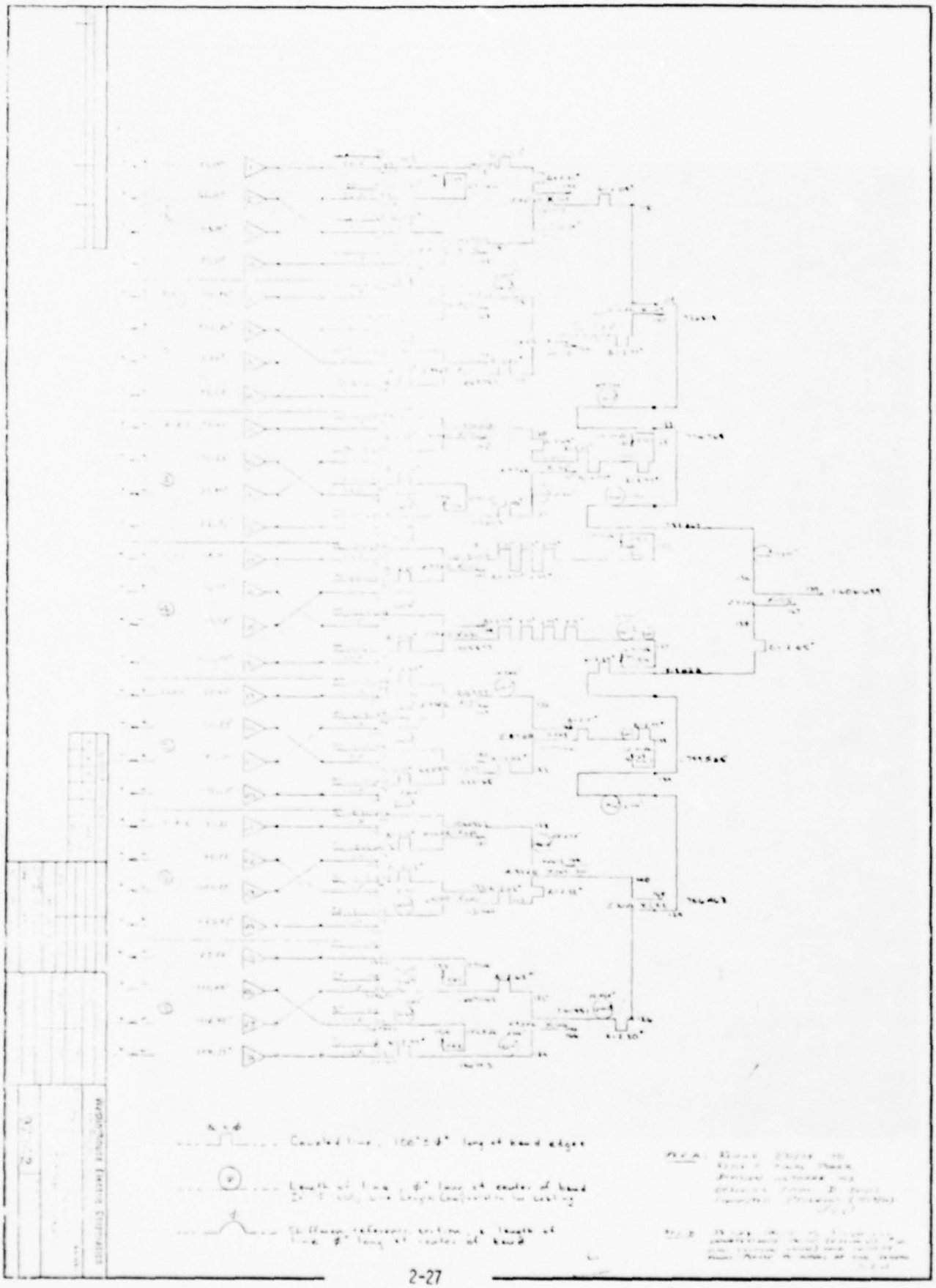

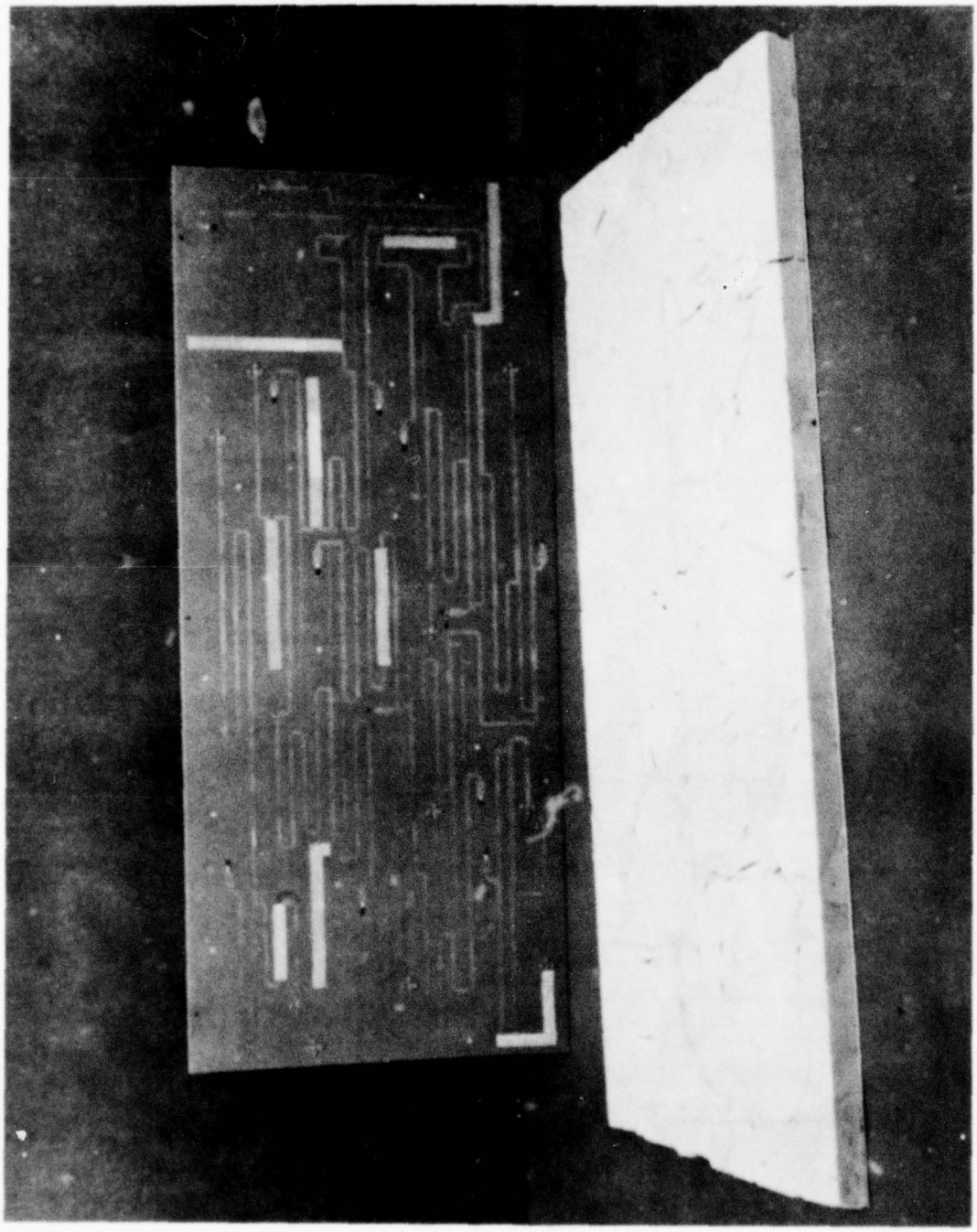

Figure 2-14 Distribution Panel For One Antenna Section

Δ (SBO)			Σ (CSB)	
AMPLITUDE (dB)	PHASE	NO.	AMPLITUDE (dB)	PHASE
- 15.48	+ 10.47°	1	- 27.93	+ 108.31°
- 11.48	+ 46.71°	2	- 28.37	- 81.33°
- 32.76	+ 73.73°	3	- 26.89	- 92.05°
- 20.73	- 38.29°	4	- 24.98	- 94.63°
- 22.60	- 2.43°	5	- 23.93	- 102.25°
- 30.27	-155.25°	6	- 22.56	+ 69.60°
- 27.99	-107.96°	7	- 21.17	- 119.04°
- 27.79	- 26.18°	8	- 19.85	- 120.53°
- 29.15	- 44.93°	9	- 19.21	- 129.67°
- 42.10	-166.64°	10	- 18.31	+ 36.17°
- 31.13	- 82.09°	11	- 17.91	- 143.70°
- 33.95	+ 81.67°	12	- 17.25	+ 26.93°
- 31.03	- 45.00°	13	- 16.55	- 153.18°
- 38.98	+ 52.24°	14	- 16.41	+ 8.68°
- 42.91	- 82.97°	15	- 16.45	- 172.23°
- 32.29	-141.01°	16	- 16.25	+ 177.45°
- 34.49	+ 96.72°	17	- 17.21	- 2.79°
- 33.00	+ 86.39°	18	- 17.61	- 7.32°
- 37.71	- 22.03°	19	- 18.46	- 9.85°
- 30.86	-155.02°	20	- 18.95	+ 157.18°
- 27.41	-159.44	21	- 19.75	+ 154.20°
- 29.19	- 65.89°	22	- 21.13	+ 143.05°
- 30.43	+133.11°	23	- 22.53	+ 134.84°
- 23.19	- 11.18°	24	- 23.66	- 50.17°
- 21.69	-138.91°	25	- 25.22	+ 123.49°
- 27.28	+ 57.35°	26	- 27.17	+ 115.42°
- 12.82	+125.44°	27	- 28.26	+ 110.50°
- 15.77	- 15.27°	28	- 28.26	+ 103.86°

TABLE 2-3

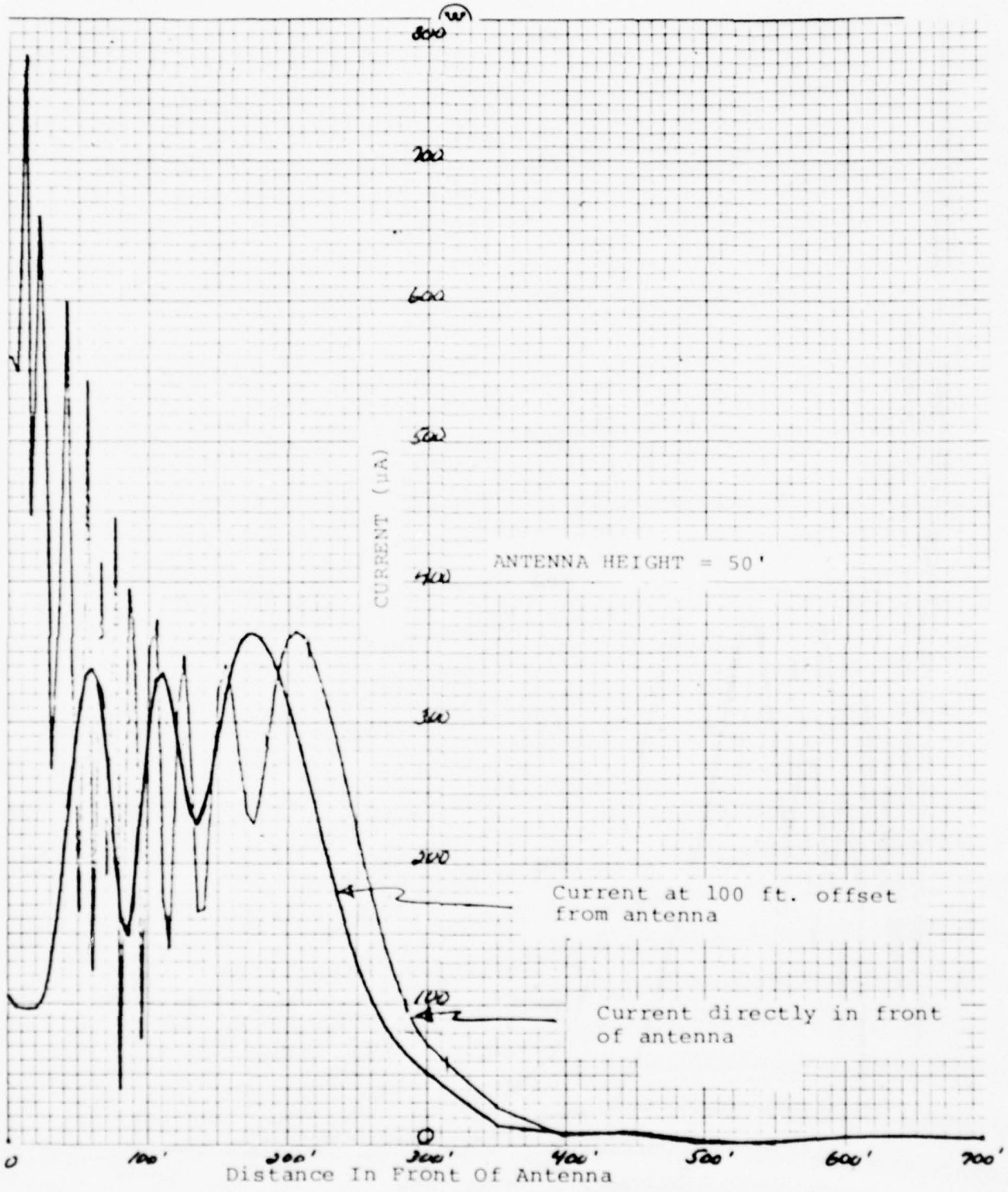

Figure 2-15 SBO Ground Currents

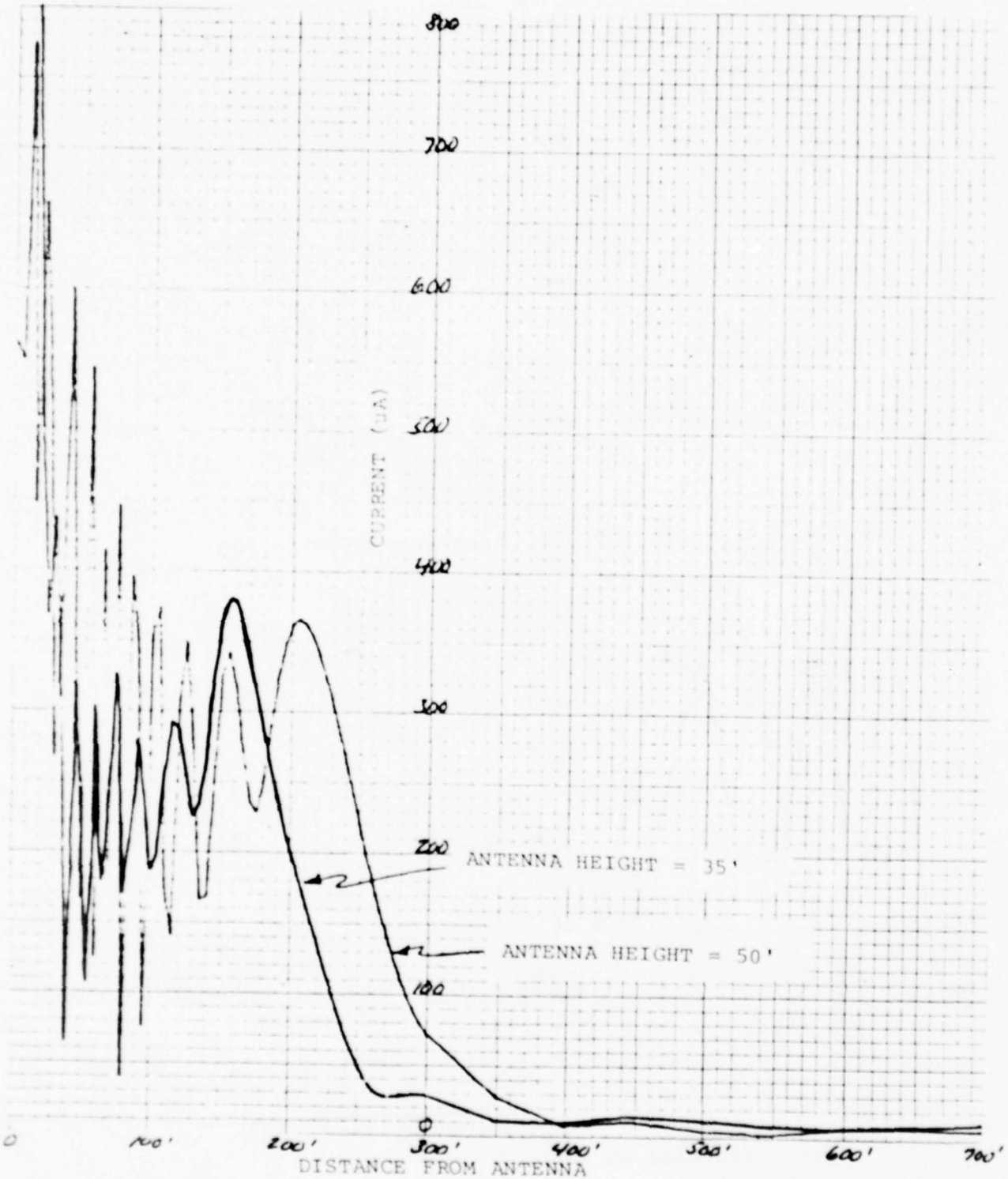

Figure 2-16 SBO Ground Currents

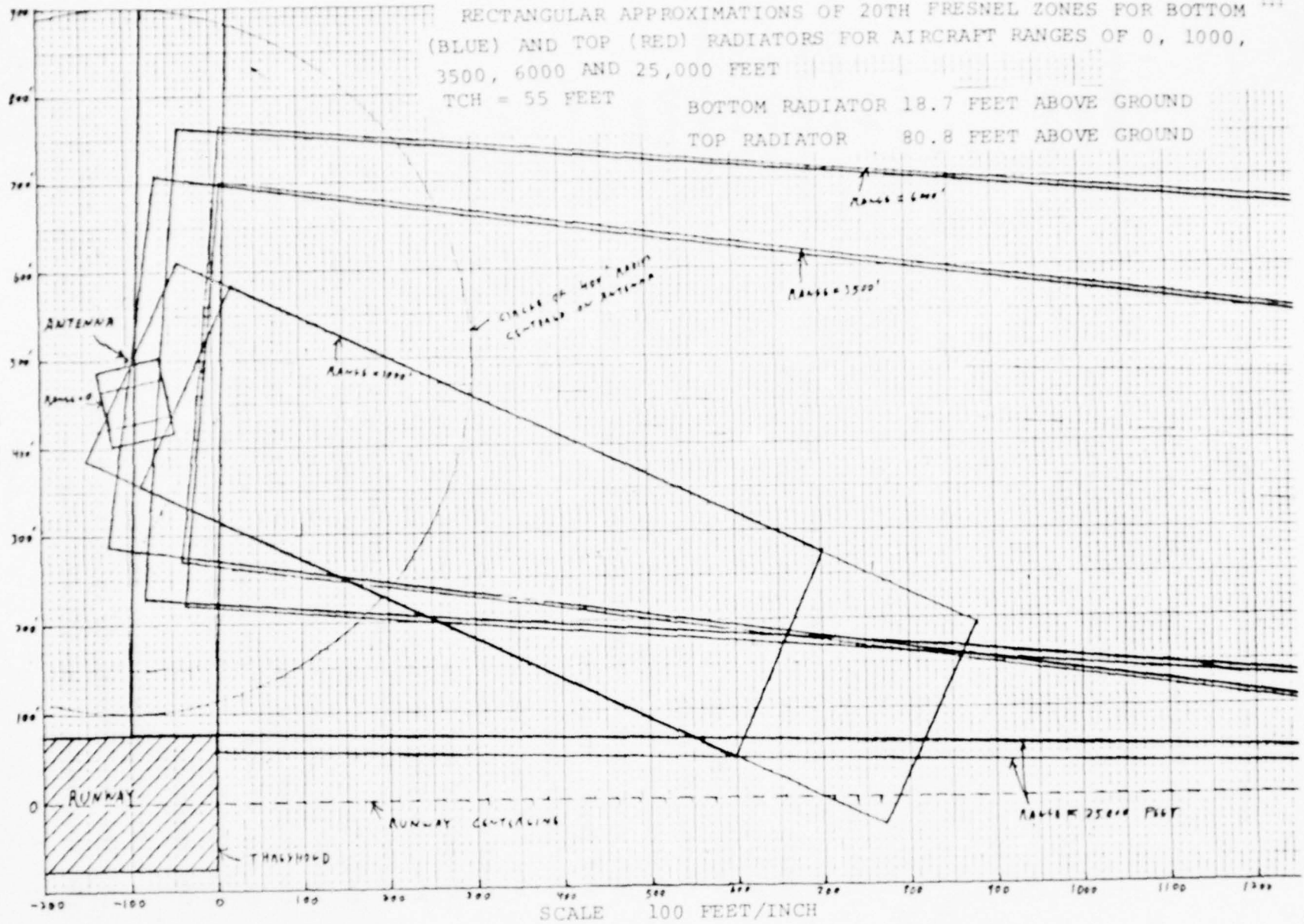

Figure 2-17 Locations Of the 20th Fresnel Zone For Various Aircraft Ranges

the 20th Fresnel Zones for five ranges.

It has been established that ground irregularities outside the 20th Fresnel Zone for a given range will have virtually no effect on the DDM at that range. This figure and the ground current information should help predict the behavior of specifically located ground irregularities.

A 30 foot square void or hole was the first surface irregularity to be investigated. Figure 2-18 shows three fly-ins with the effect of a void located 100 feet, 200 feet and 300 feet in front of the antenna. This Figure compares favorably with the ground current information which indicates that current falls off between 200 and 300 feet and has reached a minimum at distances greater than 400 feet. The DDM in Figure 2-18 for the void at 300 feet is still very good which indicates the importance of the low side lobes in reducing ground currents and thereby minimizing the effects of unwanted reflections. The DDM due to the void at 200 feet is greater than the DDM due to the void at 100 feet. This makes sense if one examines the ground current in Figure 2-15 which shows that the ground currents near 200 feet are greater than those at 100 feet. On all these curves in Figure 2-18, the voids have very little effect on DDM near threshold and this is because the voids lie outside the 20th Fresnel Zones when the aircraft is close to threshold. The curves in Figure 2-18 are perturbations about the fly-in due only to direct radiation. No image radiation was included in order to isolate the effect of the voids. Figure 2-19 shows the direct only fly-in and the direct and image fly-in. The direct fly-in is practically zero microamps at all points so the DDM in Figure 2-18 is due almost entirely to the presence of the voids.

It is necessary to determine the effect of rough ground on antenna performance to establish a criteria for the severity of the roughness. The allowed roughness will depend on position.

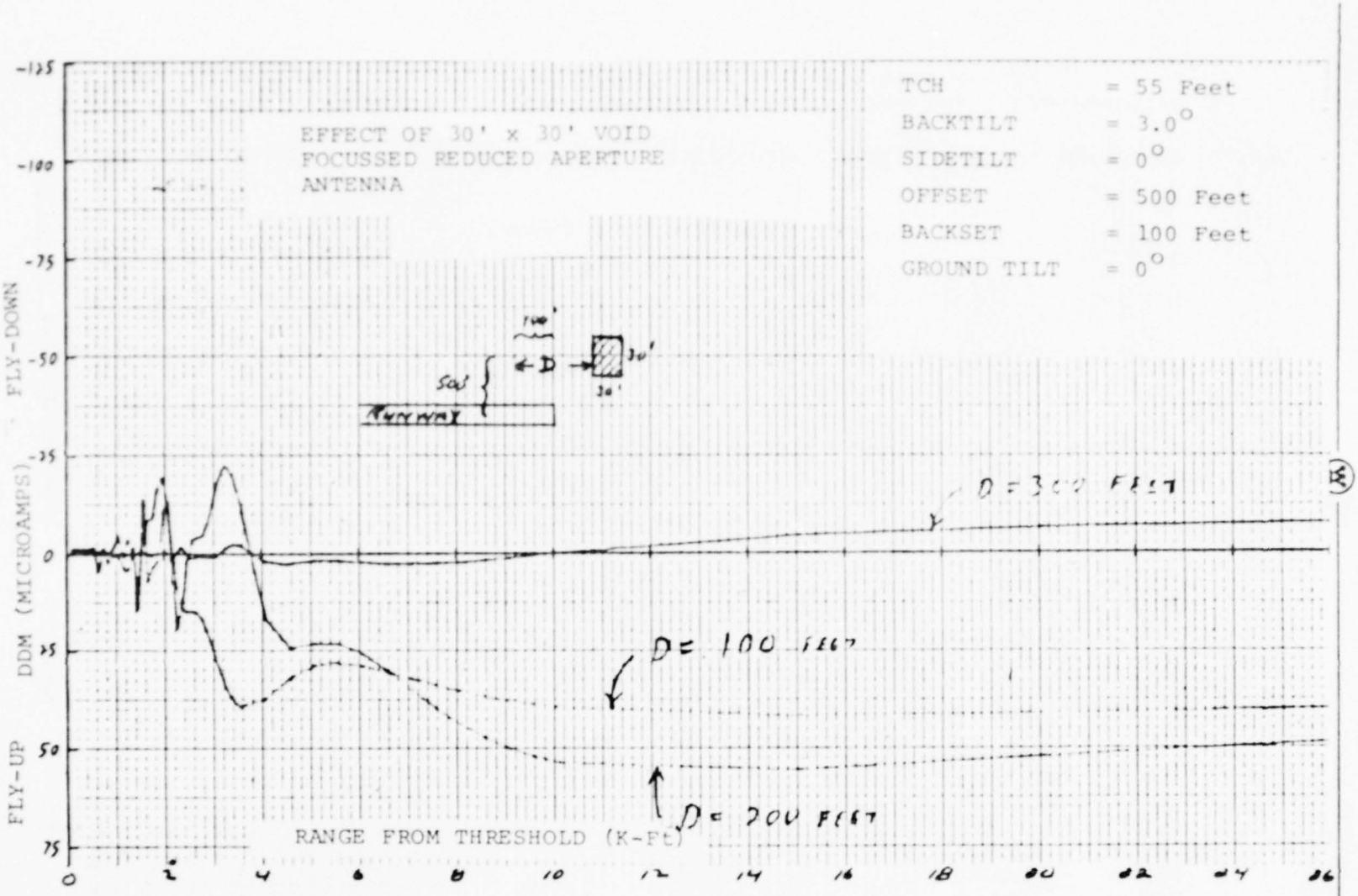

Figure 2-18 Effect Of A 30' x 30' Void At Various Locations

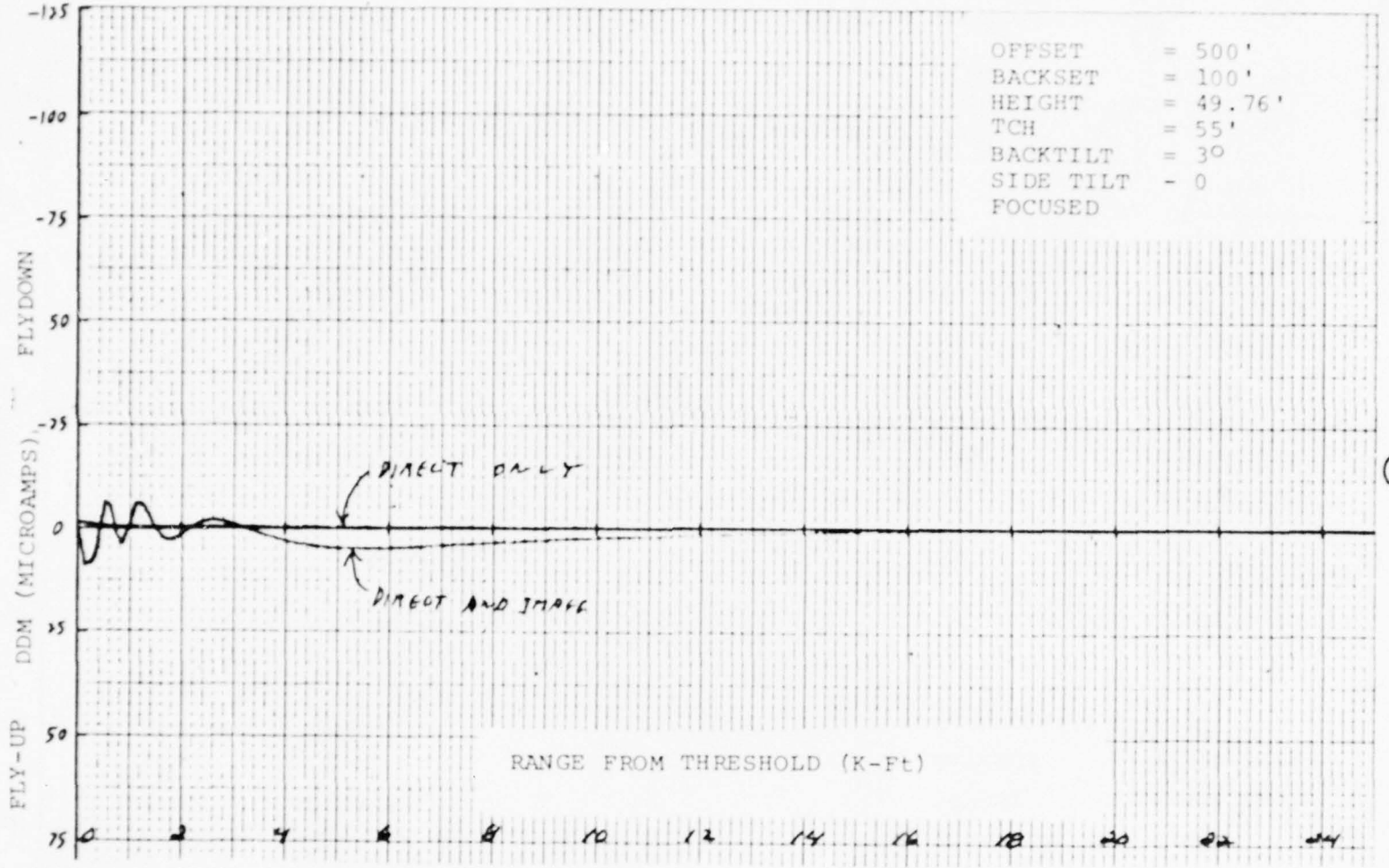

Figure 2-19 The Effect Of Including The Image Contribution For Fly-In Over Infinite Flat Ground

In other words, ground irregularities in certain areas will deteriorate antenna performance more than the same ground irregularities in another area. It is obvious that the ground underneath the antenna will have to be smoother than the ground one-thousand feet from the antenna. The problem is to find the allowable degree of roughness for various sections of ground. The rough ground can be modeled by assuming that the terrain is made up of small rectangular plates whose height above or depth below the zero ground level approximates the rough ground. Figure 2-20 shows how this would be done for a typical cross-section of ground. The size of the plates has been chosen to be five feet square. The degree of ground roughness can be defined by assigning a limit to the deviations of height and depth from zero. These deviations from zero are assumed to occur according to a normal or Gaussian distribution with 95% of the deviations lying between the limits. This is also illustrated in Figure 2-20.

The assignment of a particular deviation to a specific plate is done randomly. Ideally, the entire ground can be modeled in this fashion and limits of ground deviations established by running fly-ins for various ground deviation limits and making certain the fly-ins meet Category II specifications. However, astronomical computer times are accumulated in modeling such large areas close to the antenna. In the past, fly-in curves have been calculated using 53 data points. If a 200 foot by 200 foot section of ground were broken up into 1600 five foot square plates, the approximate computer time would be about 12800 seconds. Also, several of these runs would be necessary to give the required information on ground sensitivity. By using only six points, the cost could be reduced by about 90% per run. Another possible reduction in time could be realized by using an approximation to the calculation on the radiation reflected from the plates. This approximation would be valid if the plates were at large

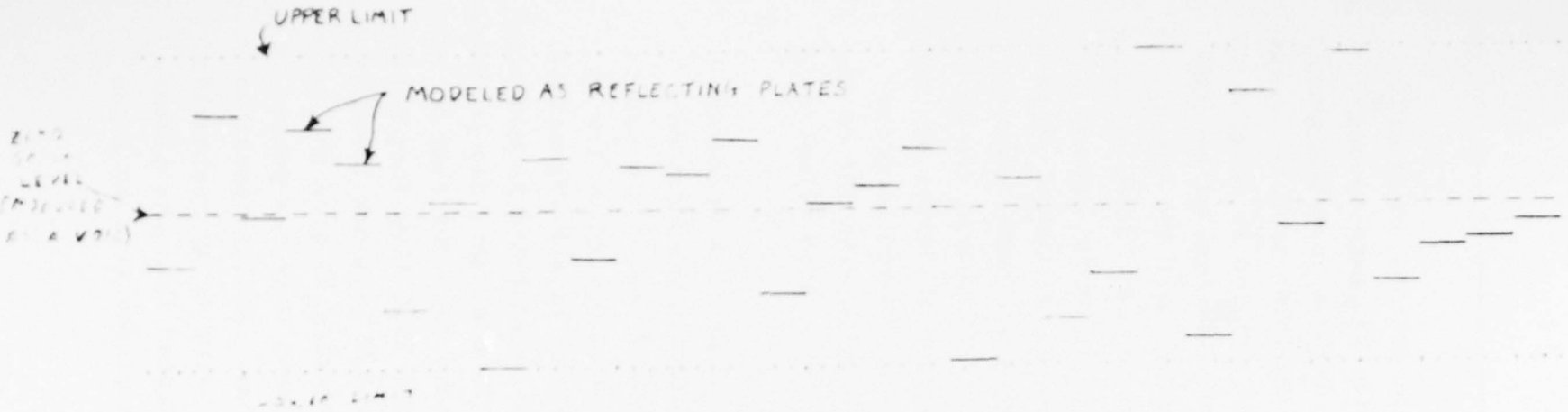

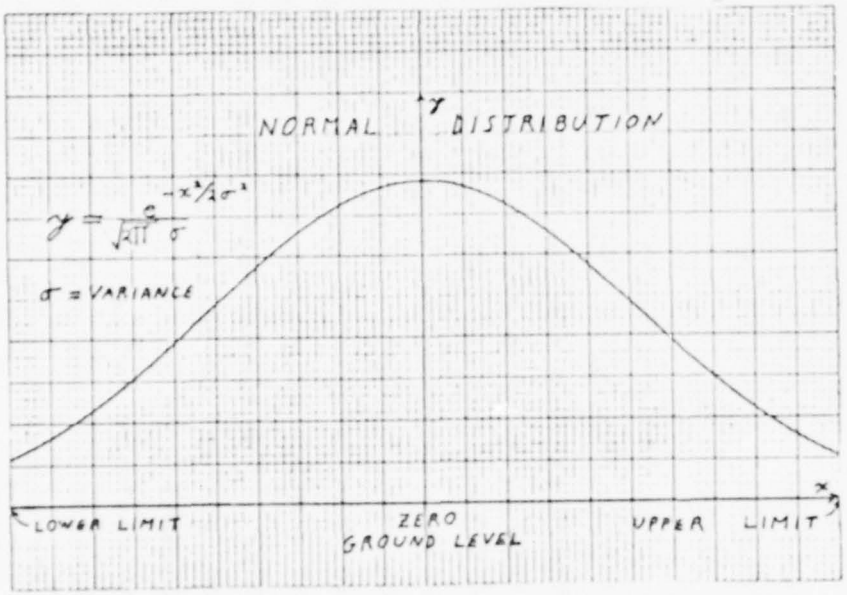

95% OF PLATE LEVELS LIE BETWEEN THE UPPER LIMIT AND THE LOWER LIMIT

Figure 2-20 Cross Section Of Rough Ground Approximation

distances from the antenna. This approximation turned out to be very complicated and it did not work.

Since modeling of the entire area around the antenna is unfeasible, the areas which are the most sensitive to ground roughness should be determined. The area of large ground currents has previously been established to lie within a radius of 200 feet of the antenna. This current drops off to a minimum at a radius of 300 feet.

The aircraft position and the radiator position define a geometric reflection point on the ground. This is the point where a line from the aircraft to the image radiator intersects the ground plane. Figure 2-21 shows the angular variation in two planes of the energy reflected from a square plate. Since this plate is located 10,000 feet from the antenna the path of the maximum reflected energy makes a small angle with the plate. This is evident in Figure 2-21. Ten degrees above this point the energy drops above 20 dB. Also, as the receiver is moved out of the y - z plane the energy is again reduced. This means that the maximum effect of a square plate is localized to a region of space defined at a small solid angle. Also, if the receiver is not at the point of maximum reflected energy, then it is in a region of space where the reflected energy varies rapidly with small changes in angular position with respect to the plate. One must be careful to sample the energy at ground points over a small enough solid angle to ensure that at least one of the measured points is reasonably close to a peak in the reflected pattern. This is to make sure the maximum effect of the plate is calculated so that worst case conditions can be investigated.

If the antenna pattern were constant the most sensitive ground would be the area above the geometrical reflection points. However, it is not constant so some method of probing the ground would be helpful in establishing the location of the

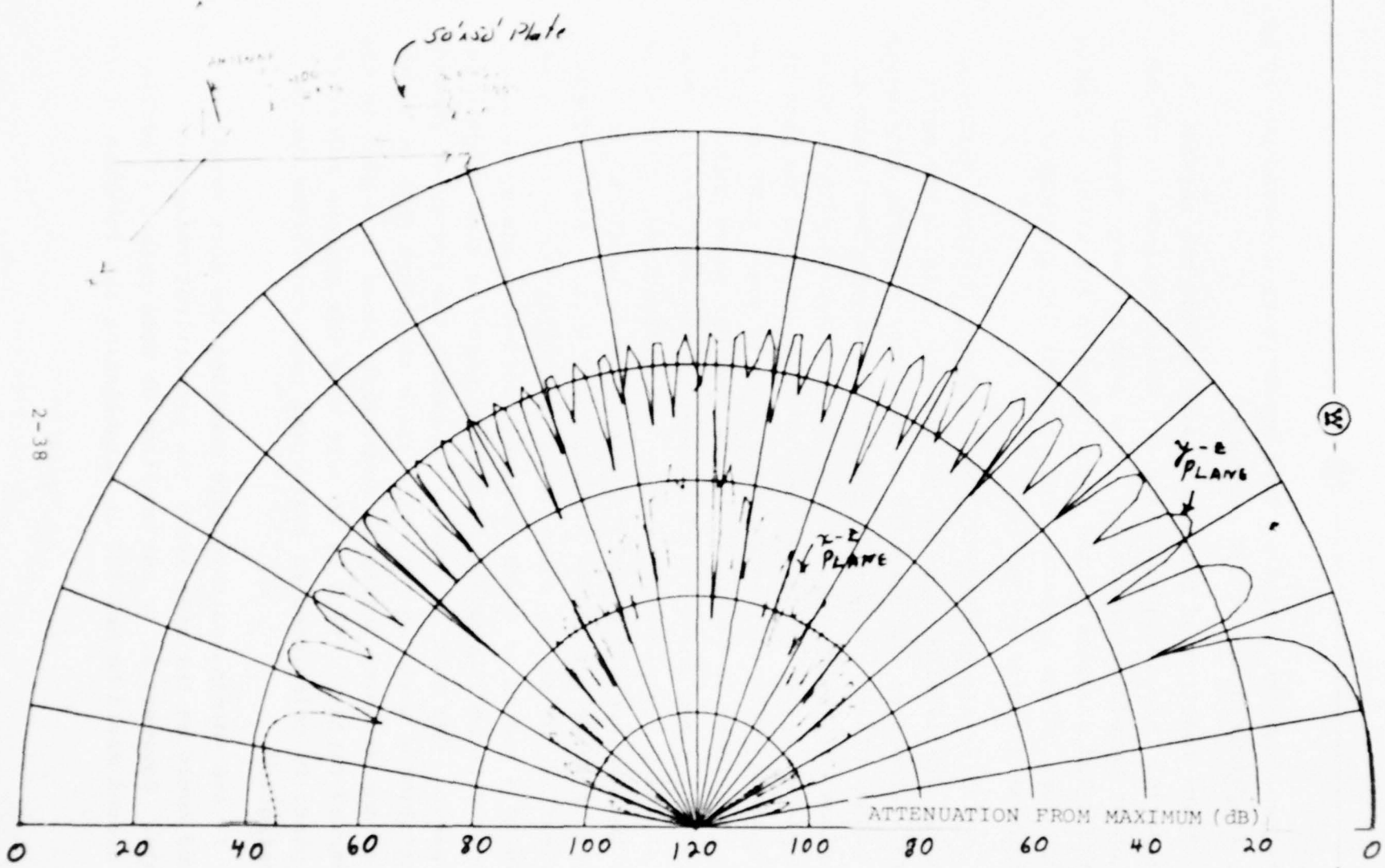

Figure 2-21 Reflected Radiation From Plate At A 500' Radius About The Plate Center

most sensitive ground. Figure 2-22 shows the location of ten 30' x 30' voids whose effect on the infinite flat plane fly-in were individually calculated. The results are shown on Figure 2-23 superimposed on a blowup of the infinite flat plane fly-in. The data was taken for six range points: 0, 1,000, 2,000, 3,500 and 2,500 feet. The only probe points which had any noticeable effect were numbers 5 and 7. Void 5 is in the reflection point region (shaded area) and it also lies along a line from the antenna to the 2,000 foot range point. So the maximum effect of that void is felt at the 2,000 foot range point and it is only above one micro-amp. This indicates that low ground current areas have little effect even if they lie in the reflection point area. Void 7 also lies in the reflection point area but it is only 220 feet from the antenna. This places it in a fairly high ground current area and Void 7 will have its largest effect at the 1,000 foot range. In this case, there is a significant change in DDM so areas of high ground current are sensitive whether or not they also lie in the reflection point area. Void 5 has virtually no effect at the 1,000 foot range and very little effect at the 2,000 foot range. This indicates the localization of the effect of a void and will permit the effect of a small area to be extrapolated to the effect of a large area, although the computer cost may be prohibitive.

It has been established that the effect of the reflected energy from a square plate is localized in a region of space defined by a small solid angle. The size of this region can be estimated by comparing Figure 2-18 and Figure 2-24. The curves in Figure 2-18 are the fly-ins obtained with 30' x 30' voids placed 100 feet, 200 feet and 300 feet directly in front of the antenna. The effect of these plates has diminished almost entirely by the time the aircraft has reached the 2000 feet range point. Figure 2-24 shows the angle swept by the line from the plate to the aircraft as the aircraft approaches threshold.

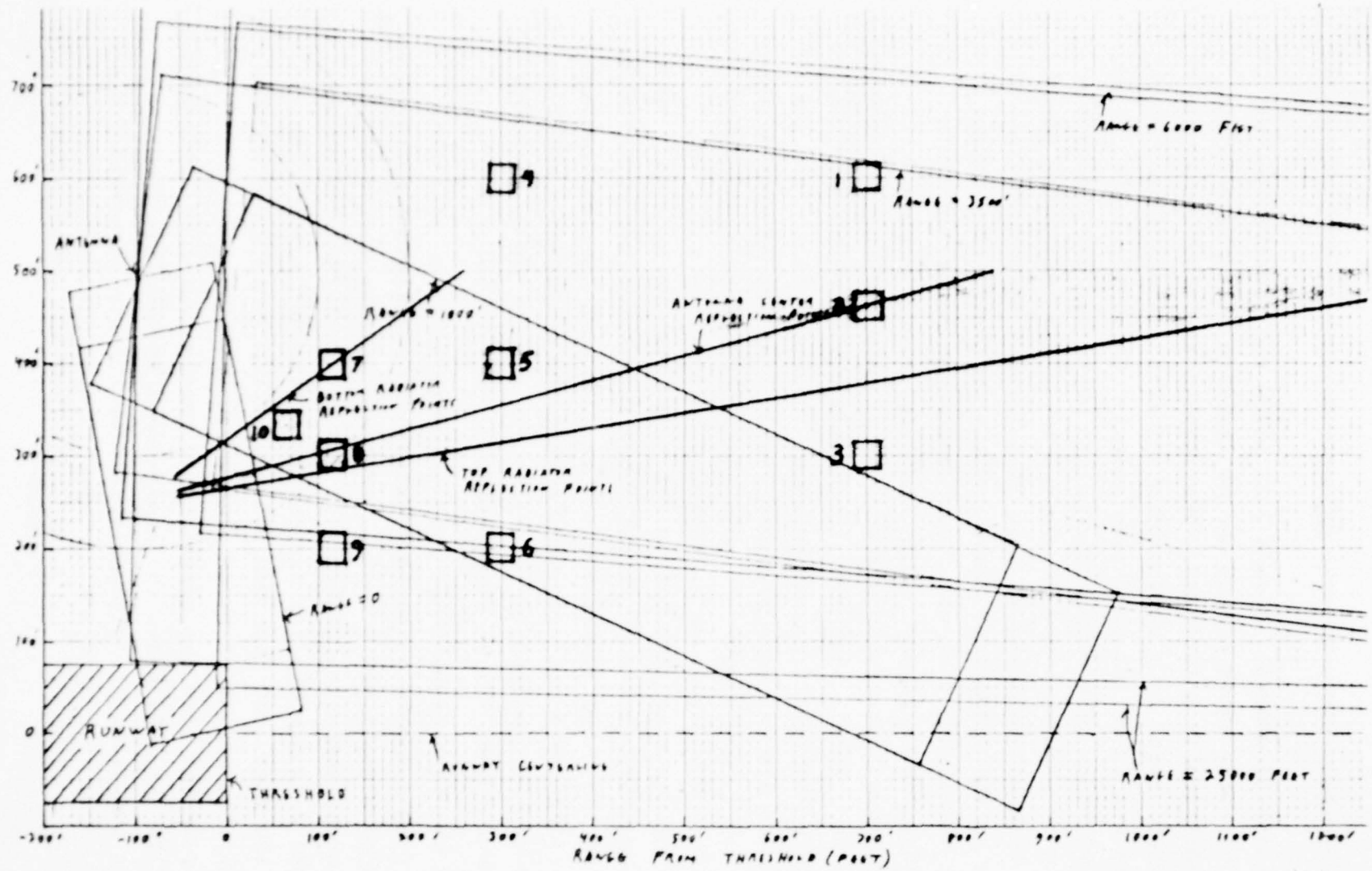

Figure 2-22 Rectangular Approximations For The 20th Fresnel Zones For Various Ranges - Location Of Ten Test Voids

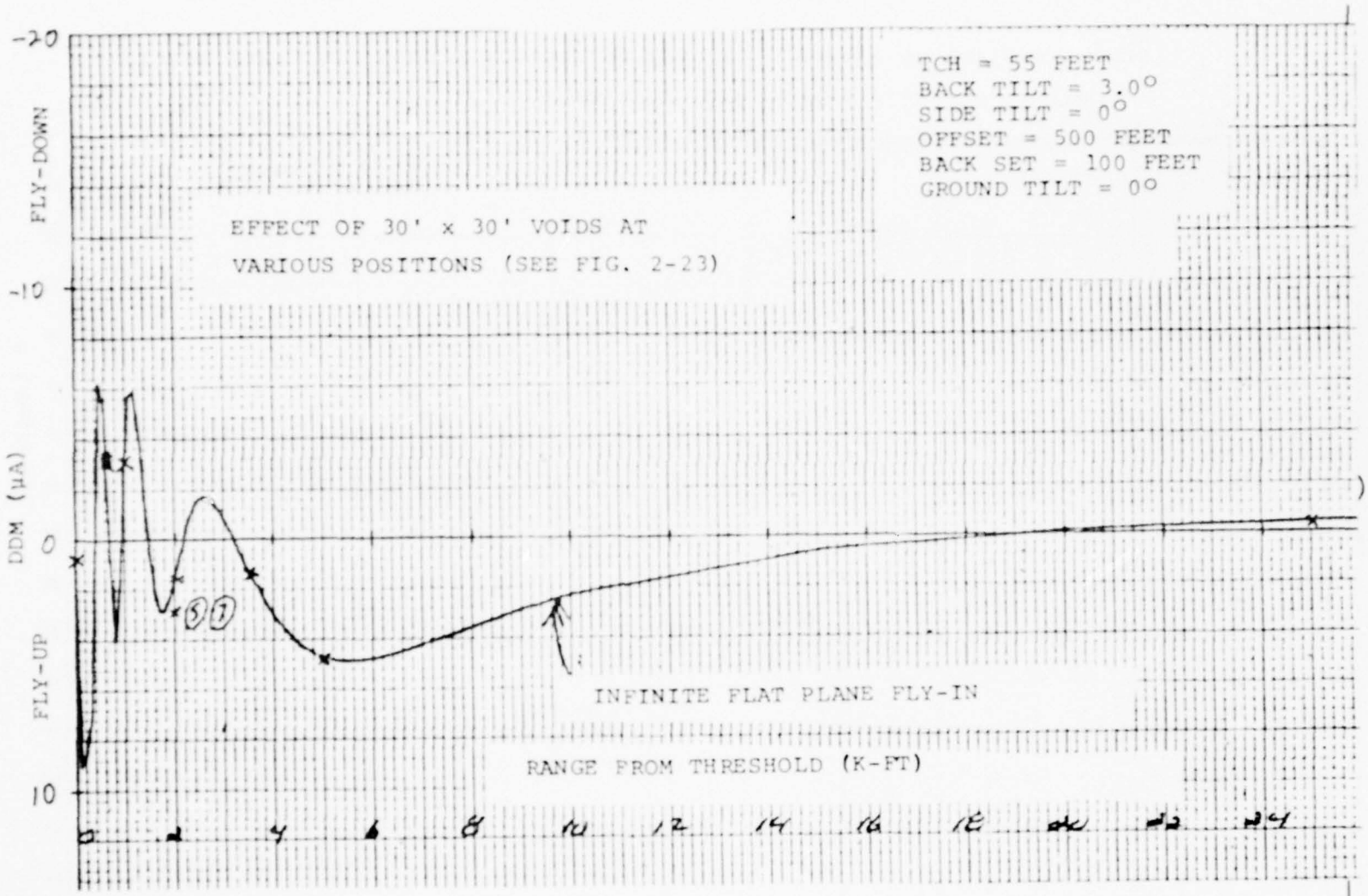

Figure 2-23 The Effect Of Ten 30' x 30' Voids Superinposed On An Expanded Scale Of An Infinite Ground Fly-In

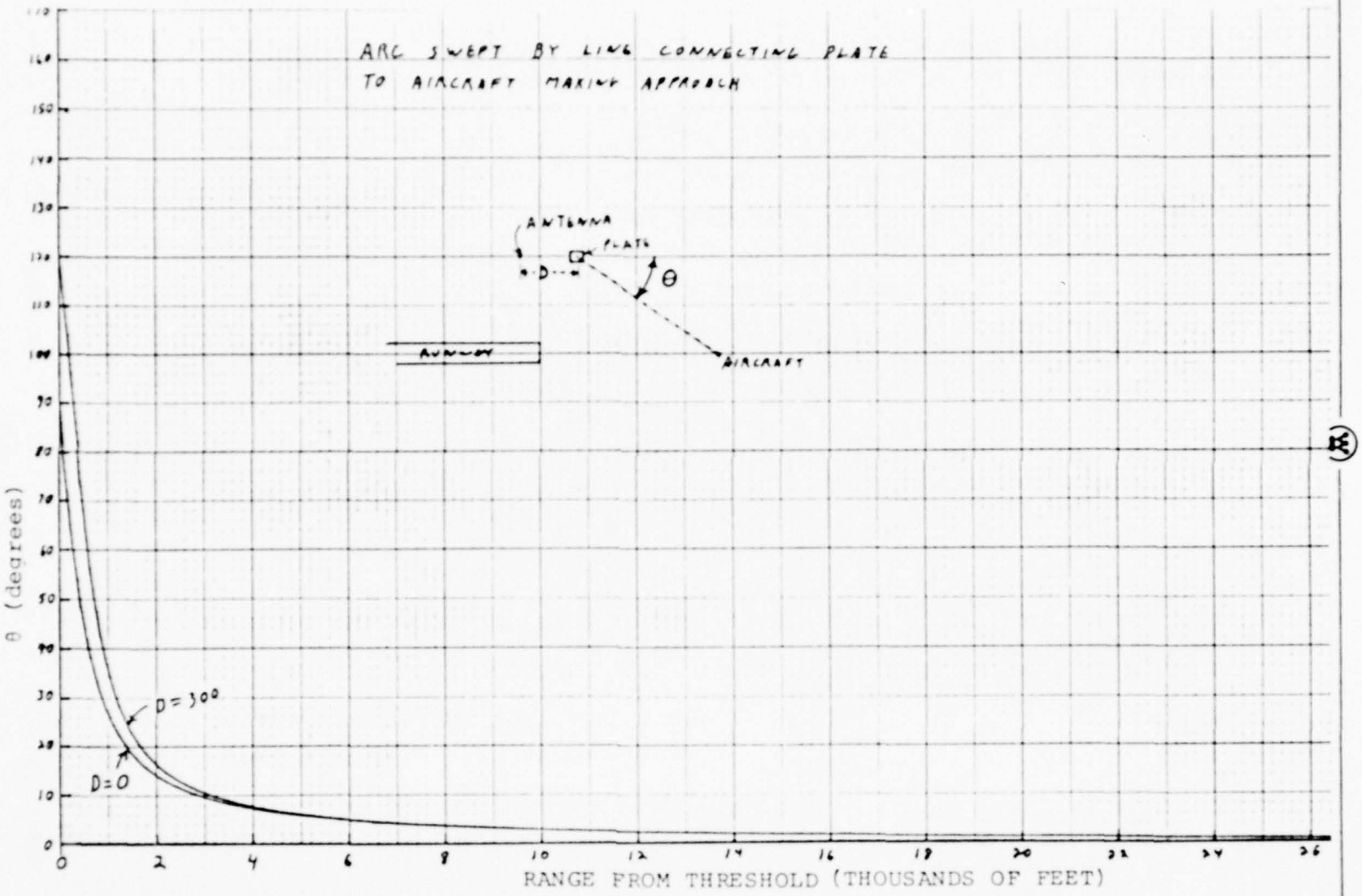

Figure 2-24 Angle From Scattering Void To Aircraft At Various Ranges

When the aircraft is 2000 feet from the threshold it has swept through an angle of about 15 degrees. Figure 2-25 shows the variation in the X-Y plane of the energy reflected from a plate that is located directly in front of the antenna. A sweep of 15 degrees from the Y-axis corresponds to about a 30 dB reduction of reflected power. This means that the major effect of a specific plate on a fly-in will occur over an interval of range values determined by this $\pm$ 15° arc. This can be seen in Figure 2-26. The size of this interval depends upon the position of the modeled area. Areas directly in front of the antenna will have the greatest cumulative effect upon the fly-in since the affected fly-in interval will extend to infinity. Areas between the approach path and the antenna will affect smaller intervals of the fly-in.

At some sites, sloping ground over a large area may be encountered. Both upslopes and downslopes were investigated and Figure 2-27 illustrates the meaning of these terms. Figures 2-28 and 2-29 show the effect of various upslopes. An upper limit for Category II performance would be about 1.5°. Figures 2-30 and 2-31 show the effect of various downslopes. An upper limit for Category II performance would be between 2° and 3°. The antenna is more sensitive to upslope than downslope because as the upslope increases, the ground at large ranges becomes illuminated by the main lobe. However, as the downslope increases, the DDM will not deteriorate until the high side lobes begin to be reflected into the path of the aircraft. As downslope increases, derogation of the DDM should occur first at short range. This is borne out by the 3° downshope curve in Figure 2-31. It should be mentioned that the sloping ground as modeled begins at the antenna position and as such would represent a worst case. Much greater ground tilts could be tolerated if the sloping ground occurred past 300 or 400 feet from the antenna site.

For many problem sites, the primary terrain feature is an

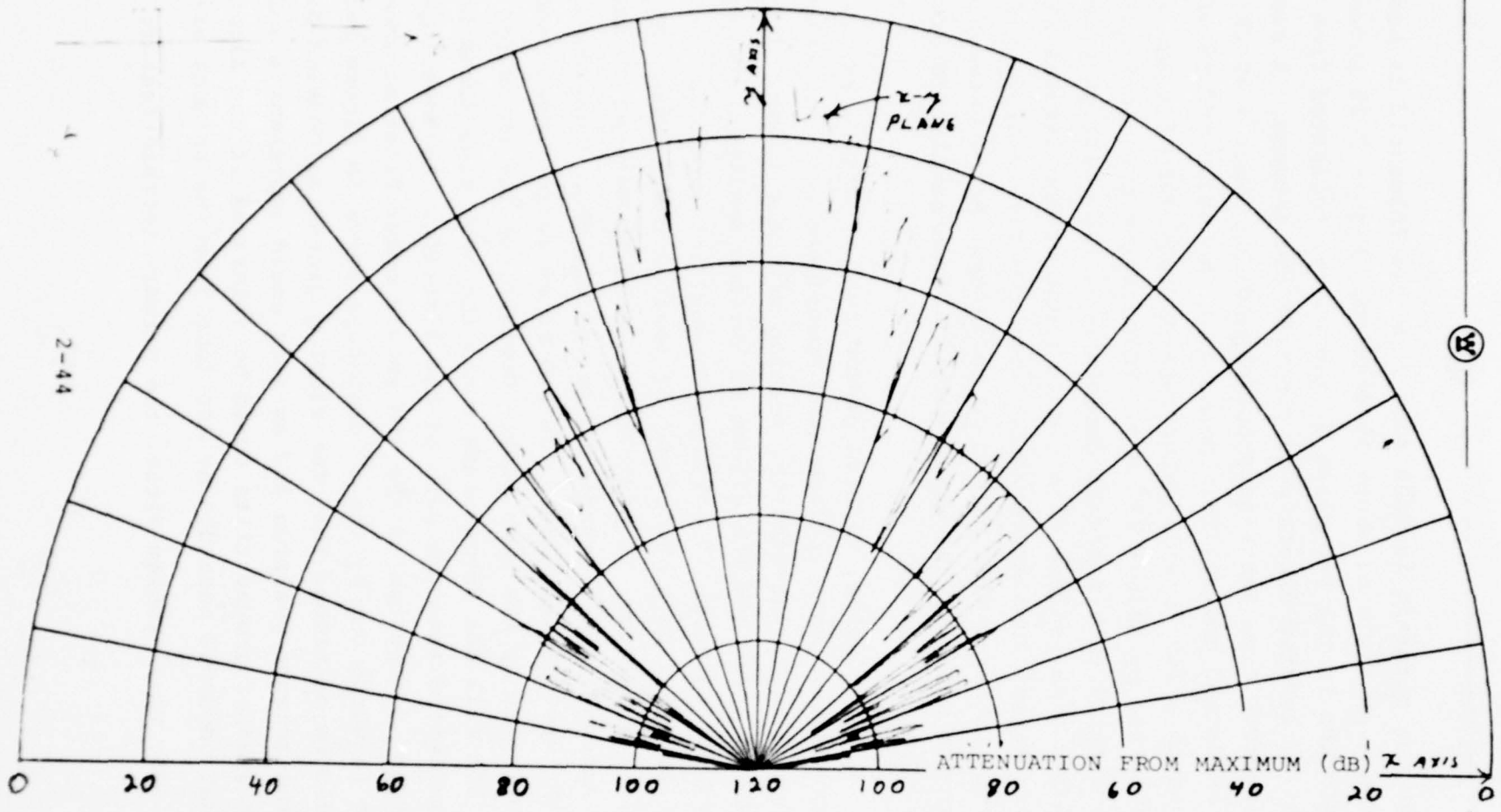

Figure 2-25 Energy Scattered By A Plate Directly In Front Of The Antenna

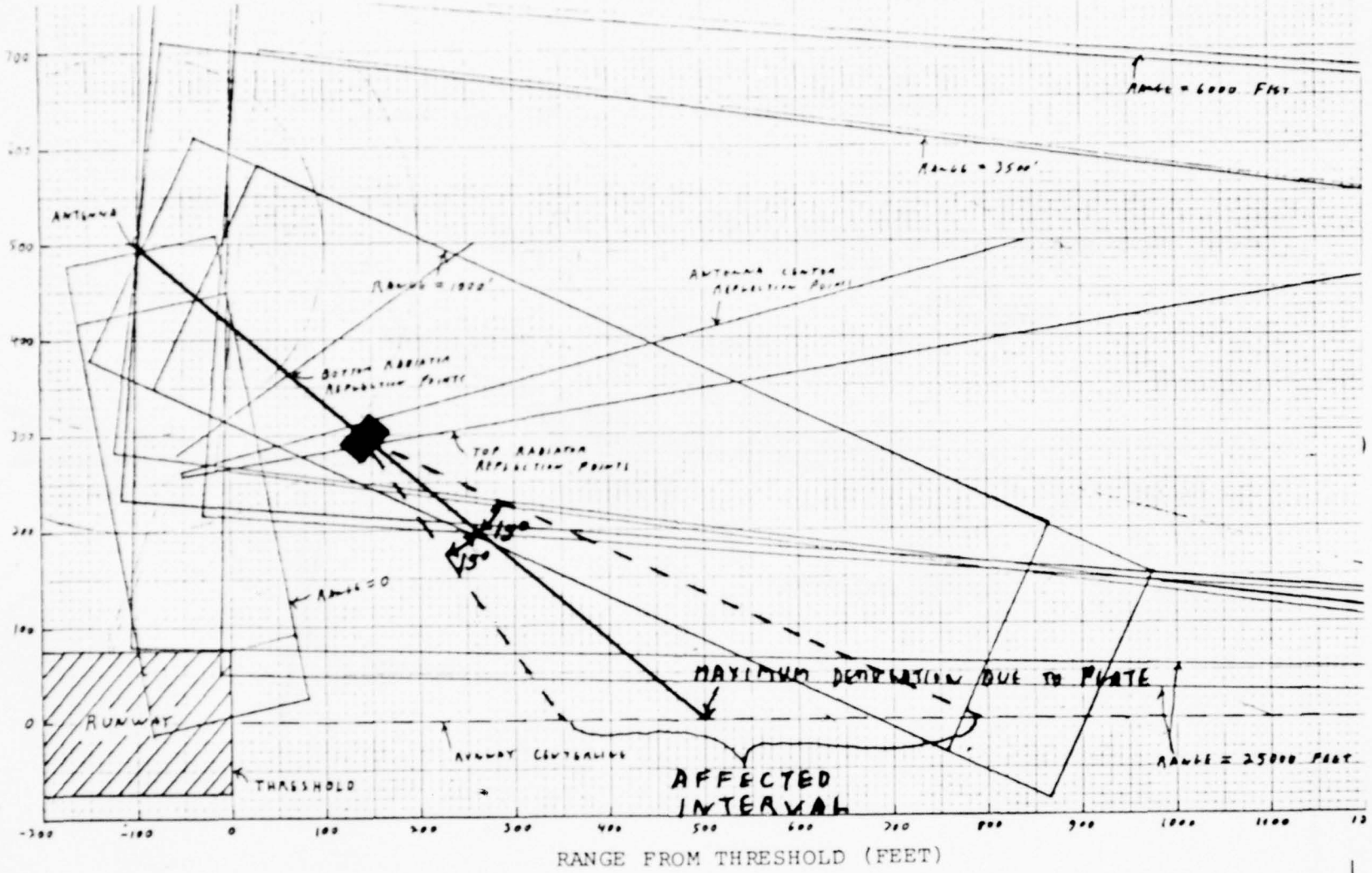

Figure 2-26 Area Of Greatest Effect Due To Scattering From A Plate

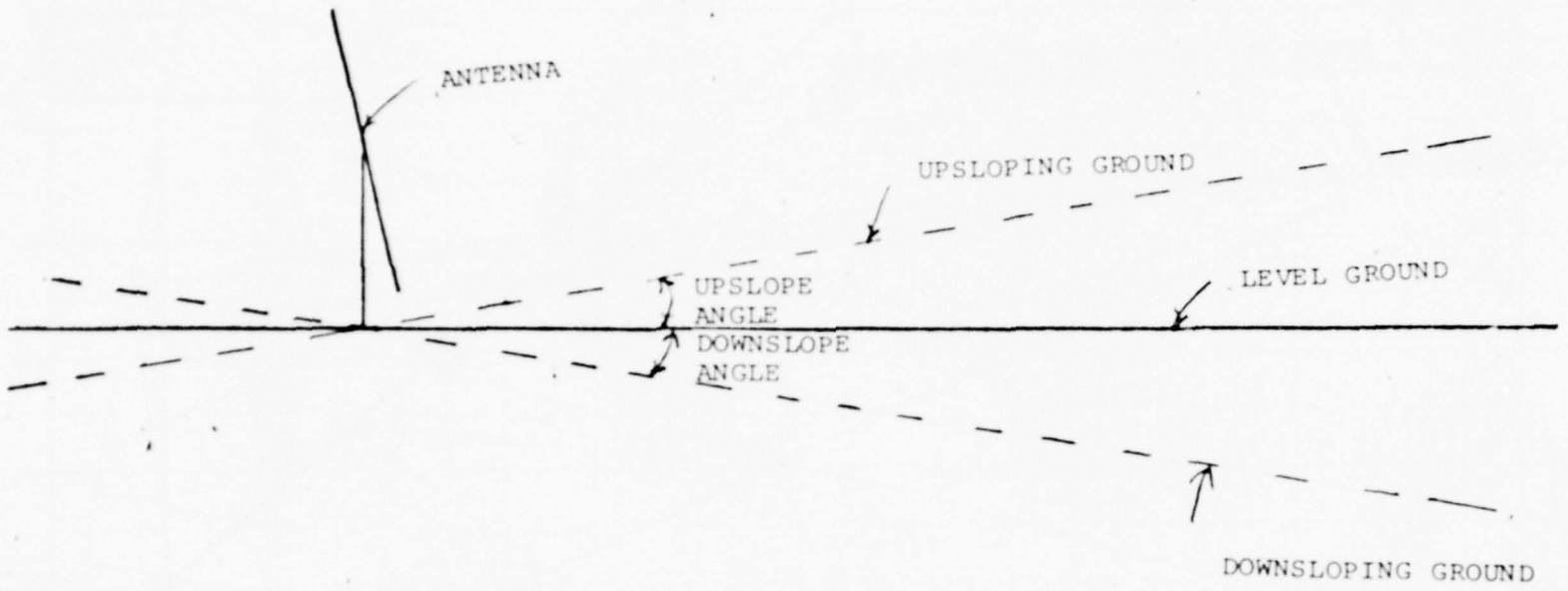

Figure 2-27 Definition Of Sloping Ground

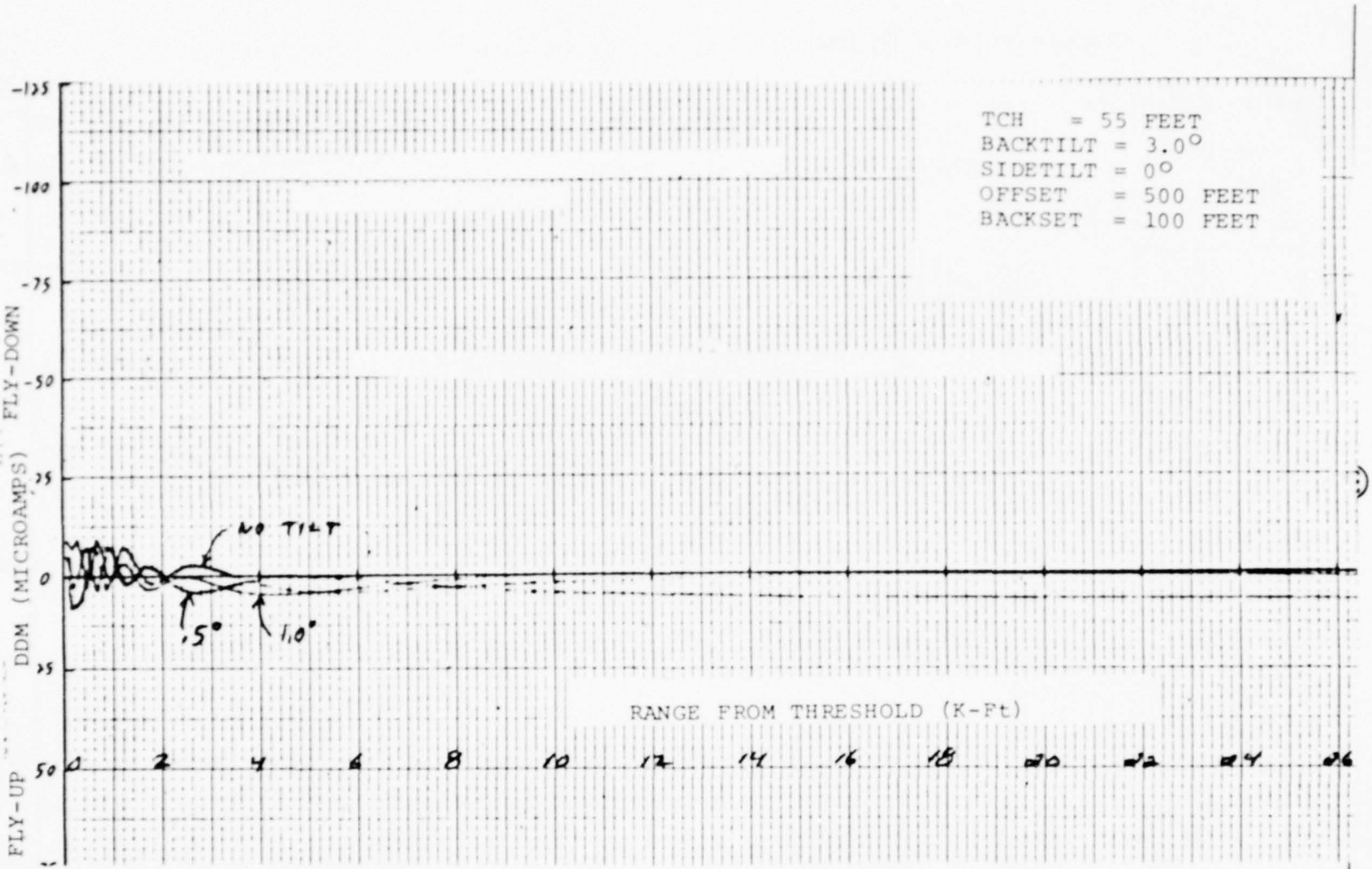

Figure 2-28 The Effect On Fly-In For Various Up Sloping Grounds

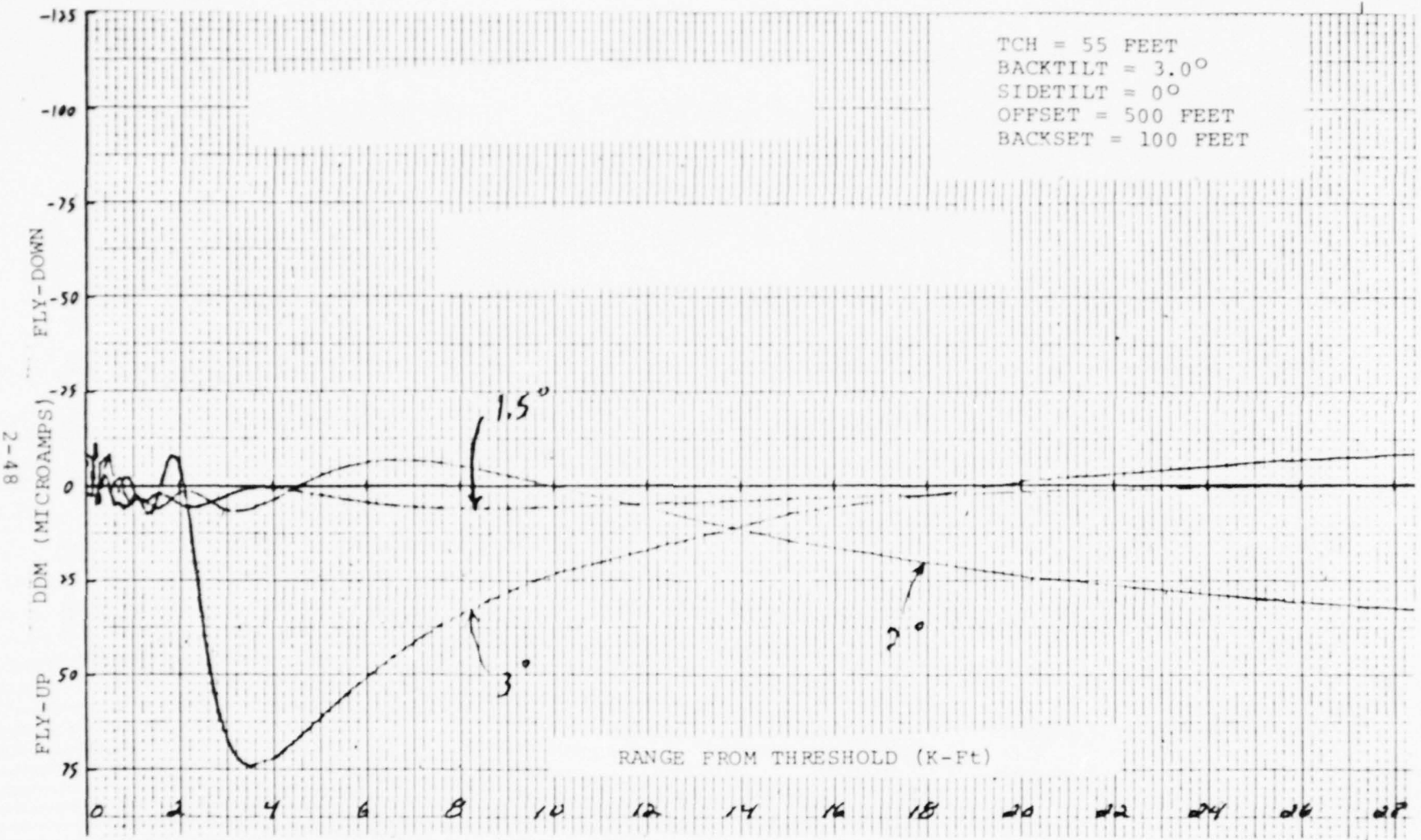

Figure 2-29 The Effect On Fly-In For Various Up Sloping Grounds

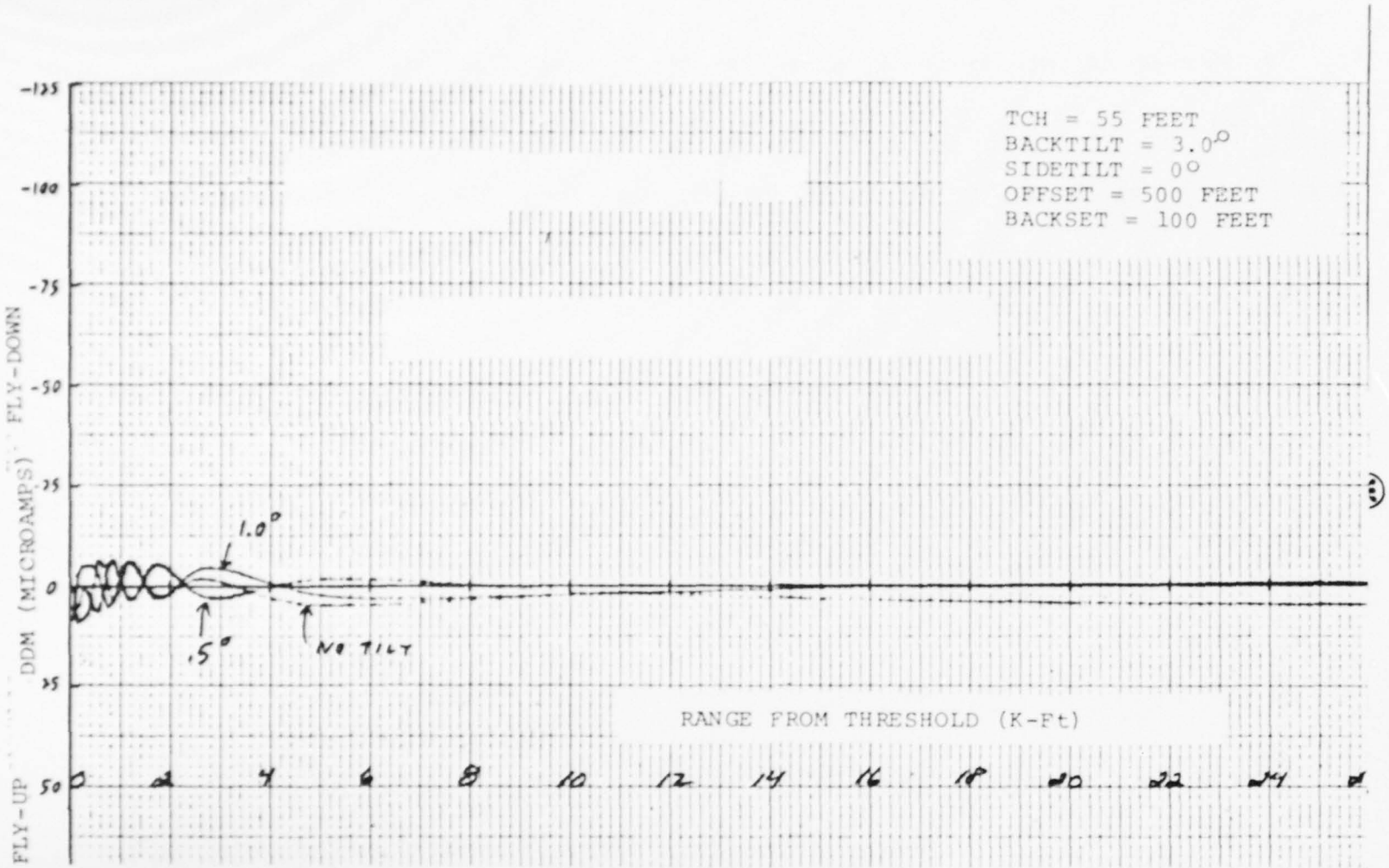

Figure 2-30 The Effect On Fly-In For Various Down Sloping Grounds

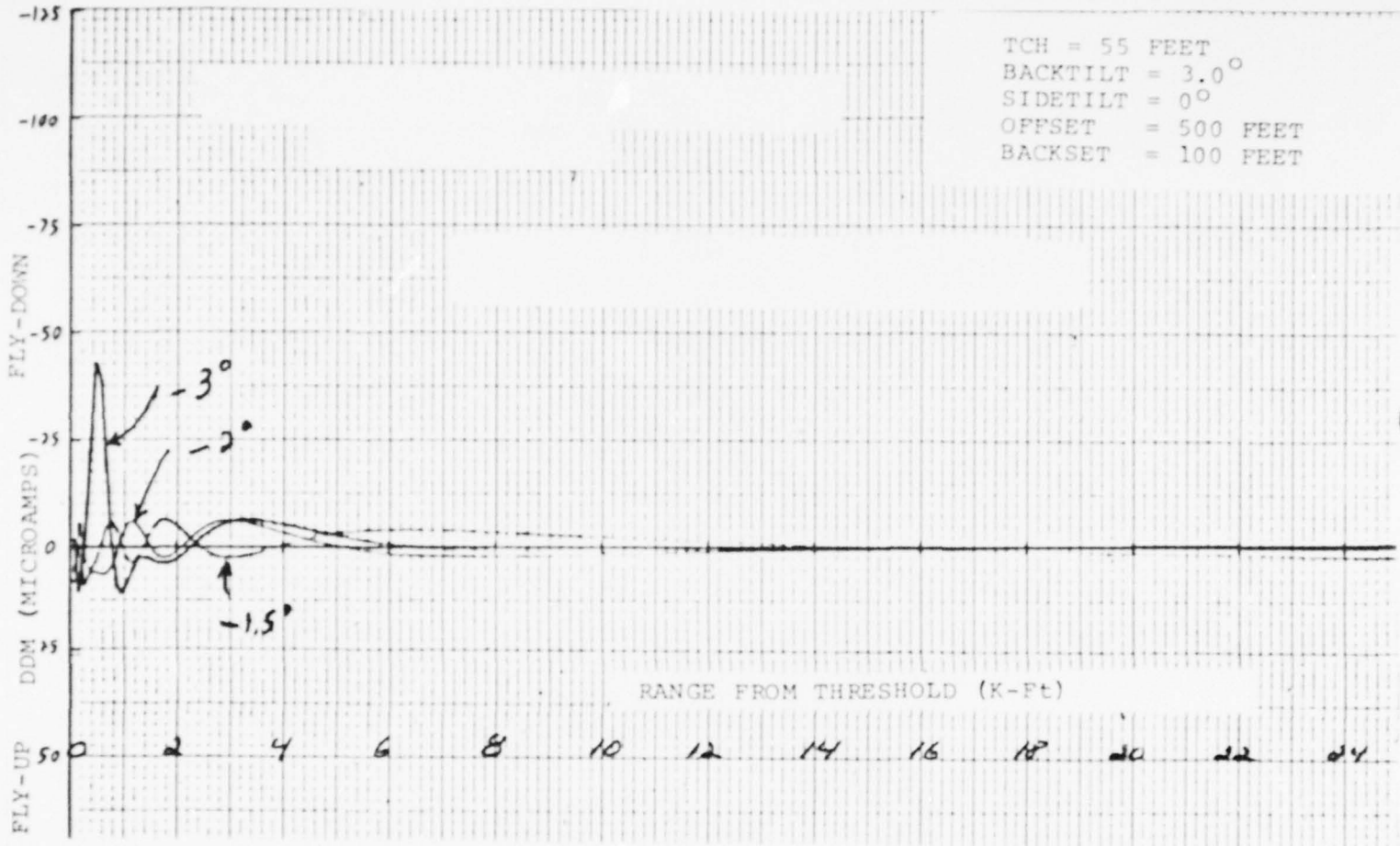

Figure 2-31 The Effect On Fly-In For Various Down Sloping Grounds

abruptly terminated ground plane. This could arise if the runway is situated upon a plateau or large embankment or in mountainous regions. In the case investigated, the edge of an infinite half-plane was perpendicular to the runway centerline and placed at various distances in front of the antenna. For the first series of graphs, the antenna was offset 500 feet and backset 100 feet. The center of the antenna was 49.76 feet above the ground and this established a threshold crossing height of 55 feet. Figure 2-32 shows fly-ins for four edge distances. It has been previously established that the ground currents for an antenna height of 50 feet do not begin to diminish until one has reached a point 200 feet in front of the antenna and become negligible at about 300 feet in front of the antenna. One would expect an edge located 200 feet or less in front of the antenna to have a significant effect upon antenna performance and Figure 2-32 does show that the transition from unacceptable to acceptable antenna performance occurs for an edge located between 200 and 300 feet in front of the antenna. If the edge is placed directly under the antenna there will be no image contributions and no edge diffraction contributions. As one can see, the curve does show that it is practically zero over the whole range. Figure 2-33 is an expanded scale version of Figure 2-32 with range values from threshold to 3000 feet.

Figure 2-34 is a more detailed investigation of edges located between 200 and 300 feet in front of the antenna. It appears that the edge will have to be at least 300 feet in front of the antenna to insure acceptable results. Figure 2-35 is an expanded version of Figure 2-34.

If the offset and T.C.H. are maintained and the antenna is moved back from threshold the antenna height will decrease. If it is moved back 310 feet from threshold the antenna center will be 38.75 feet above the ground and the bottom radiator will be about 8 feet above the ground. This gives sufficient clearance

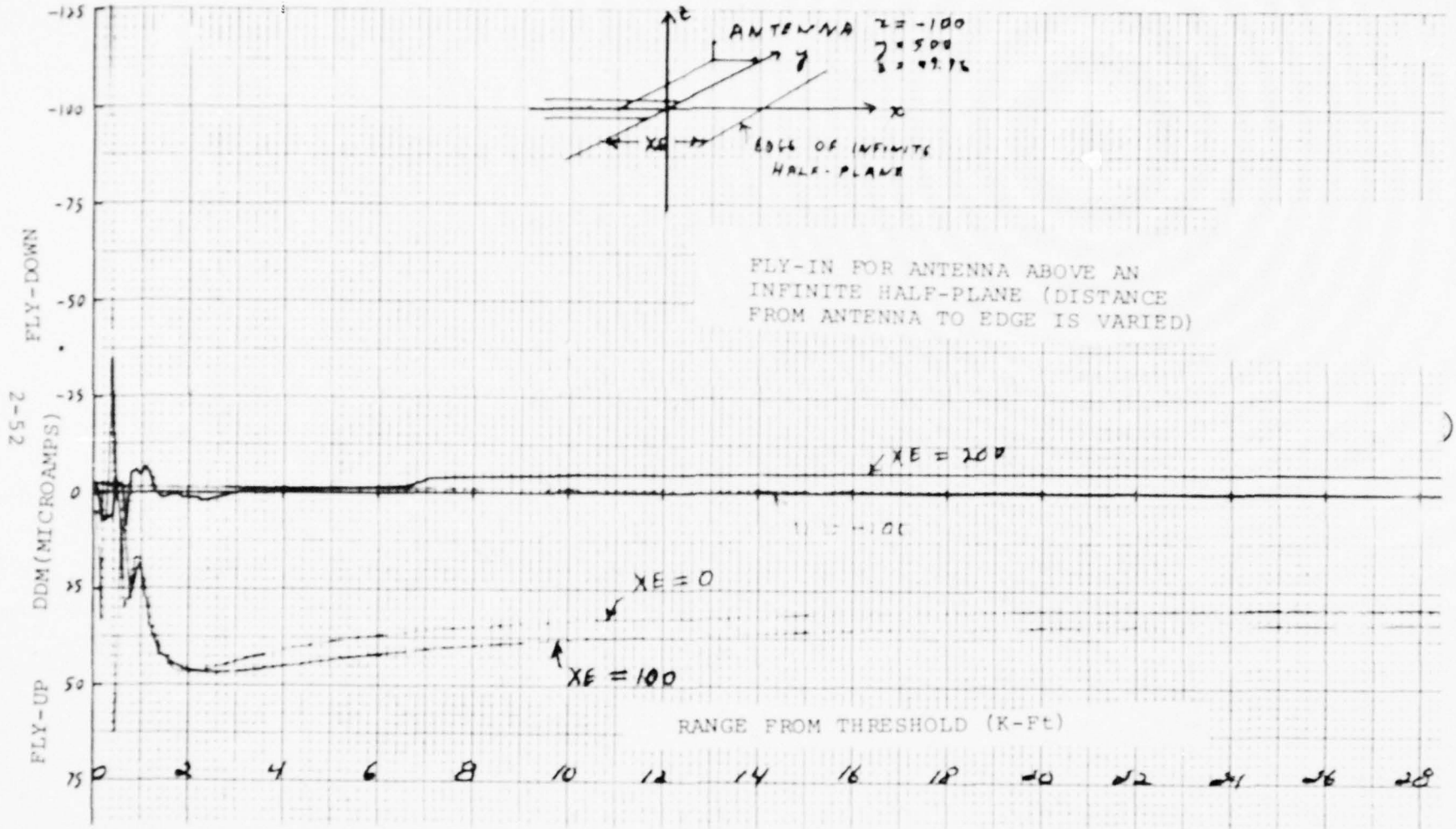

Figure 2-32 Antenna Performance Over An Abruptly Terminated Ground Plane

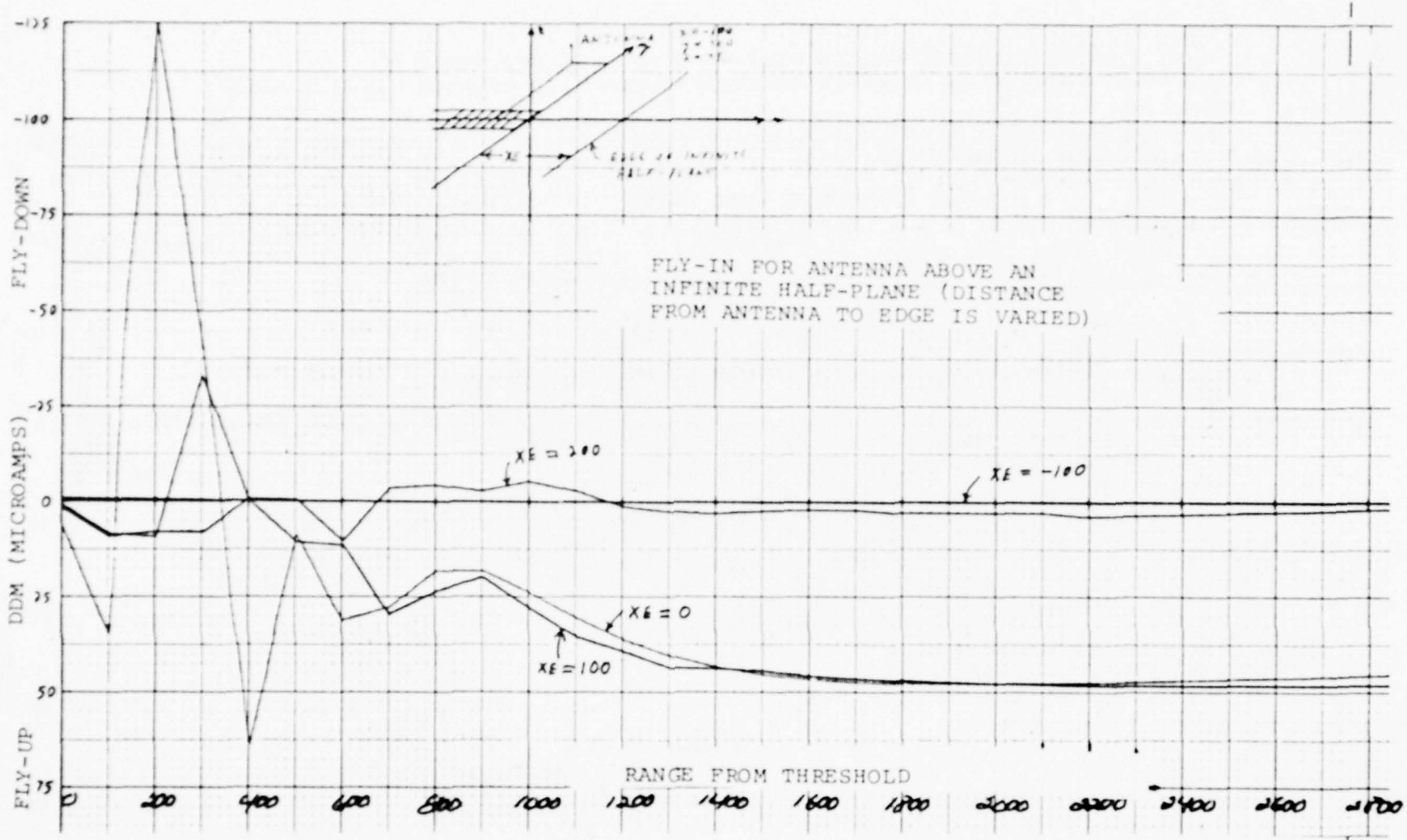

Figure 2-33 Data Of Figure 2-32 On An Expanded Scale

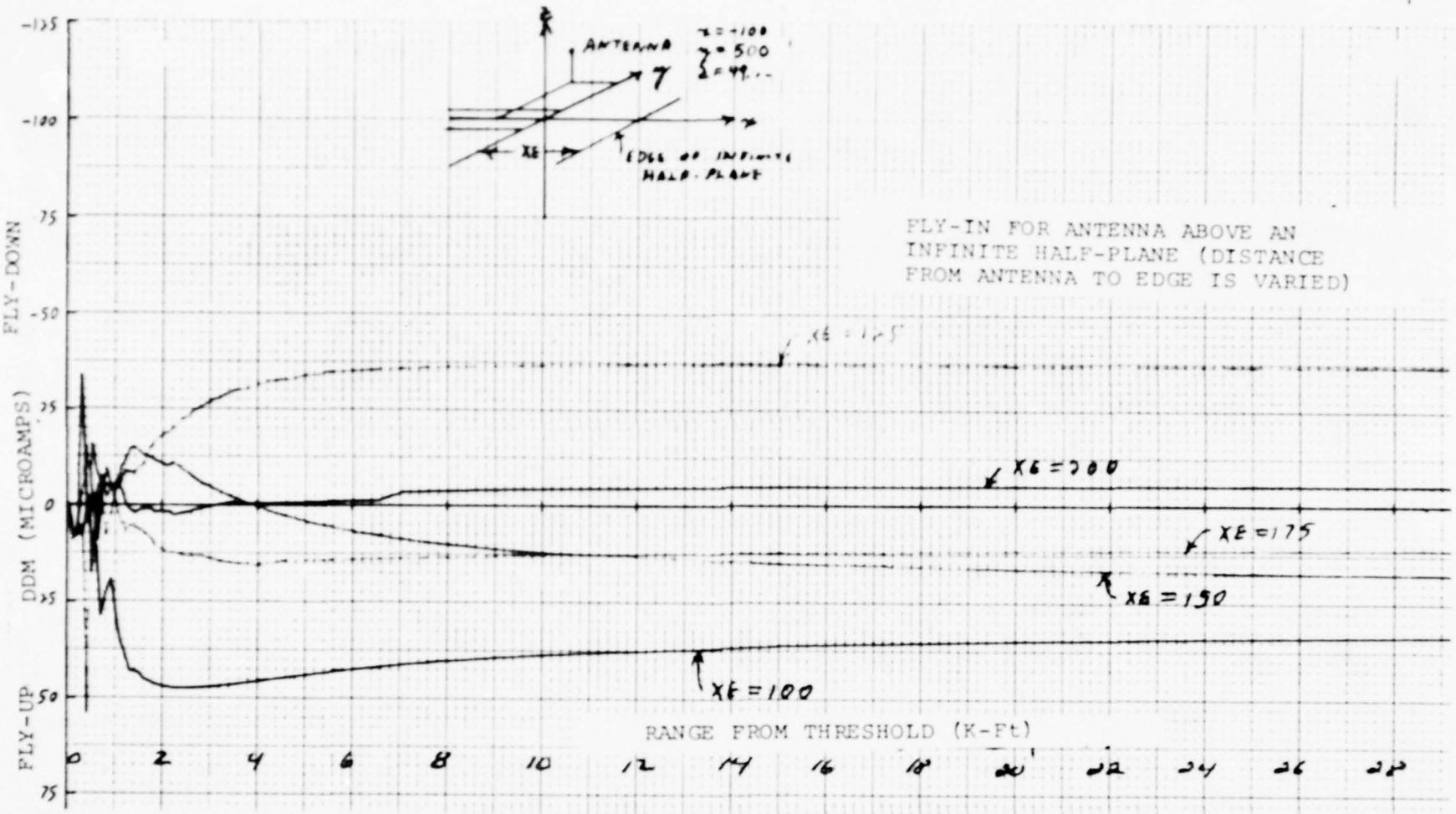

Figure 2-34 Antenna Performance Over An Abruptly Terminated Ground Plane For Various Locations Of The Discontinuity

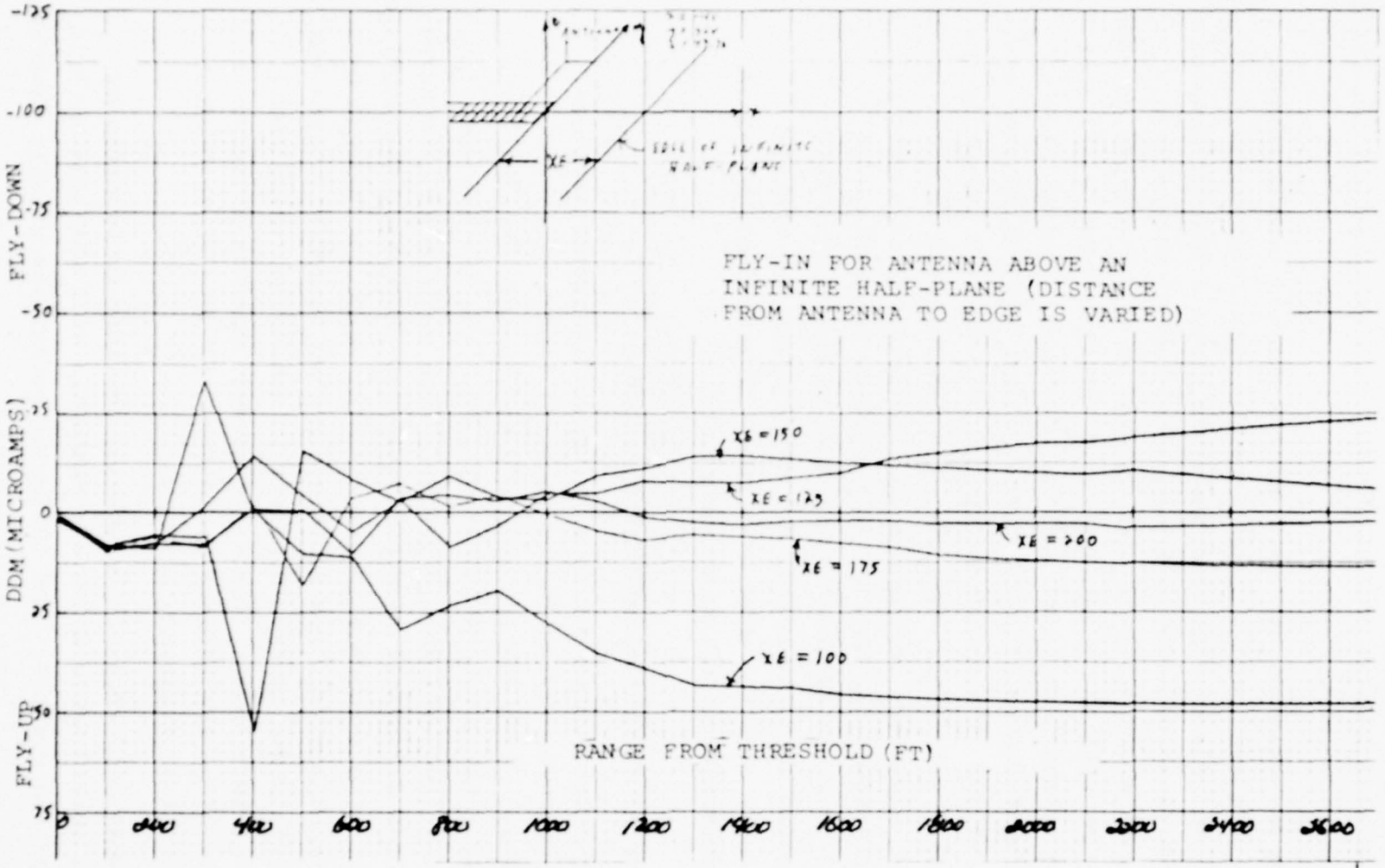

Figure 2-35 Data Of Figure 2-34 On An Expanded Scale

for snow accumulation and is about the minimum usable antenna height. The next set of graphs are for this antenna position. Shorter half-planes should be possible since a smaller area of ground is illuminated by the high sidelobes of the pattern. Figure 2-36 shows a fly-in with an edge at threshold and an edge directly beneath the antenna. Since the threshold is 310 feet from the antenna, the edge will not be heavily illuminated so antenna performance should be good. Also, an edge beneath the antenna should give an ideal fly-in. Figure 2-37 shows fly-ins for edges located 200, 225, 250, 275 and 300 feet in front of the antenna. Since the antenna is lower, these curves should be slightly better than similar curves shown in Figure 2-34. Figure 2-38 is an expanded version of Figure 2-37. This demonstrates that the Dipole Broadside Array can operate successfully at sites with very short truncated ground planes where conventional ILS will not work.

2.2 MECHANICAL CONFIGURATION AND ASSEMBLY

The antenna assembly is made up of 7 separate sections each of which is 110.48 inches long, 34 inches wide, and 9 inches deep. Each section weighs approximately 200 lbs. The assembled antenna length is 64'- 5 1/2". The antenna walls are fabricated from .062 inch aluminum. Each section is terminated in extruded structural aluminum angle for connecting the sections together. The antenna elements, four of which are located in each antenna section, are inbedded in foam in order to give the unit rigidity and to eliminate air in the cavity which could become moisture laden. There are no wall spacing adjustments necessary since the antenna is designed to operate throughout the glide slope frequency band.

Access into each of the antenna sections is provided by aluminum cover panels which are removable even with the antenna assembled and erected. The following paragraphs briefly describe

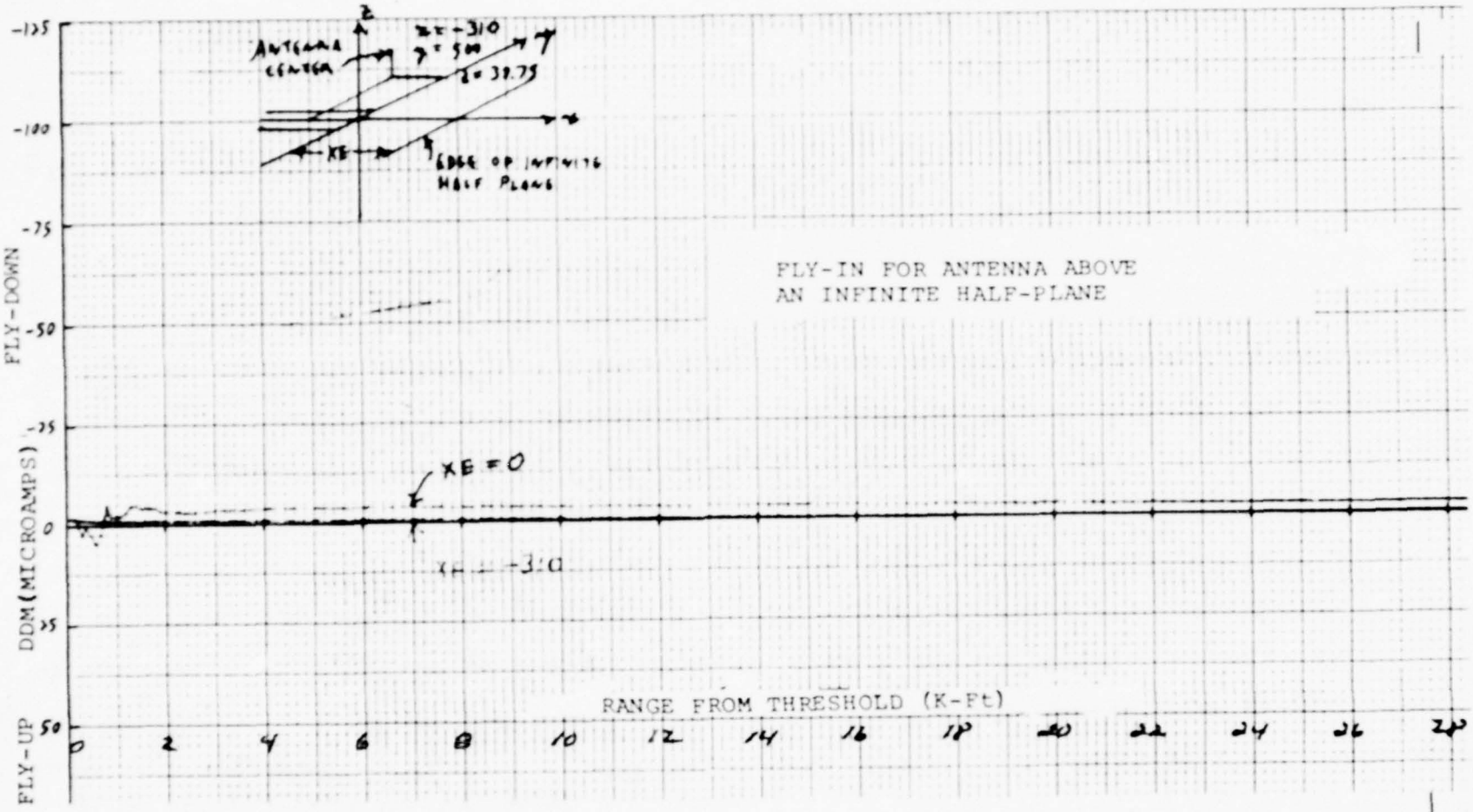

Figure 2-36 The Effects Of An Infinite Edge Discontinuity At Threshold And Directly Below The Antenna

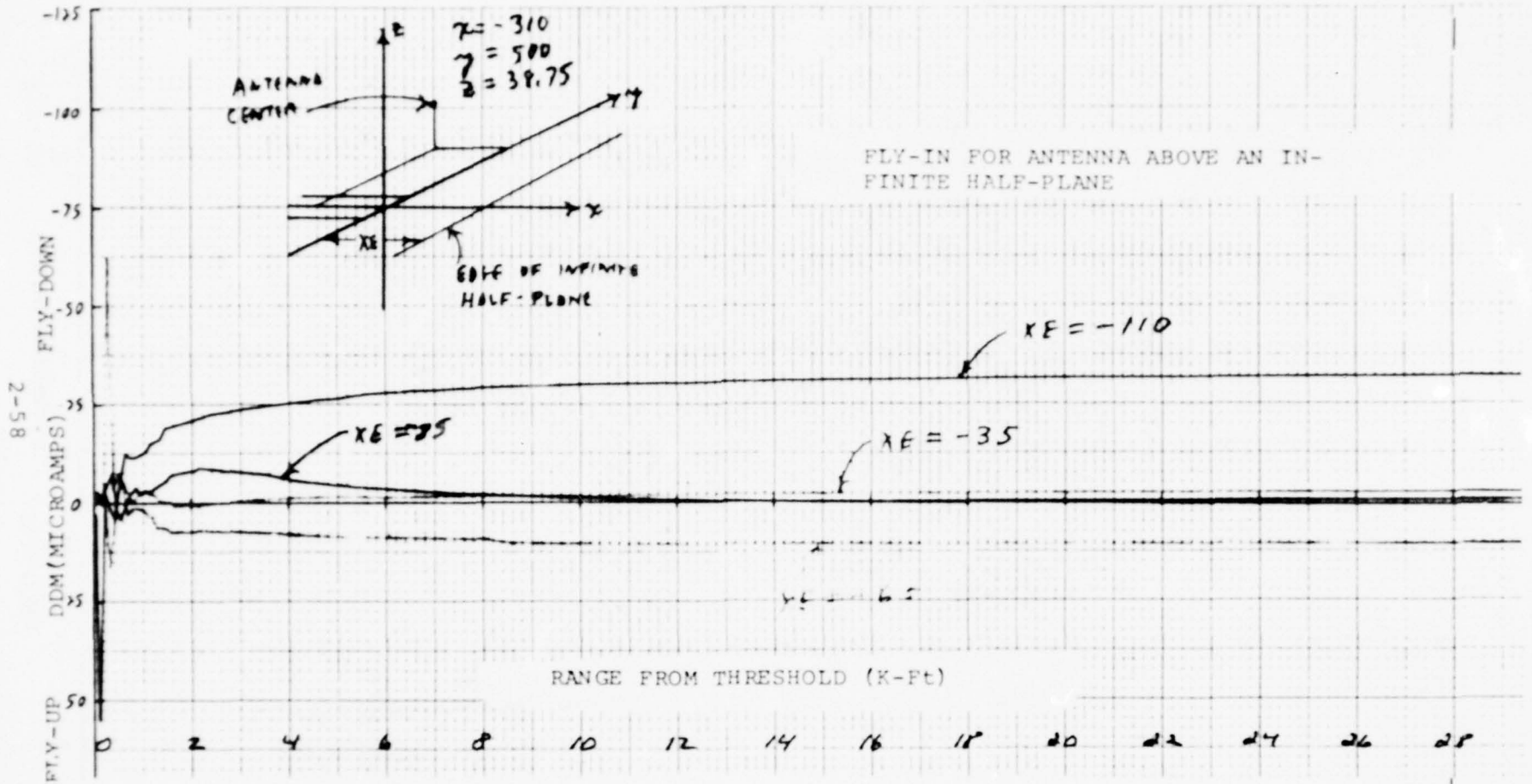

Figure 2-37 The Effects Of Edge Discontinuities At Various Locations

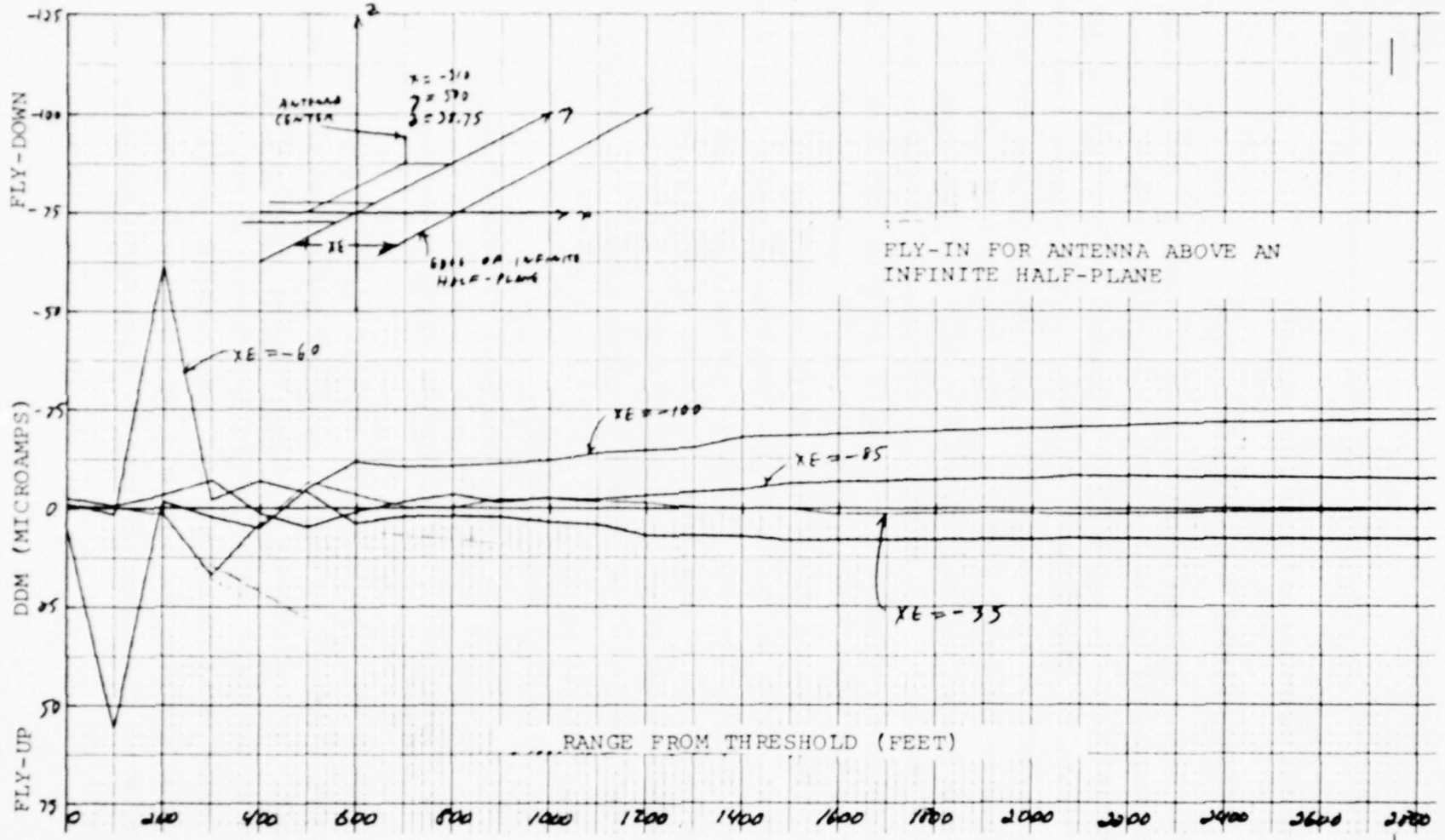

Figure 2-38 Data Of Figure 2-37 On An Expanded Scale

the antenna assembly and erection procedure.

2.2.1 Antenna Siting And Site Preparation

The dipole broadside antenna may be sited on either side of the designated ILS runway with primary consideration given to parallel taxiways and aircraft movement in front of the glide slope location. The lateral placement of the antenna from the runway centerline must comply with the lateral offset criteria described in FAA Order 6750.16A. This distance is a function of antenna height but may not be less than 250 feet from the runway centerline. The antenna in its present configuration is mechanically sideways focused with the focal distance (array center to R/W centerline) set at 500 feet; however, placement within $\pm$ 200 feet of this offset distance has been proven to be acceptable. When determining the longitudinal backset distance from the runway threshold the major criteria is to locate the physical midpoint of the antenna (center of Section No. 4) at a point which places it on a line with the desired glide path. The factors which must be considered when siting the antenna are:

1. Desired Glide Angle.
2. Threshold Crossing Height.
3. Elevation of runway threshold and elevation of ground at antenna.
4. Elevation of R/W centerline opposite antenna location.

Although the antenna may be located directly abeam of the runway threshold it may not be sited forward of the runway threshold. As the antenna is sited further downfield from the runway threshold the height of the center of the antenna above ground level is reduced and consideration should be given to maintaining the bottom of the antenna at a reasonable distance above the ground (6 feet is a practical minimum distance).

Site preparation for installation of the dipole broadside antenna should include maintaining level ground with no severe terrain discontinuities directly in front of the main antenna foundation for a distance of approximately 200 feet. This will serve to simplify the antenna erection procedure and to minimize signal derogation.

2.2.2 Antenna Tower Assembly

The support structure for this antenna is designed to mount the antenna to a steel tower made up of Rohn No. 65G triangular tower sections. The number of tower sections required is a function of antenna placement. During the site testing of the antenna system at Lynchburg, Virginia, a total of 7 65G tower sections were employed. Each of the Rohn 65G sections is 10' - 1" in length and weighs 178 lbs.

2.2.3 Attachment of Antenna to Main Tower Assembly

The seven antenna sections are attached to the main tower assembly. All assembly work is done directly on the tower since it is an integral part of the antenna structure. Each of the seven dipole broadside array sections are coded with Section No. 1 located at the bottom and Section No. 7 being located at the top of the tower. The antenna sections are fastened to the tower by the use of brackets as shown on Figure 2-41. These brackets are fabricated from extruded structural aluminum angle. The bracket layout on the tower is shown in Figure 2-40. The antenna sections are joined to the brackets and to each other by 3/8 inch and 1/4 inch bolts going through the antenna flanges. Each of the eight brackets are also identified with a code number (F1 through F6) and installation must be made with the proper sequence as shown in Figure 2-40. Although there are eight brackets employed two sets of the brackets are identical. Each antenna section remains rectangular with curvature obtained

by inserting tapered shims at each joint. Antenna section No. 4 remains vertical with respect to the tower with the other sections angled as shown in Figure 2-40. It is to be noted that the antenna is installed such that the antenna curvature is focused towards the runway which is being instrumented. The antenna can be installed on either side of a runway by interchanging the mounting brackets with the top to the bottom and with the bracket overhang on the opposite side. Six choke splice plates are provided to cover the side of the antenna section where the thick end of the shim is installed. A parts list for the antenna assembly is given in Figure 2-39.

2.2.4 Antenna Base Assembly

The antenna base assembly is designed to allow movement of the antenna in both a longitudinal and lateral direction. The backtilt of the tower is set to the desired glide slope angle. Generally no side tilt is incorporated into the antenna system; however, it provides erection clearances during antenna installation. A sketch of the base assembly is shown in Figure 2-43.

2.2.5 Antenna Erection Procedure

An antenna installation requires that first the three concrete foundations be poured, two for the main braces and one for the main base assembly. A typical antenna foundation layout is shown in Figure 2-44.

The main braces are assembled by building up two members consisting of seven (typical) Rohn type 55 tower sections terminated on the bottom by anchor hinges and on the top by the brace top plate. These two brace members are tied together by the tower hinge which, in turn, attaches to the tower hinge bracket located on one of the type 65G tower sections. If a large enough crane is available, all tower and antenna assembly

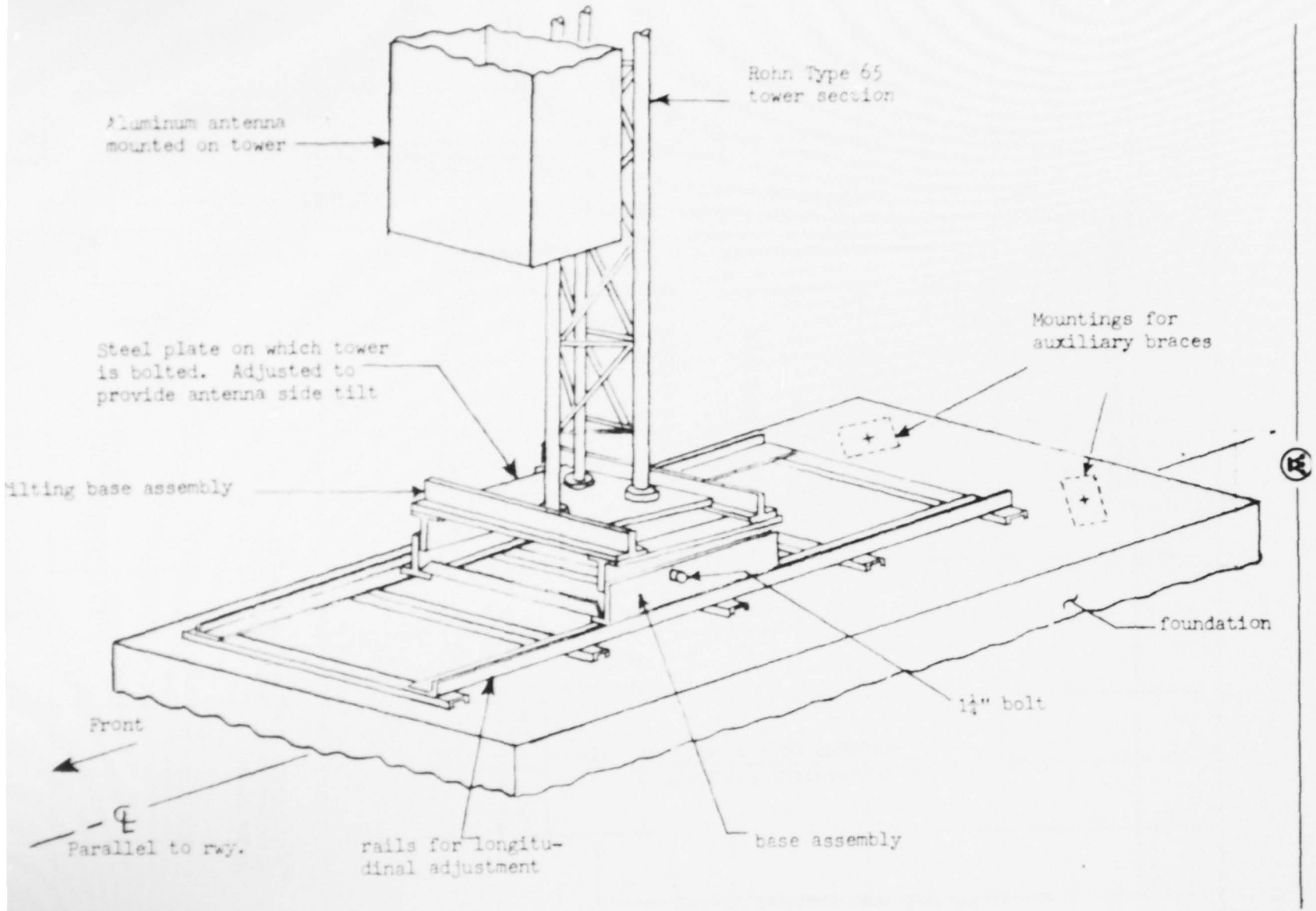

Figure 2-43 Antenna Base Assembly

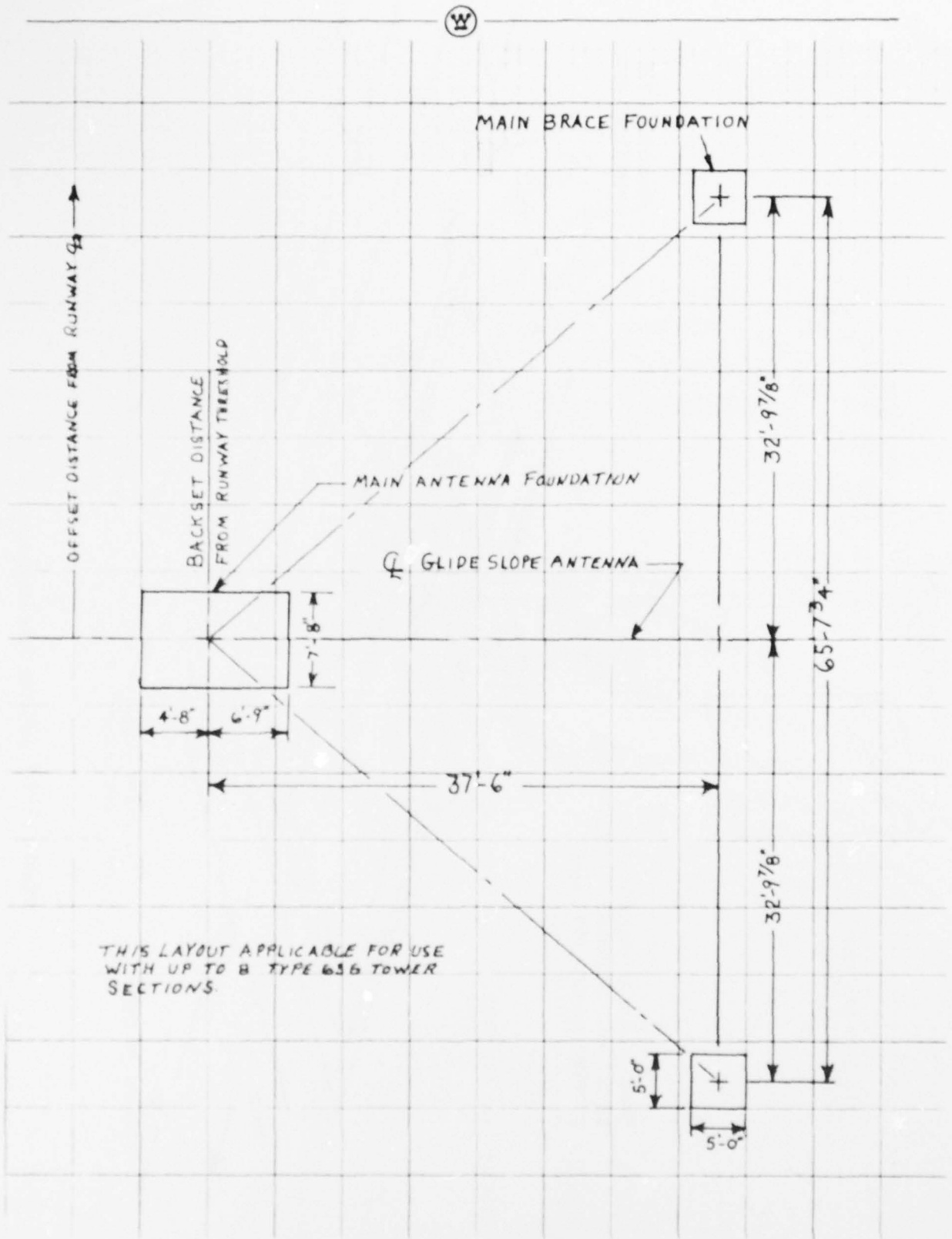

Figure 2-44 Typical Foundation Layout For Dipole Broadside Antenna Array.

is done on the ground with the entire structure being raised upon completion. This antenna erection procedure was validated at the Lynchburg, Virginia, test site. The bottom of the tower is not permanently secured to the base assembly until after flight check in order to allow for minor changes in the glide angle setting.

...THETIC IDENTITIES ARE FOR ...INGHOUSE REFERENCE ONLY

QTY	CODE IDENT NUMBER	PART NO.	I M	DESCRIPTION
6		[illegible]		SPACER SPACE
6		[illegible]		SPACE SPACE
6		MS24033C48		SCREW, FLAT HD [illegible]
18		MS24033C50		SCREW, FLAT HD [illegible]
18		MS24033C52		SCREW, FLAT HD [illegible]
24		MS24033C54		SCREW, FLAT HD [illegible]
32		MS51957-47		SCREW, PAN HD [illegible]
6				CABLES
8				CABLES, MONITOR
84		MS35338-141		LOCKWASHER #6
68		MS15795-816		FLAT WASHER #6
84		32BC14E704D		NUT, HEX #6-4
84		330CR3D3H424A		BOLT, HEX HD [illegible]
		MS35649-264		NUT, HEX #8-32
		MS15795-841		FLAT WASHER #8
		MS35338-137		LOCKWASHER #8
6		7710128-76		SPACER
6		7710128-74		SPACER
6		7710128-71		SPACER
36		MS15795-820		FLAT WASHER 5/8
244		MS15795-816		FLAT WASHER 3/8
300		MS15795-812		FLAT WASHER 1/4
96		MS35338-166		LOCKWASHER 5/8
196		MS35338-141		LOCKWASHER 3/8
150		MS35338-139		LOCKWASHER 1/4
96		32BC412AE2		NUT, HEX 5/8-11
196		MS35649-2264		NUT, HEX 3/8-16
150		MS35649-2264		NUT, HEX 1/4-20
96		[illegible]		BOLT, HEX HD [illegible]
36		MS[illegible]		SCREW, PAN HD [illegible]
72		MS[illegible]		SCREW, PAN HD [illegible]
176		[illegible]		BOLT, HEX HD [illegible]
96		[illegible]		BOLT, HEX HD [illegible]
6		[illegible]		BOLT, HEX HD [illegible]
90		[illegible]		BOLT, HEX HD [illegible]
60		[illegible]		BOLT, HEX HD [illegible]

V=VENDOR ITEM B=BULK MATERIAL — PARTS LIST

1. FOR UNDERSIDE OF SECTION 2 WITH COVERS REMOVED SEE DETAIL 'D' SHT 5
2. FOR UNDERSIDE OF SECTION 6 WITH COVERS REMOVED SEE DETAIL 'E' SHT 5
3. 14/2 TYPE 'SVO' 120 V. BLACK, NEOPRENE JACKET
4. PANDUIT #SST-4
5. CROUSE HINDS #FSCC1
6. CROUSE HINDS #DS1006

FOR ELEVATION VIEW SEE FIG 2-40

SHEET REVISION STATUS					
5	4	3	2	1	SHEET NO.
					CATEGORY REV. LTR.

REVISIONS				
ZONE	LTR	DESCRIPTION	DATE	APPROVED
	—	DRAWING RELEASED		

ITEM	DESCRIPTION	GOVT SPEC	Ⓦ SPEC	FIND NO.
				43
				42
				41
	CHEE SPLICE			40
	CHEE SPLICE			39
	SCREW, FLAT HD #8-32 X .38			38
	SCREW, FLAT HD #8-32 X .50			37
	SCREW, FLAT HD #8-32 X .75			36
	SCREW, FLAT HD #10-32 X .50			35
	SCREW, PAN HD #10-32 X .62			34
	CABLES			33
	CAP, BS, MOUNTING			32
	LOCKWASHER #10			31
	FLAT WASHER #10			30
	NUT, HEX #10-32			29
	BOLT, HEX HD #10-32 X 1.50			28
	NUT, HEX #8-32			27
	FLAT WASHER #8			26
	LOCKWASHER #8			25
	SPACER			24
	SPACER			23
	SPACER			22
	FLAT WASHER #4			21
	FLAT WASHER #2			20
	FLAT WASHER #1			19
	LOCKWASHER #2			18
	LOCKWASHER #1			17
	LOCKWASHER #4			16
	NUT, HEX #4-40			15
	NUT, HEX #2-56			14
	NUT, HEX #1-72			13
	BOLT, HEX HD #2-56 X 2.50			12
	SCREW, PAN HD #2-56 X .62			11
	SCREW, PAN HD #1-72 X .31			10
	BOLT, HEX HD #4-40 X .62			9
	BOLT, HEX HD #4-40 X .25			8
	BOLT, HEX HD #4-40 X .62			7
	BOLT, HEX HD #2-56 X .62			6
				5
				4
				3
				2
				1

ITEM	QUAN	DOCUMENT NUMBER	PART NO	DESCRIPTION	GOVT SPEC	Ⓦ SPEC	FIND NO.
							40
							39
	2						38
	1			POWER DIVIDER NO 7			37
	1			POWER DIVIDER NO 6			36
	1			POWER DIVIDER NO 5			35
	1			POWER DIVIDER NO 4			34
	1			POWER DIVIDER NO 3			33
	1			POWER DIVIDER NO 2			32
	1			POWER DIVIDER NO 1			31
	1	354D003H-1		COVER W/GASKET Ⓓ			30
	1	354D003H-2		JUNCTION BOX, 3 WAY Ⓔ			29
	1	SERA0003H-7		ANTENNA SECTION ASSY			28
	1	SERA0003H-6		ANTENNA SECTION ASSY			27
	1	SERA0003H-5		ANTENNA SECTION ASSY			26
	1	SERA0003H-4		ANTENNA SECTION ASSY			25
	1	SERA0003H-3		ANTENNA SECTION ASSY			24
	1	SERA0003H-2		ANTENNA SECTION ASSY			23
	1	SERA0003H-1		ANTENNA SECTION ASSY			22
	6	SERA0003H-14		SHIM, SIDE			21
	6	SERA0003H-13		SHIM, BOTTOM			20
	6	SERA0003H-12		SHIM, MIDDLE			19
	6	SERA0003H-11		SHIM, TOP			18
	1	SERA0003H-10		MOUNTING FRAME			17
	1	SERA0003H-9		MOUNTING FRAME			16
	1	SERA0003H-8		MOUNTING FRAME			15
	1	SERA0003H-7		MOUNTING FRAME			14
	2	SERA0003H-6		MOUNTING FRAME			13
	2	SERA0003H-5		MOUNTING FRAME			12
	14	354D003H-15		BASE PLATE - SSB			11
	24	SERA0003H-16		CLAMP			10
	2	354D003H-16		ANCHOR PORCELAIN ASSY			9
	1	SERA0003H-17		TOWER BASE WELDED			8
	1	SERA0003H-18		TOWER BASE ASSEMBLY			7
	1	SERA0003H-19		TOWER BASE ASSY			6
	100	354D003H-20		CABLE TIES Ⓕ			5
	FT	354D003H-21		CABLE Ⓖ			4
		354D003H-1		CONDUIT ASSEMBLY			3
		SERA0003H-22		TOWER SECTION ASSY			2
							1

PARTS LIST

PARTS LIST

SEE FIG 2-40

UNLESS OTHERWISE SPECIFIED DIMENSIONS ARE IN INCHES
DO NOT SCALE. TOLERANCES ON DIM
2 PLACE ± | 3 PLACE ± | ANGLES ±
Ⓢ SPEC MISSILE APPLIES
PROCESS SPEC

NEXT ASSY | USED ON
APPLICATION

Westinghouse Electric Corporation

C POLE BROADSIDE SLIDE SLOPE ARRAY ASSEMBLY

SIZE D | CAGE CODE NO. 97942 | DWG NO. 354D003

SCALE | WEIGHT | SHEET 1 OF 5

2-67/68

FIG 2-3 PARTS LIST

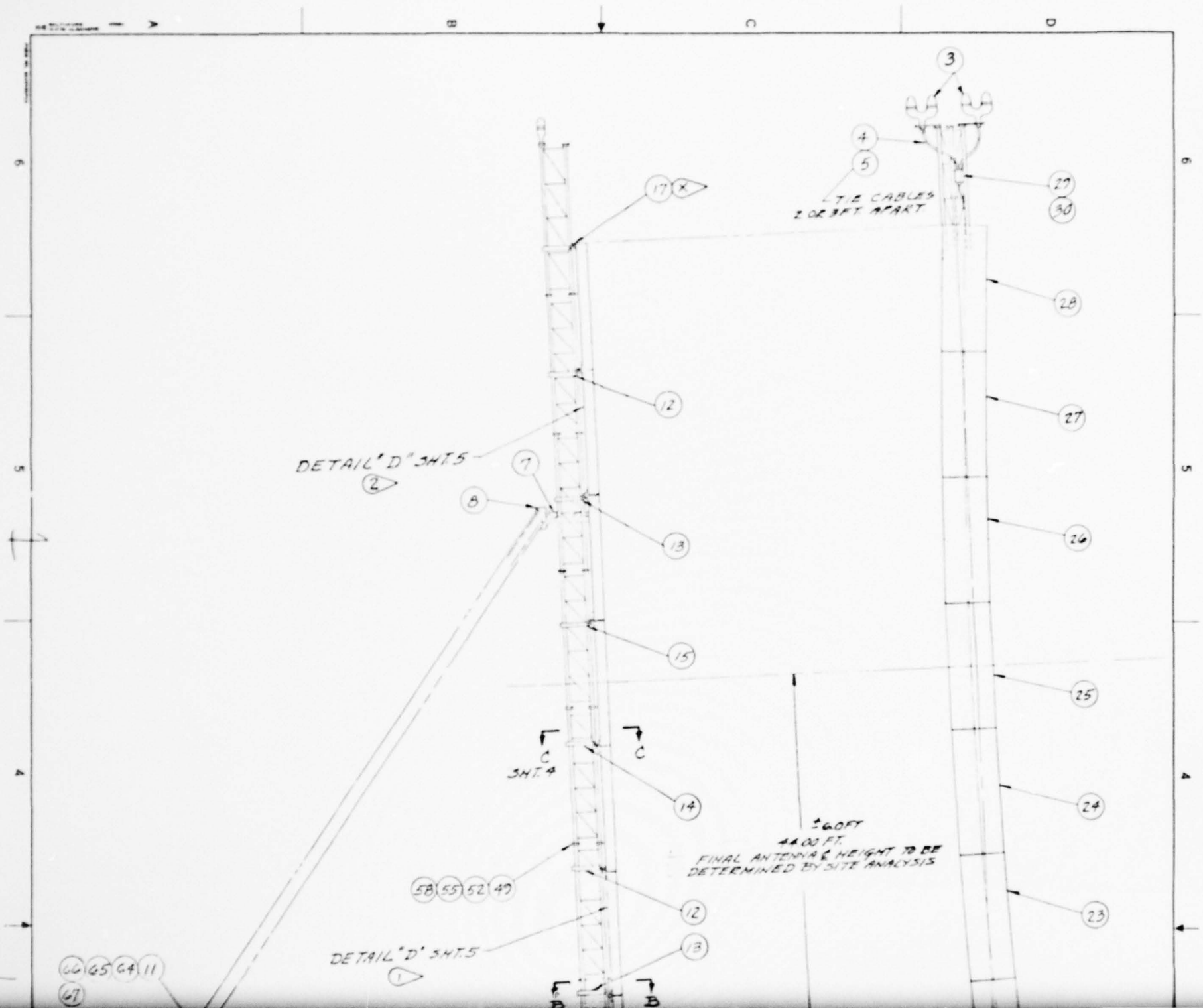
3
4
5
LTE CABLES 2 OR 3FT APART
17
16
29
30
28
12
27
DETAIL "D" SHT 5
2
7
8
13
26
15
25
C
SHT 4
C
14
24
140FT
44.00 FT.
FINAL ANTENNA & HEIGHT TO BE DETERMINED BY SITE ANALYSIS
58
55
52
49
12
23
DETAIL "D" SHT 5
1
13
66
65
64
11
67
B
B

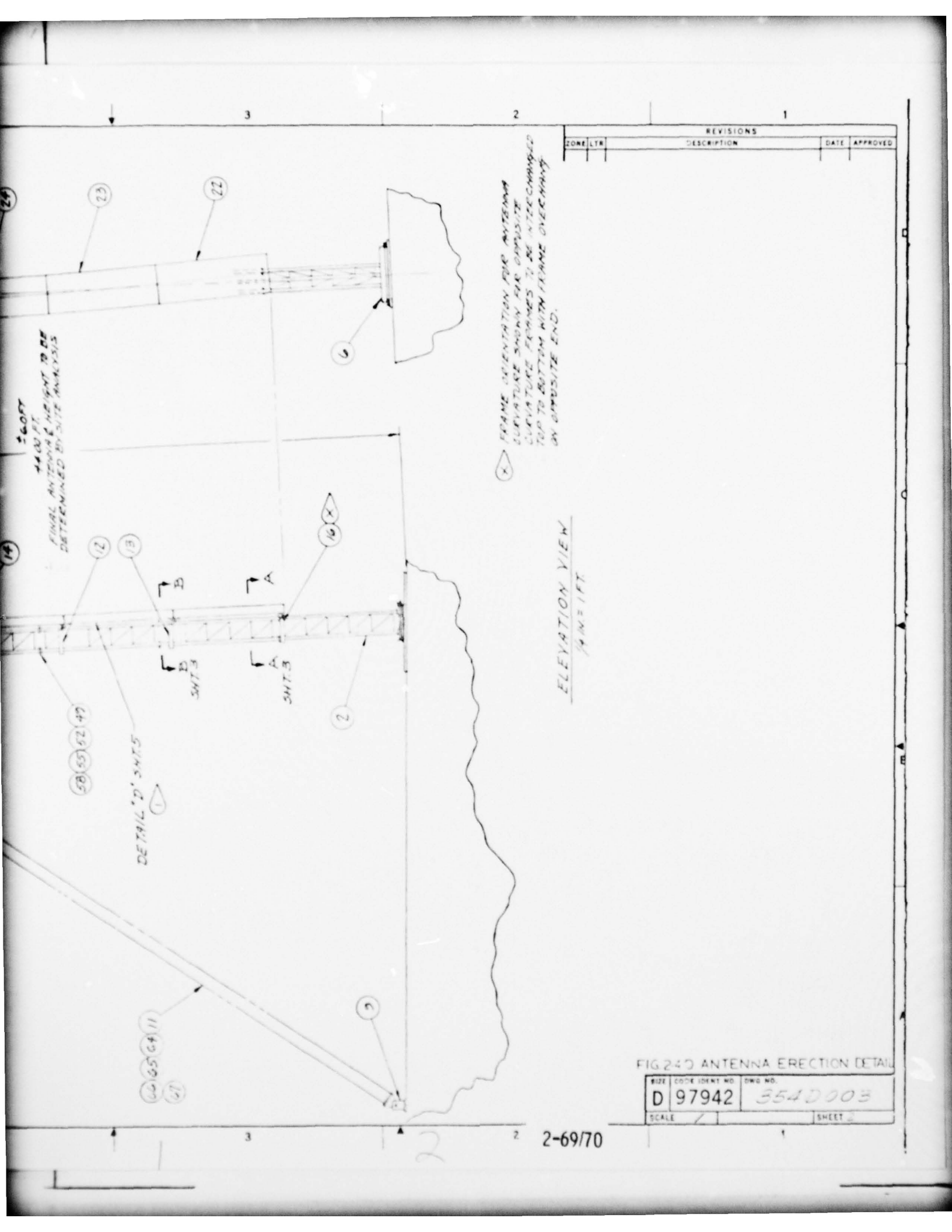
REVISIONS
ZONE LTR DESCRIPTION DATE APPROVED
±60FT
1460 FT.
FINAL ANTENNA HEIGHT TO BE
DETERMINED BY SITE ANALYSIS
FRAME ORIENTATION AND ANTENNA
ELEVATION SHOWN AS VIEWED
FROM OPPOSITE END.
ELEVATION VIEW
1/4IN = 1FT.
DETAIL 'D' SHT.5
SHT.3
SHT.3
FIG 24 D ANTENNA ERECTION DETAIL
SIZE D
CODE IDENT NO. 97942
DWG NO. 354D003
SCALE
SHEET
2-69/70

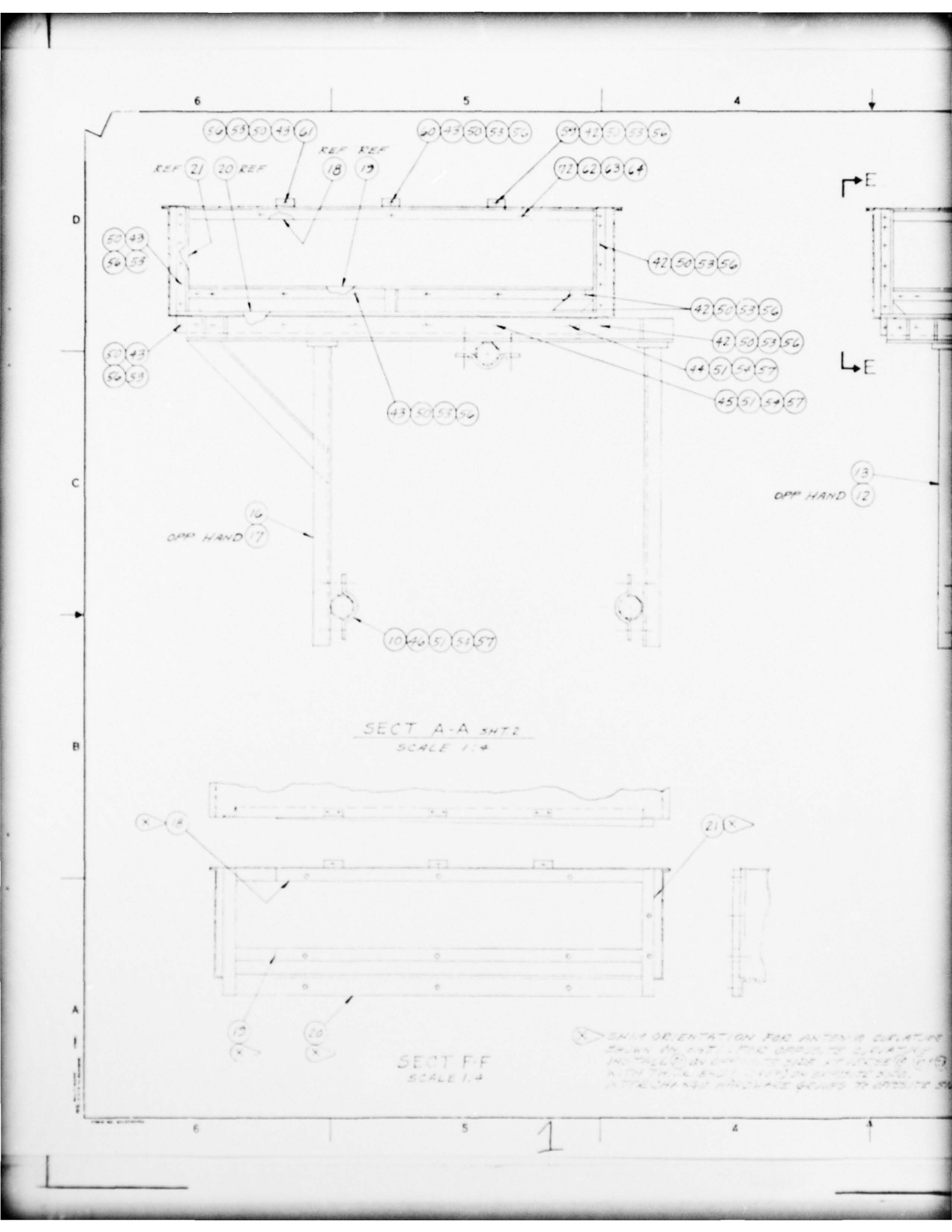
6
5
4
D
C
B
A
REF
REF
REF
OPP HAND
OPP HAND
E
E
SECT A-A SHT 2
SCALE 1:4
SECT F-F
SCALE 1:4
1

REVISIONS				
ZONE	LTR	DESCRIPTION	DATE	APPROVED

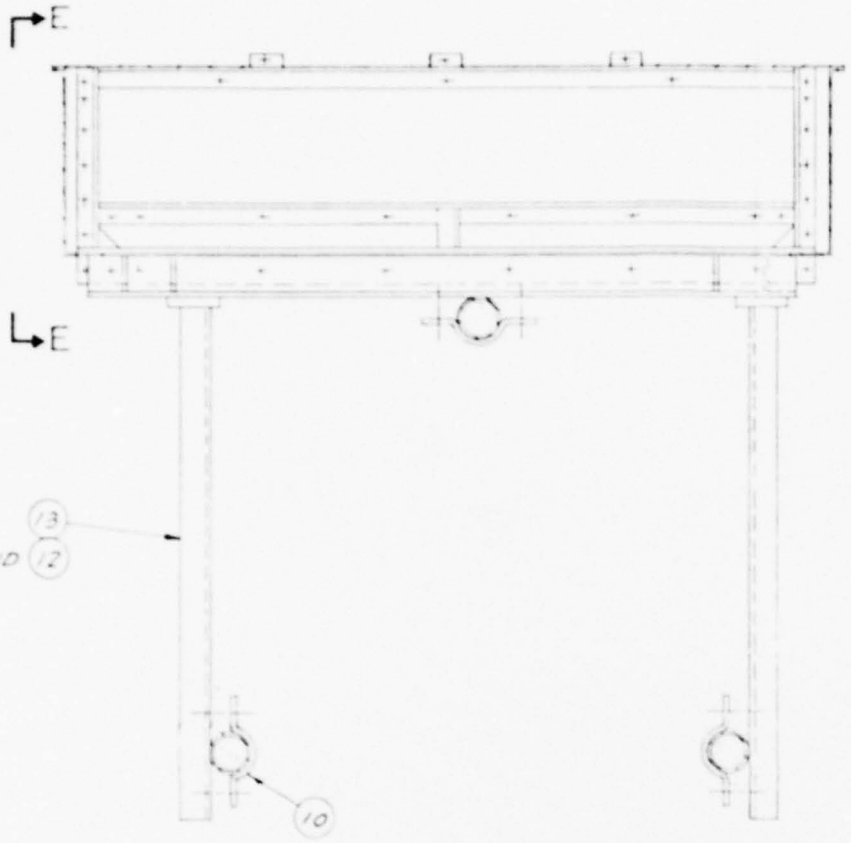

SECT B-B SHT 2
SCALE 1:4

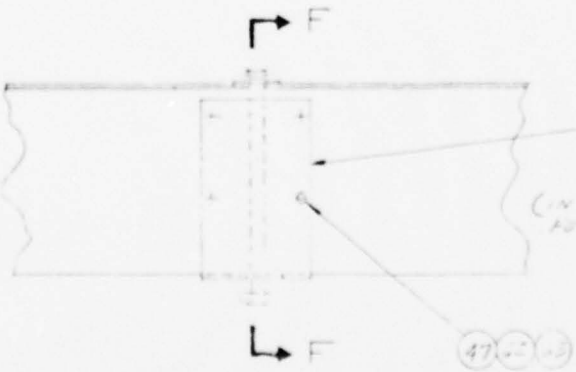

SECT E-E
SCALE 1:4

FIG 241 ANTENNA INSTALLATION DETAILS

SIZE	CODE IDENT NO.	DWG NO.
D	97942	354D003
SCALE		SHEET

2-71/72

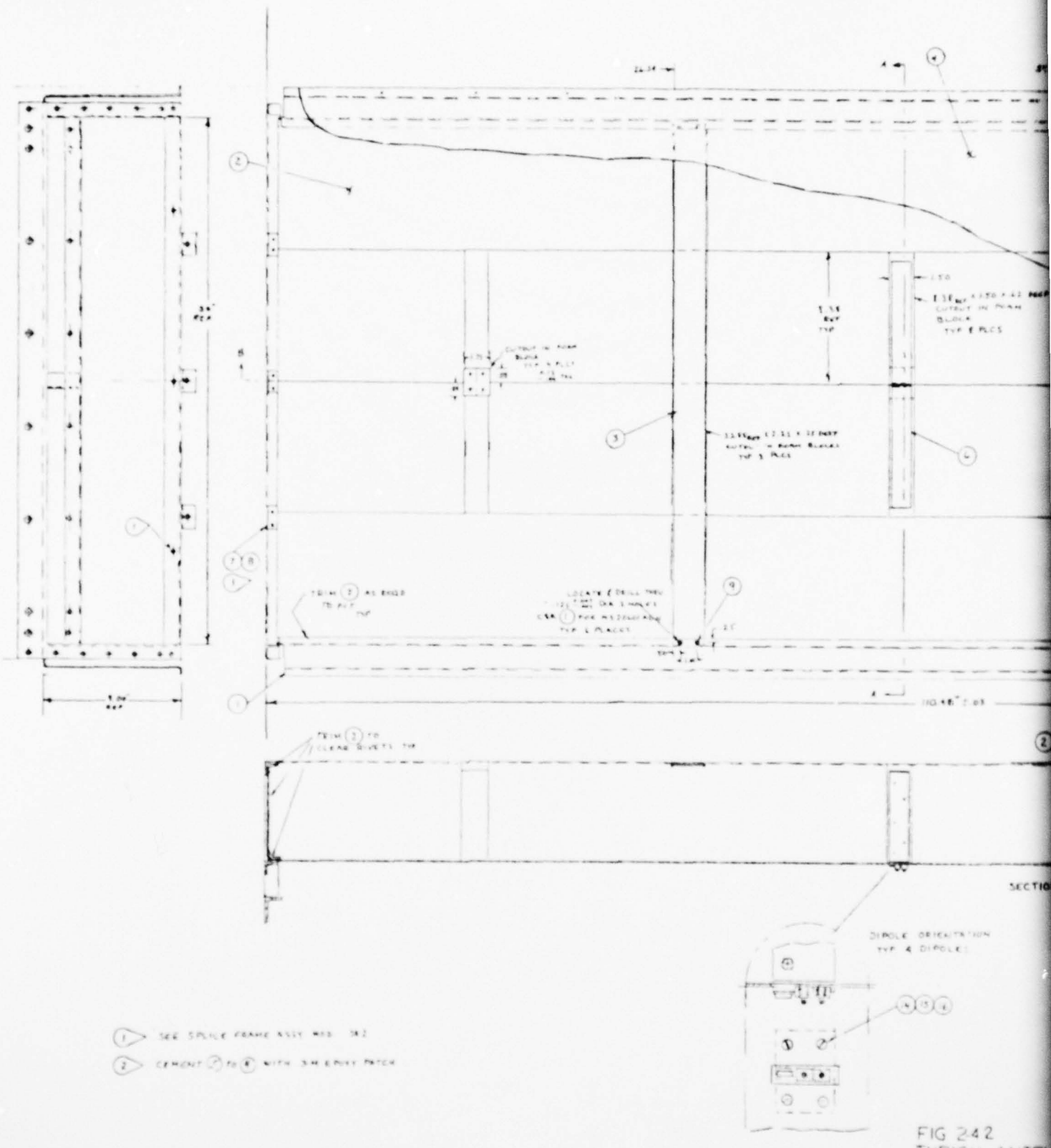

(1) SEE SPLICE FRAME ASSY MKS 382

(2) CEMENT (7) TO (8) WITH 3M EPOXY PATCH

FIG 242
TYPICAL ANTEN

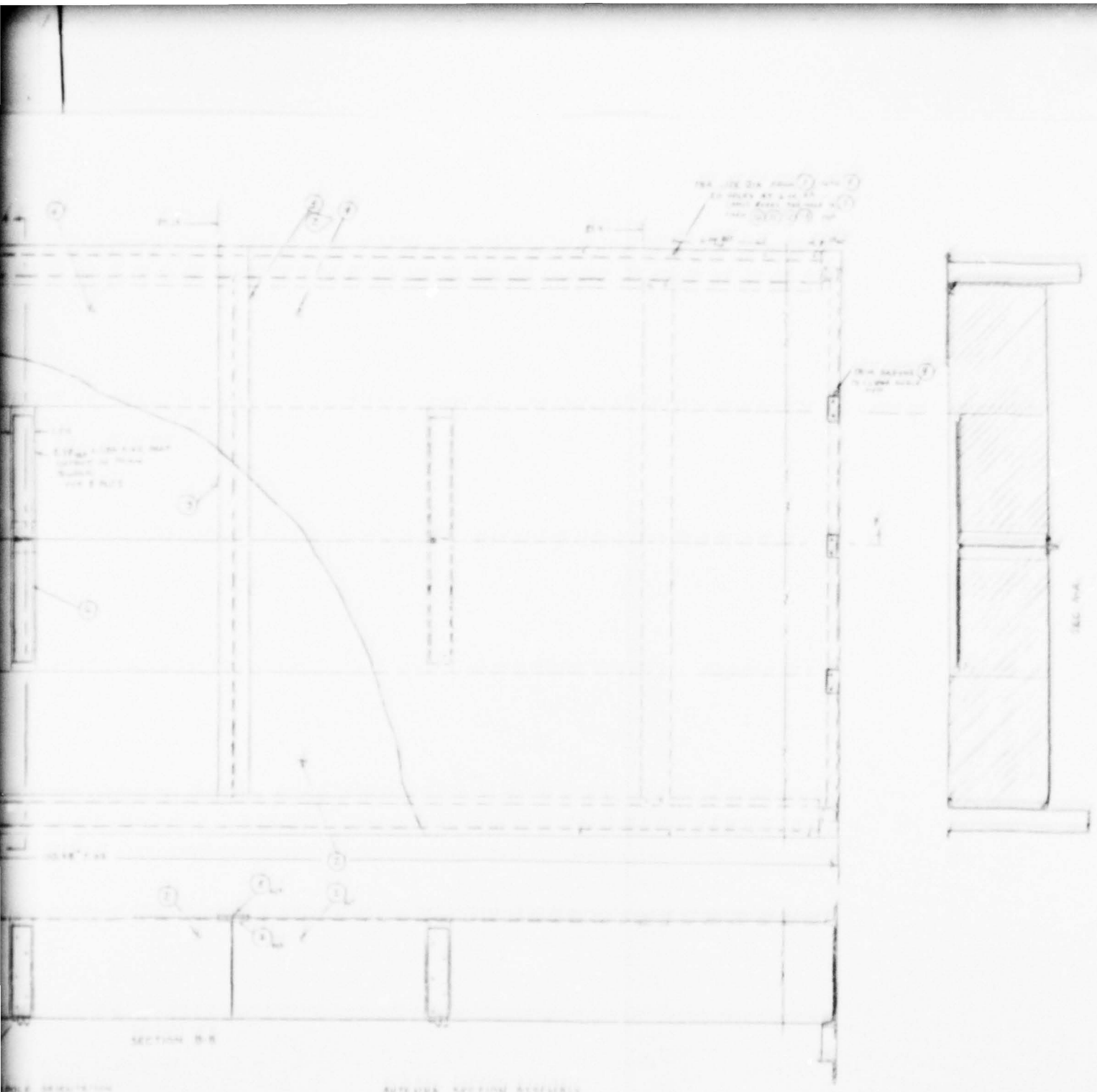

SECTION B-B

ANTENNA SECTION ASSEMBLY

			QTY
1			
2			
3			
4			
5			
6			
7			
8			
9			
10			
11			
12			
13			
14			
15			
16			

FIG 242
TYPICAL ANTENNA SECTION

FIG 242
TYPICAL ANTENNA SECTION

3.0 MONITOR SYSTEM

As a preliminary to the design of a monitor system capable of monitoring the excitation of a multi element array, an extensive analysis was performed. The purpose was to determine: (1) which elements have a significant effect in the far field pattern and what is the nature of their effect, and (2) how tightly must each element be monitored (i.e. detectable phase and amplitude variation). The analysis included introducing faults into the antenna and measuring on the antenna range the effect on the SBO pattern, and using the flyability computer model to predict the effective DDM variations as seen by an aircraft.

Due to the complexity and expense associated with measuring patterns for an array of this size, patterns were only taken for certain catastrophic cases. These are presented in Figures 3.1 through 3.34, and are summarized in the following table:

Figure	Antenna Condition
3.1	SBO pattern for normal (no fault)
3.2	SBO pattern element #1 open circuit
3.3	SBO pattern element #2 open circuit
3.4	SBO pattern element #4 open circuit
3.5	SBO pattern element #5 open circuit
3.6	SBO pattern element #10 open circuit
3.7	SBO pattern element #11 open circuit
3.8	SBO pattern element #13 open circuit
3.9	SBO pattern element #14 open circuit
3.10	CSB & SBO patterns for normal(no fault)
3.11	CSB pattern element #1 short circuit
3.12	SBO pattern element #1 short circuit
3.13	CSB pattern element #2 short circuit

Figure	Antenna Condition
3.14	SBO pattern element #2 short circuit
3.15	CSB pattern element #4 short circuit
3.16	SBO pattern element #4 short circuit
3.17	CSB pattern element #5 short circuit
3.18	SBO pattern element #5 short circuit
3.19	CSB pattern element #10 short circuit
3.20	SBO pattern element #10 short circuit
3.21	CSB pattern element #11 short circuit
3.22	SBO pattern element #11 short circuit
3.23	CSB pattern element #13 short circuit
3.24	SBO pattern element #13 short circuit
3.25	CSB pattern element #14 short circuit
3.26	SBO pattern element #14 short circuit
3.27	CSB pattern 3dB error in board #1
3.28	SBO pattern 3dB error in board #1
3.29	CSB pattern 38° phase error in board #1
3.30	SBO pattern 38° phase error in board #1
3.31	CSB pattern 3dB error in board #7
3.32	SBO pattern 3dB error in board #7
3.33	CSB pattern 38° phase error in board #7
3.34	SBO pattern 38° phase error in board #7

The effects of various faults can best be understood by making reference to the relative amplitude distribution across the array. Figure 3-40 shows both the CSB and SBO amplitudes. The CSB has a maximum at the array center (elements 12 through 17), and is very nearly a cosine on a pedestal. As one would expect, perturbation of these elements will produce the greatest effect on the CSB pattern. The SBO pattern has heavily driven elements near the ends (elements 1-4 and 25-28). These elements primarily determine the SBO guidance lobes and the depth of the guidance null. The center elements for SBO (elements 13-16) do critically

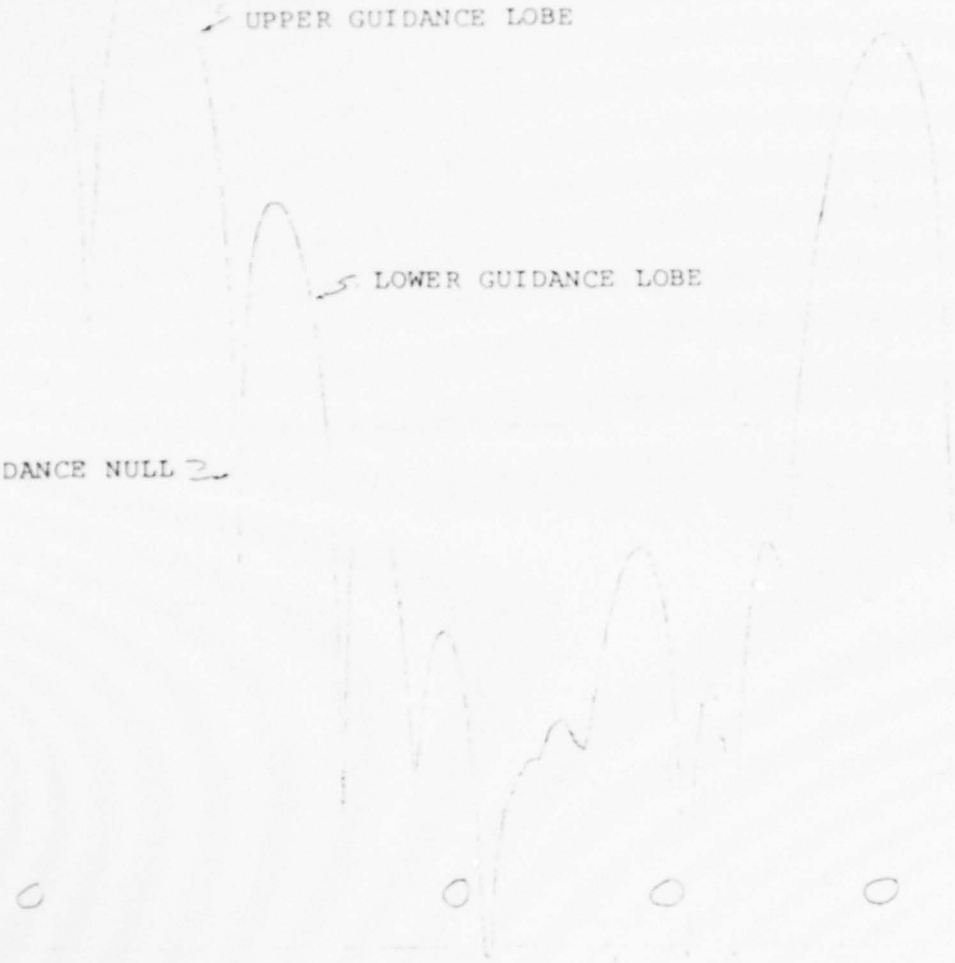

FIGURE 3.1 - SBO PATTERN FOR NORMAL (NO FAULT)

3.2 - SBO PATTERN ELEMENT #1 OPEN CIRCUIT

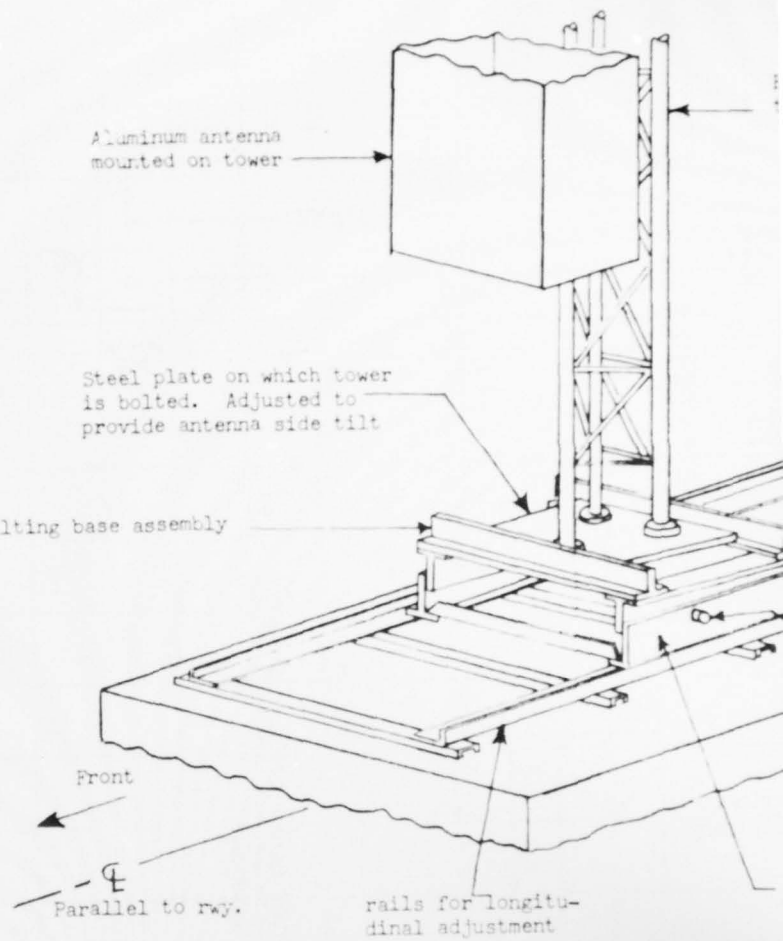

Figure 2-43 Antenna Base Assembly

AD-A077 042 WESTINGHOUSE DEFENSE AND ELECTRONIC SYSTEMS CENTER B--ETC F/G 9/5
DIPOLE BROADSIDE GLIDE SLOPE ARRAY.(U)
MAY 79 R S LITTLEPAGE , R RAJNIC DOT-FA74WA-3353
UNCLASSIFIED FAA-RD-79-69 NL

2 OF 3
AD-
A077042

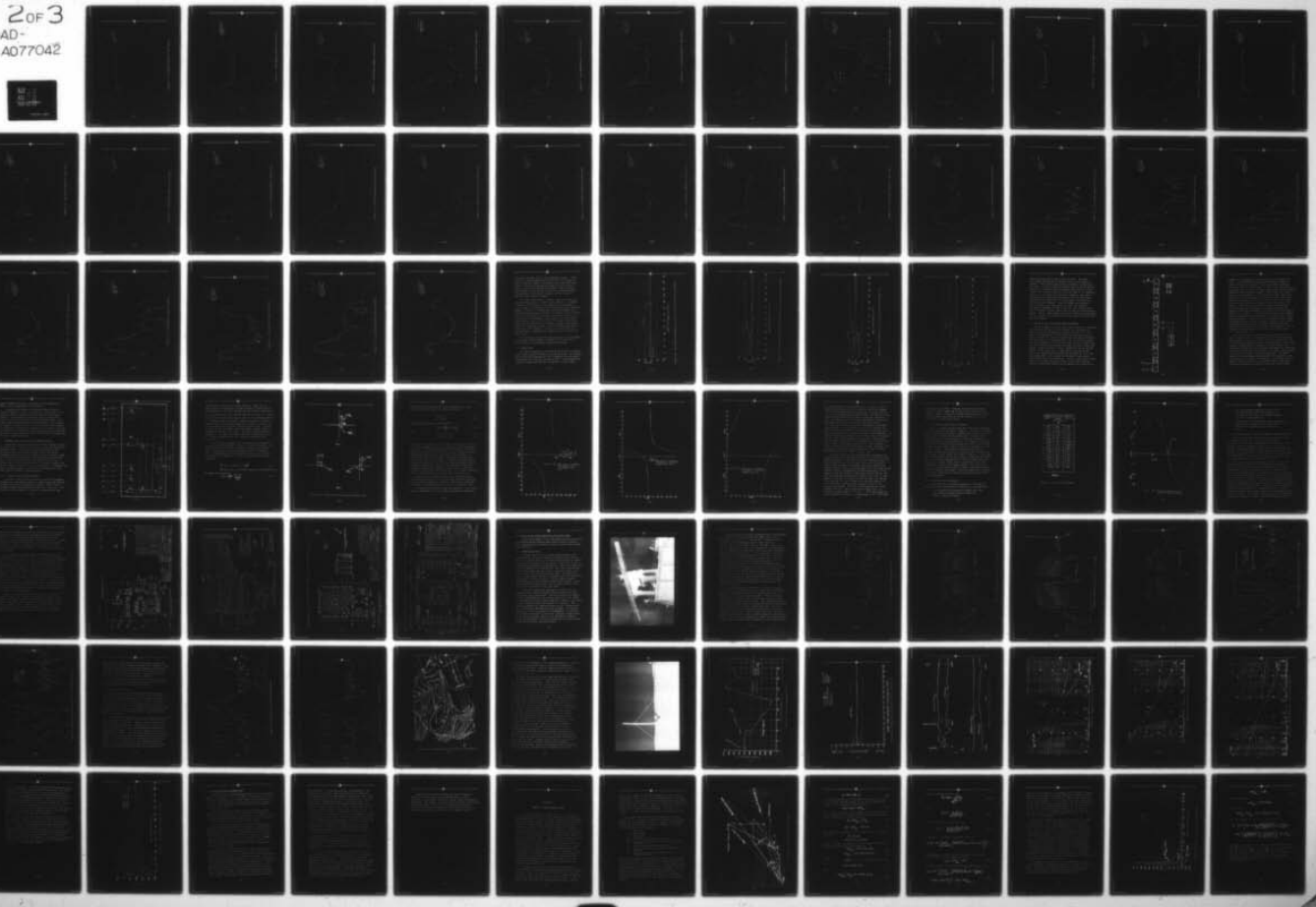

FIGURE 3.3 - SBO PATTERN ELEMENT #2 OPEN CIRCUIT

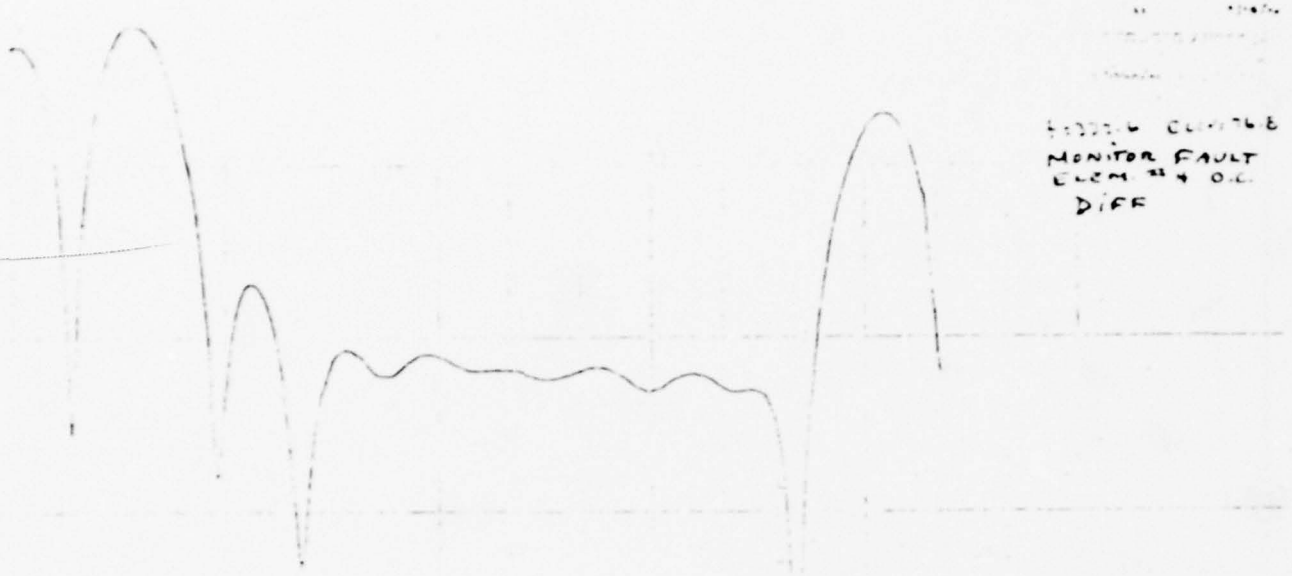

FIGURE 3.4 - SBO PATTERN ELEMENT #4 OPEN CIRCUIT

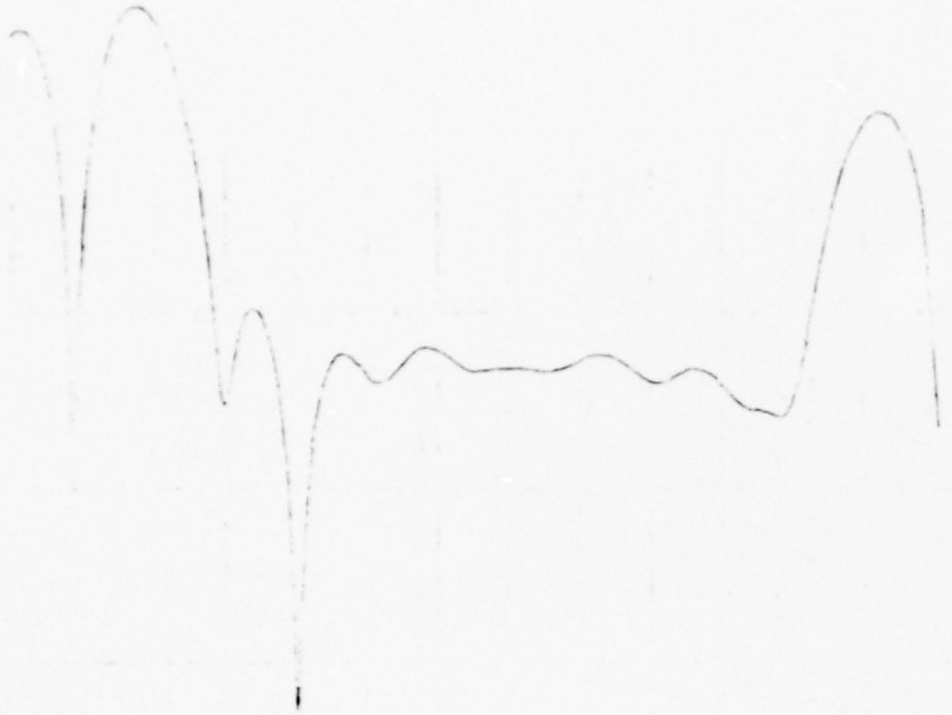

FIGURE 3.5 - SBO PATTERN ELEMENT #5 OPEN CIRCUIT

FIGURE 3.6 - SBO PATTERN ELEMENT #10 OPEN CIRCUIT

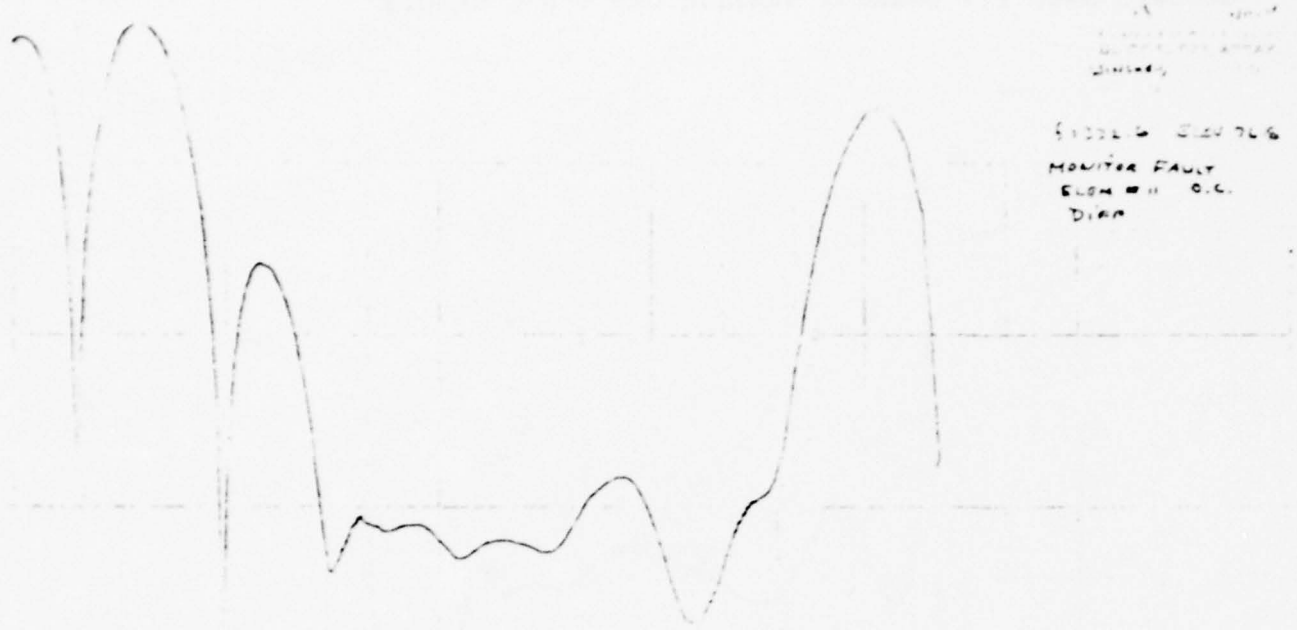

FIGURE 3.7 - SBO PATTERN ELEMENT #11 OPEN CIRCUIT

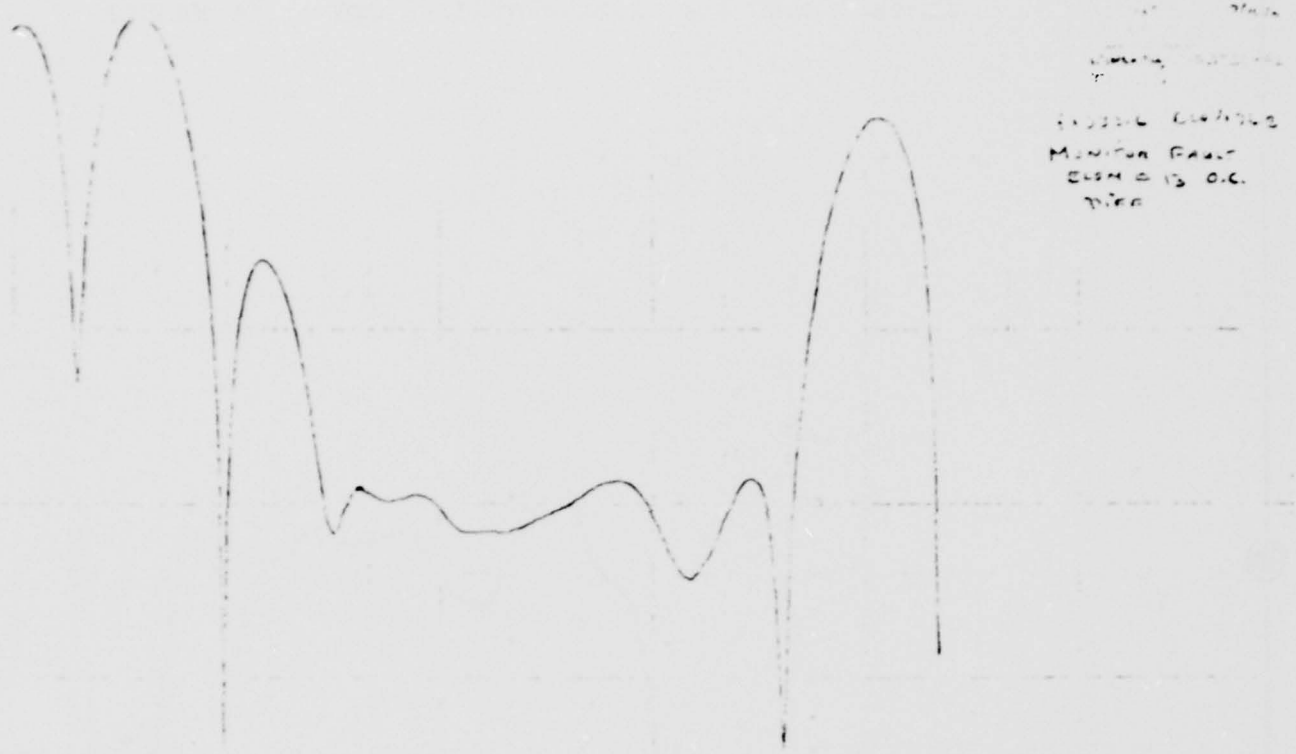

FIGURE 3.8 - SBO PATTERN ELEMENT #13 OPEN CIRCUIT

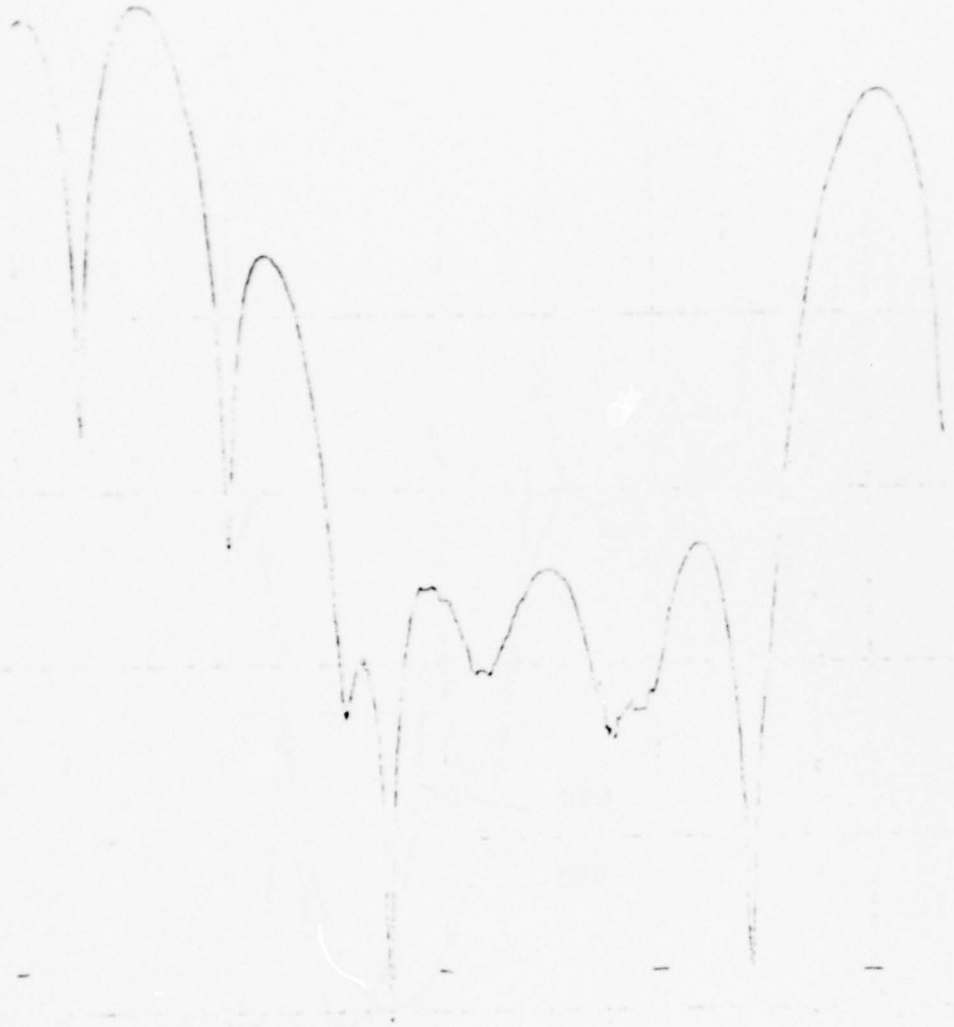

FIGURE 3.9 - SBO PATTERN ELEMENT #14 OPEN CIRCUIT

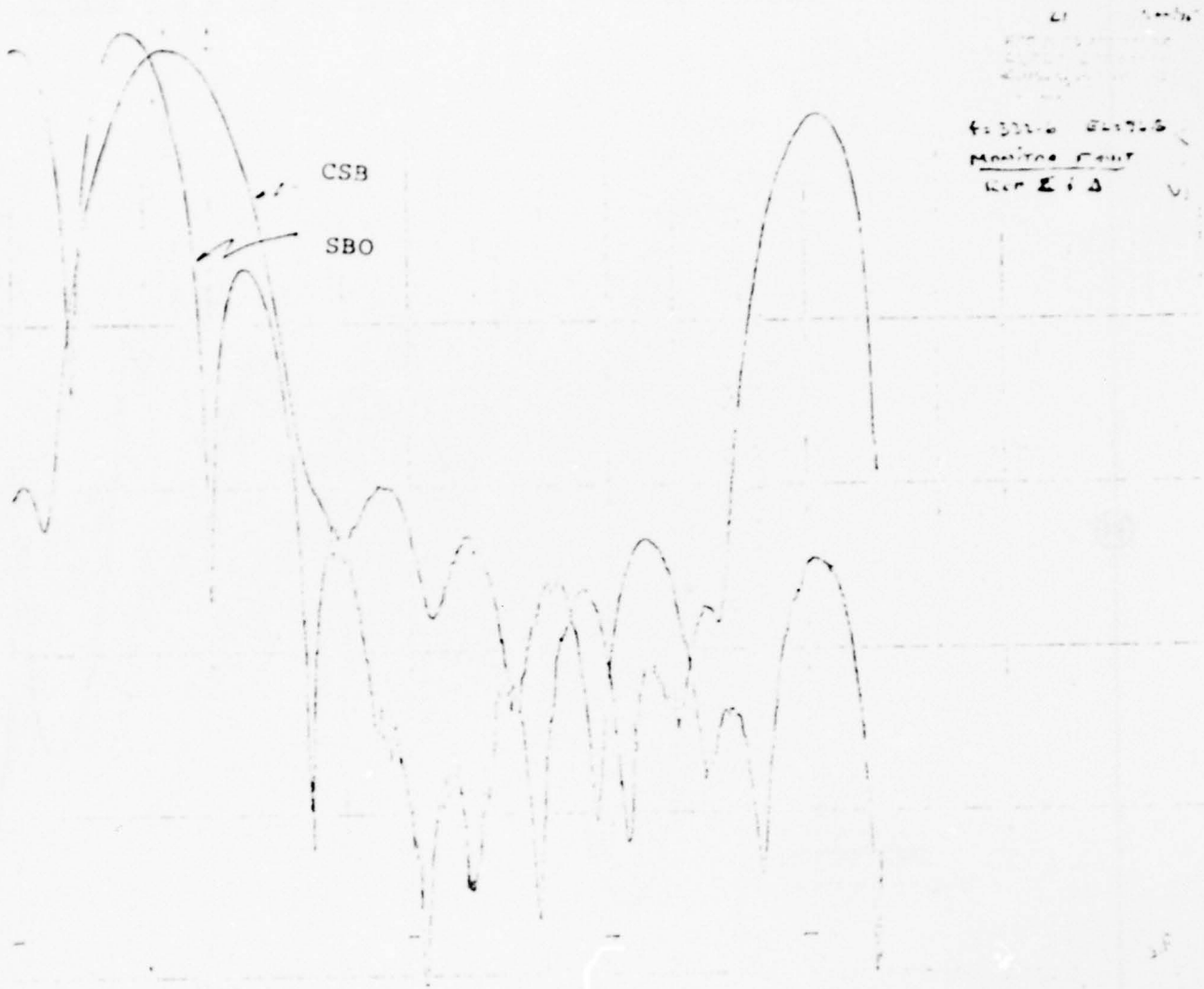

FIGURE 3.10 - CSB & SBO PATTERNS FOR NORMAL (NO FAULT)

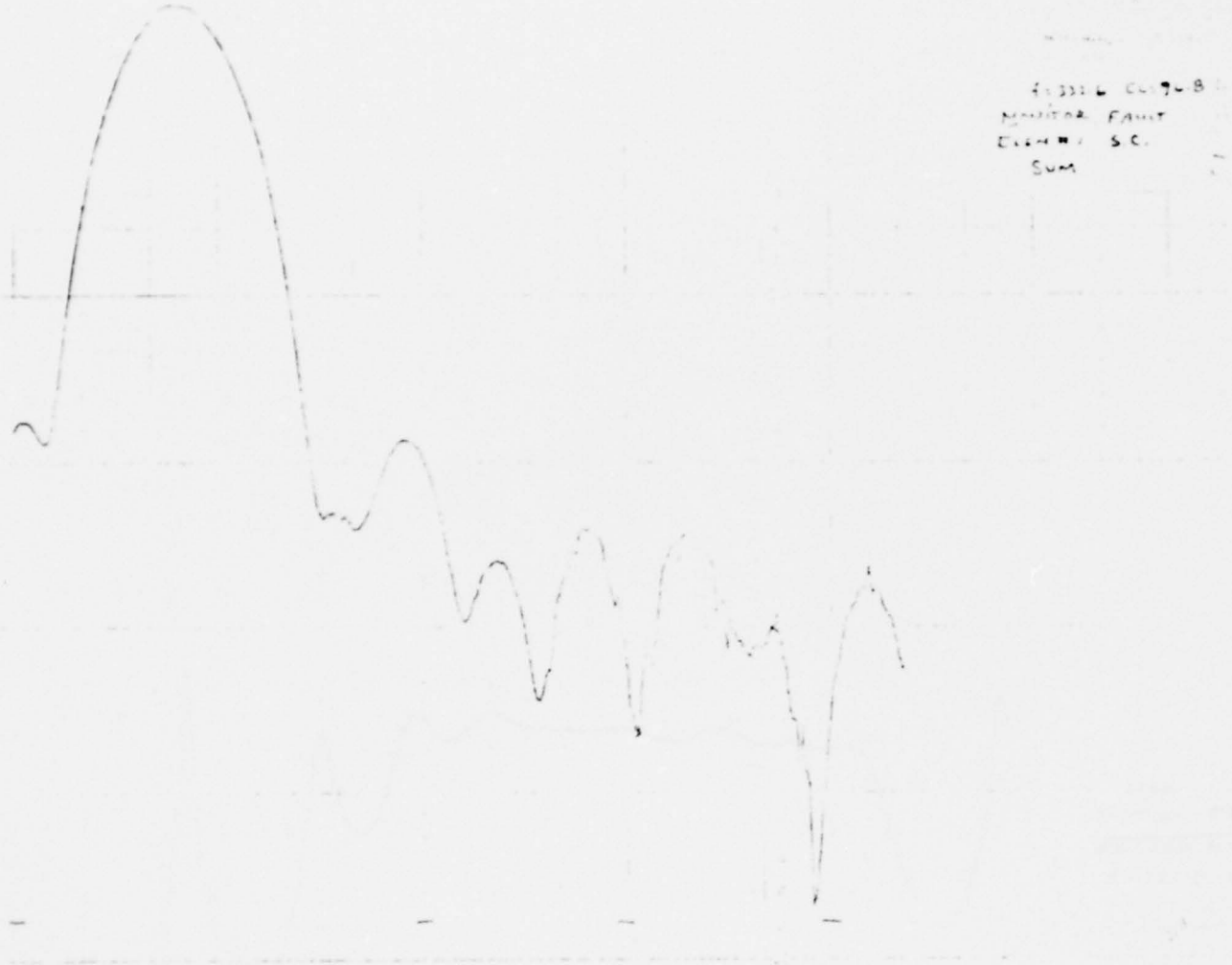

FIGURE 3.11 - CSB PATTERN ELEMENT #1 SHORT CIRCUIT

FIGURE 3.12 - SBO PATTERN ELEMENT #1 SHORT CIRCUIT

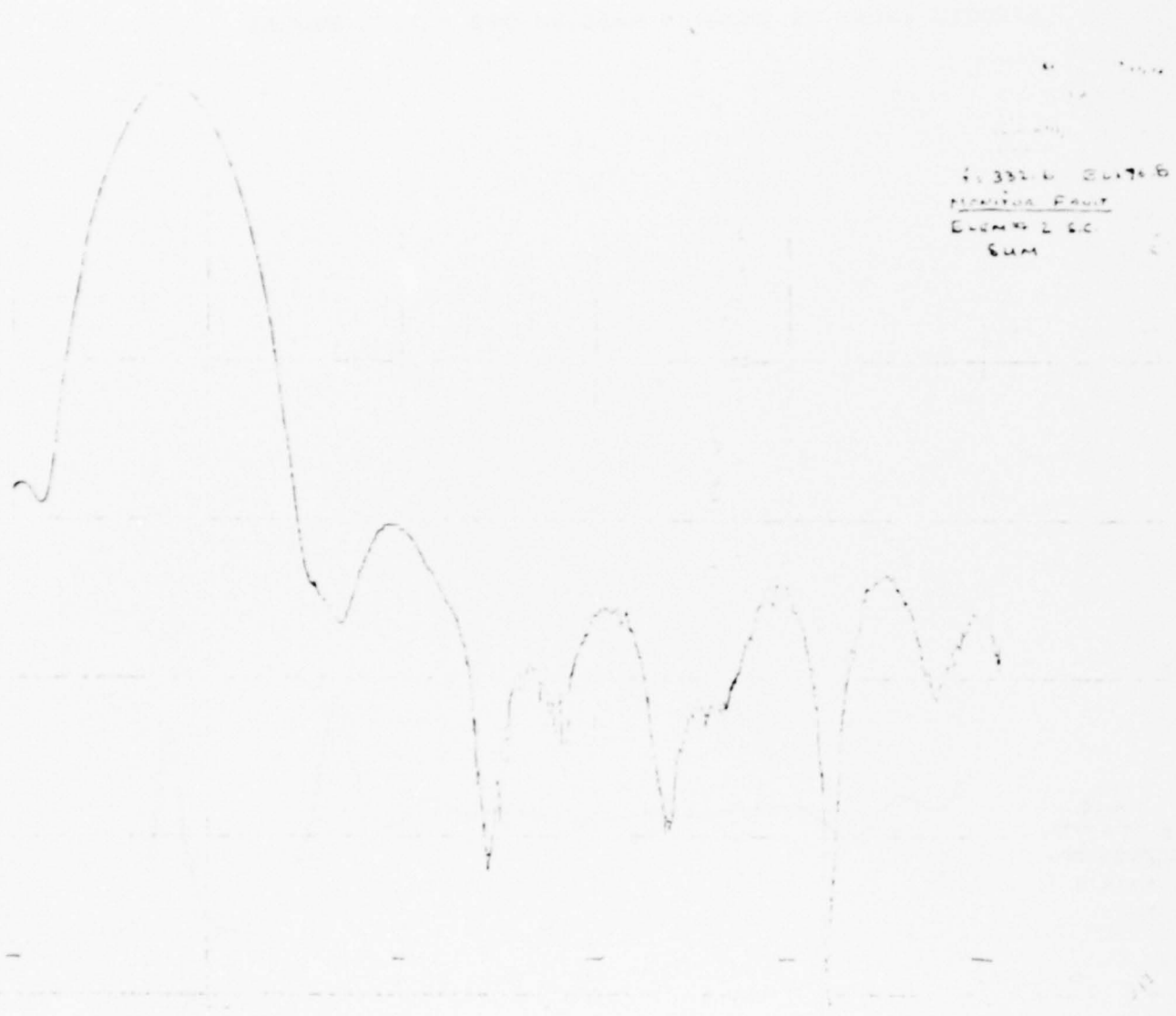

FIGURE 3.13 - CSB PATTERN ELEMENT #2 SHORT CIRCUIT

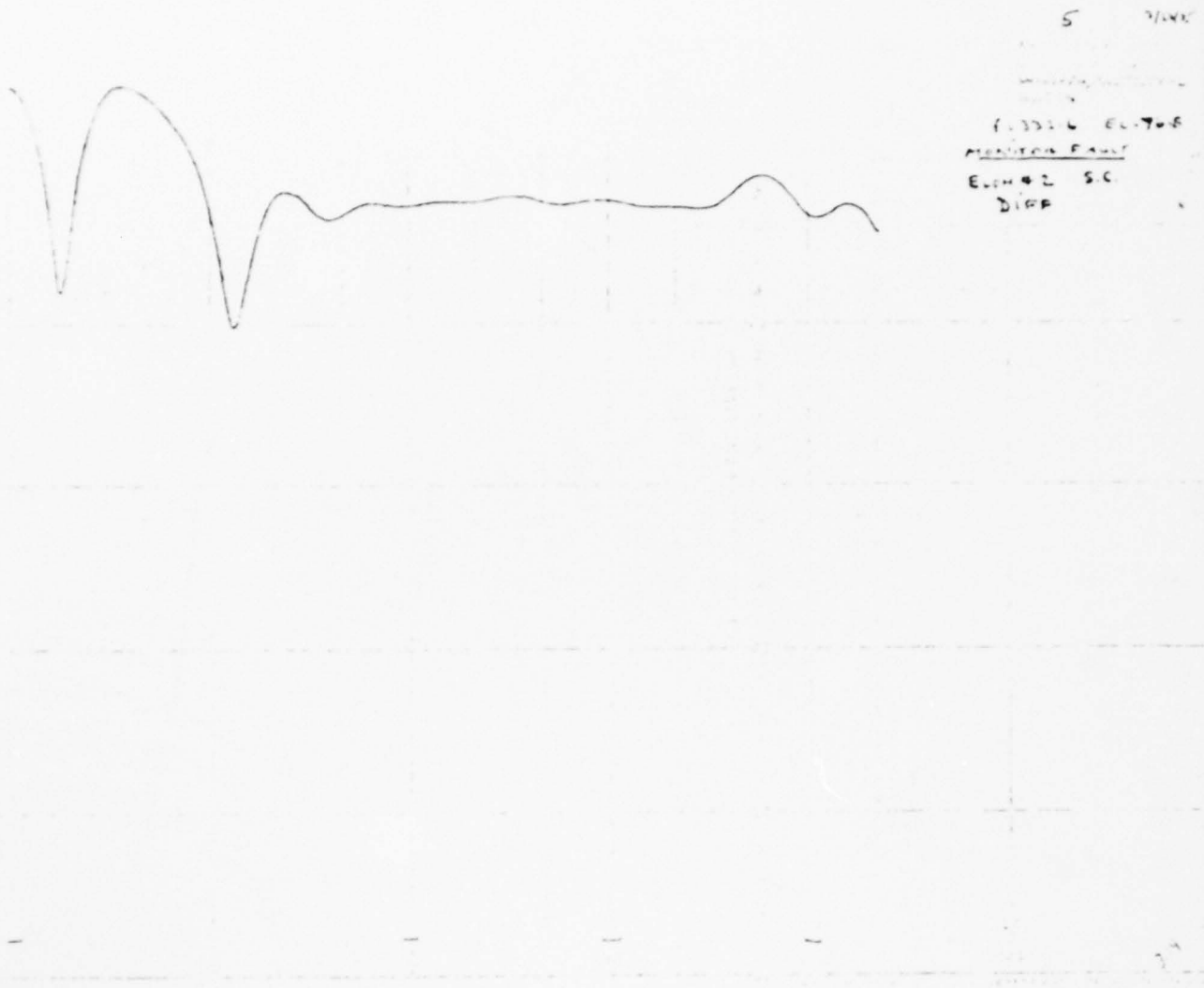

FIGURE 3.14 - SBO PATTERN ELEMENT #2 SHORT CIRCUIT

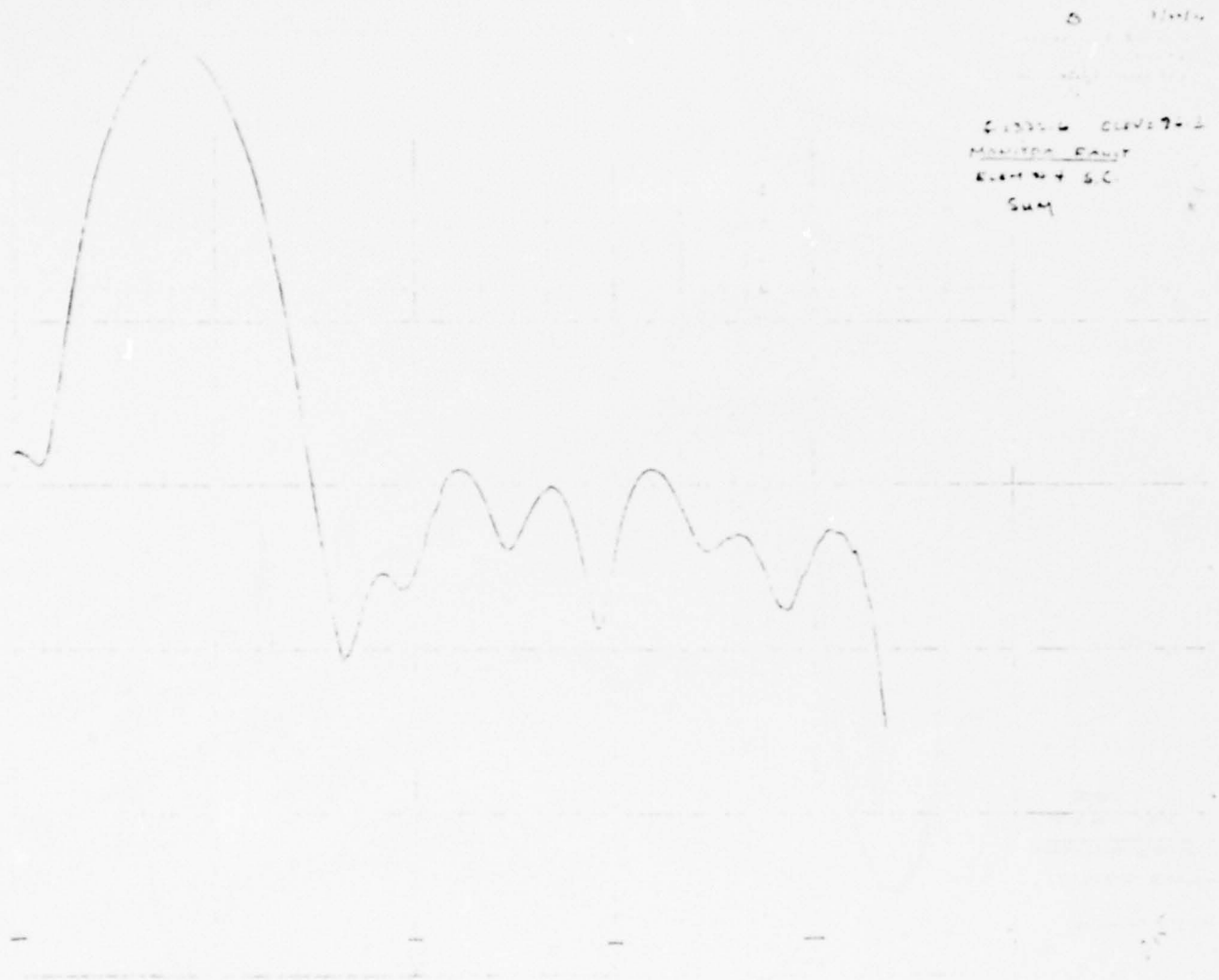

FIGURE 3.15 - CSB PATTERN ELEMENT #4 SHORT CIRCUIT

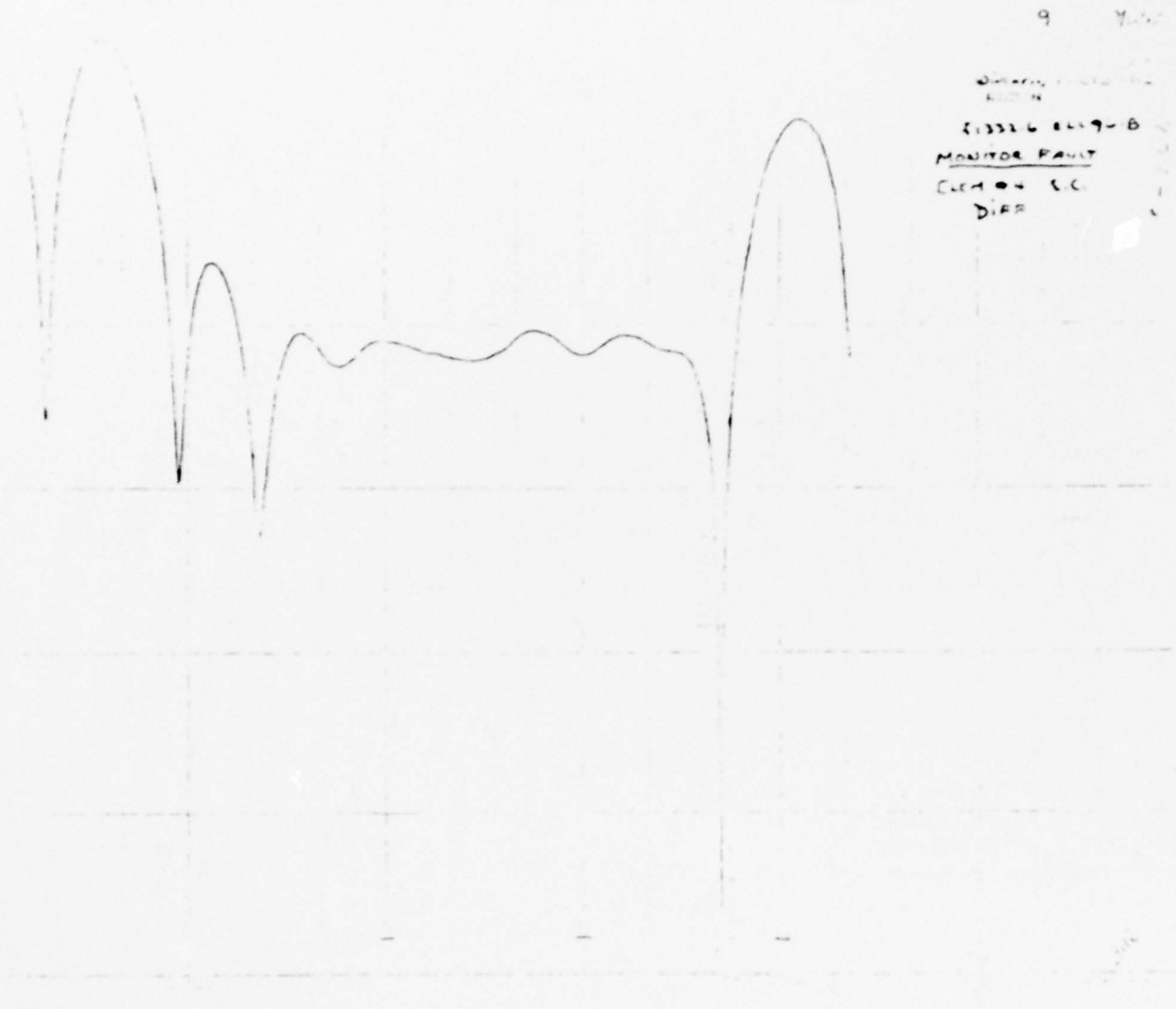

FIGURE 3.16 - SBO PATTERN ELEMENT #4 SHORT CIRCUIT

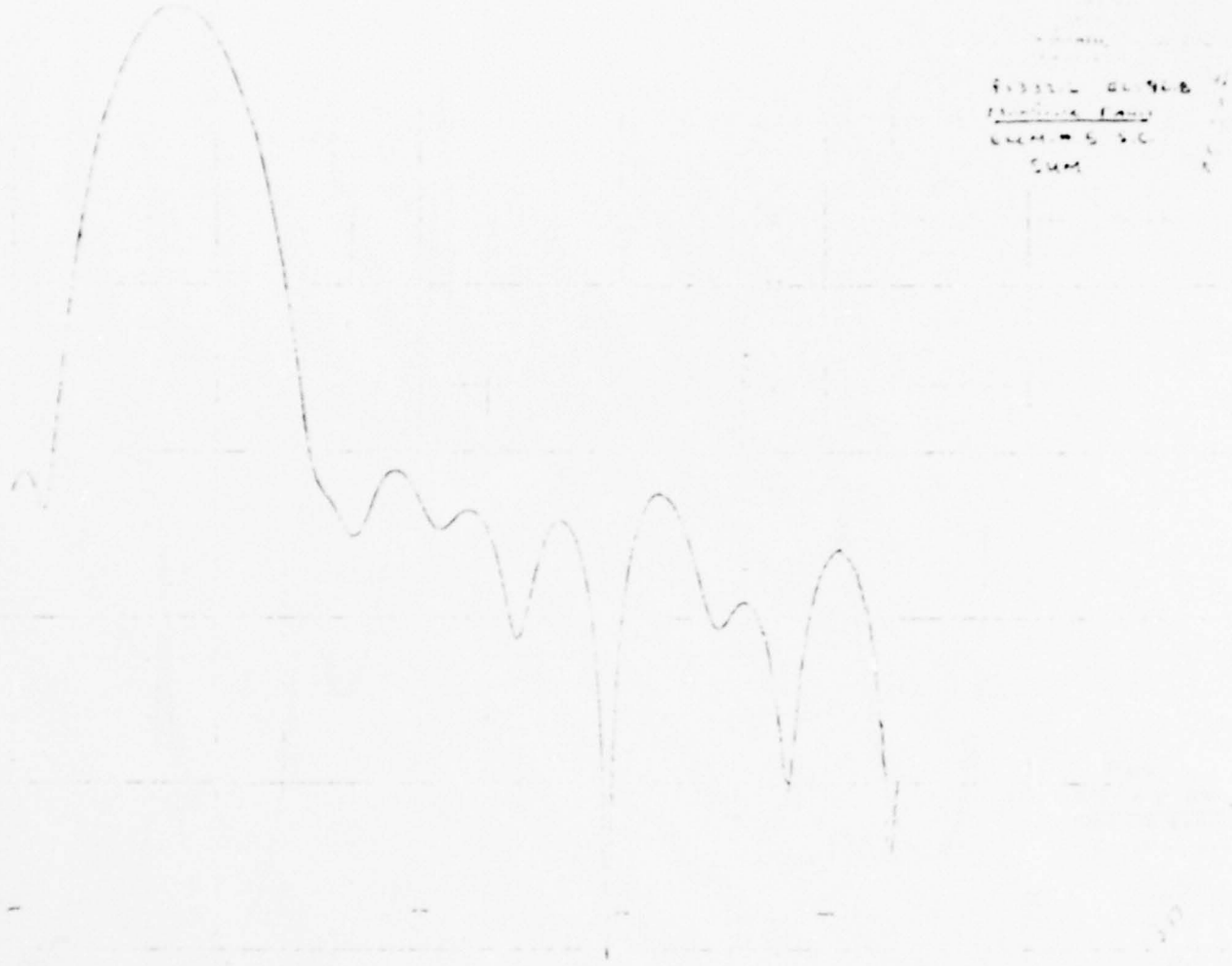

FIGURE 3.17 - CSB PATTERN ELEMENT #5 SHORT CIRCUIT

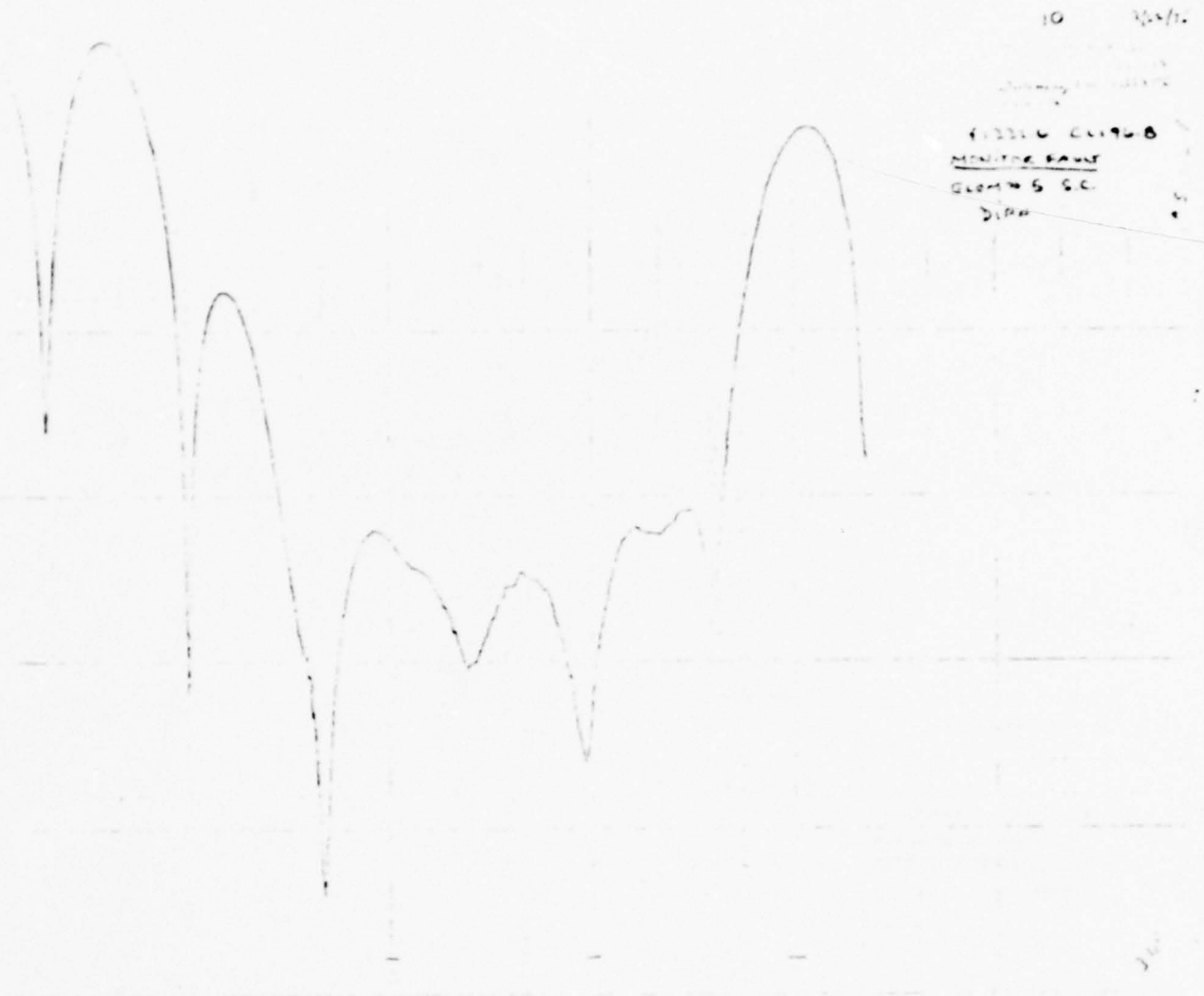

FIGURE 3.18 - SBO PATTERN ELEMENT #5 SHORT CIRCUIT

FIGURE 3.19 - CSB PATTERN ELEMENT #10 SHORT CIRCUIT

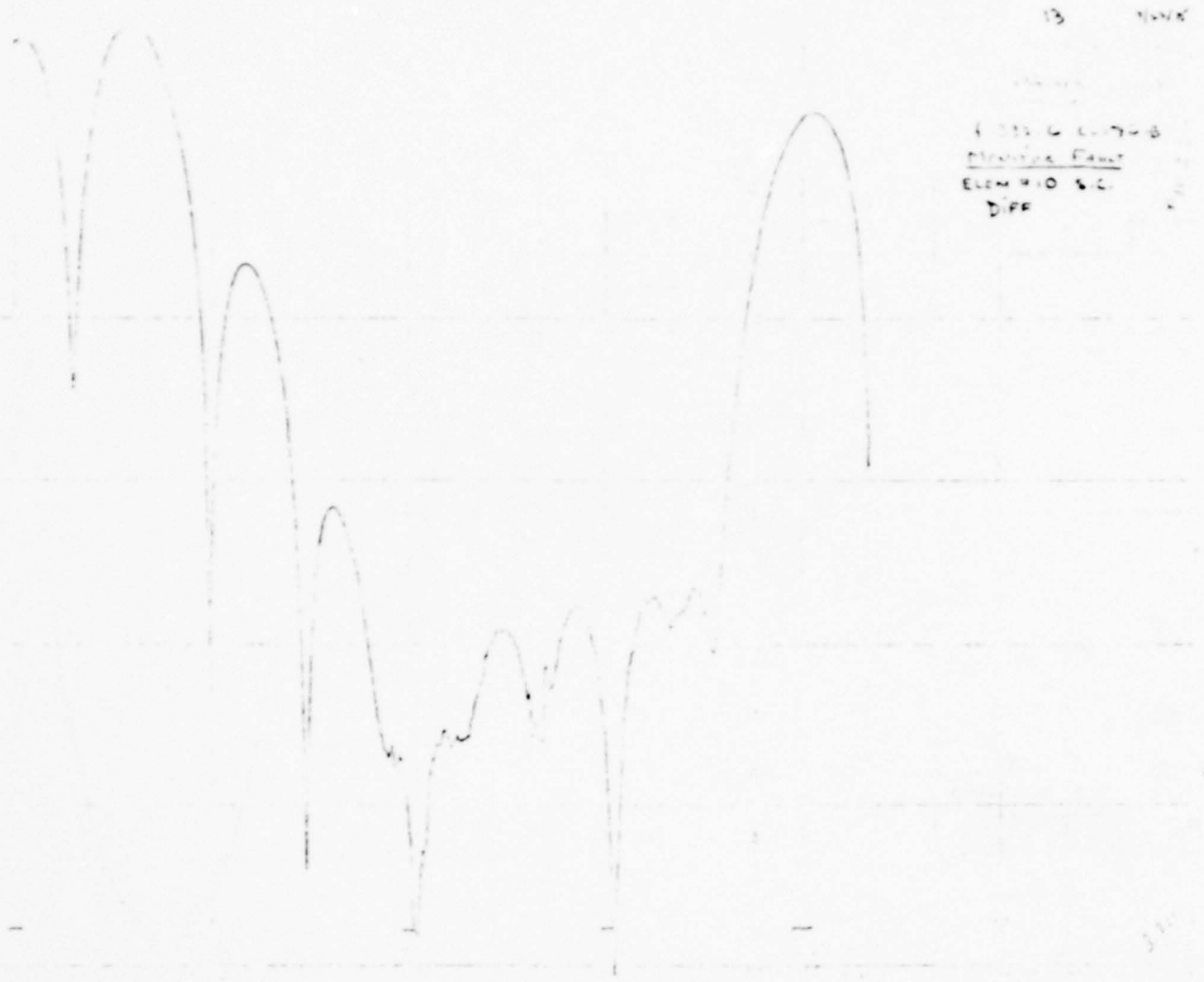

FIGURE 3.20 - SBO PATTERN ELEMENT #10 SHORT CIRCUIT

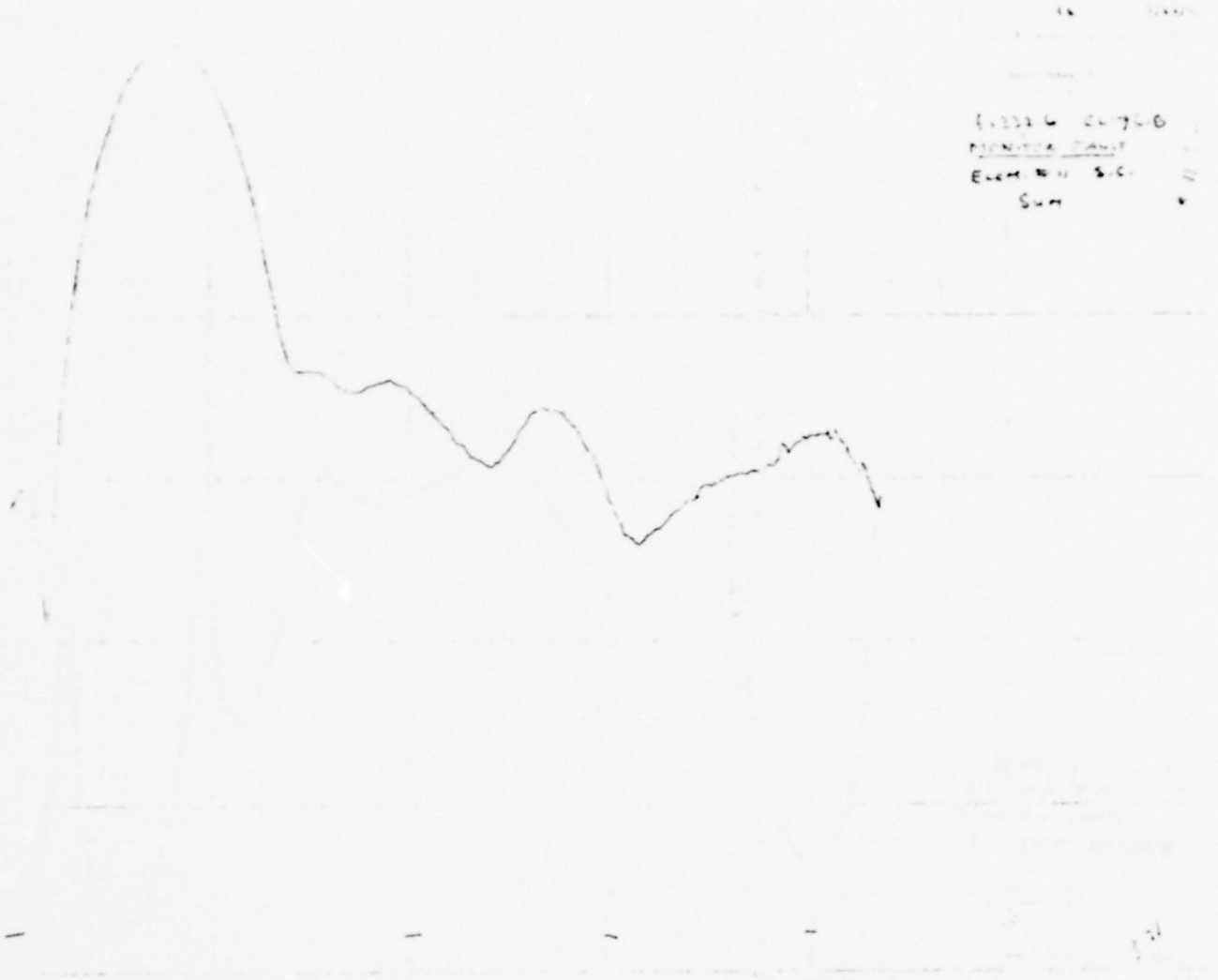

FIGURE 3.21 - CSB PATTERN ELEMENT #11 SHORT CIRCUIT

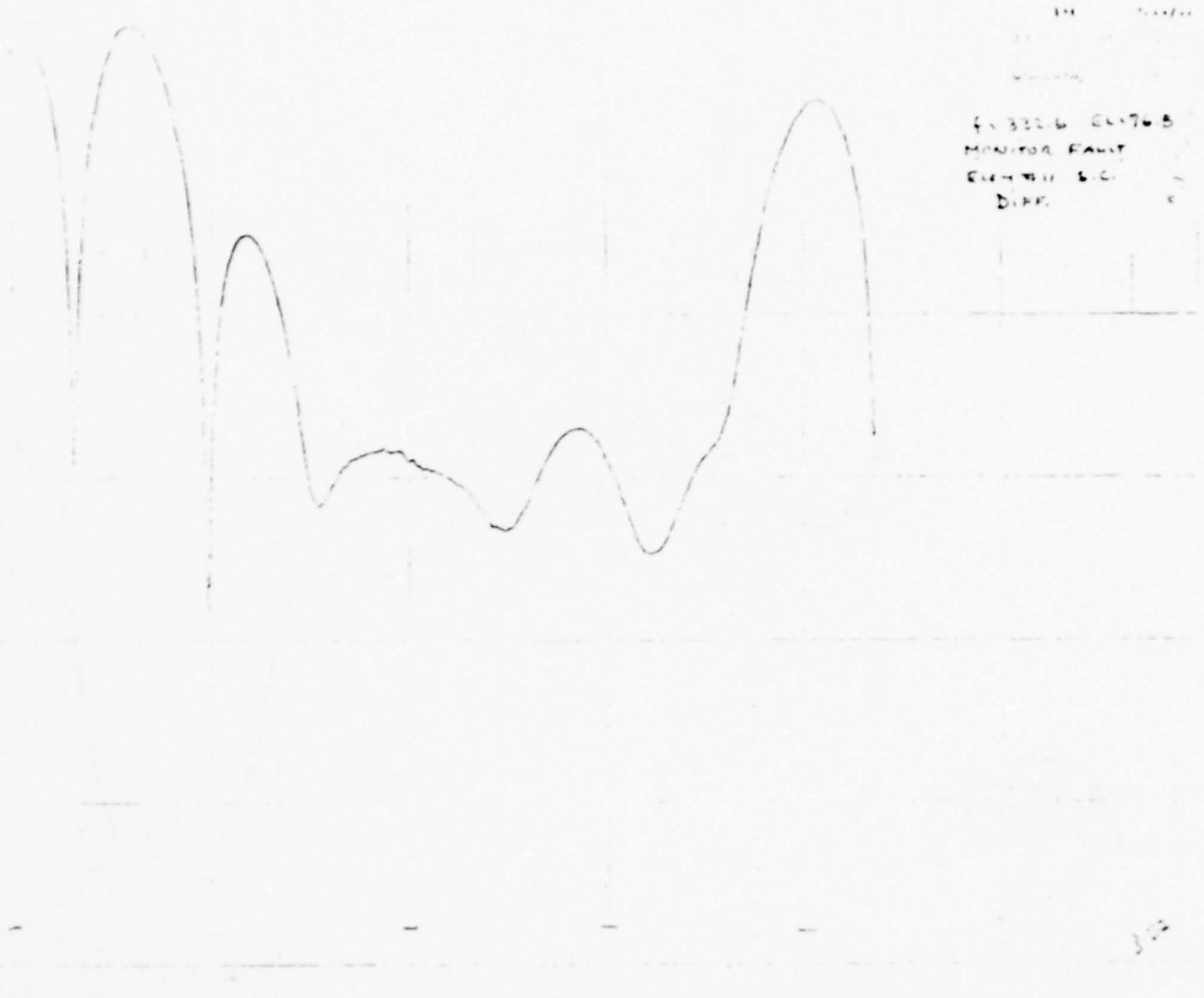

FIGURE 3.22 - SBO PATTERN ELEMENT #11 SHORT CIRCUIT

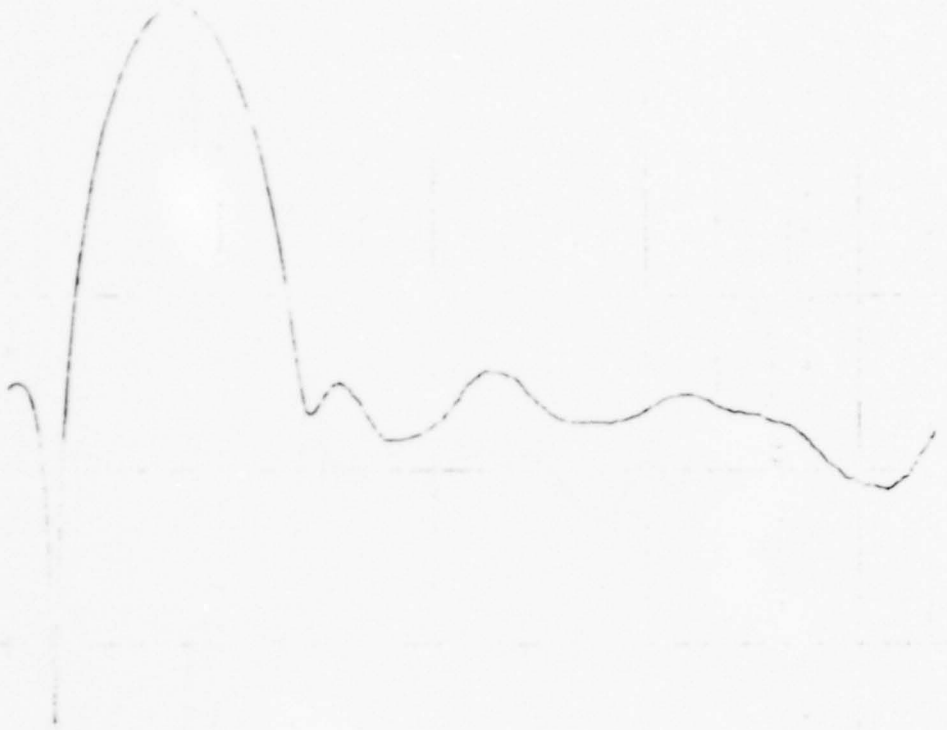

FIGURE 3.23 - CSB PATTERN ELEMENT #13 SHORT CIRCUIT

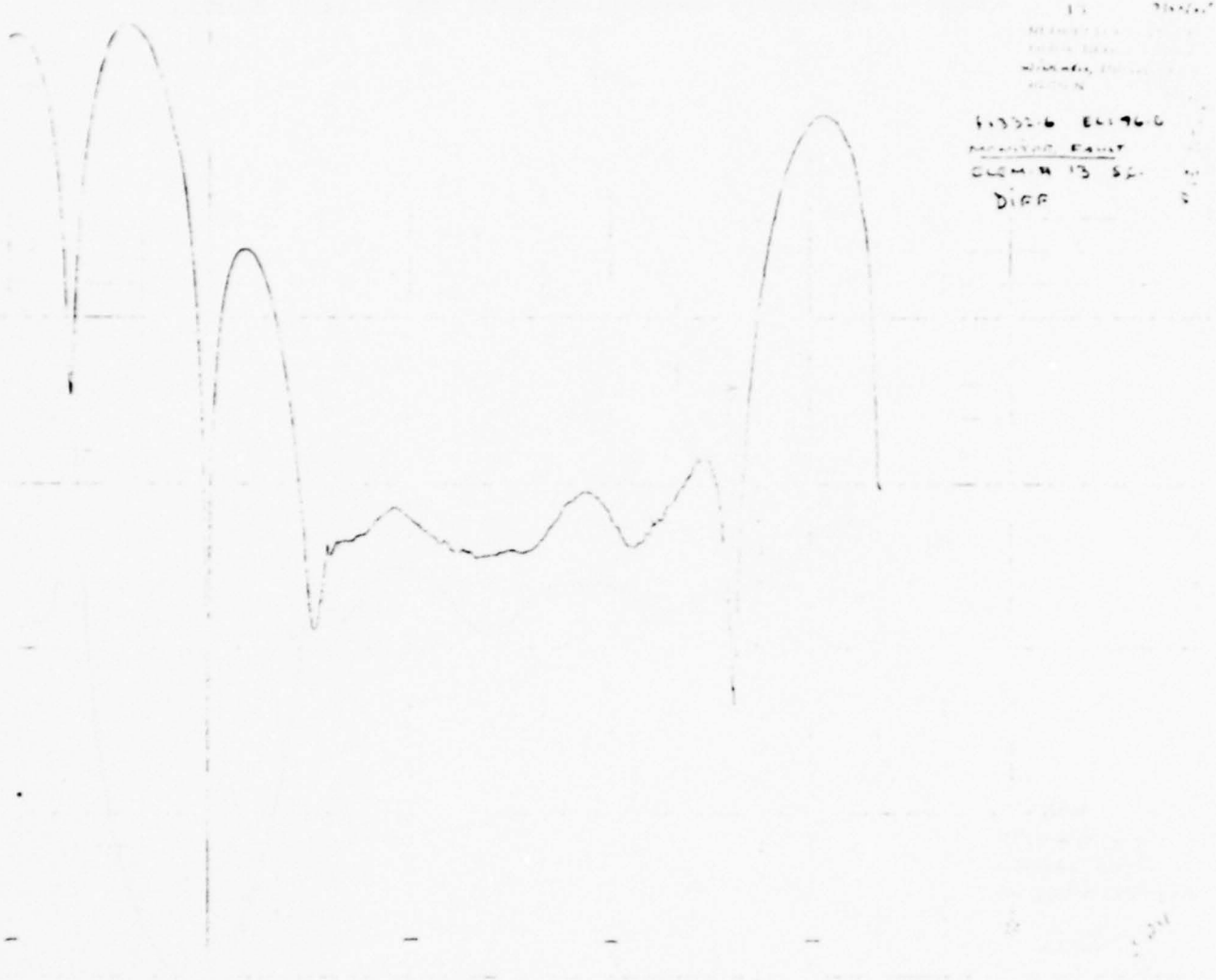

FIGURE 3.24 - SBO PATTERN ELEMENT #13 SHORT CIRCUIT

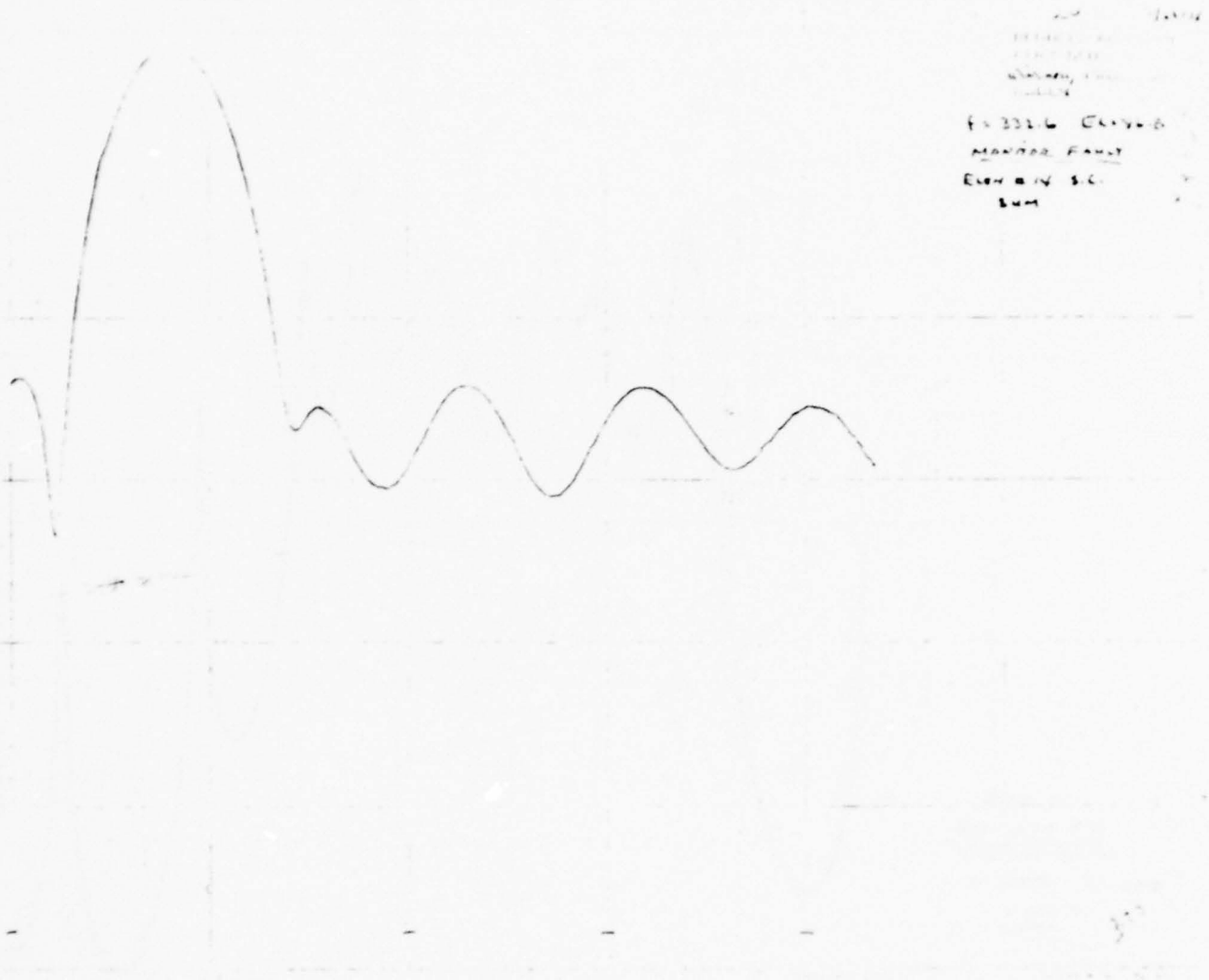

FIGURE 3.25 - CSB PATTERN ELEMENT #14 SHORT CIRCUIT

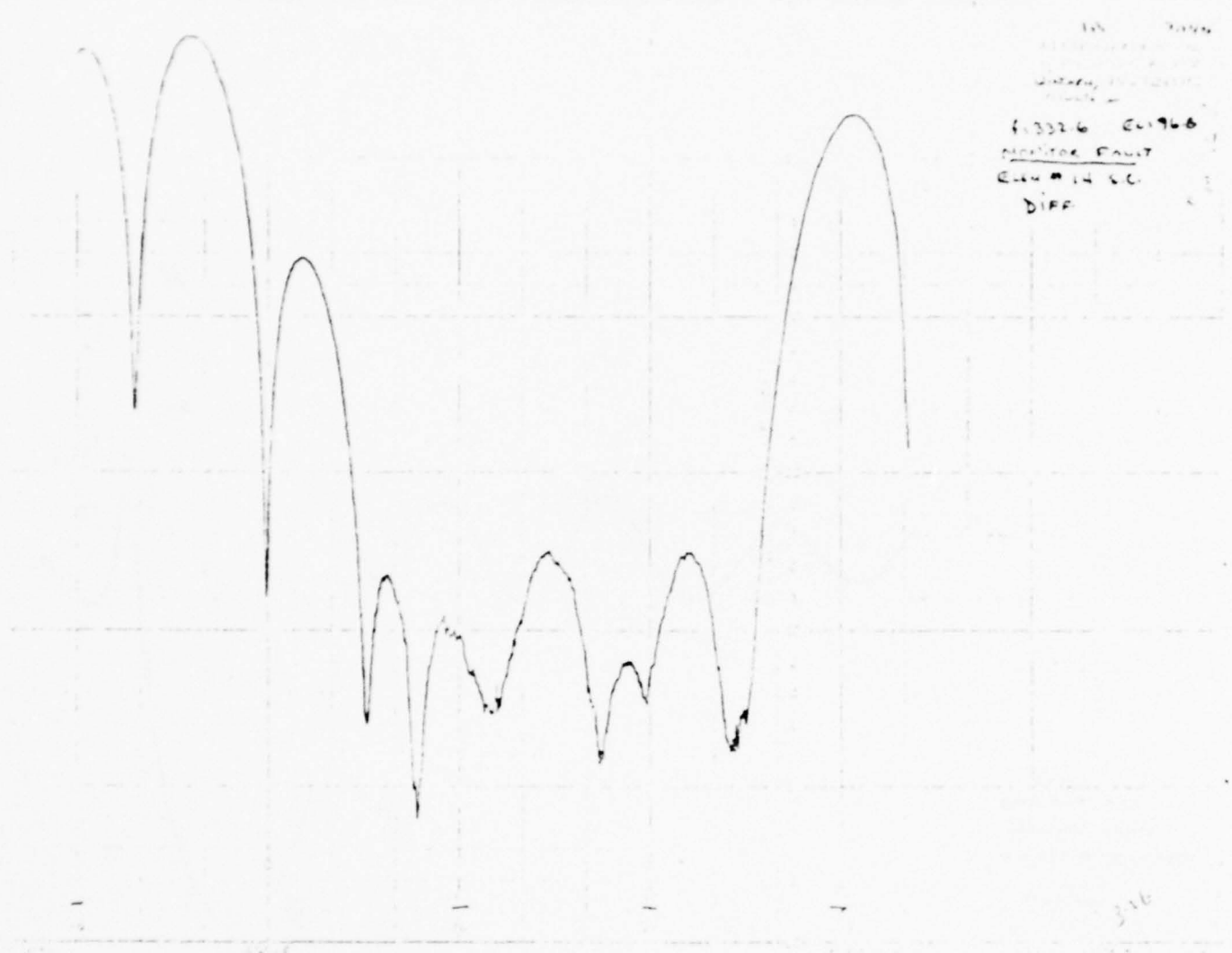

FIGURE 3.26 - SBO PATTERN ELEMENT #14 SHORT CIRCUIT

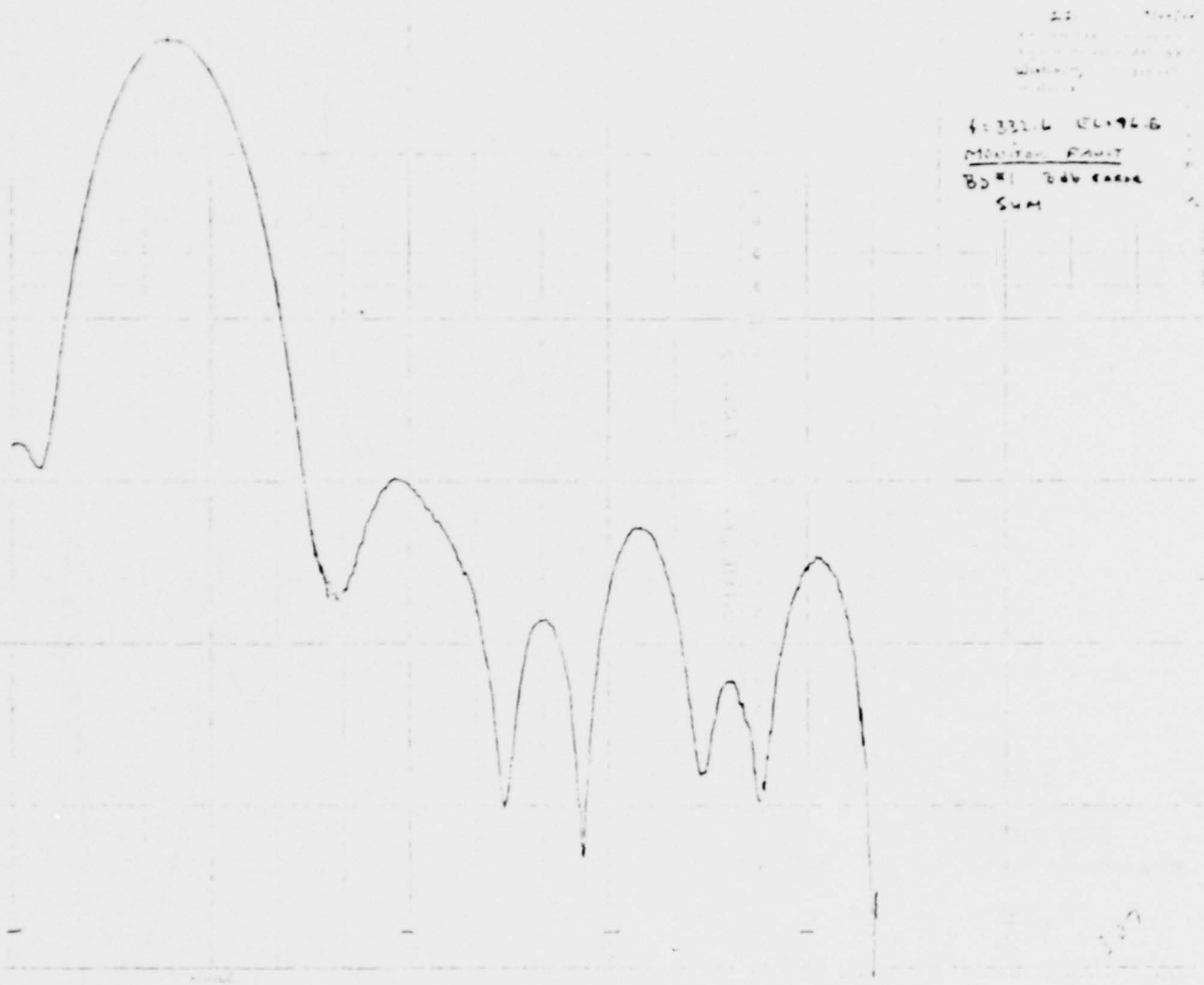

FIGURE 3.27 - CSB PATTERN 3DB ERROR IN BOARD #1

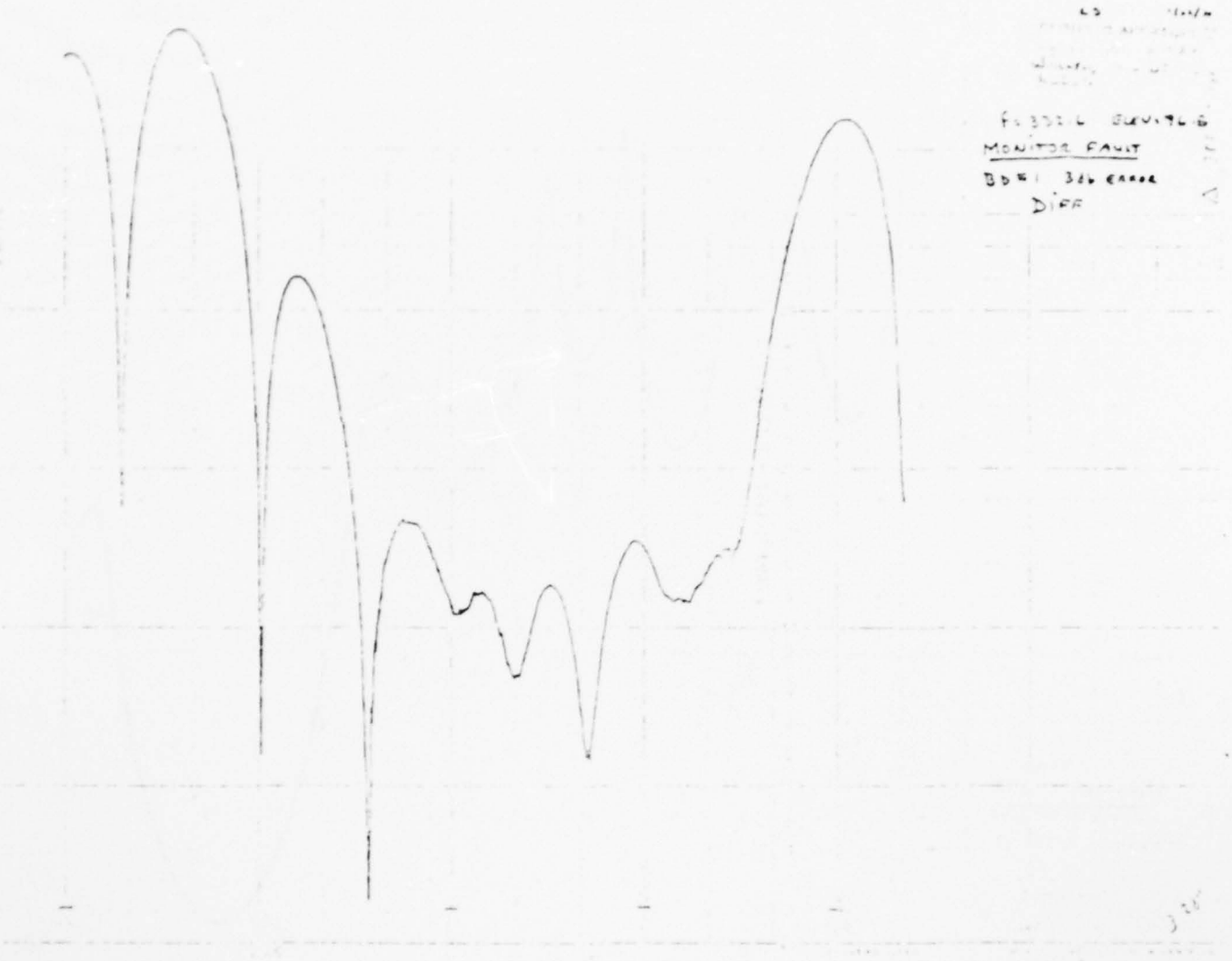

FIGURE 3.28 - SBO PATTERN 3DB ERROR IN BOARD #1

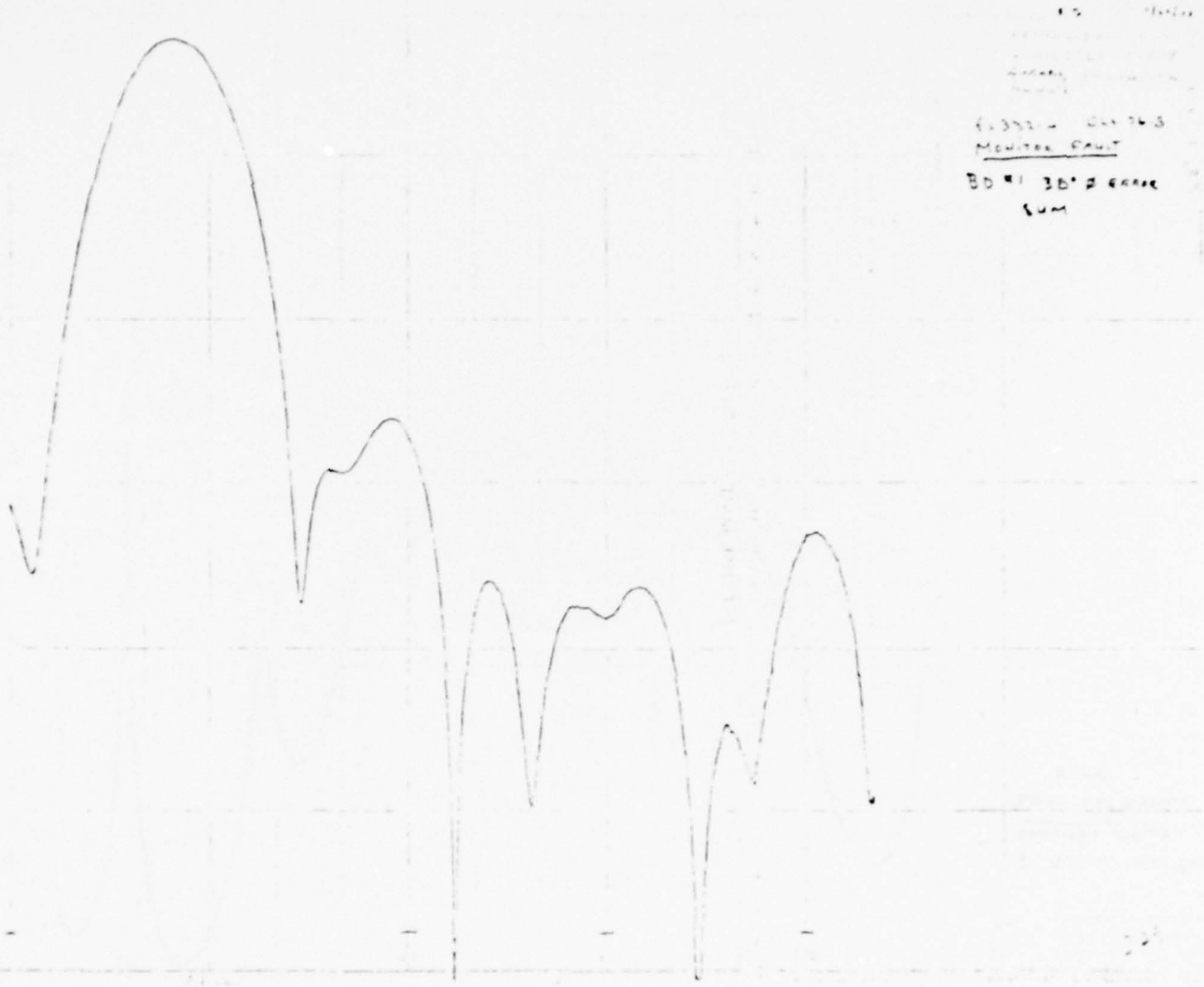

FIGURE 3.29 - CSB PATTERN 38° PHASE ERROR IN BOARD #1

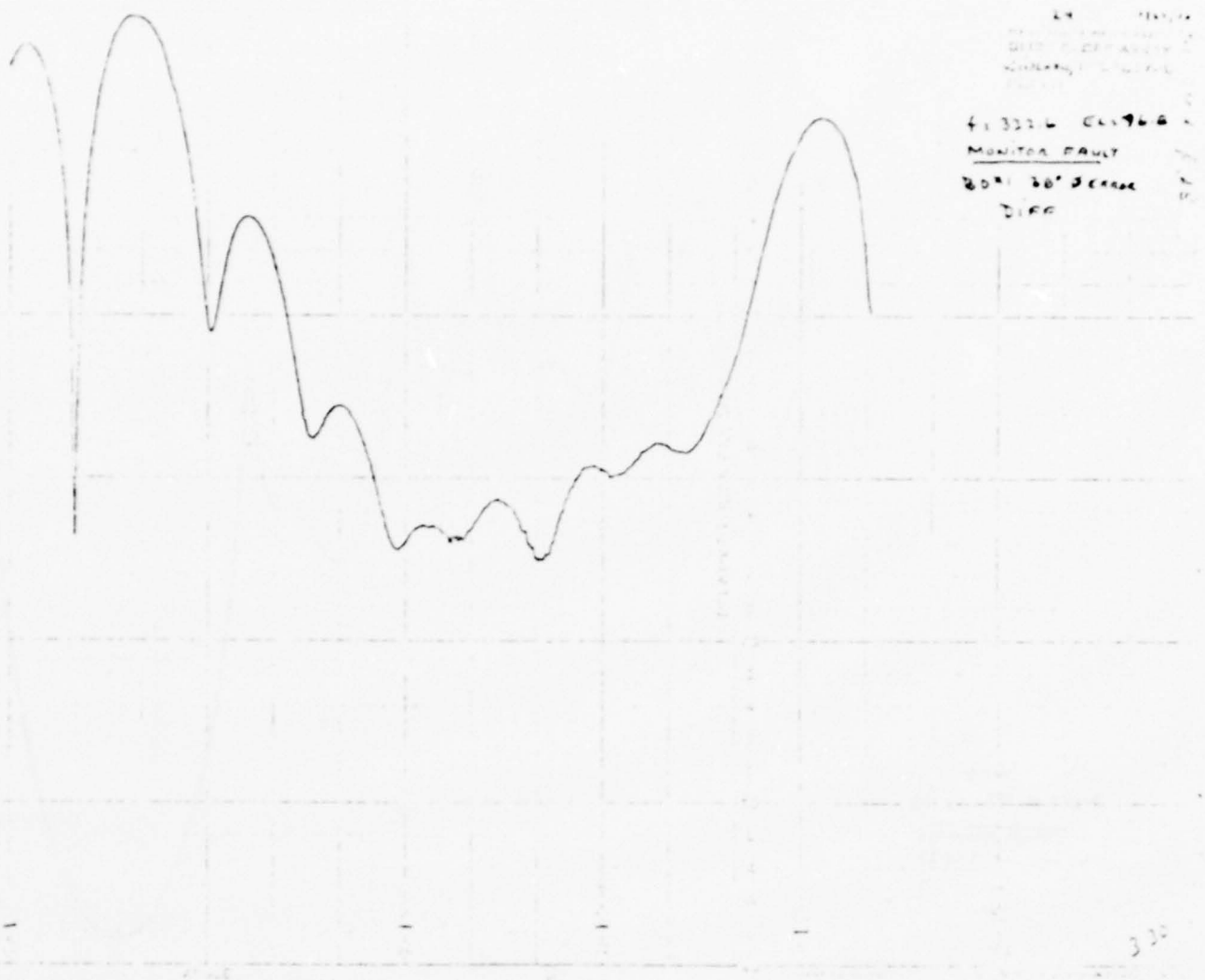

FIGURE 3.30 - SBO PATTERN 38° PHASE ERROR IN BOARD #1

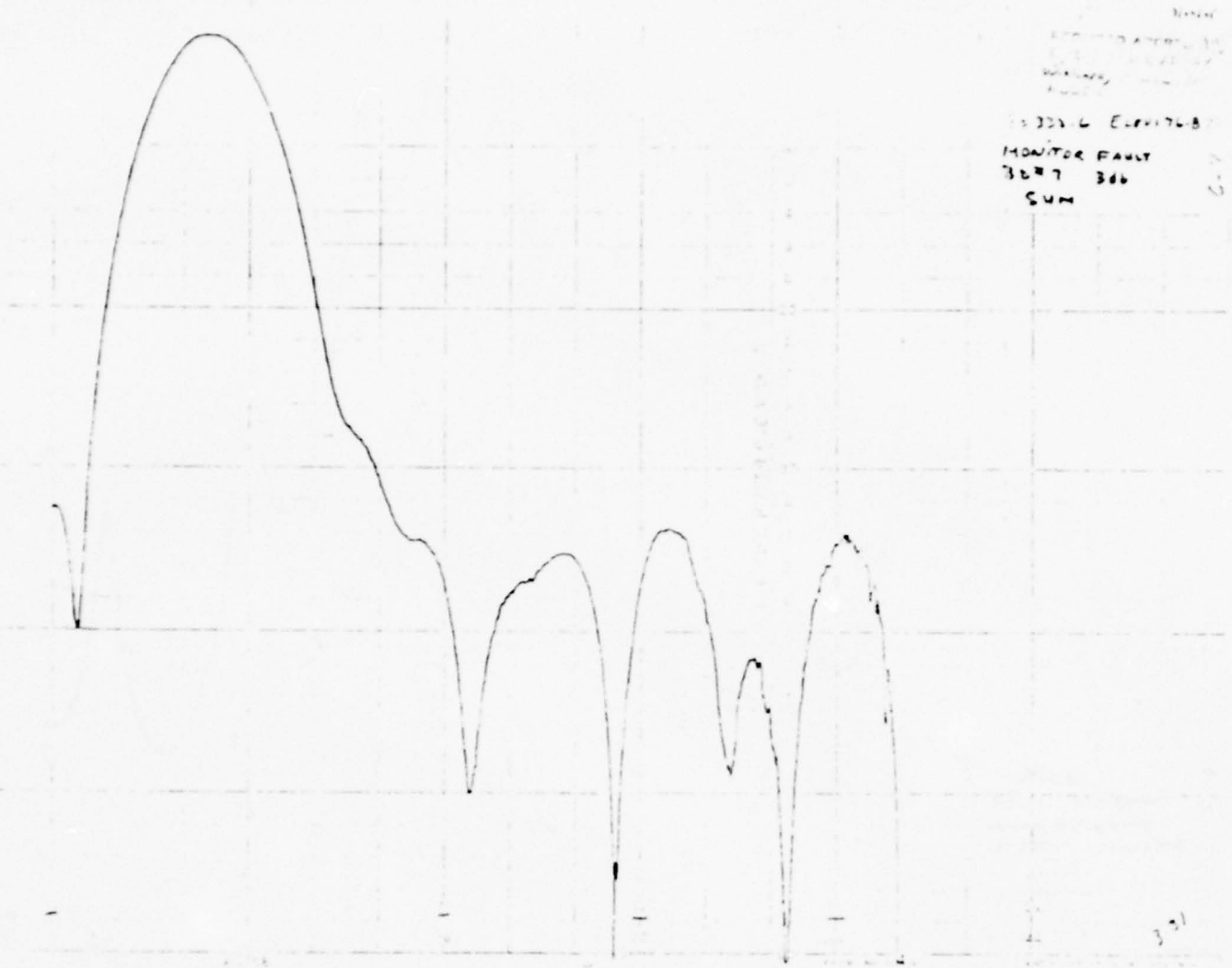

FIGURE 3.31 - CSB PATTERN 3DB ERROR IN BOARD #7

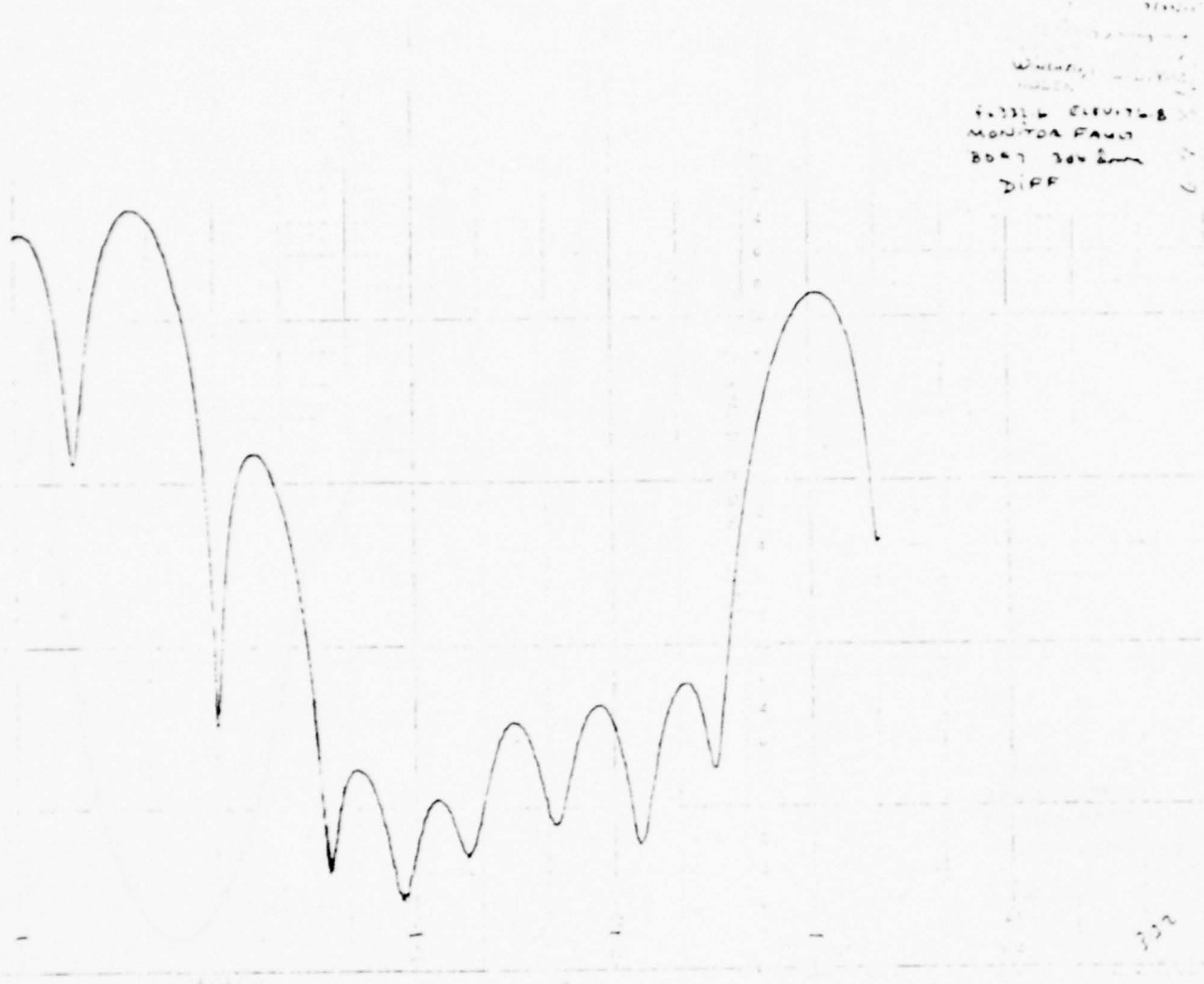

FIGURE 3.32 - SBO PATTERN 3DB ERROR IN BOARD #7

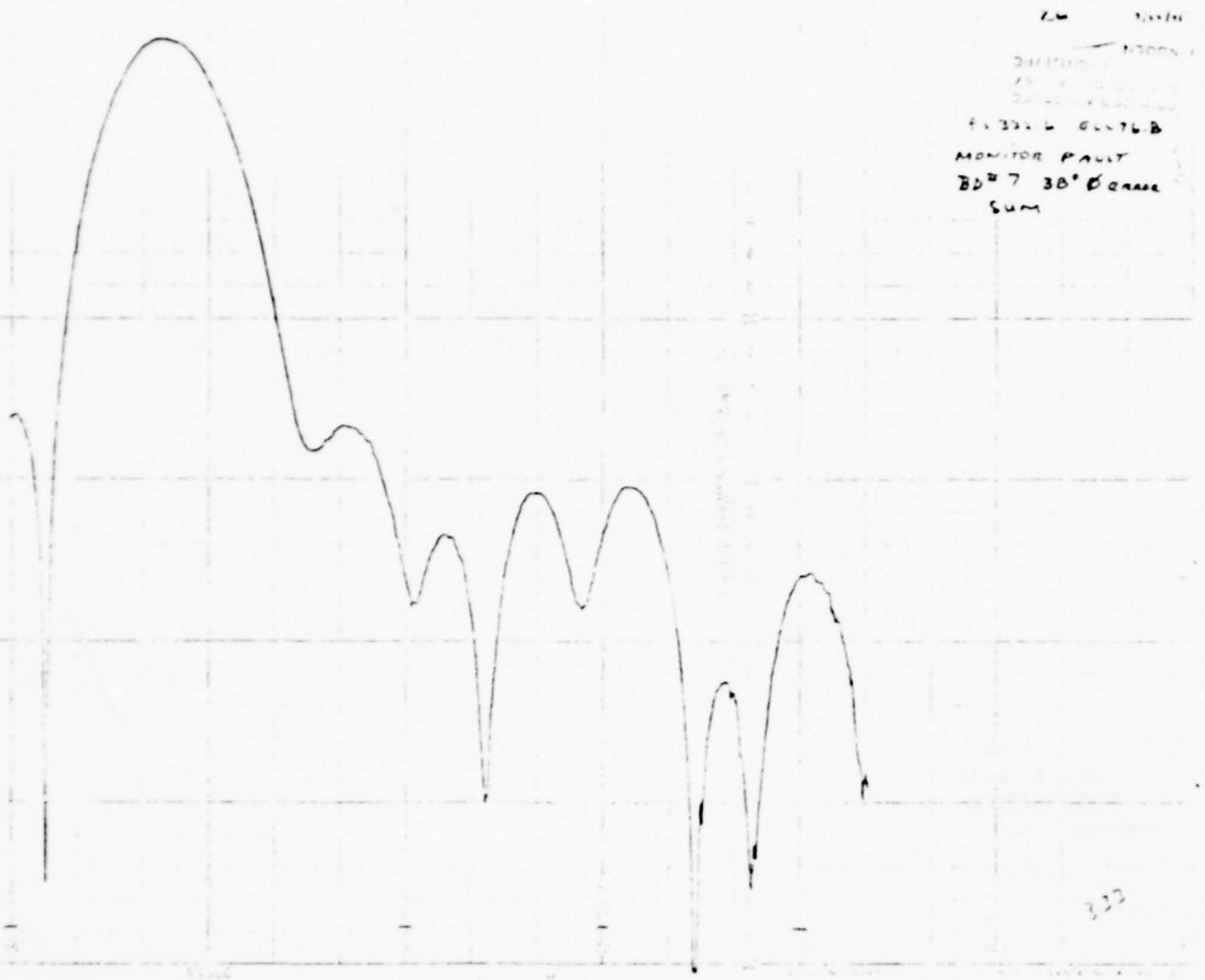

FIGURE 3.33 - CSB PATTERN 38° PHASE ERROR IN BOARD #7

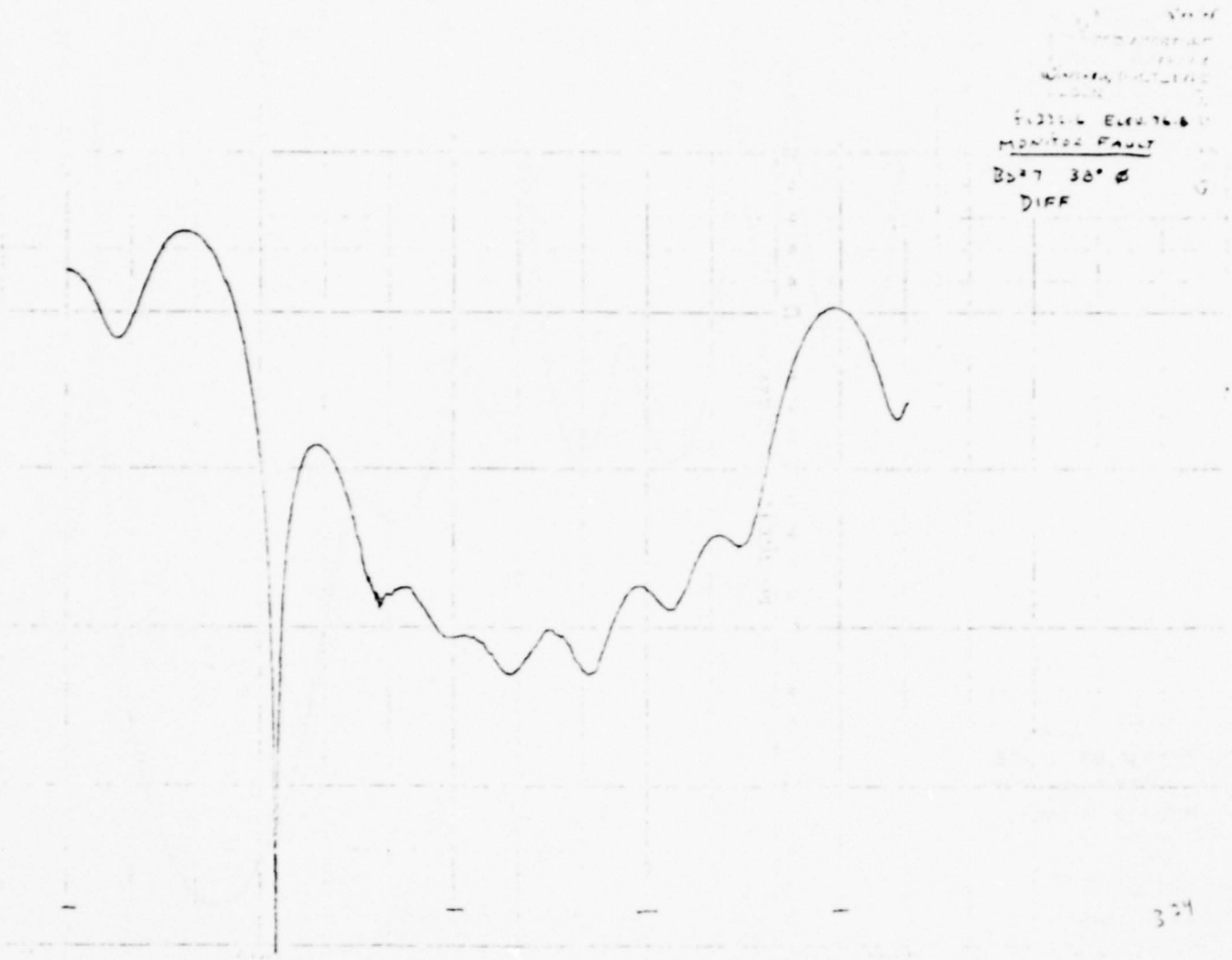

FIGURE 3.34 - SBO PATTERN 38° PHASE ERROR IN BOARD #7

effect the sidelobe level in the surpressed region. Hence, an error in these elements will only effect the flyability based on how the pattern interacts with the particular site terrain. The same considerations apply to the analysis of faults in particular distribution boards. Based on these measurements, it was decided to monitor critical SBO phase and amplitude from outboard elements, and CSB phase and amplitude from central elements.

As a test of the effect of small, random errors to the lightly driven elements (5 → 10 and 19 → 24), a computer simulation of the effect on the flyability was performed. In all cases a 3° glide path over an infinite ground plane was assumed. Figure 3-35 compares the normal performance with randomly applied errors to elements 5 through 10 and 19 through 24 of 10°, 15°, and 25° in phase. These do not result in a loss of CAT II performance. Figure 3-36 is the same type of computation for errors of 30° and 35° in phase. Each curve represents the worst case of a number of random applications. Figure 3-37 shows the results of a 10° uniformly distributed phase error over elements 5 through 10 and 19 through 24. The same type of computation is shown in Figure 3-38 for 15° phase error.

The following section describes the design and development of a monitor system capable of detecting all faults which would produce an unacceptable antenna performance.

3.1 INTRODUCTION

The Dipole Broadside Glide Slope Array consists of twenty eight dipole elements stacked in a vertical array. Two independent distribution systems are used to generate the particular illumination functions for the CSB and SBO. These systems are mounted on common distribution boards with a single cable

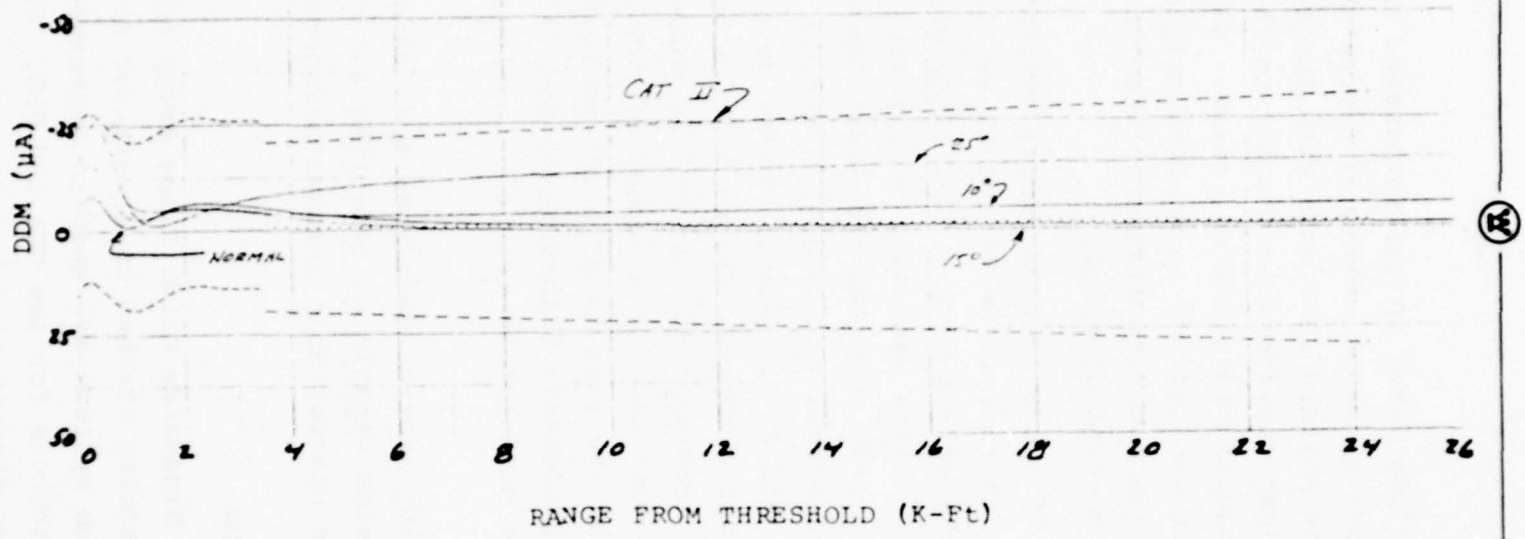

Figure 3-35 The Effect Of Random Applied Phase Errors To Non-Critical Elements

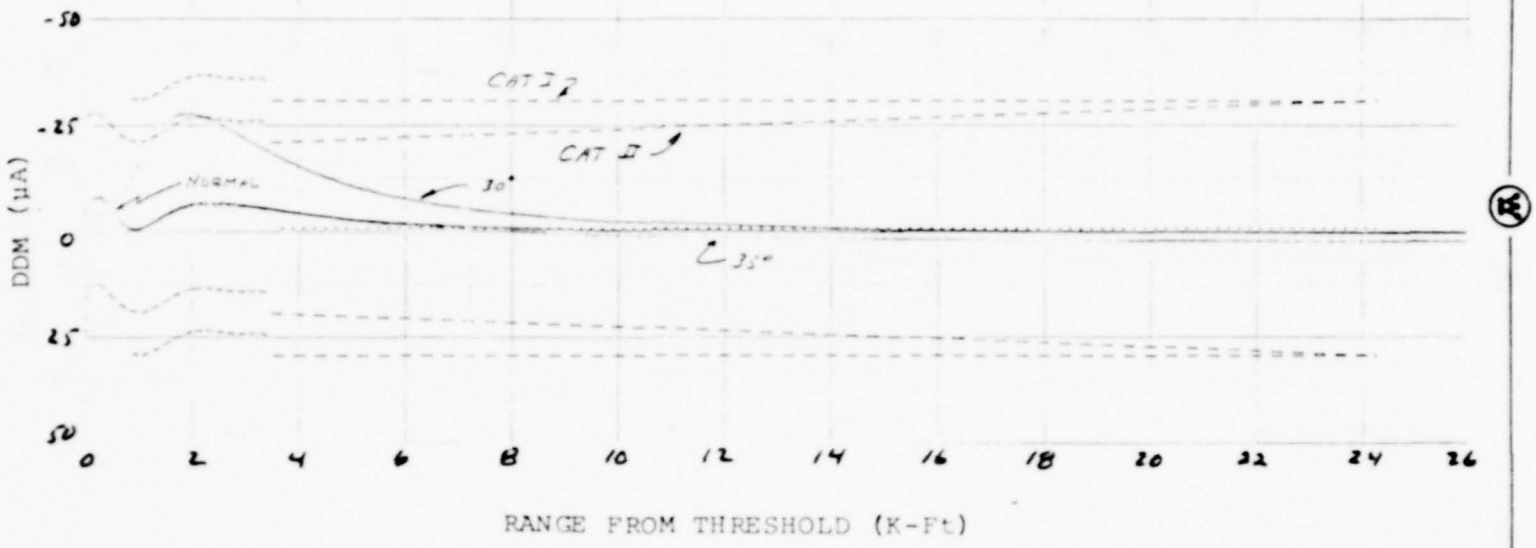

Figure 3-36 The Effect Of Randomly Applied Phase Errors To Non-Critical Elements

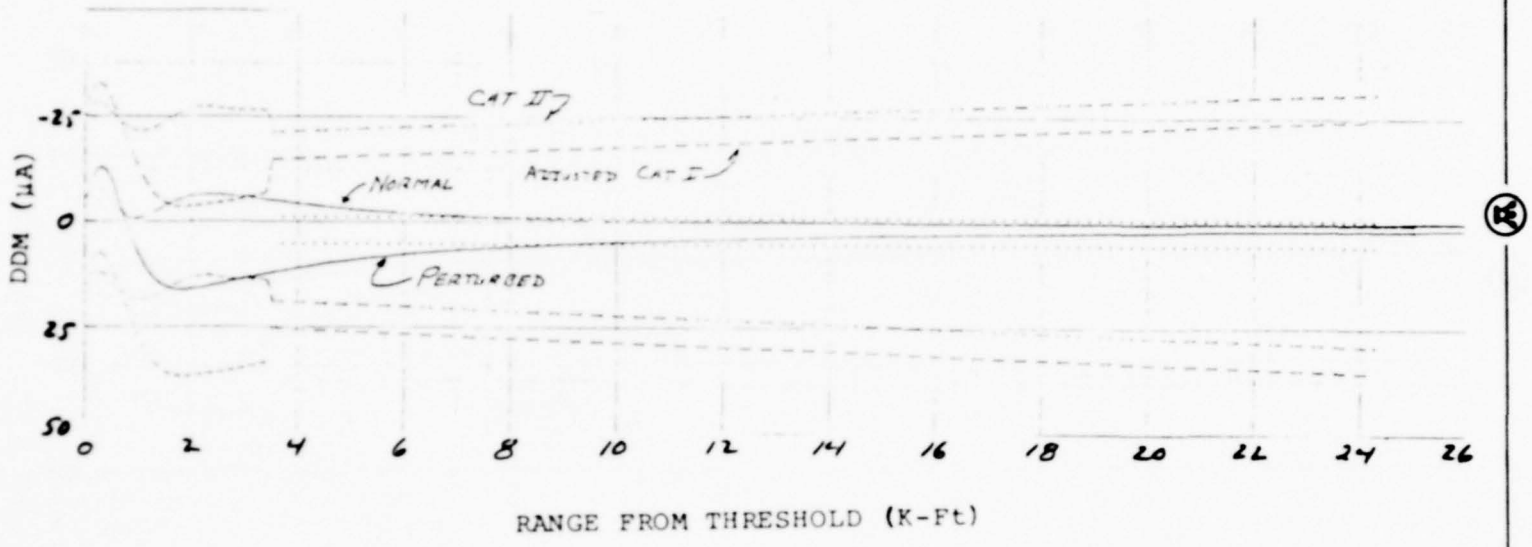

Figure 3-37 The Effect Of A 10° Uniformly Distributed Phase Error

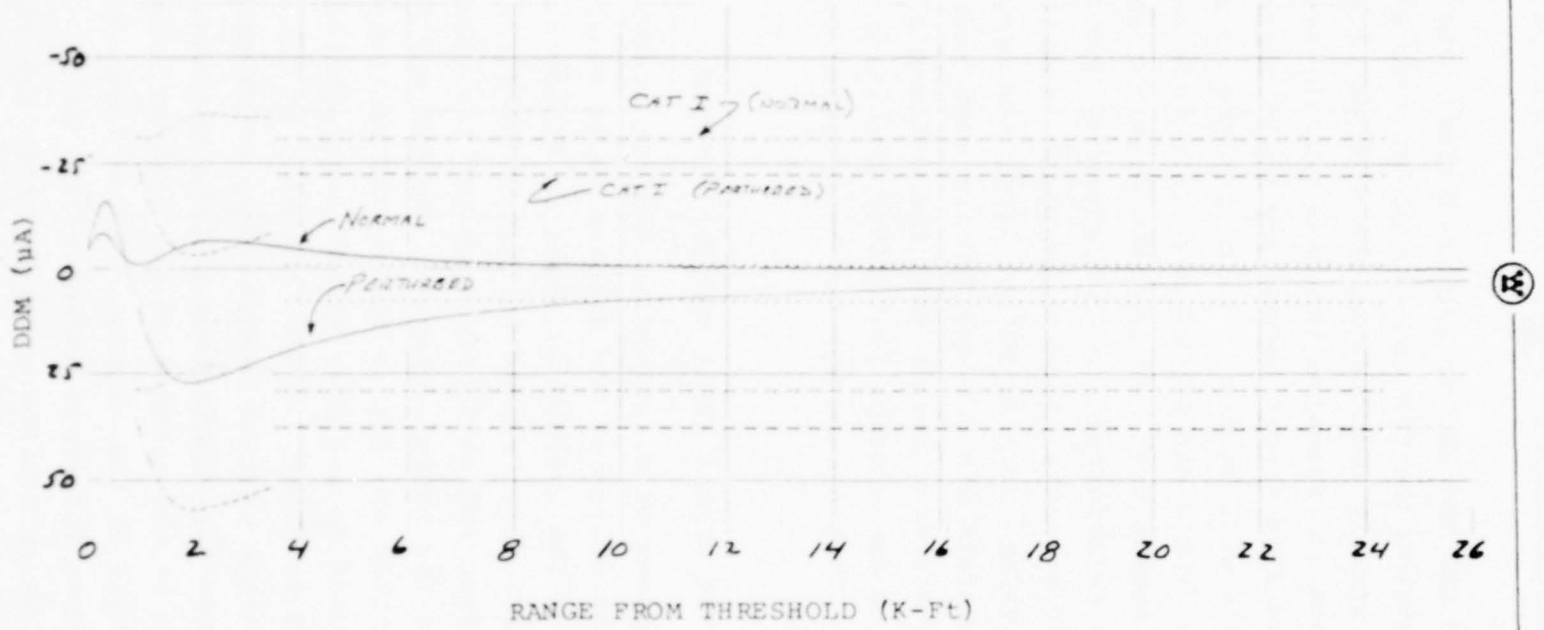

Figure 3-38 The Effect Of A 15° Uniformly Distributed Phase Error

delivering both CSB and SBO to each radiator. The phase relationship between the CSB and SBO varies from element to element. This greatly complicates the problem of monitoring the array. Since an effective integral monitor system requires sampling the radiated energy beyond any point where a failure could occur, this will require a pick up probe in the immediate vicinity of the dipole and beyond any connectors and cables. The probe will couple both CSB and SBO, with the same phase relationship as established for that element, and different than every other element. Since this phase relationship is not a cardinal value, such as 90° or 180°, the circuitry necessary to separate the CSB and SBO for each radiator would be very complex and more costly than the antenna's distribution system. Hence, a new concept in monitor combining was developed for this array. This system has not been tested in conjunction with the antenna.

3.2 THEORY OF THE DIPOLE ARRAY MONITOR NETWORK

The development of an effective monitor system is absolutely predicated on the design of the antenna to be monitored. A wiring diagram of the antenna is shown in Figure 3.39. The antenna is mechanically divided into seven sections, each of which contains four radiating elements and the required CSB and SBO distribution for those elements. The CSB and SBO signals from the transmitter are fed to the center section, number four, and are distributed up and down the array by series connections between adjacent sections. Hence, elements at the top and the bottom of the array have no common cable paths except the connection between the transmitter and the antenna. This lack of a common path is the essence of the monitor technique to detect cable faults on the antenna. Since a common fault cannot occur for the upper and lower halves of the array, one can develop a cable fault monitor which compares the excitation of

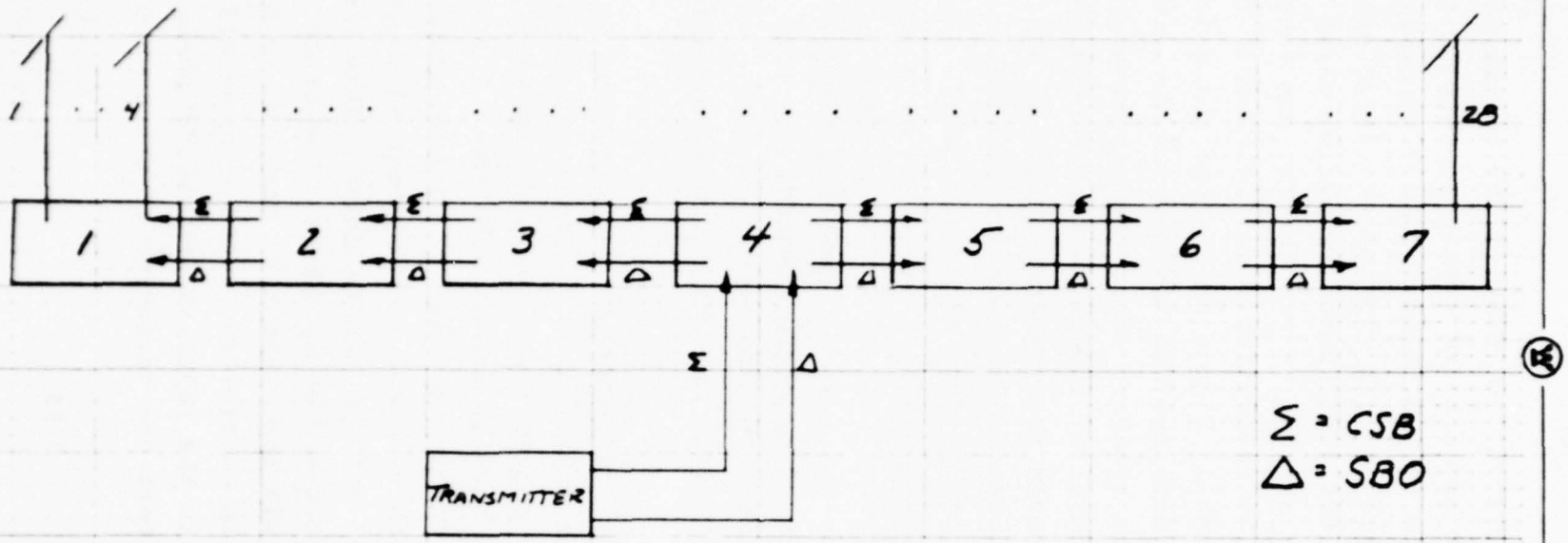

Figure 3-39 Dipole Array Wiring Diagram

elements in the upper half array to those in the bottom half array. It is desirable in any monitor combining network to limit the number of outputs to the minimum number necessary to monitor all fault conditions. In view of the large number of Wilcox Mark 1-D's in use, the ideal number would be three channels compatible with the Wilcox system. Since "width" and "angle" account for two channels, it is desirable to limit cable fault detection to a single channel. Figure 3-40 shows the relative amplitude distribution of both the CSB and SBO for the array. Note that both patterns are symetric about the center of the array. (This is not the case for the phase distributions). This indicates that if signals from symetric elements are combined, the signal strengths will be equal with equal monitor sensitivity. However, if inputs from all twenty eight elements were manifolded into a single output, there would be a corresponding decrease in sensitivity for any single element. These considerations gave rise to the idea of detecting cable faults by comparing the excitation of symetric elements and time sharing this information into a single output channel. This is accomplished by an array of diode switches coupled radially to a common output line.

The "width" and "angle" measurements are performed in a more customary fashion. Examination of Figure 3-40 indicates that elements at the array center are heavily driven with CSB while extreme elements are heavily driven with SBO. The "width" channel is established by combining a signal derived from element #14 (large CSB) with a signal from element #1 (large SBO) such that the resultant CSB and SBO are in phase. This channel will be tuned to detect broad and sharp alarm. The "angle" channel will have element #14 and element #1 combined to give the resultant CSB and SBO in quadrature. This channel will be tuned to detect variation in the relative SBO to CSB phase. These two channels will detect any variation in CSB to SBO

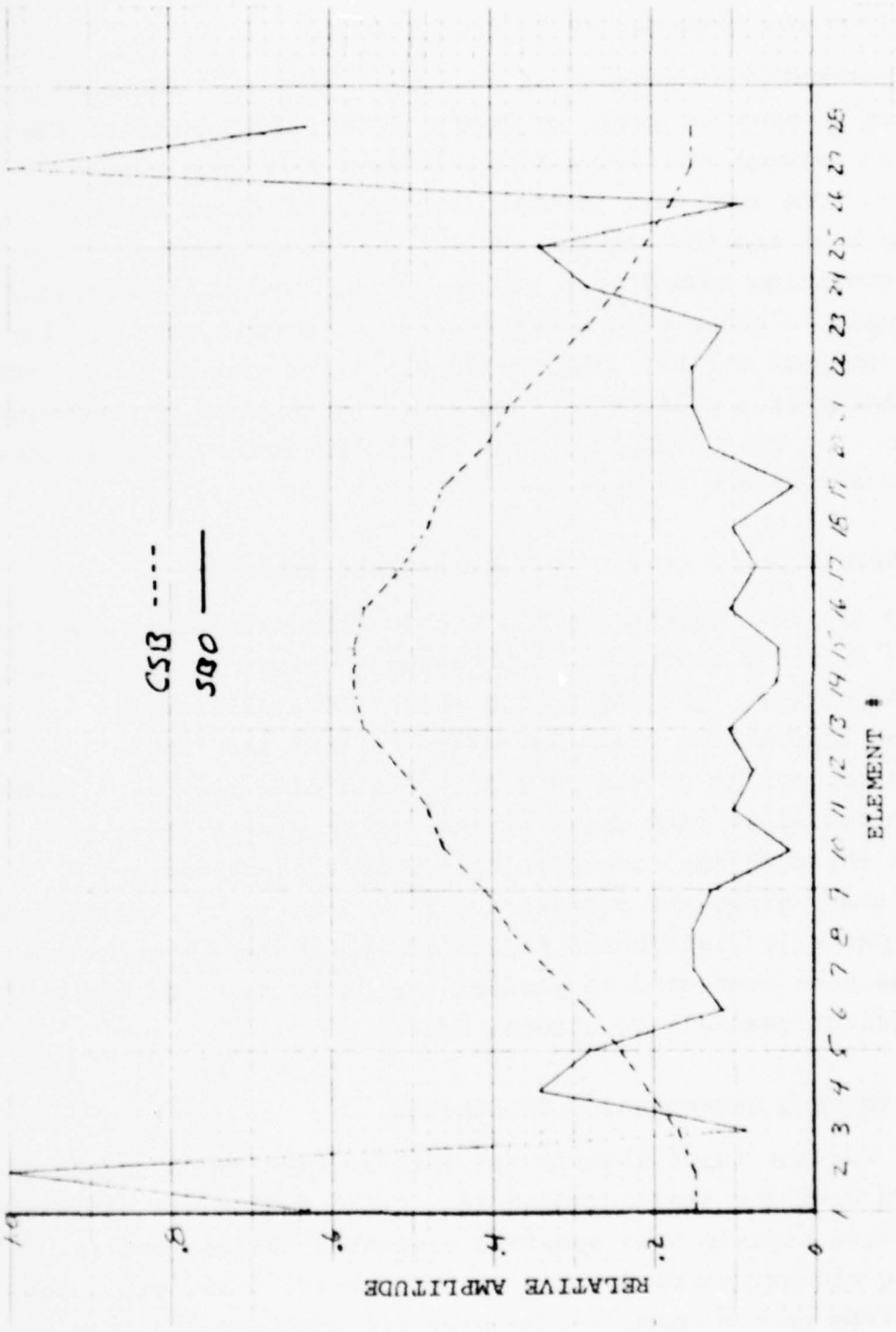

Figure 3-40 Dipole Array Amplitude Distribution

phase and amplitude either originating in the transmitter or cables from the transmitter to the antenna.

A conceptional drawing of the above described monitor combining network is given in Figure 3-41. The inputs to the combining network are derived from probes near each dipole radiator. One must bear in mind that each of these probes picks up both the CSB and SBO of the particular dipole. This simple combining network has no way to separate these signals. For example, a phase shifter in a given line will vary equally the CSB and SBO in that line, resulting in no change to the DDM. To determine if a network of this type was capable of producing responses for which meaningful alarm limits could be established required a computer analysis.

3.3 COMPUTER MODEL OF THE MONITOR NETWORK RESPONSE

The monitor concept for the Dipole Broadside Array consists of three distinct functions each having a unique and separately generated output. The SBO to CSB phase and amplitude are monitored through two channels called "width" and "angle". Complete monitoring of the path angle will also require a tower tilt monitor since path angle varies directly with tower back tilt. A third channel monitors all cable connections and assures that, given the correct SBO to CSB phase and amplitude, this is properly distributed to all 28 radiators. A mathematical model has been generated to predict the performance of these three monitor channels to antenna faults.

3.3.1 Antenna Interconnection Monitor

All monitor input signals are derived from 20 dB couplers implanted near the dipole radiators. Cable faults are detected by comparing signals from symetric elements. Hence, one is comparing element pairs defined by 1-28, 2-27, 3-26, etc. The signals from each element of the pair are combined and then

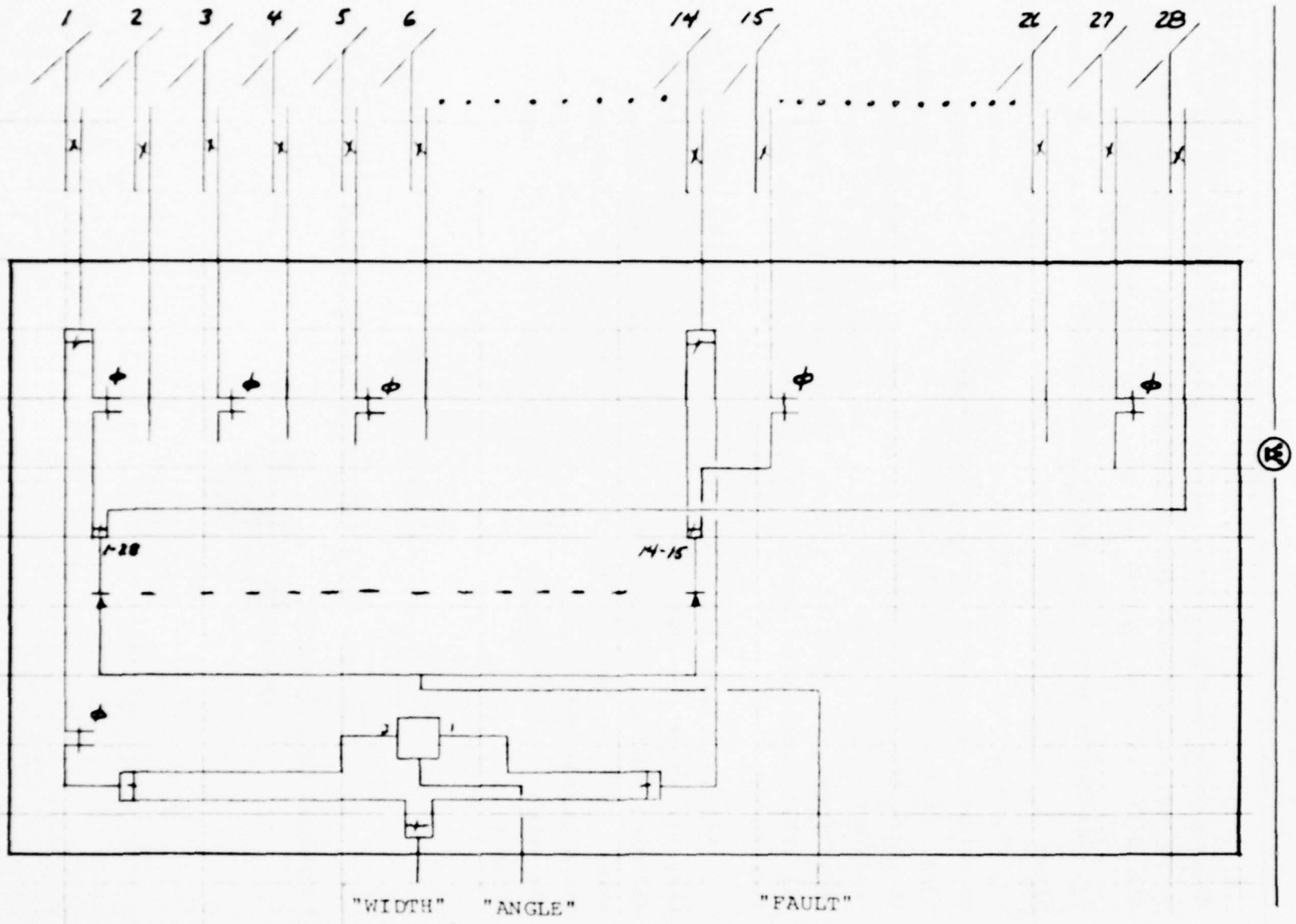

Figure 3-41 Concept Of Monitor Combining Network

sequentially coupled to the output terminal. Each pick up probe samples a signal with a format as shown in Figure 3-42(a). The amplitudes of the CSB_i and SBO_i and the relative phase angle θ_i, are determined by the required excitation for the i th element. Since θ_i varies across the array, there is no convenient method to change θ_i within the monitor combining network. Since all combined pairs feed into the same output channel, they must all have the same initial DDM and identical alarm limits. In order to allow the initial DDM's to be made equal, a phase shifter is provided in one arm of each pair. An analysis was performed to determine: (1) that the initial DDM's can be made equal, and (2) that reasonable faults will produce a measurable DDM variation.

Figure 3.42(b) represents the signals from two elements as they arrive at the combiner. There is no loss in generality in assuming that the CSB from one element defines the principal axis. In this case the angle ϕ between the CSB of elements i and n corresponds exactly to the phase shifter in the circuit. The output of the combiner is a CSB (total) and an SBO (total) given by,

$$\vec{C_T} = (C_i + C_n \cos\phi)\,\hat{i} + C_n \sin\phi\,\hat{j} \qquad (3.1)$$

$$\vec{S_T} = (S_i \cos\theta_i + S_n \cos\theta n)\,\hat{i} + (S_i \sin\theta_i + S_n \sin\theta n)\,\hat{j} \qquad (3.2)$$

The resultant DDM is given by,

$$DDM \propto Re\,\frac{SBO}{CSB} = \frac{\vec{S_T} \cdot \vec{C_T}}{|\vec{C_T}|^2} \qquad (3.3)$$

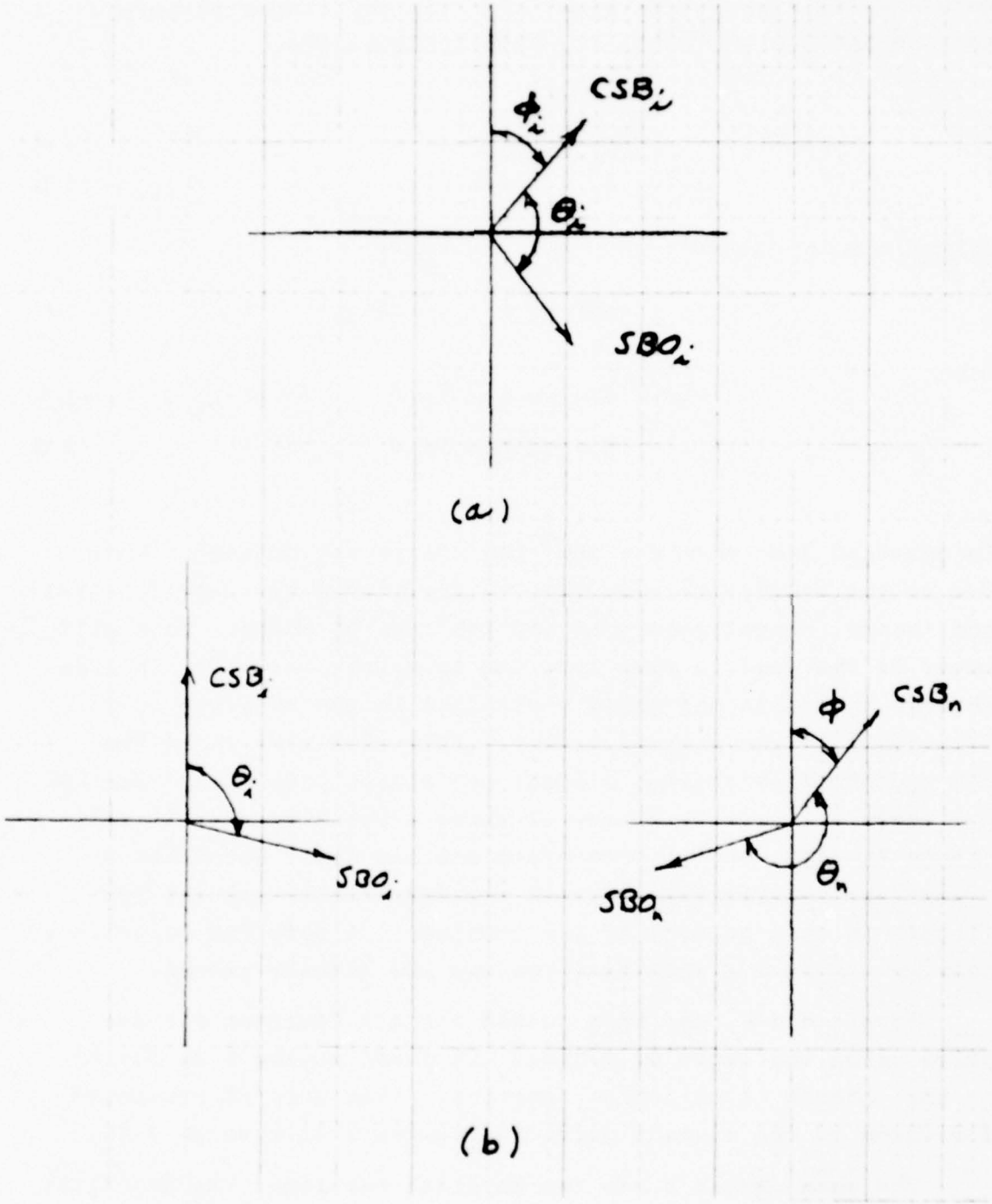

Figure 3-42 Signal Format At Combining Network Input

Reference to Figure 3-40 shows that the amplitudes of both the CSB and SBO are equal for symetric elements,

$$C_i = C_n = C \tag{3.4}$$

$$S_i = S_n = S. \tag{3.5}$$

Solving equation (3) under this condition yields,

$$DDM \propto \frac{1}{2} \frac{S}{C} \left\{ A + B \tan \frac{\phi}{2} \right\} \tag{3.6}$$

with

$$A = \cos \theta_i + \cos \theta_n \tag{3.7}$$

$$B = \text{Sin } \theta_i - \text{Sin } \theta_n \tag{3.8}$$

In equation 3-6 when $\phi = 180^\circ$ the DDM is not defined. This is due to the assumption that the CSB amplitudes are exactly equal and, hence, cancel when combined 180° out of phase. This will never be the case in real life due to slight variation in loss through the cable and small variations in the coupling coefficients of the pick up probes. Note also that since the CSB and SBO from a given element are always phase displaced by the angle θ, there is no way of using a phase shifter to only change the SBO vector. Therefore one can never establish a quadrature relationship between the CSB (total) and the SBO (total) in this portion of the combiner. A zero DDM is achieved only by tuning a ϕ such that the two SBO signals cancel.

Equation 3-6 has been solved for all fourteen element pairs using the ratio of S/C and the phase angles θ as defined by the antenna illumination function. This data is presented for three of the element pairs in Figures 3-43 through 3-45.

The phase angle ϕ has two physical meanings. In the first case it represents the initial phase displacement between the

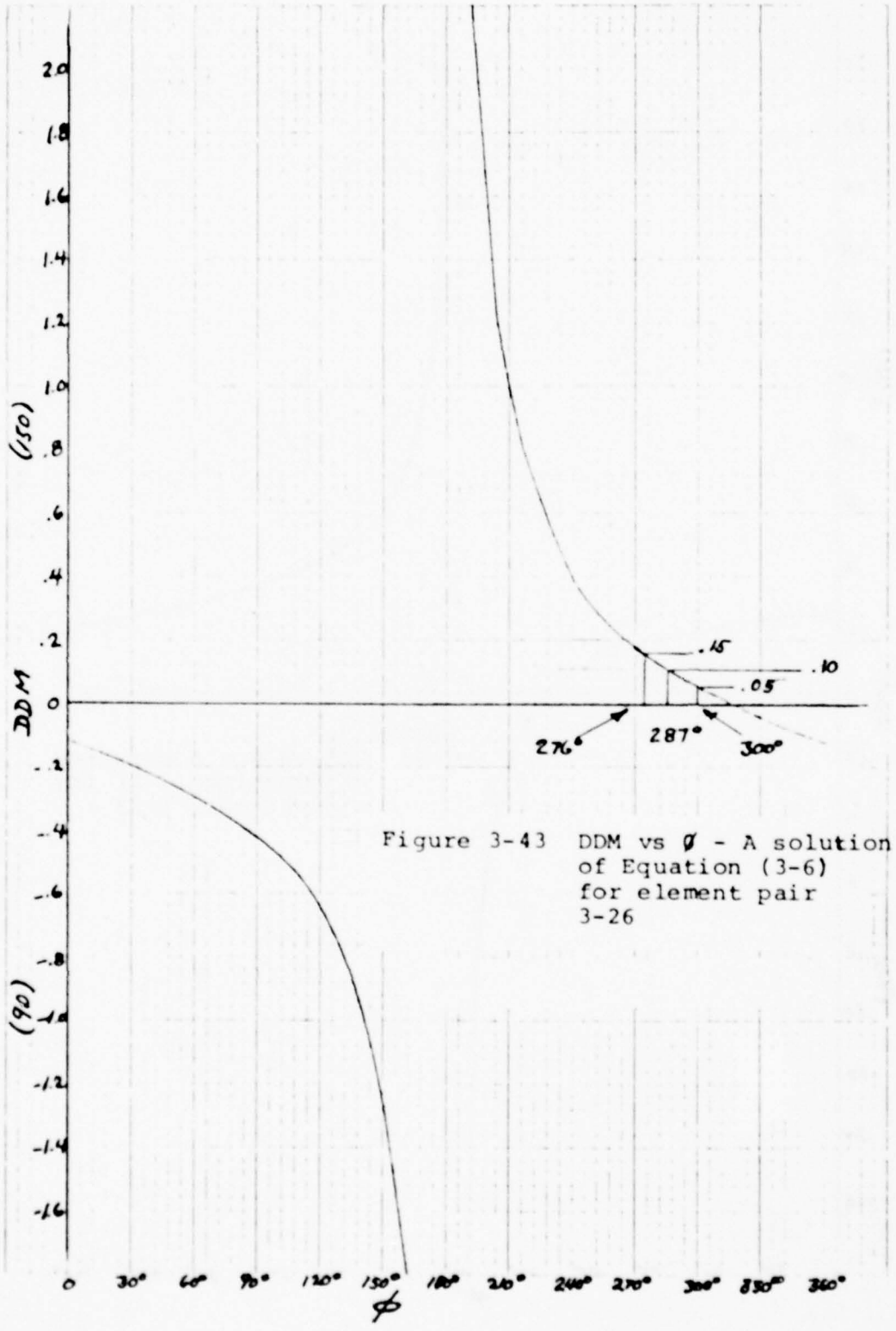

Figure 3-43 DDM vs Ø - A solution of Equation (3-6) for element pair 3-26

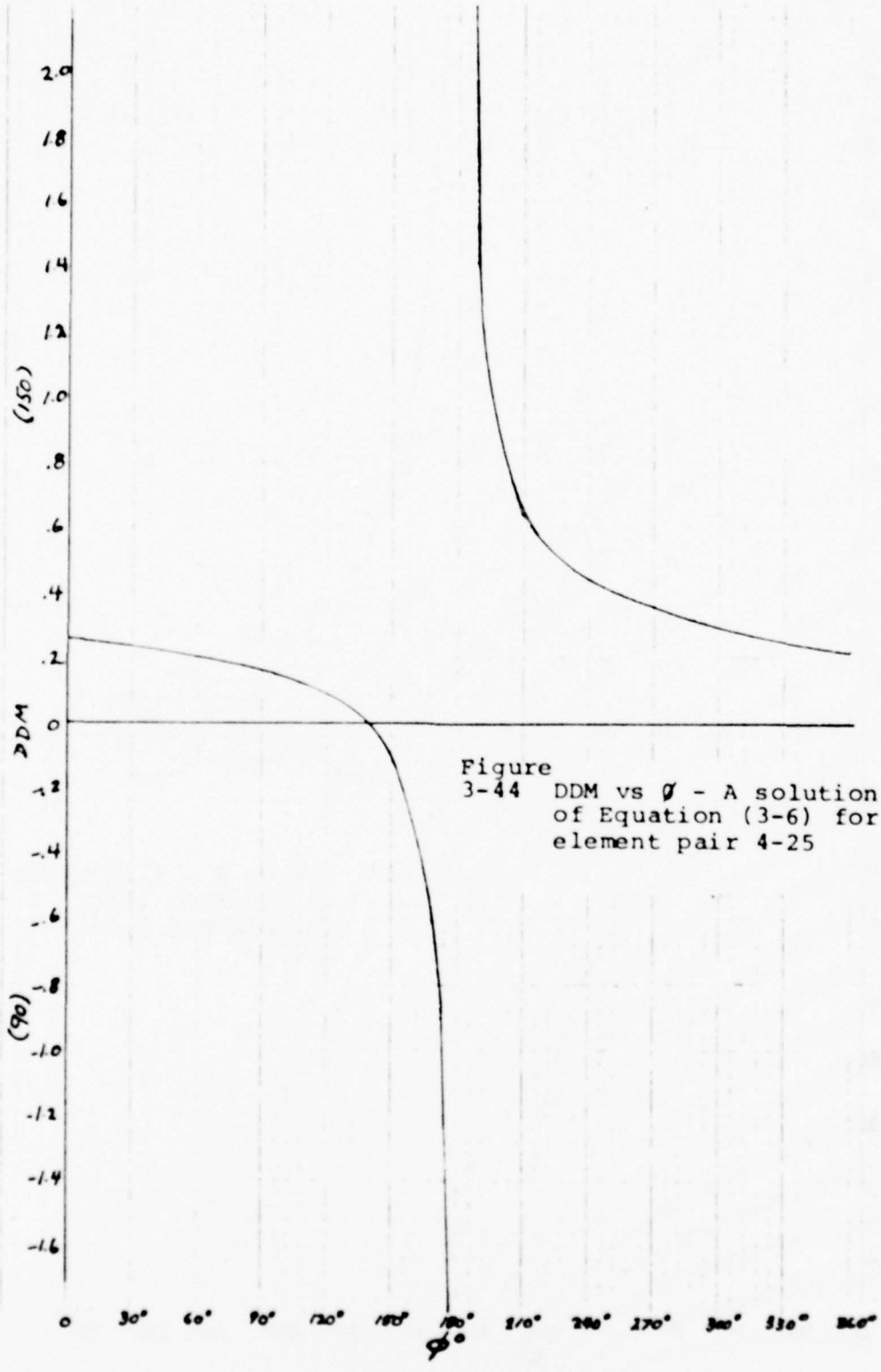

Figure
3-44 DDM vs Ø - A solution of Equation (3-6) for element pair 4-25

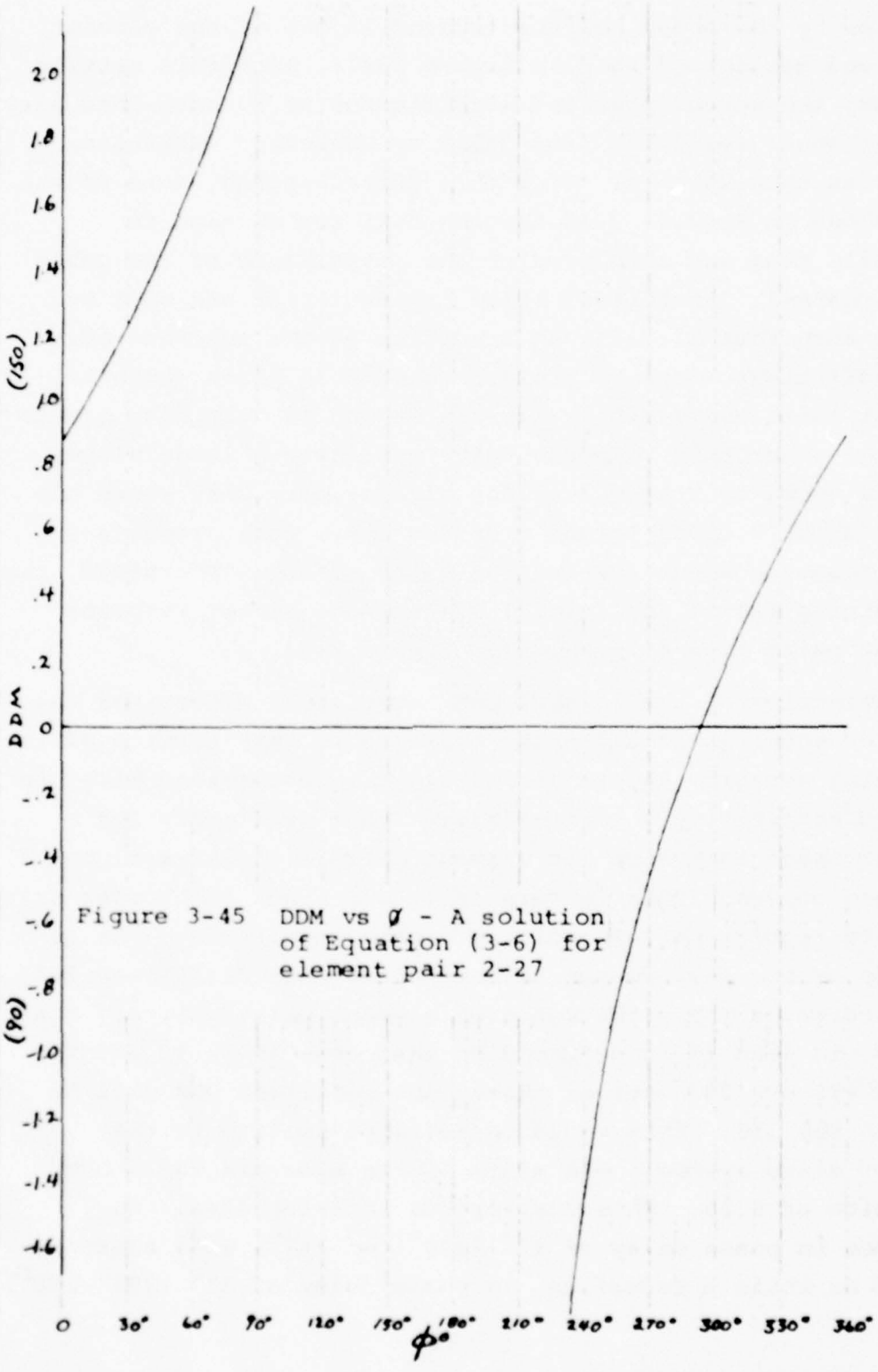

Figure 3-45 DDM vs Ø - A solution of Equation (3-6) for element pair 2-27

two CSB components of the element pair. As such, it can be adjusted by the phase shifter located in one of the element lines and designated as ø in Figure 3-41. Once this setting is made, the second physical significance of ø comes into play; phase changes resulting from cable or connector variations appear as changes in ø. With this understanding, data of the type shown in Figures 3-43 through 3-45 can be used to initially tune and then predict the performance of the cable fault channel. An initial value (no fault) of DDM must be chosen such that it falls on a portion of the response curve with sufficient slope to yield a reasonable alarm response. For element pairs where either the CSB or SBO is very much greater than the other this response curve will have a large slope. This is shown in Figure 3-45 for element pair 2-27 where the SBO is about 7 times larger than the CSB. This produces a large response about any initial value of DDM. Therefore, the determining factor for initial DDM are the slower response element pairs like 4-25 shown in Figure 3-44.

Selection of the initial DDM immediately determines the required settings of all phase shifters in this portion of the combining network. Alarm limits are then determined based in desired sensitivity. A given alarm limit will occur for a smaller phase variation for element pairs with large slope response curves. This is very desirable since the harder driven elements require correspondingly tighter monitoring. As an example of how performance is determined consider Figure 3-43. This indicates the performance of element pair 3-26. If the phasor in line #3 is adjusted so that the CSB in #3 and the CSB in #26 are 287° out of phase, the resultant DDM will be 0.10 in the 150. This would be adjusted to zero in the monitor alarm system. The alarm limits show are for a DDM variation of 0.05. This corresponds to about 43μa. An increase in phase delay of 13° (300° - 287°) will alarm in the 90 Hz while a reduction in phase delay of 11° (287°-276°)

will alarm in the 150Hz. Although the discussion has been directed to phase, amplitude variations will produce similar effects. Table 3-1 shows the response characteristics of all fourteen element pairs for an initial setting of .10 in the 150 Hz and $\pm$ .05 DDM alarm limit.

3.3.2 Width and Angle Monitor Channels

SBO to CSB amplitude and phase are continuously monitored through the "width" and "angle" channels. Prior to the element pair combination some energy is sampled from elements #1 and #14. Element #1 is largely SBO and element #14 is largely CSB. A phase shifter is in series with the input from element #1 in order to provide a tuning capability. The remaining circuitry is designed such that if ϕ is adjusted to give the CSB and SBO in phase at the "width" channel, they are in quadrature at the "angle" channel. Again using the actual values from the antenna illumination function, a calculation was performed for the response of the "width" and "angle" channels. It was found that if the phase shifter ϕ was adjusted to make the CSB element #1 be 191° advance compared to the CSB from element #14, the CSB (total) and SBO (total) were in quadrature at the angle channel and in phase at the width channel. This resulted in an "angle" channel normal output of ODDM and an 84μa variation for $\pm$ 15° change in SBO phase. The width channel has a nominal .3 DDM (150) output with a 51μa (90) broad alarm and an 97μa (150) sharp alarm.

3.3.3 Summarization of Analysis

The results of the preceeding analysis of the monitor response for the configuration of Figure 3-41 indicates that:

1. It is possible to economically sample data from all radiating elements using a sequencing monitor combining network.

ELEMENT PAIR	INITIAL PHASE SETTING ϕ_0	ALARM RESPONSE
1-28	161°	± 2°
2-27	300°	± 4°
3-26	287°	± 12°
4-25	116°	± 15°
5-24	93°	± 19°
6-23	48°	± 25°
7-22	117°	± 25°
8-21	357°	± 40°
9-20	305°	± 60°
10-19	157°	± 12°
11-18	166°	± 12°
12-17	195°	± 10°
13-16	211°	± 15°
14-15	190°	± 10°

TABLE 1

Table 3-1 Fault Channel Response

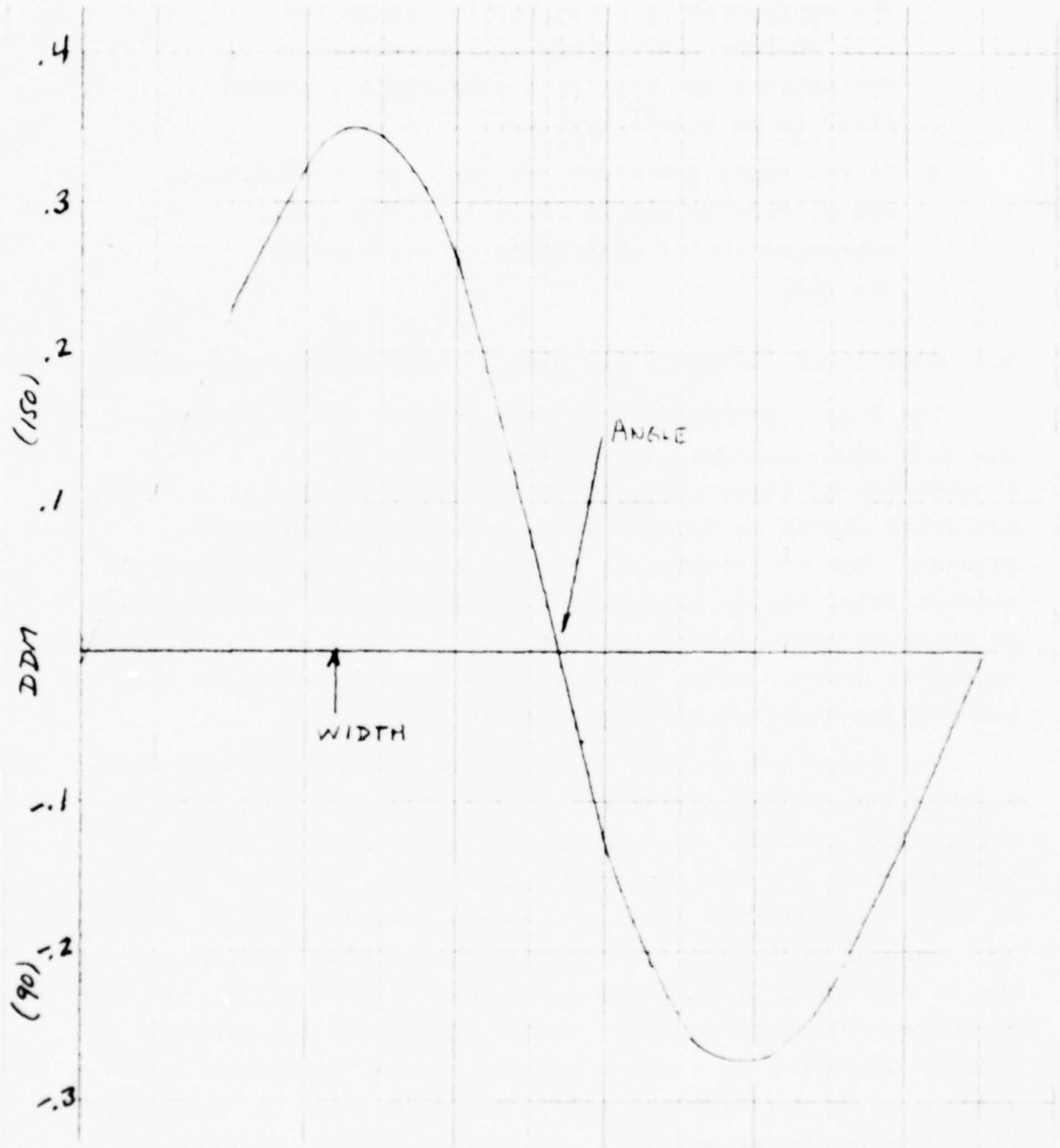

Figure 3-46 Monitor Response Of The Width and Angle Channels

2. The configuration presented in Figure 3-41 will monitor every cable and connector in the antenna and provide a measurable response prior to an alarm condition.

3. Course angle and width are monitored continuously and provide an output which is a very close approximation of what would be measured in the air.

3.4 FUNCTIONAL DESIGN OF THE DIPOLE MONITOR COMBINING NETWORK

The Dipole Broadside G/S Array monitor combining network was designed, constructed, and preliminary tested. It consists of three basic sub-assemblies, mounted in a single box which itself is mounted on the center section of the antenna. The sub-assemblies consist of the logic and control circuit (A1), the RF combining and switching circuit (A2), and an array of phase shifters to provide the correct initial signals to the RF board. Since final testing was not completed only preliminary drawings are presented at this time.

The logic and control sub-assembly, shown in Figure 3-47, provides power and control for the fourteen position diode switch, CR1 to CR14. The diodes are normally back biased at approximately 5 V when the switch is "off". When the driver is "on", the selected diode is forward biased by the 5V supply and current limited by R27 through R40. Visual indication that the RF switching is sequencing properly is provided by an array of LED's, CR15 through CR28. Clock pulses are generated by U1 (52555) operating as a multivibrator in the "automatic" mode and as a one-shot in the "manual" mode. The clock rate in "automatic" is controlled by R4 and C16. Integrated circuit U2 (55452) serves as a buffer and inverter between the clock and the binary counter U3 (5493). The counter provides a four bit binary word to the demultiplexer U5 (54154). The demultiplexer performs a

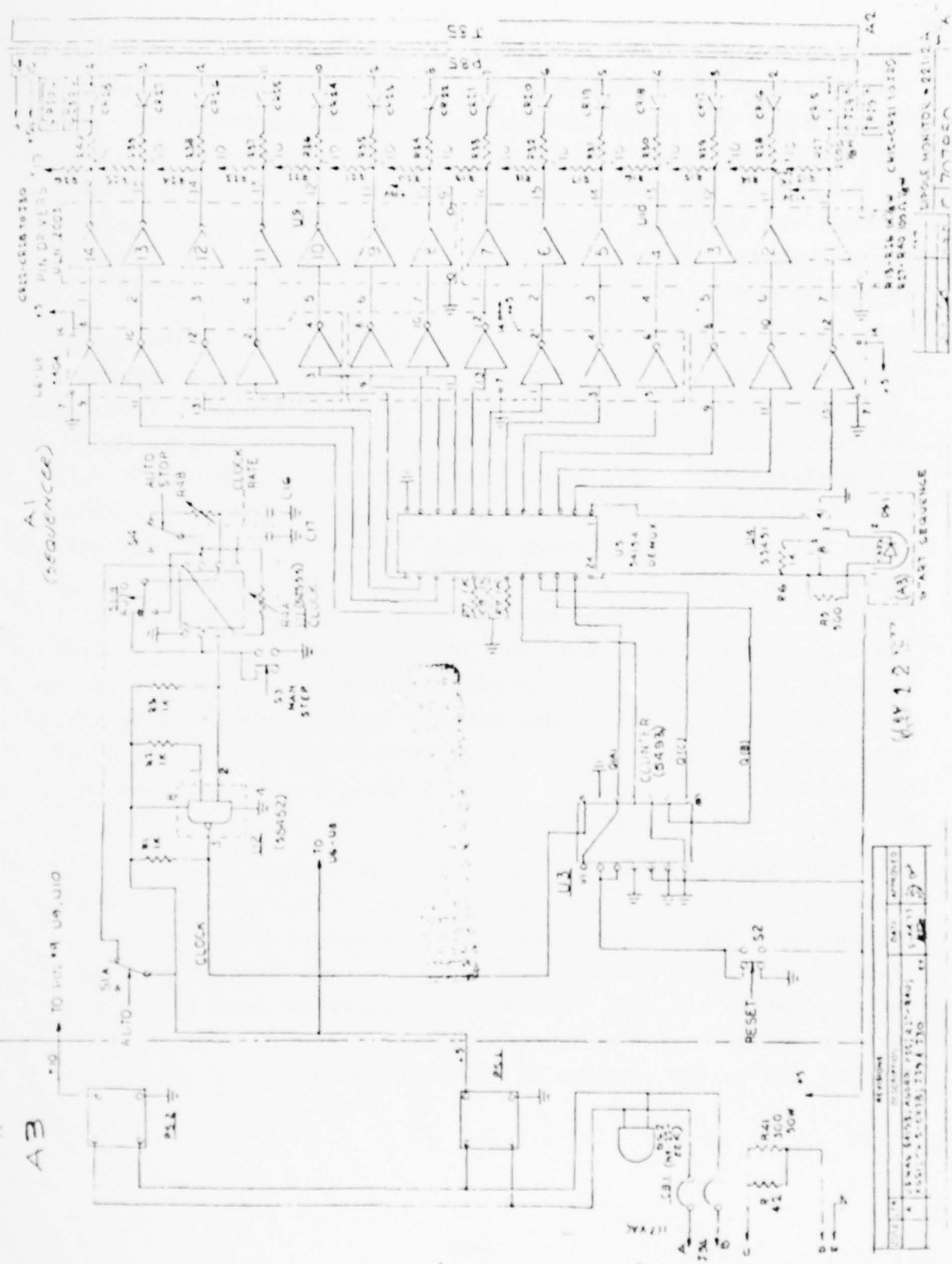

Figure 3-47 Logic & Control Subassembly Schematic

decoding and commutating function so that each of its 16 outputs changes state sequentially as the binary word value increases. Output #1 of the demultiplexer switches the LED driver U4 (55451) to indicate "start sequency" on the front panel. Outputs #2 and #15 of the demultiplexer are used to drive the switch drivers via inverters U6 through U8. Output #16 is ignored. The mechanical layout of the logic circuit and control is shown in Figure 3-48.

The RF combining board is shown in Figure 3-49 with the mechanical layout given in Figure 3-50. This differs slightly from the conceptual layout of Figure 3-41 in that more flexability for tuning is provided. This will insure the ability to match the analysis of Section 3.3. Phase shifters Z1 through Z14 provide the tuning required to set the initial DDM to the same value for each of the element pairs. The switching diodes are arranged in a radial combining network so that the same impedance is seen in each of the fourteen switched positions. The signals for the "width" and "angle" channels are taken from dividers Z34 and Z35. A 3 dB pad is included in elements 15 and 28 in order to maintain equal signals to the element pairs since energy was coupled out of 1 and 14. Two phase shifters, Z36 and Z37, insure that the proper signal formats can be achieved in the "width" and "angle" channels.

The overall layout of the monitor combining network is shown in Figure 3-51. This box is mounted on the back of the antenna with cables connected to the pick-up probes through J1-J28. The fault channel output is J31, the "width" is J32, and the "angle" is J33. These will require RF cables to the monitor system in the equipment shelter. An A.C. line cord must be run up the antenna to the monitor combining network.

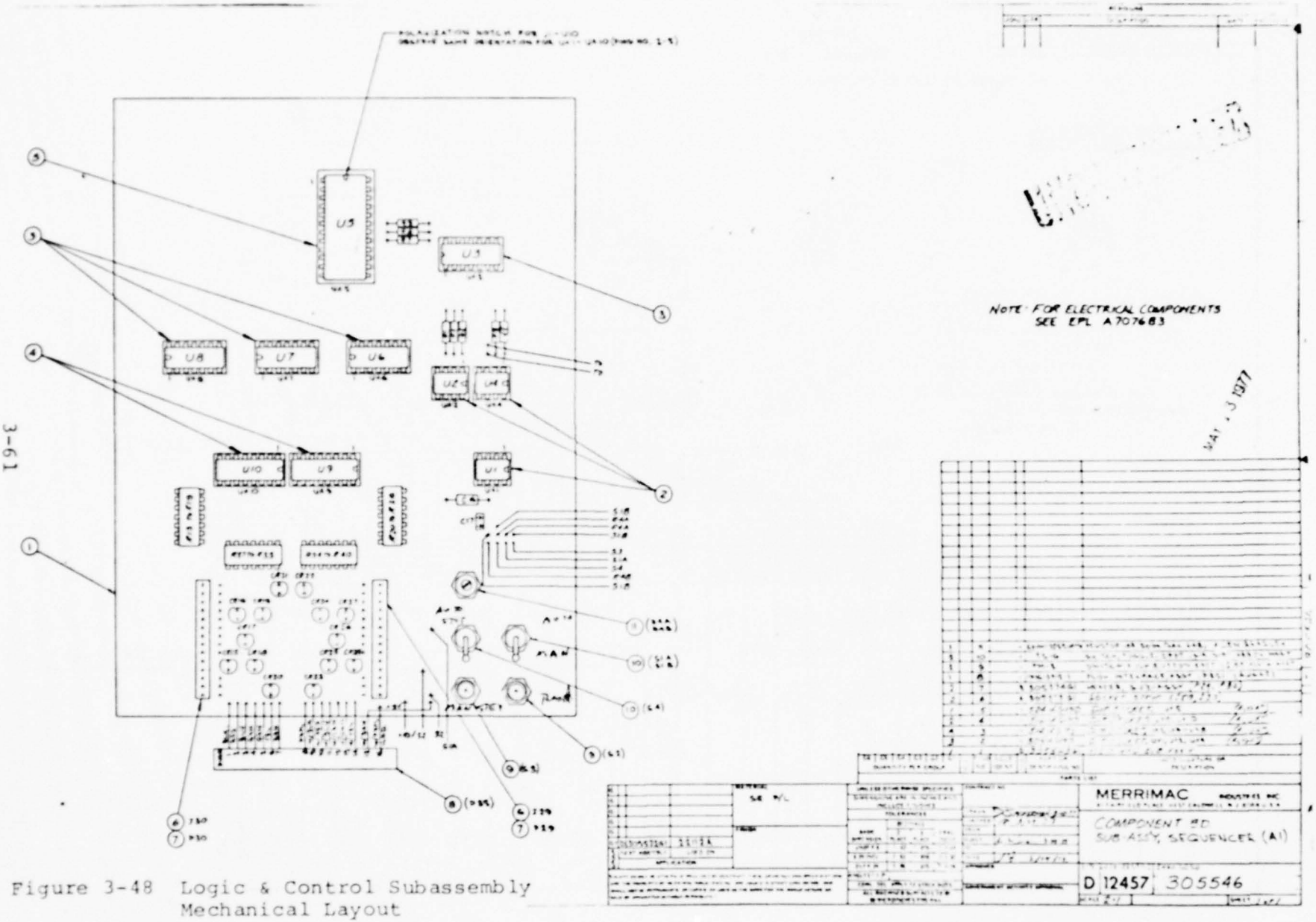

Figure 3-48 Logic & Control Subassembly Mechanical Layout

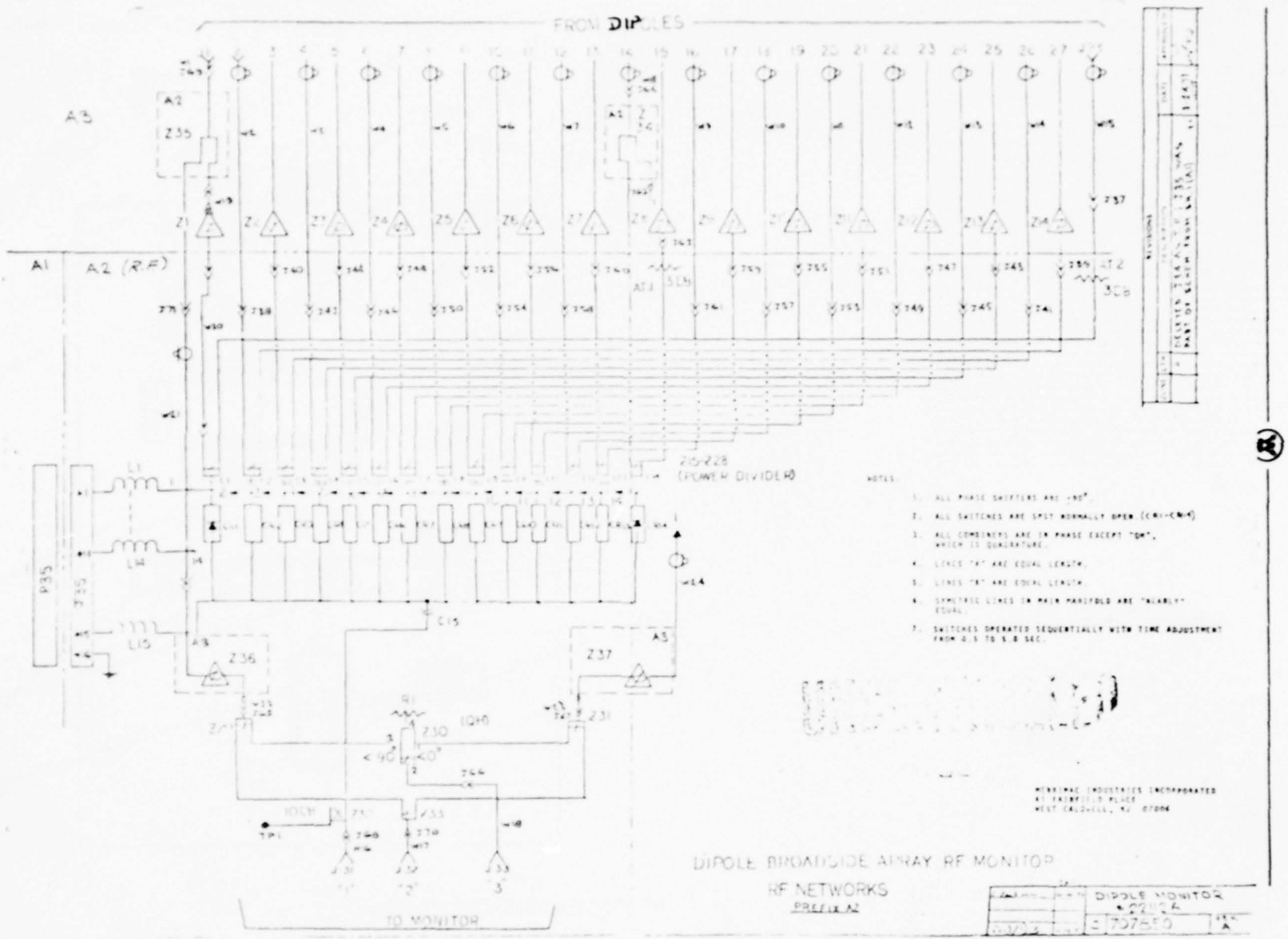

Figure 3-49 RF Combining Circuit Schematic

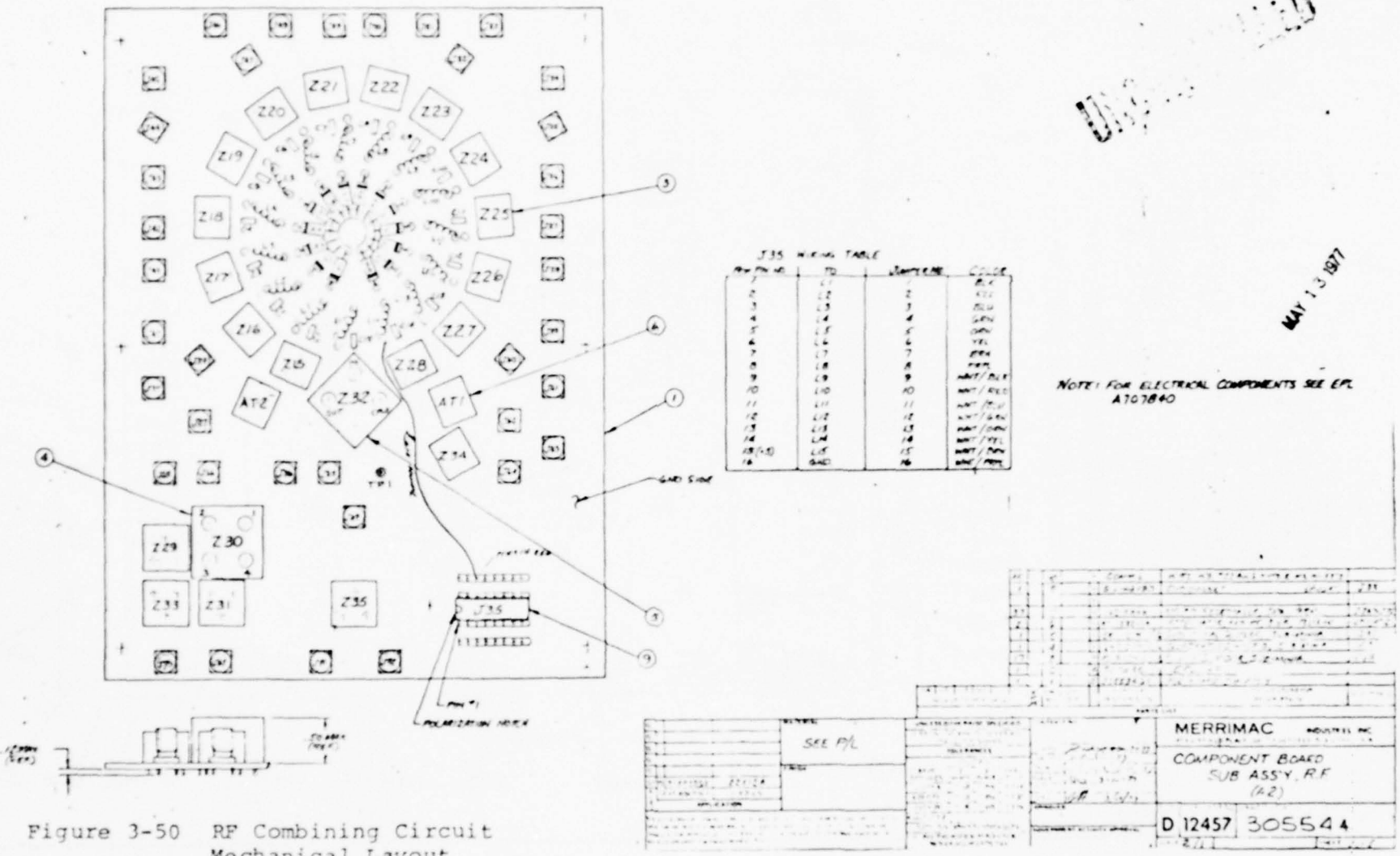

Figure 3-50 RF Combining Circuit Mechanical Layout

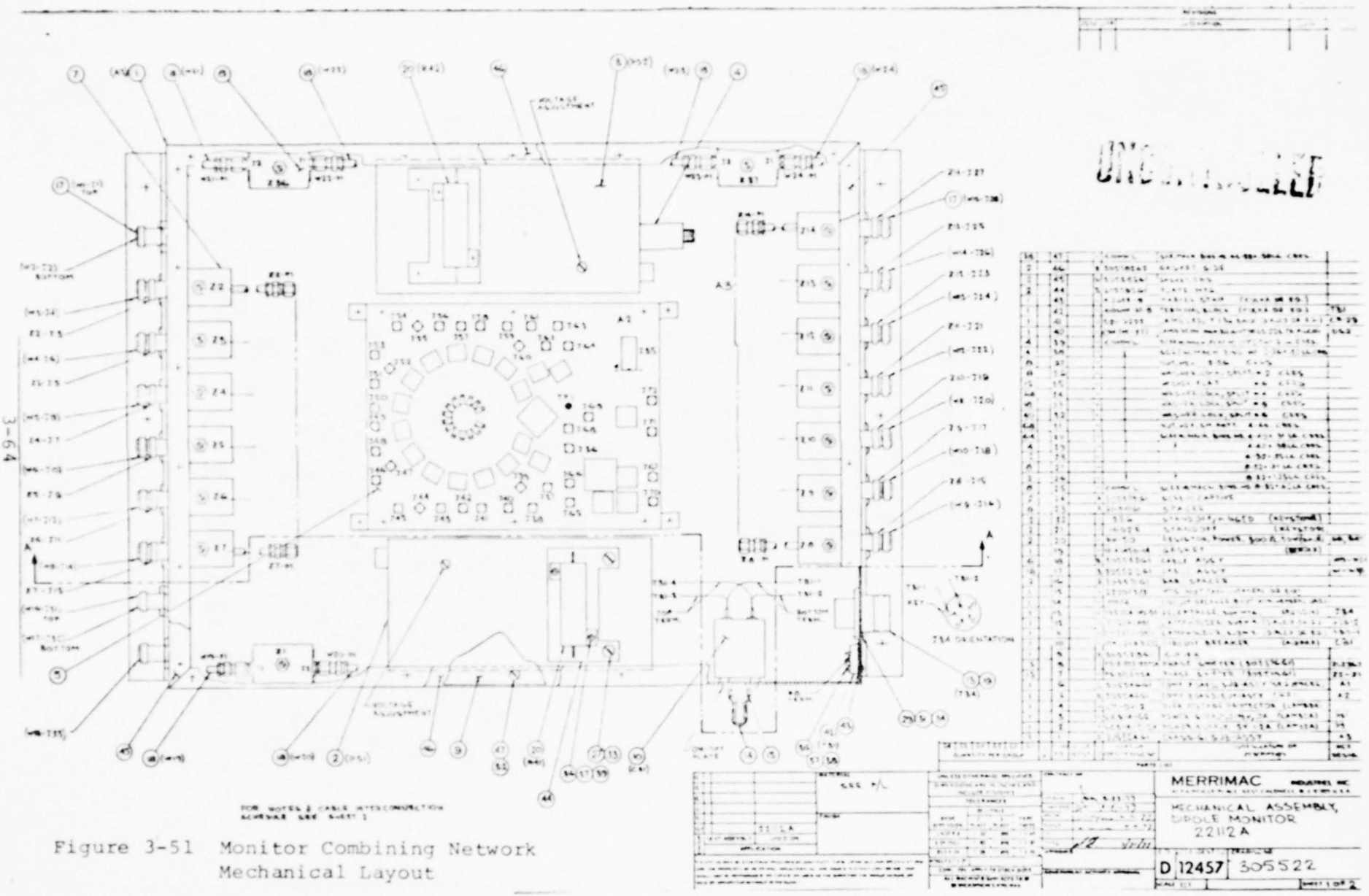

Figure 3-51 Monitor Combining Network Mechanical Layout

4.0 TESTS OF THE DIPOLE BROADSIDE GLIDE SLOPE ARRAY

The Dipole Broadside Glide Slope Array has been tested both on the Westinghouse antenna range, where radiation patterns were measured, and in Lynchburg, Virginia, where flight checks were conducted.

4.1 ANTENNA RANGE TESTS

The final tuning of the antenna was performed on the antenna range. Figure 4-1 shows the antenna mounted on the pedestal. Notice that during pattern measurements the antenna is mounted horizontally, 80' in the air, rather than in the normal vertical operating configuration. These tests were made using the antenna in a receive mode. The source antenna was located 1700' away near the ground. Since this range is not in the far field of the antenna under test, the source was itself a four element dipole array phased to provide plane wave illumination of the test array. Prior to making pattern measurements, the range characteristics were measured. These include measuring reflections from all fixed targets, to be applied as a correction to the test data.

As with any large array designed to produce very low sidelobes over a specific angular region, analysis can only provide an initial excitation. The final tuning was computer aided and performed with the antenna under test. The output of the antenna is fed to a phase sensitive receiver, the output of which is both plotted and inputed to a computer. The computer compares the measured pattern to the theoretically best pattern which was determined by analysis. A synthesis program is run which generates a recommendation for a phase and/or amplitude change to a specific radiating element which will produce a pattern closer to the theoretical optimum. Using this technique, the final pattern was a virtual overlay of the theoretically predicted pattern.

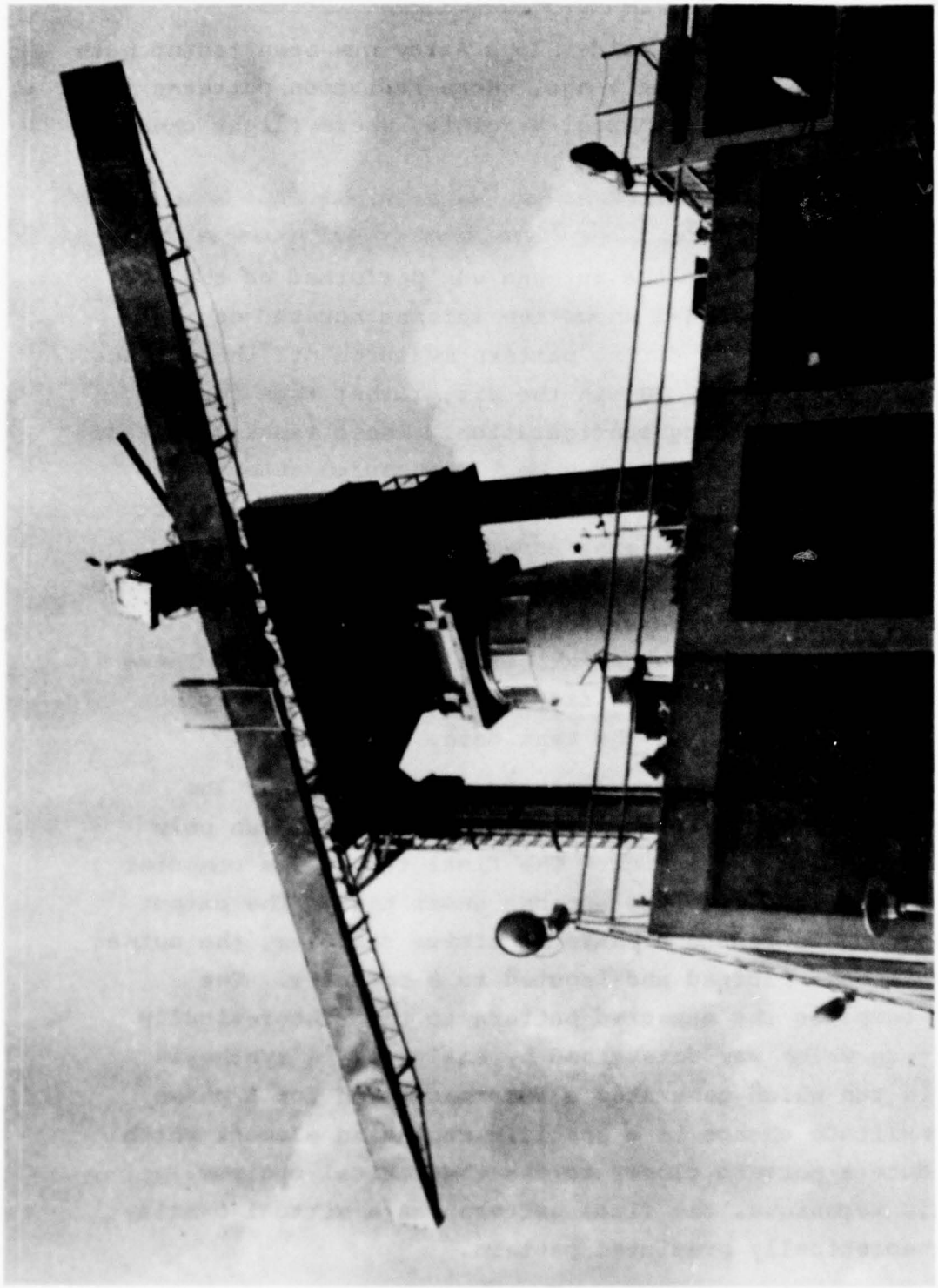

Figure 4-1 Antenna Range Mounted For Pattern Measurements

A design goal was to produce an antenna which could operate over the entire glide slope frequency band with no tuning adjustments. Due to F.C.C. restrictions, measurements were confined to three frequencies spaced across the band: (1) 329.6 MHZ, (2) 332.6 MHZ, and (3) 334.7 MHZ. Over this range of frequencies, there is no variation of the CSB pattern. This is expected since there are no critically tuned parameters associated with this pattern. A 360° CSB pattern is given in Figure 4-2 for the center frequency of 332.6 MHZ. Since the SBO pattern is tailored to supress sidelobes over a critical angular region, it is slightly frequency dependent. The design goals were achieved over the entire frequency range. Figures 4-3 through 4-5 show 360° plots of the SBO at the three test frequencies. An expanded plot is given in Figure 4-6 for both the CSB and SBO, at the center frequency of 332.6 MHZ. This shows that the SBO sidelobes are surpressed to an average value of 20 db below the lower guidance lobe and to an angular range of 16° below the glide path angle. These are antenna characteristics which would yeild excellent flyability over very severe terrain.

The array elements are located on a circular arc whose focal point is the runway center line. This type of mechanical focusing is designed to prevent the customary near field defocusing and to produce a planar guidance. This effect was measured on the antenna range by tilting the array both above and below its normal horizontal plane. This allows patterns to be measured as would be seen by an aircraft approaching parallel to the runway center line but displaced by +100' and -100'. These results are given respectively in Figures 4-7 and 4-8. Comparison of this data to the on center line data of Figure 4-6 indicates a negligible glide path angle change as represented by the location of the guidance null. Hence, the array provides planar guidance and the antenna curvature is not critical with

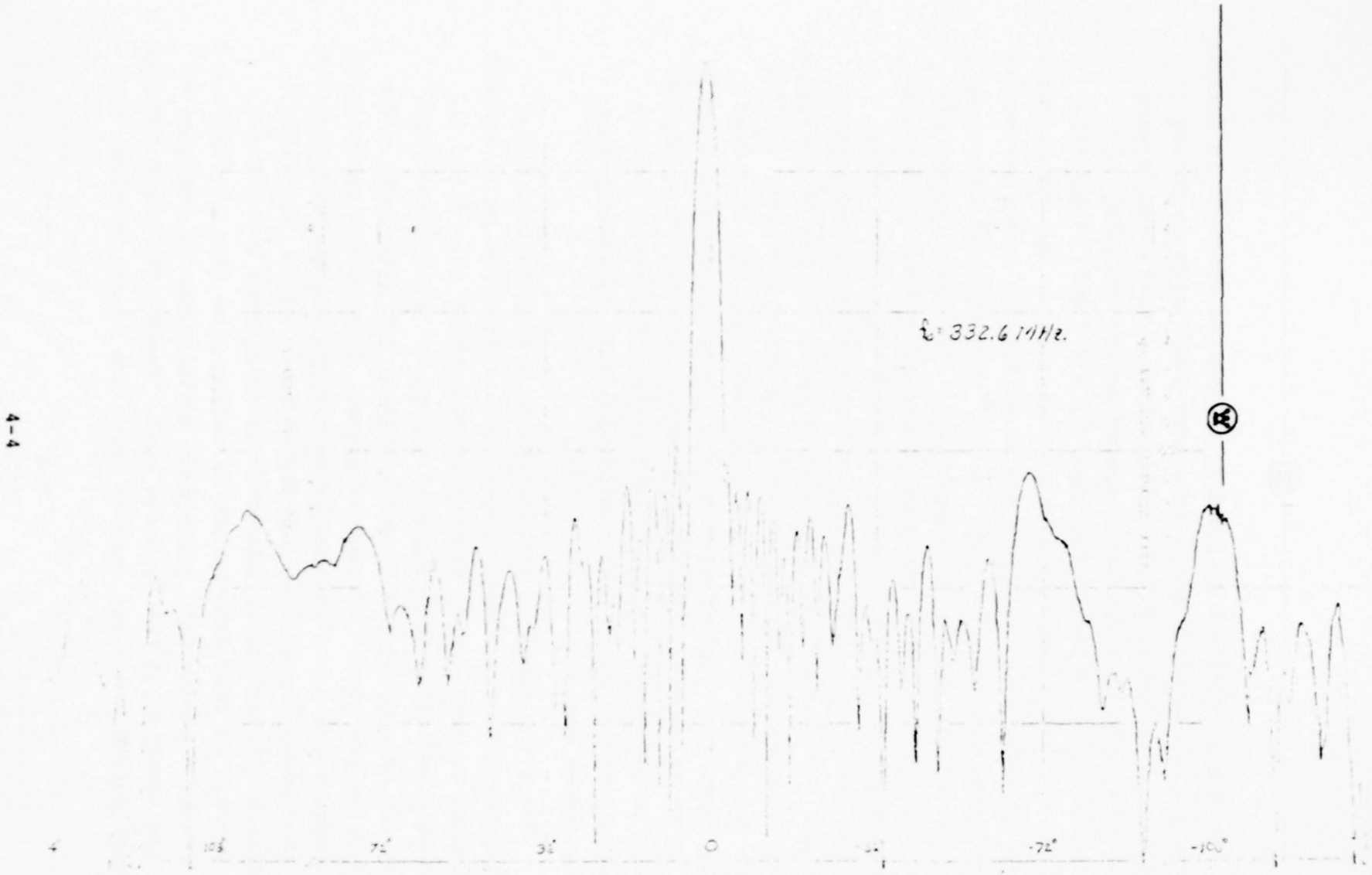

Figure 4-2 CSB Pattern Over 360°

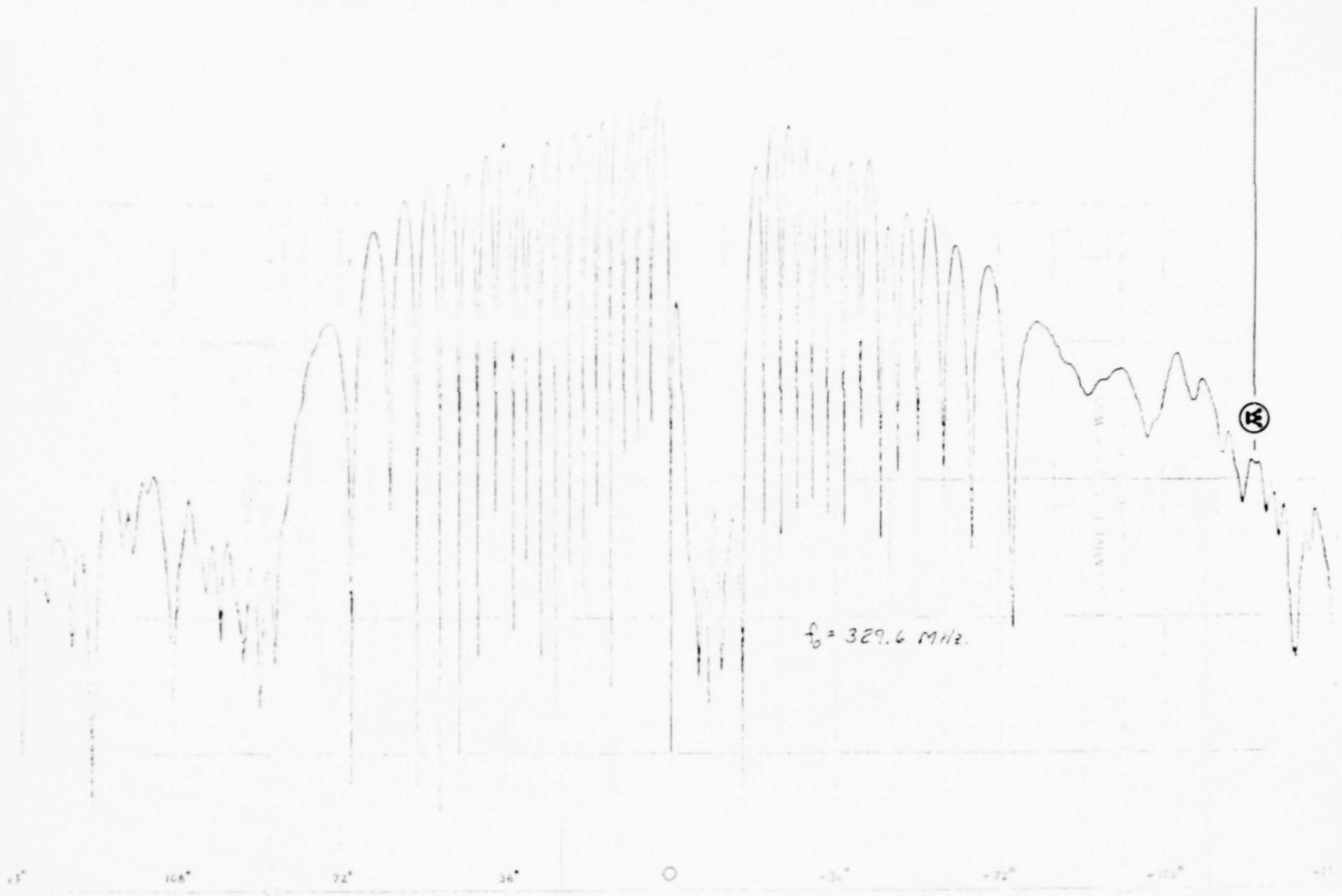

Figure 4-3 SBO Pattern Over 360° (f_o = 329.6 MHz)

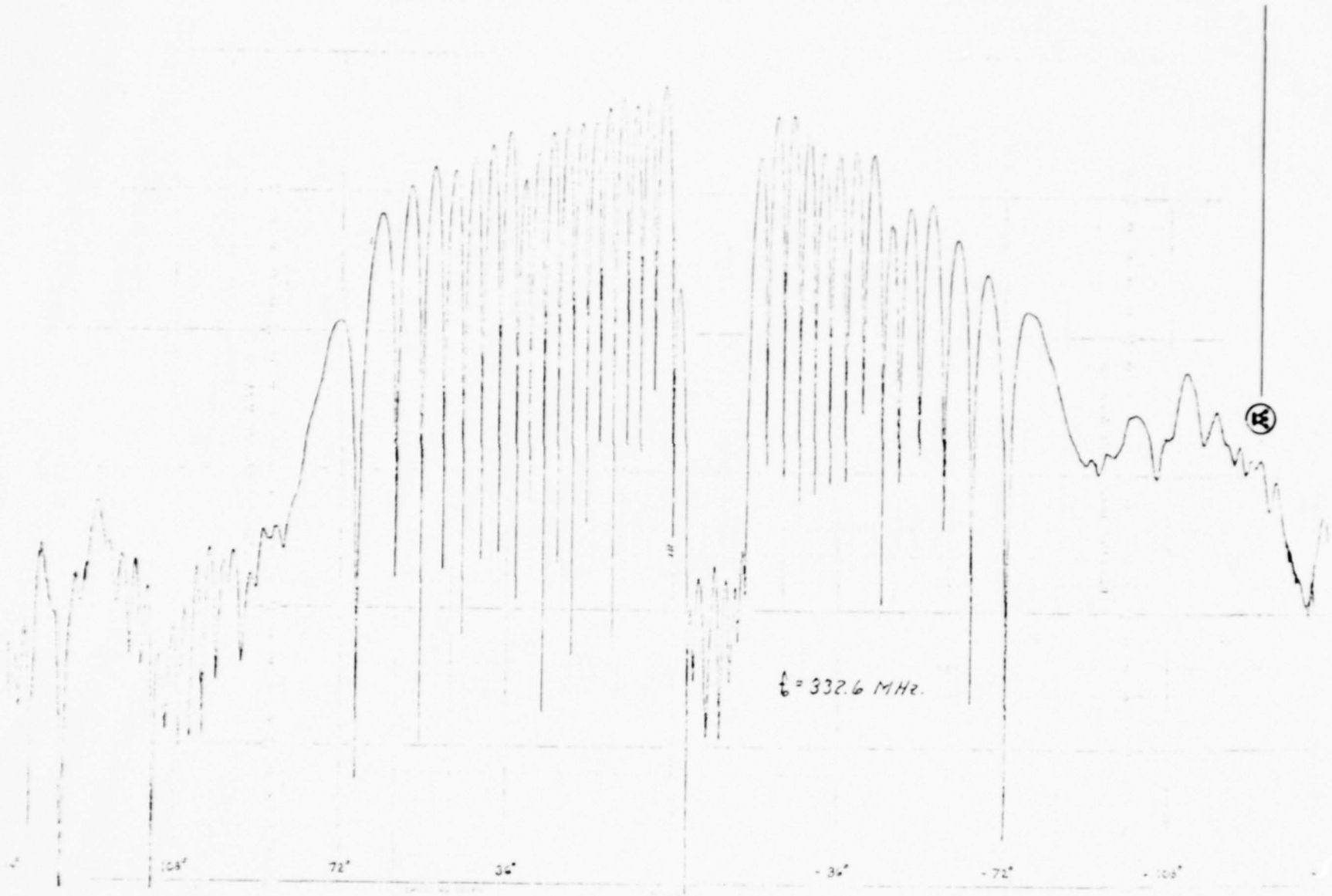

Figure 4-4 SBO Pattern Over 360° (f_o = 332.6 MHz)

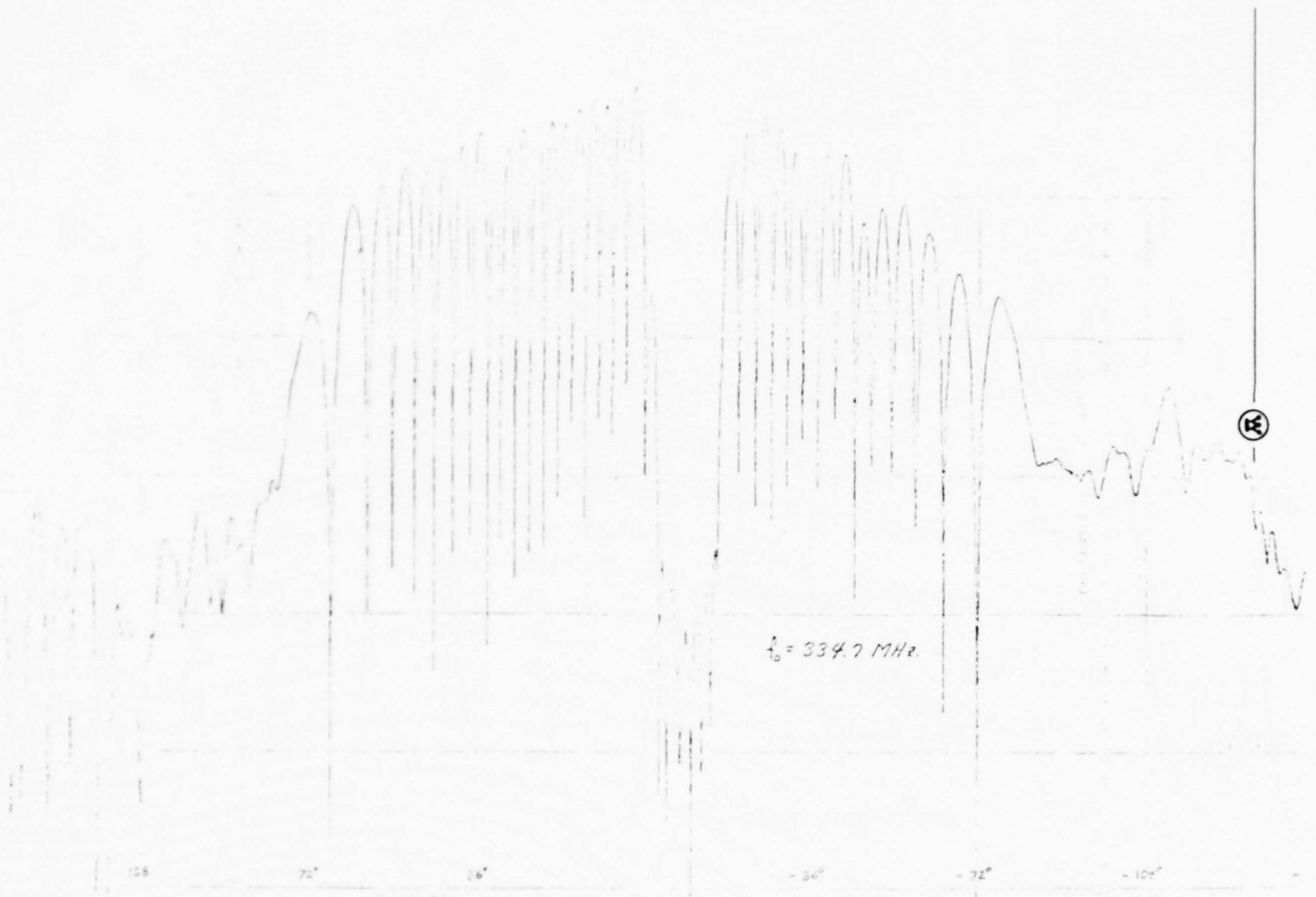

Figure 4-5 SBO Pattern Over 360° (f_o = 334.7 MHz)

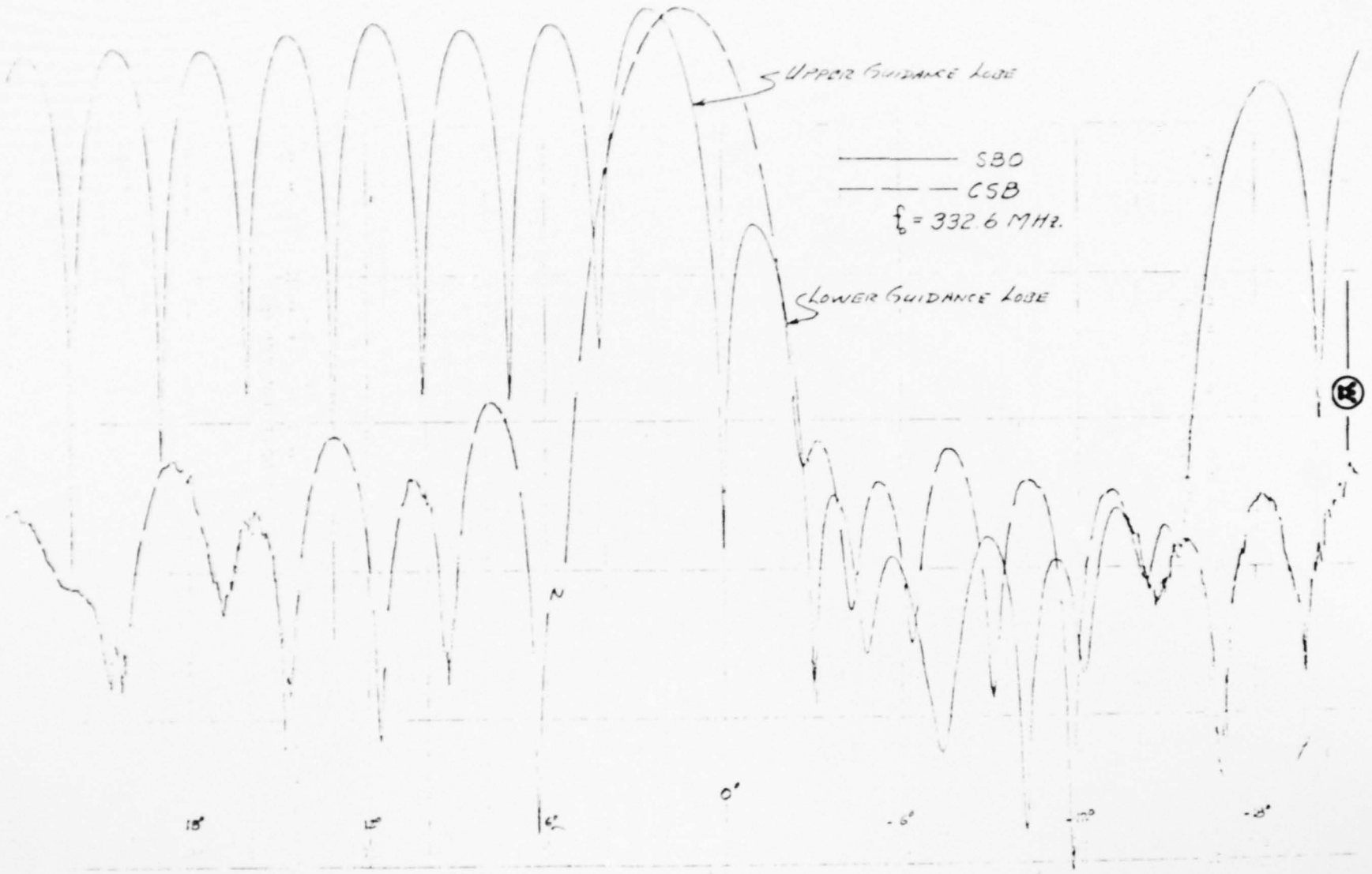

Figure 4-6 An Expanded Plot of CSB and SBO for f_o = 332.6 MHz

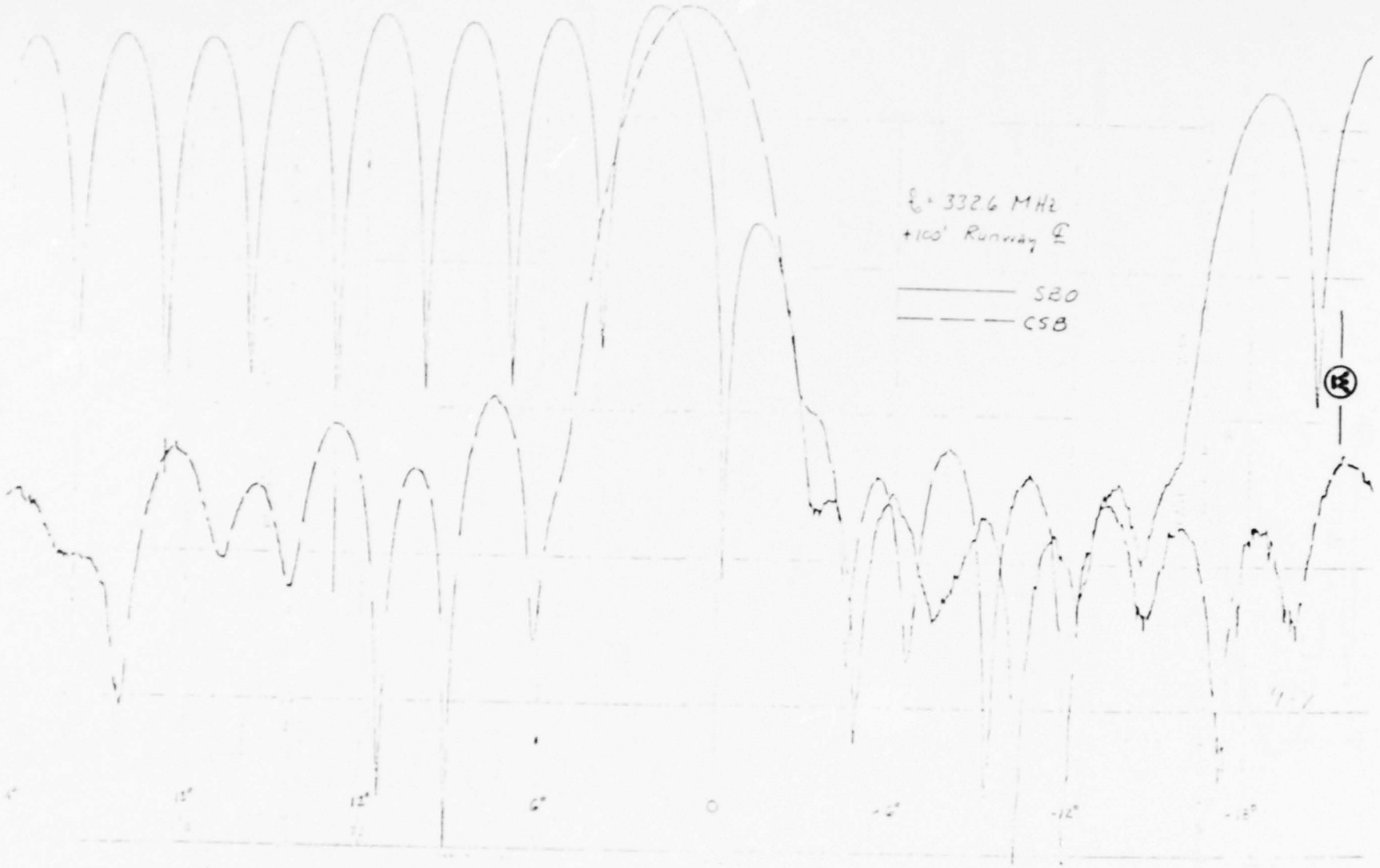

Figure 4-7 Antenna Pattern For A Cut At +100' Off Runway Center Line

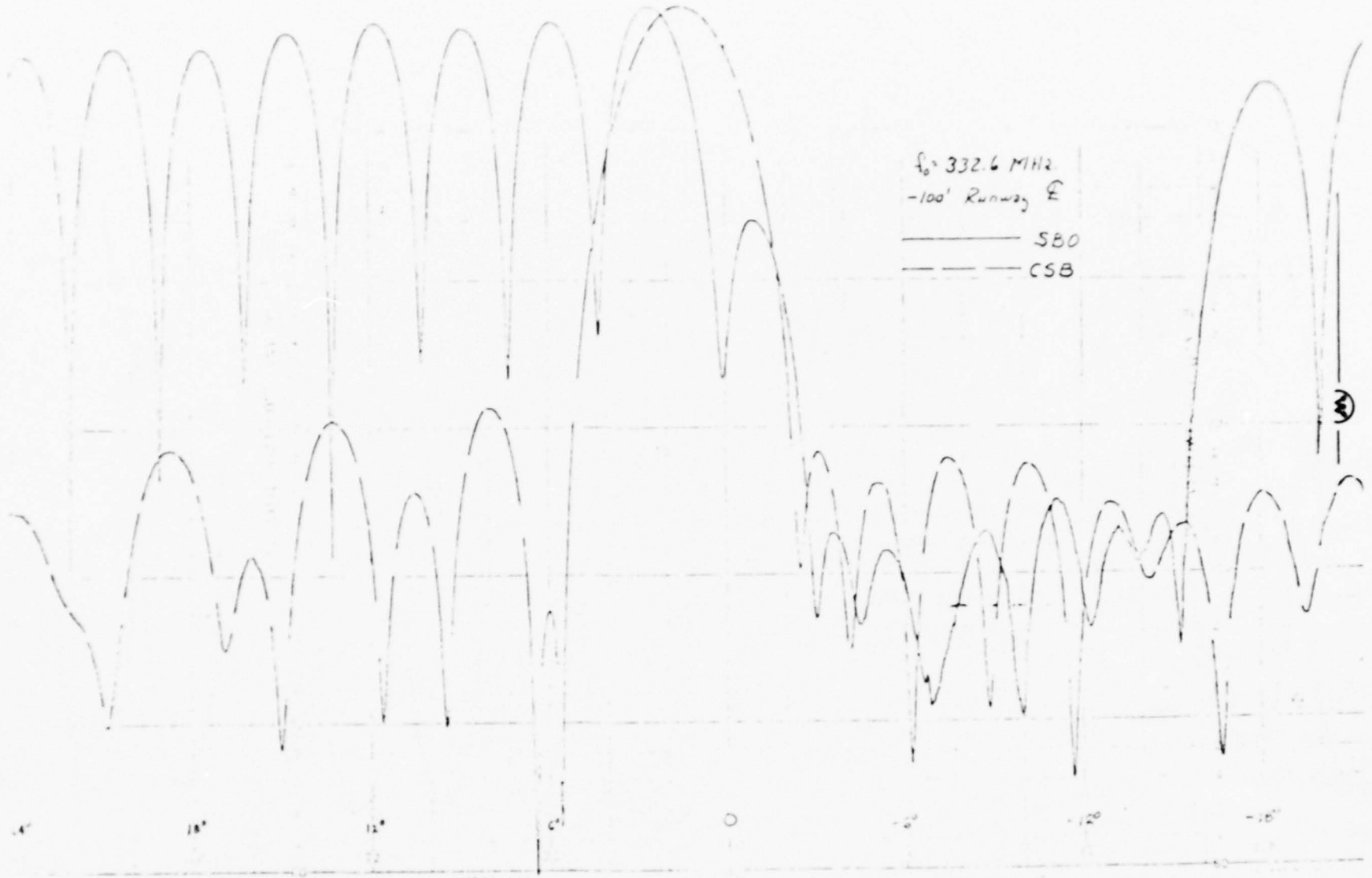

Figure 4-8 Antenna Pattern For A Cut at -100' Off Runway Center Line

respect to the runway center line. Glide slope antennas are also required to provide usable guidance at the localizer course extremes. This was tested by measuring patterns corresponding to aircraft approaching from $+8^{O}$ and -8^{O} off azimuth. This data is given in Figures 4-9 and 4-10. Again, the array performance is such that good flyability is achieved.

The data presented in this section is for the final tuned antenna excitation, and represents only a small fraction of the total patterns generated during this program.

4.2 ANTENNA FLIGHT CHECKS

Flights checks were performed on the Dipole Broadside Glide Slope Array in Lynchburg, Virginia, during the summer of 1976, by Dr. Richard McFarland of Ohio University Avionics Laboratory under contract to the F.A.A. During these tests, a connector design problem was discovered which resulted in numerous cable failures. This has been corrected, but did cause a large amount of invalid flight check data. Enough runs were made with the correct antenna excitation to demonstrate the antenna performance.

The antenna site was chosen to provide a test of performance over a rough ground approach. This did not correspond to any physical runway at Lynchburg. However, the site was chosen to have an approach path along the center line of runway 35-17 in order to provide the pilot with azimuthal guidance since there was no localizer. The ficticious middle marker was at the threshold of RW35. The ficticious threshold was at a point on RW35. Figure 4-11 shows the antenna location relative to RW35-17. For test purposes this represents an antenna with a backset of 200', offset of 560', for a threshold crossing height of 55'. The terrain both in front of the antenna and between the antenna and runway center line is quite rough.

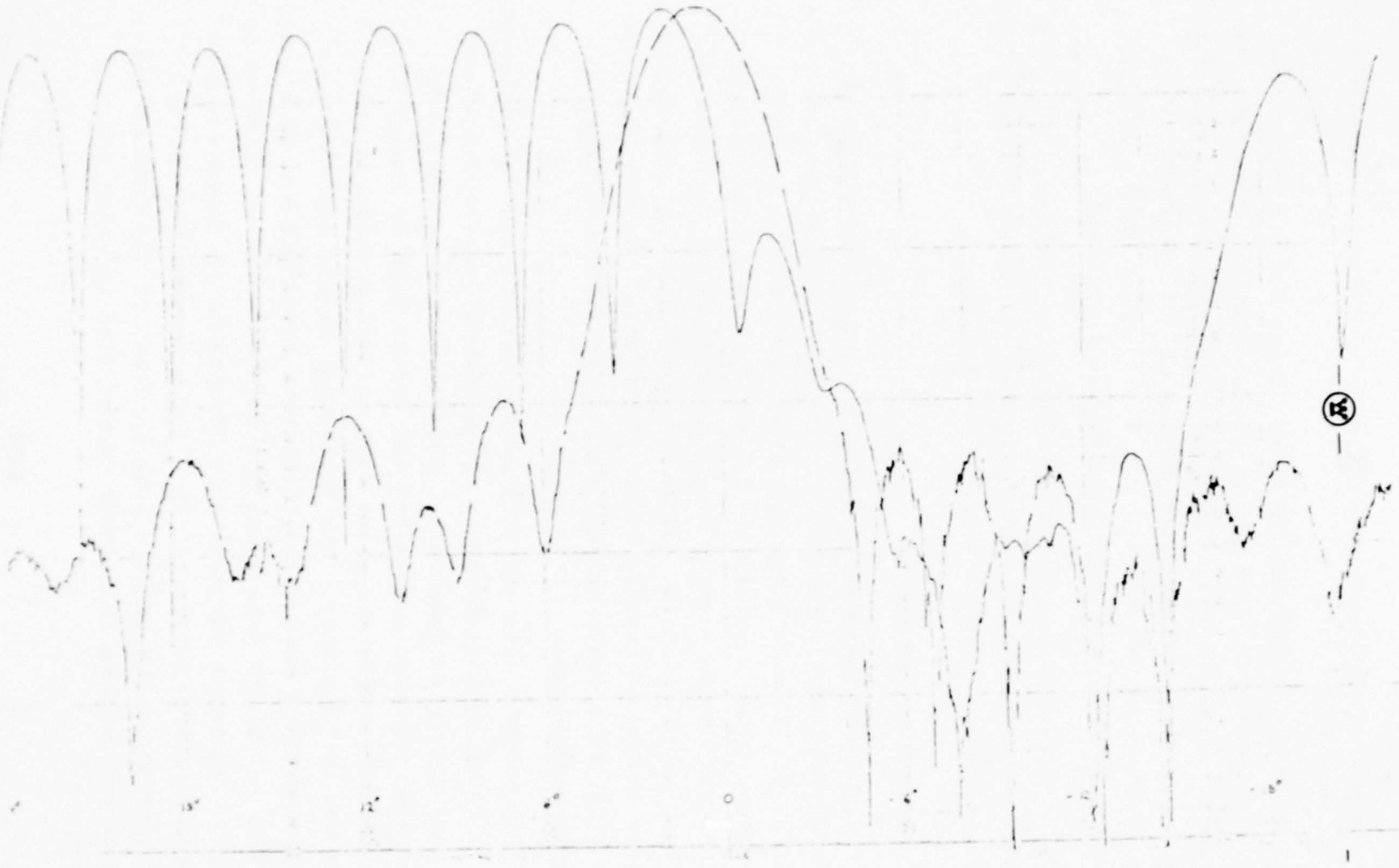

Figure 4-9 Antenna Pattern For +8° Off Azimuth Approach

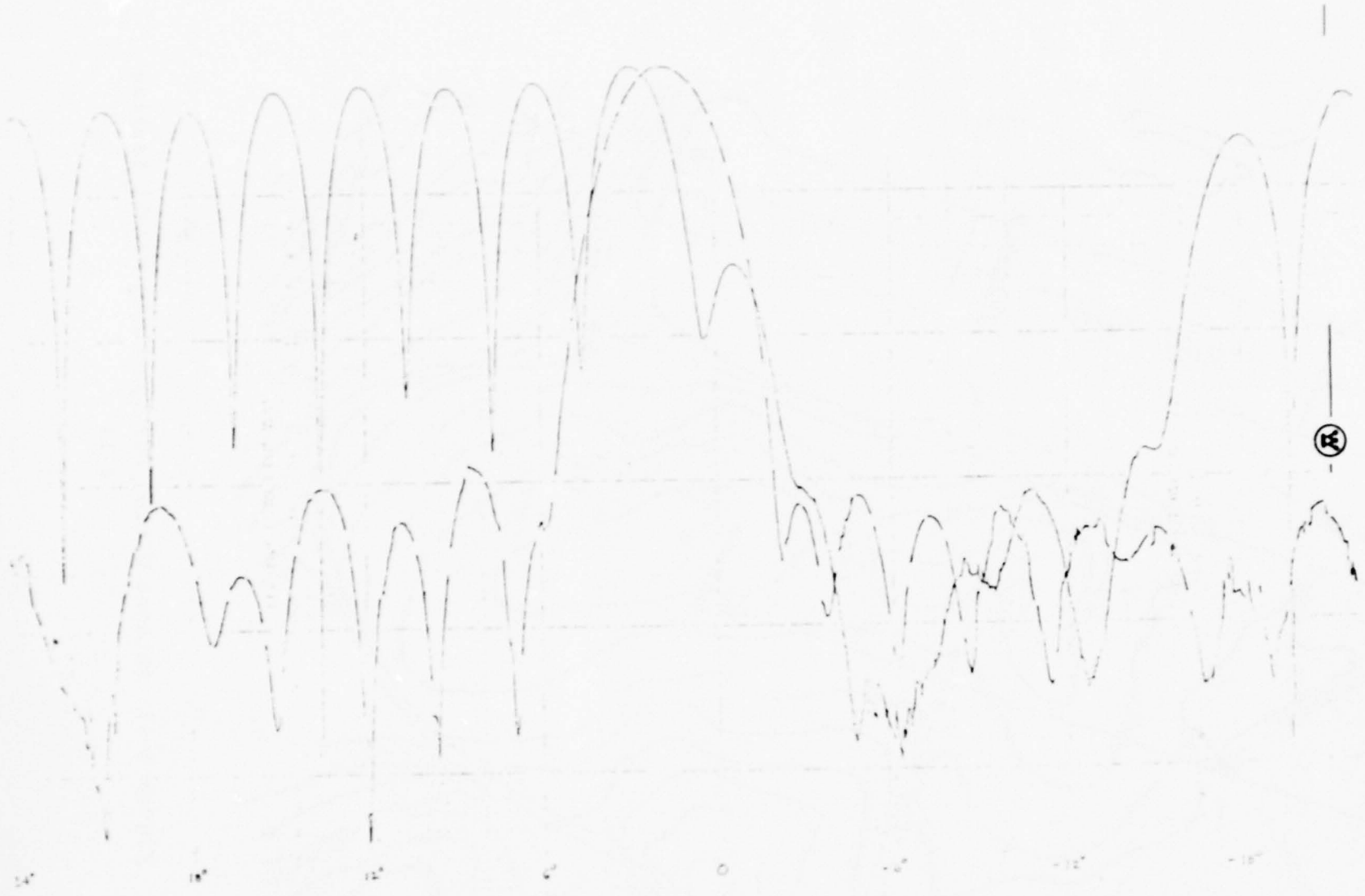

Figure 4-10 Antenna Pattern For -8° Off Azimuth Approach

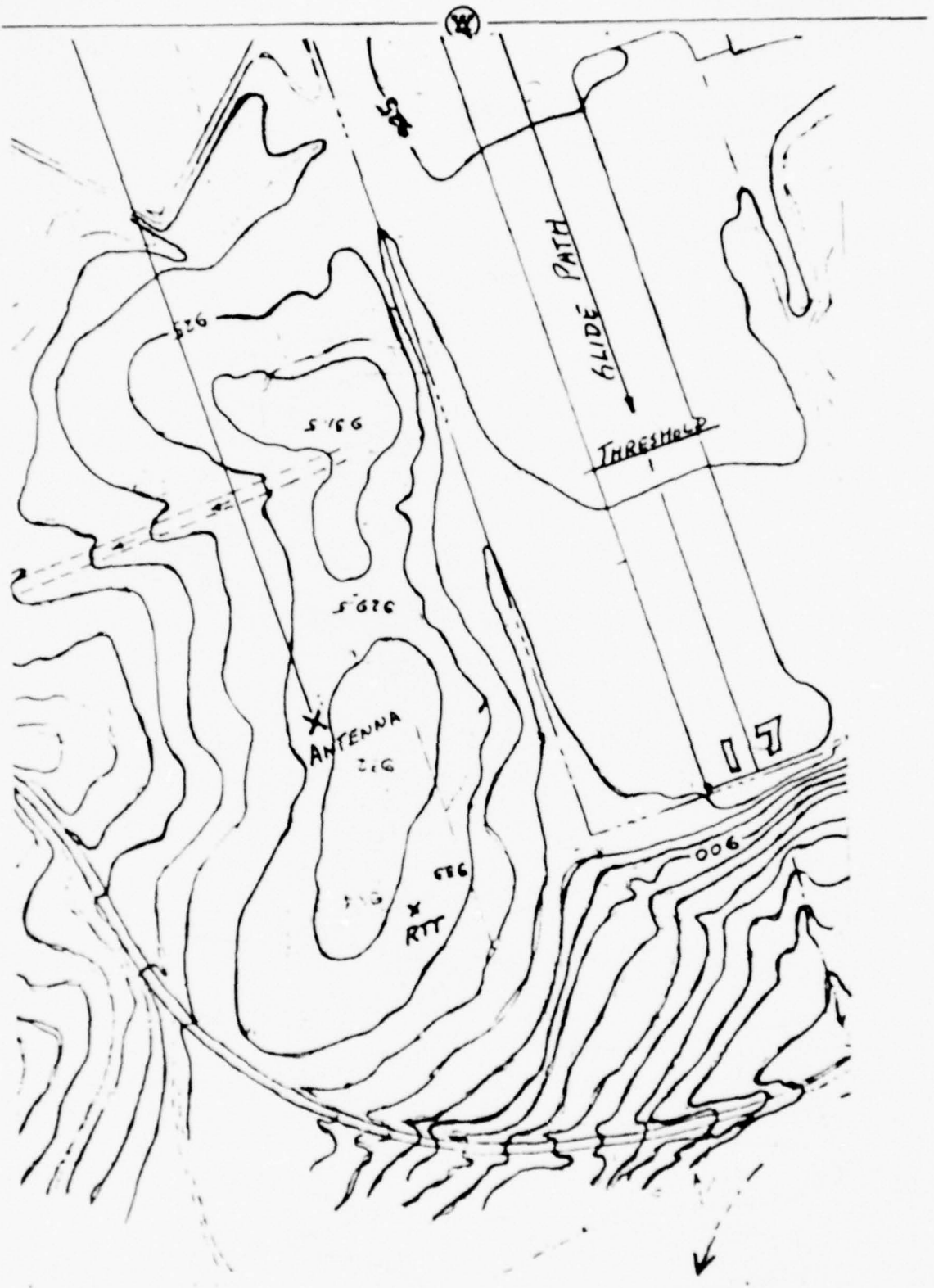

Figure 4-11 Antenna Siting For Lynchburg Flight Testing

Figure 4-12 is a photograph of the antenna installation. Figure 4-13 shows ground profiles both in front of the antenna and under the approach path. Note the large ditch within 600' of the antenna. The nearest mountain obstruction is almost 0.5° at a range of 2 n mi.

A normal commissioning flight check was performed including: (1) RTT runs, (2) level runs, (3) below path clearance runs, and (4) off azimuth approaches. This site was computer modeled for the Dipole Broadside Array and the predicted fly-in data is given in Figure 4-14. A typical measured fly-in is given in Figure 4-15, for a case when there were no cable faults. This data would be excellent for an image system over very flat ground let alone the severe terrain at this site. The agreement is quite close to the computer model. The maximum roughness in zones 1 and 2 is less than 8 μA. There is a slight flair up near threshold. There is no measurable scattering off the mountain top. This is uncorrected data just as it appeared at the output of the differential amplifier. If the correction for the RTT tracking error were applied, it would further smooth this data, particularly near threshold. An analysis of the RTT tracking error is given as an appendix to this report. Figure 4-16 is a level run. The transition is very linear and symetrical. The angle is a little high at 3.3°, indicating that the antenna backtilt should be decreased. Figures 4-17 and 4-18 are level runs at $+8^{\circ}$ and -8° off azimuth angles respectively. The slight shift in angle is consistent with the measured antenna pattern changes for off azimuth given in Figures 4-9 and 4-10. The only flight check test for which the antenna did not perform excellently was the below path clearance. Example data is given in Figure 4-19, which includes both the antenna signal and a theodelite track of the airplane. However, it was known prior to testing at this site that clearances would be marginal at 1000' to

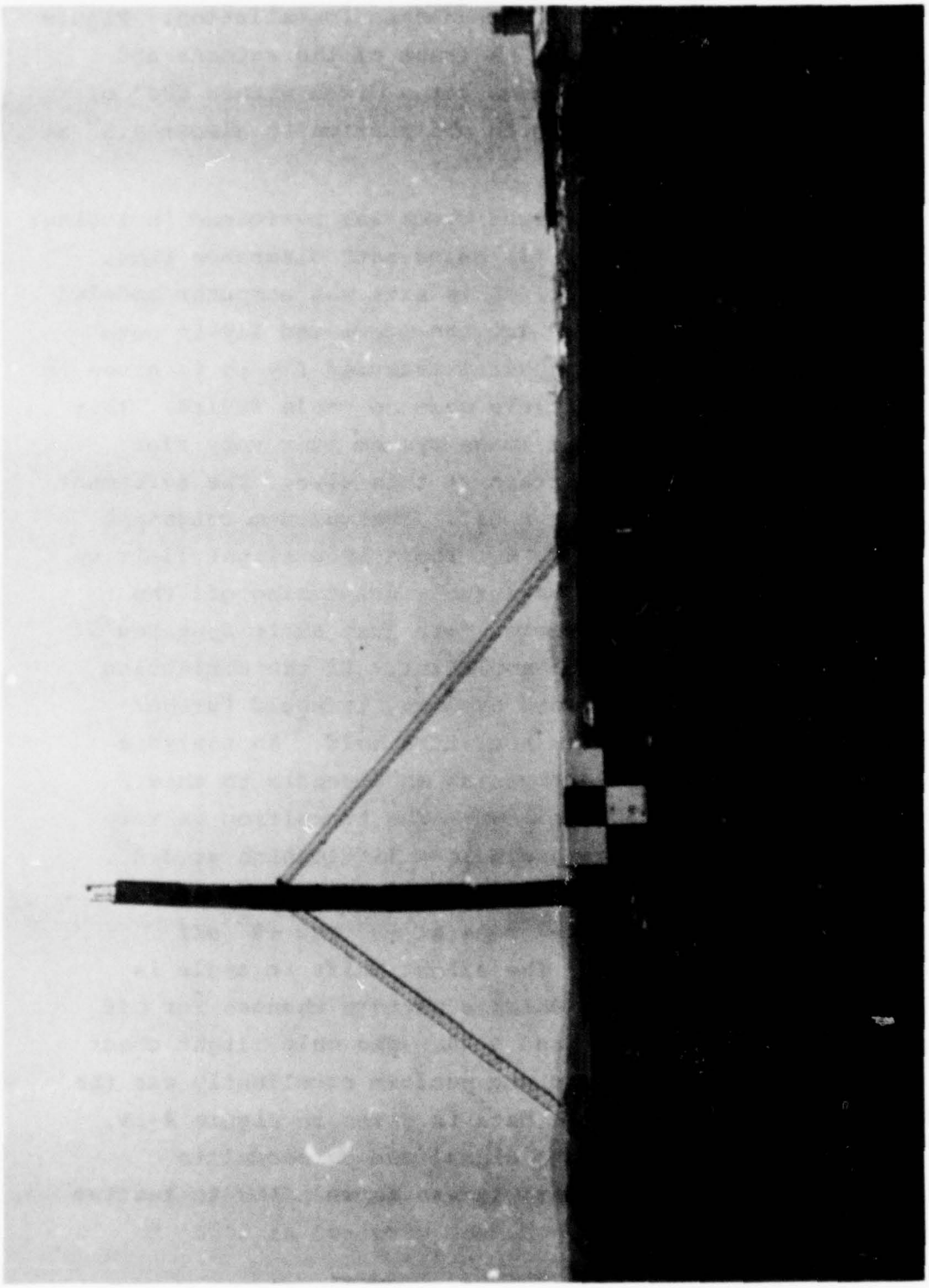

Figure 4-12 Antenna Erected At The Lynchburg Test Site

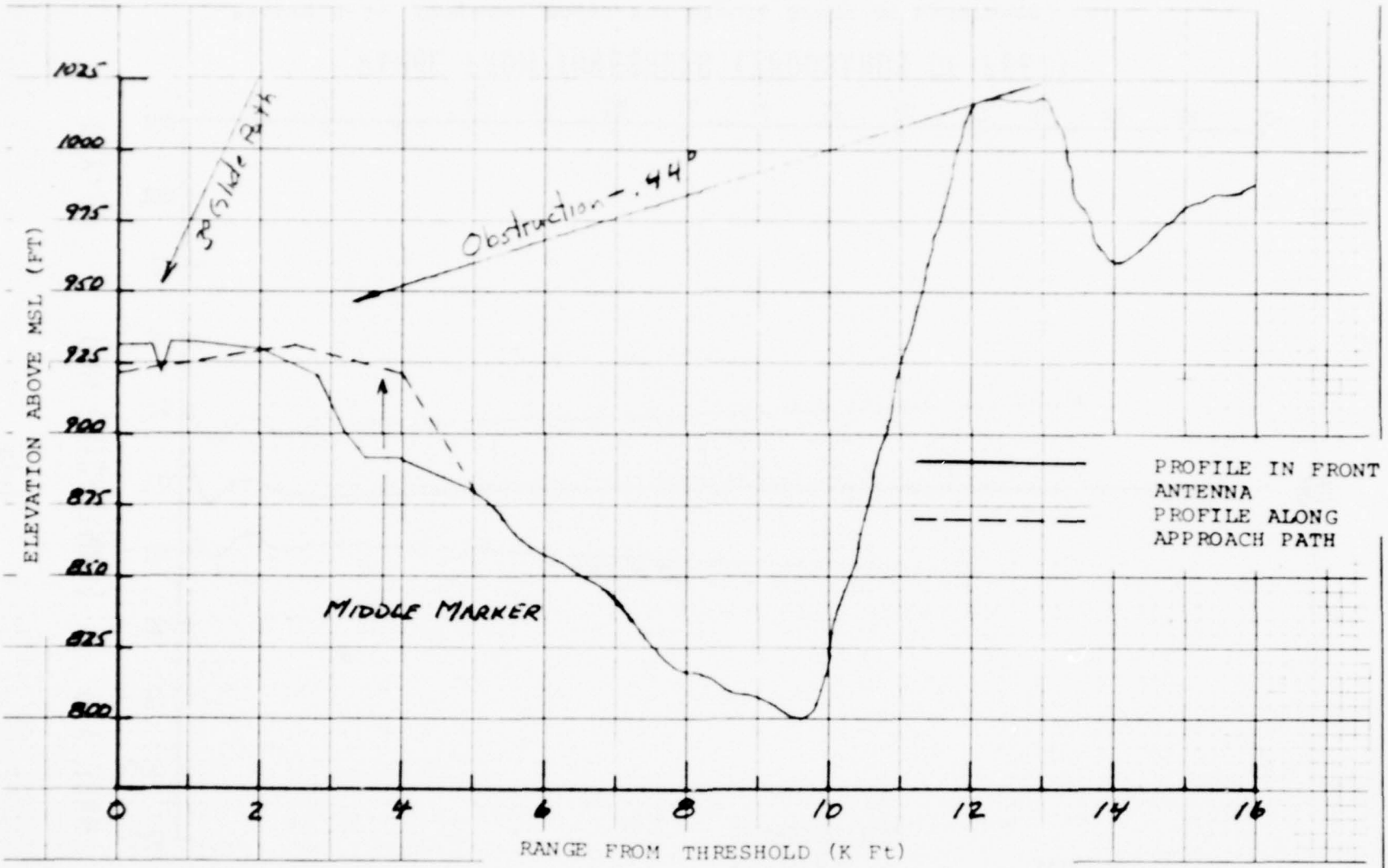

Figure 4-13 Approach Path Ground Profiles

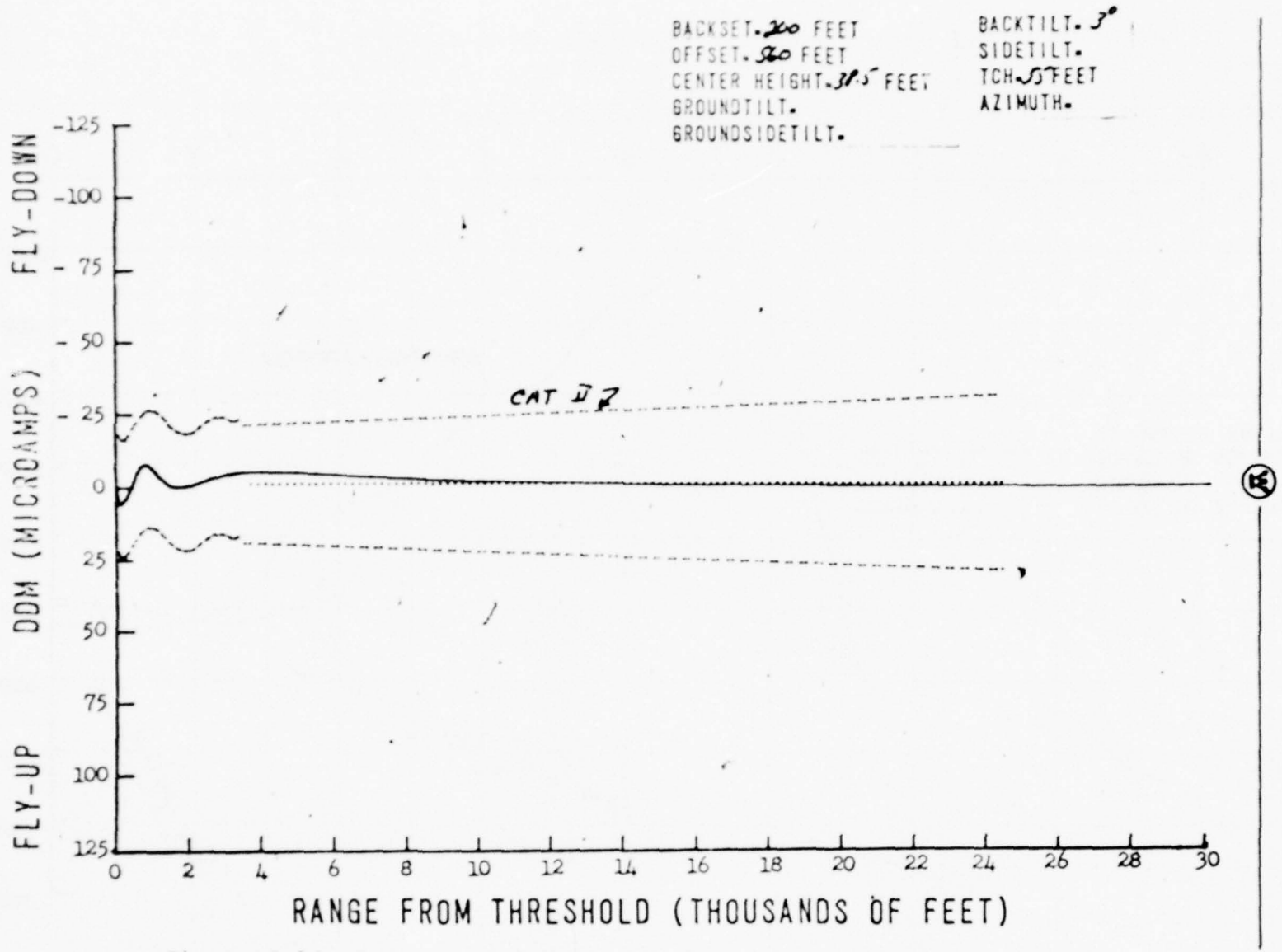

Figure 4-14 Computer Model For Dipole Array At Lynchburg, Va.

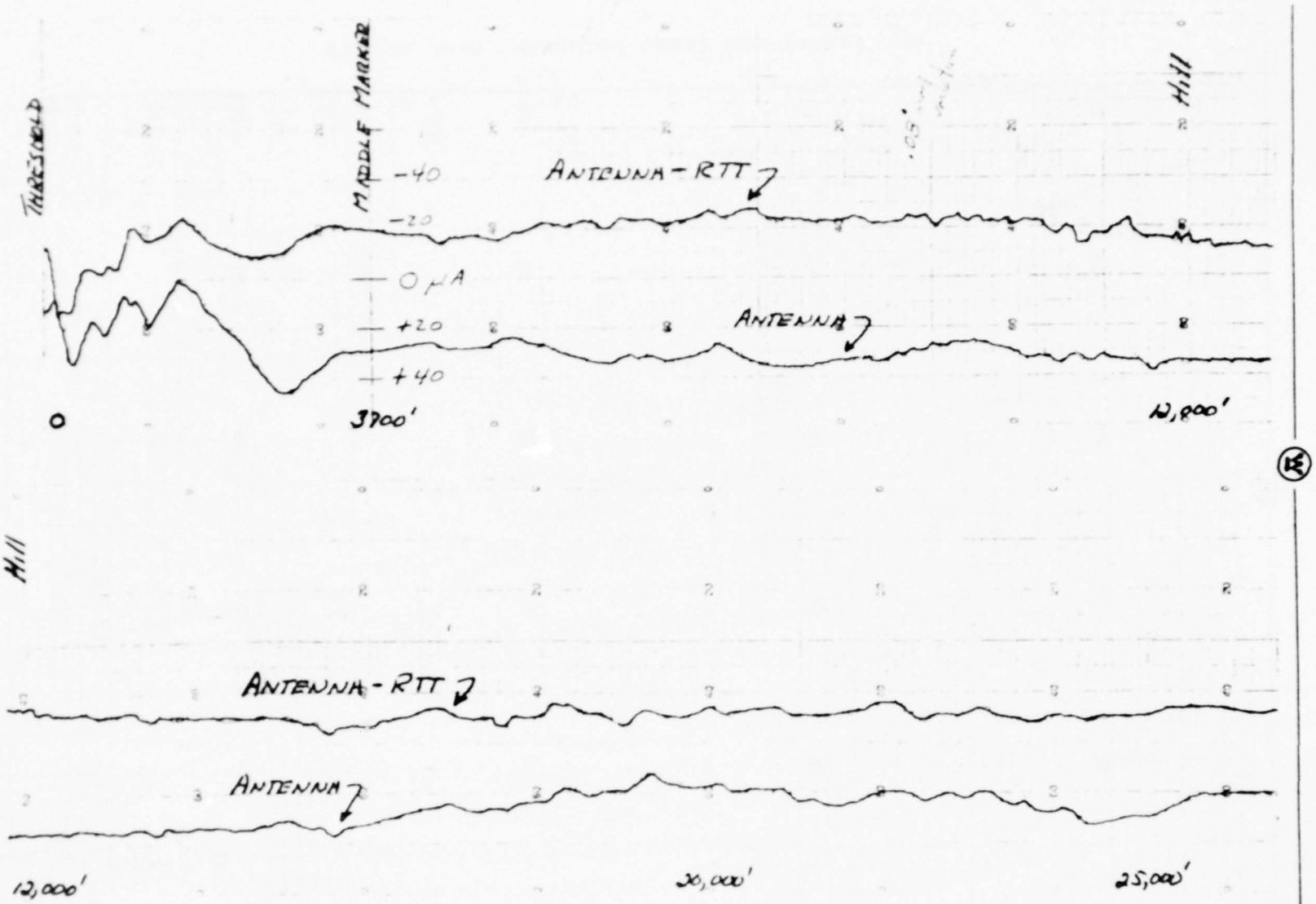

Figure 4-15 Typical Measured RTT Fly In Data

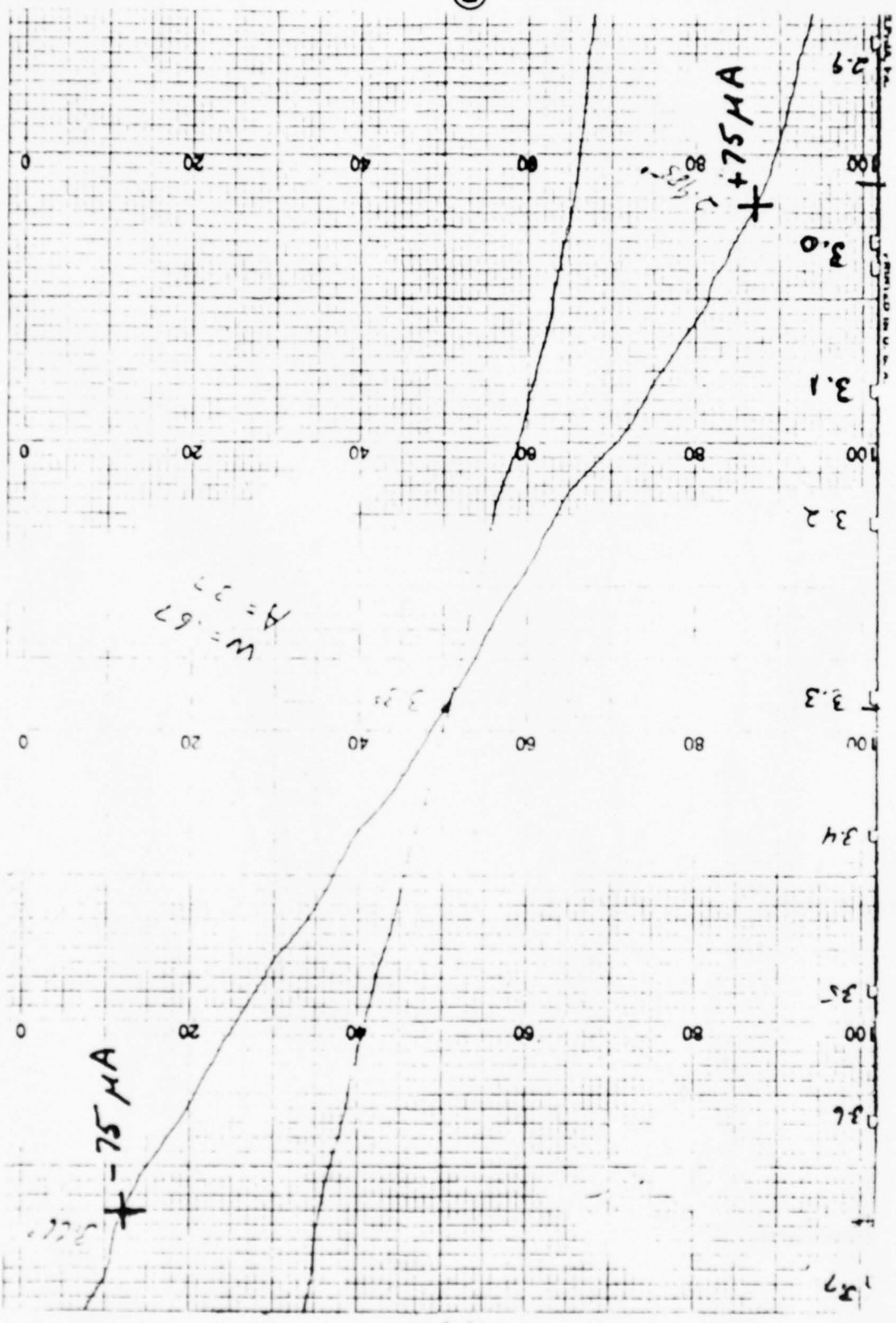

Figure 4-16 Measured Level Run Transition

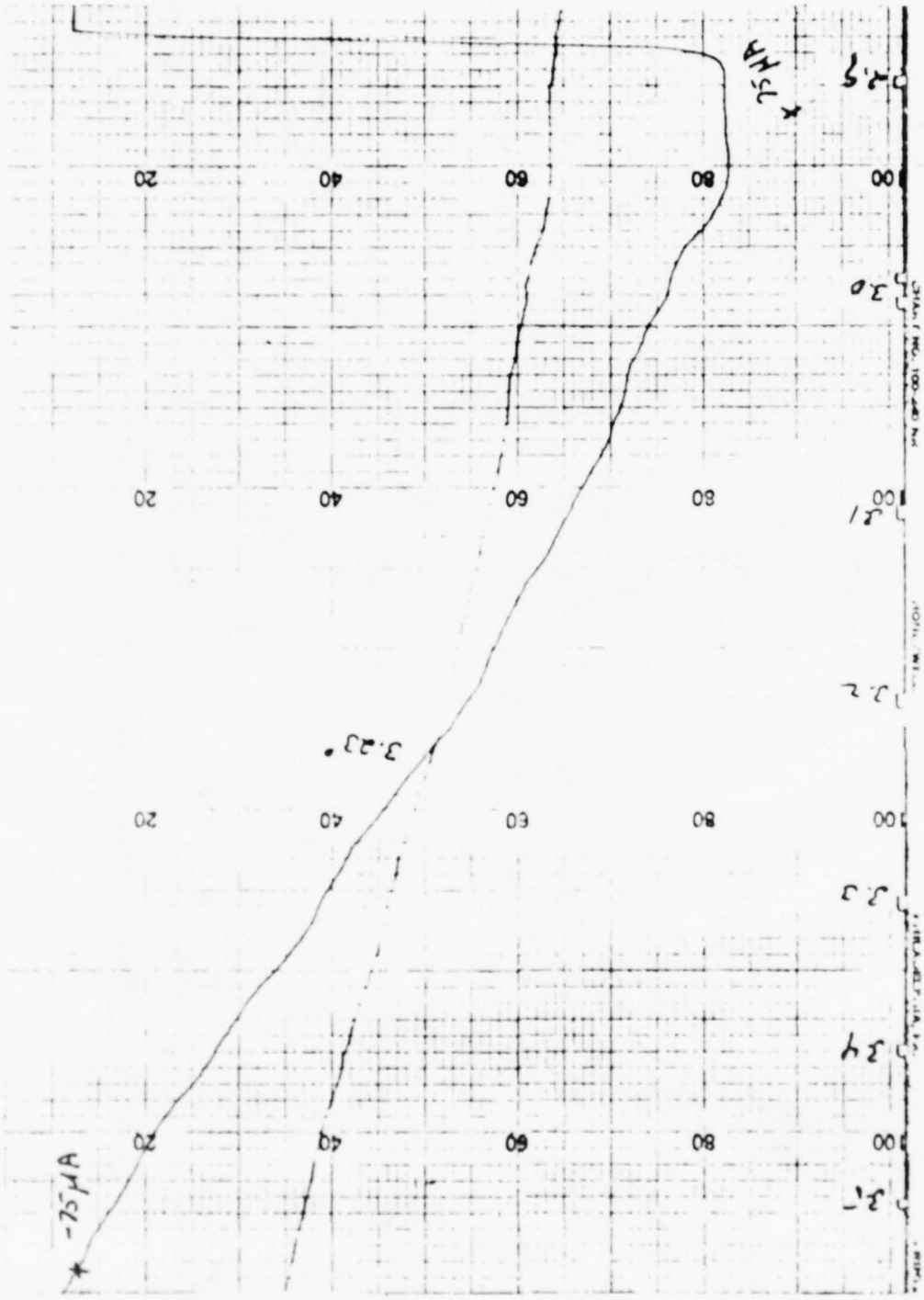

Figure 4-17 Measured Level Run For +8° Off Azimuth Approach

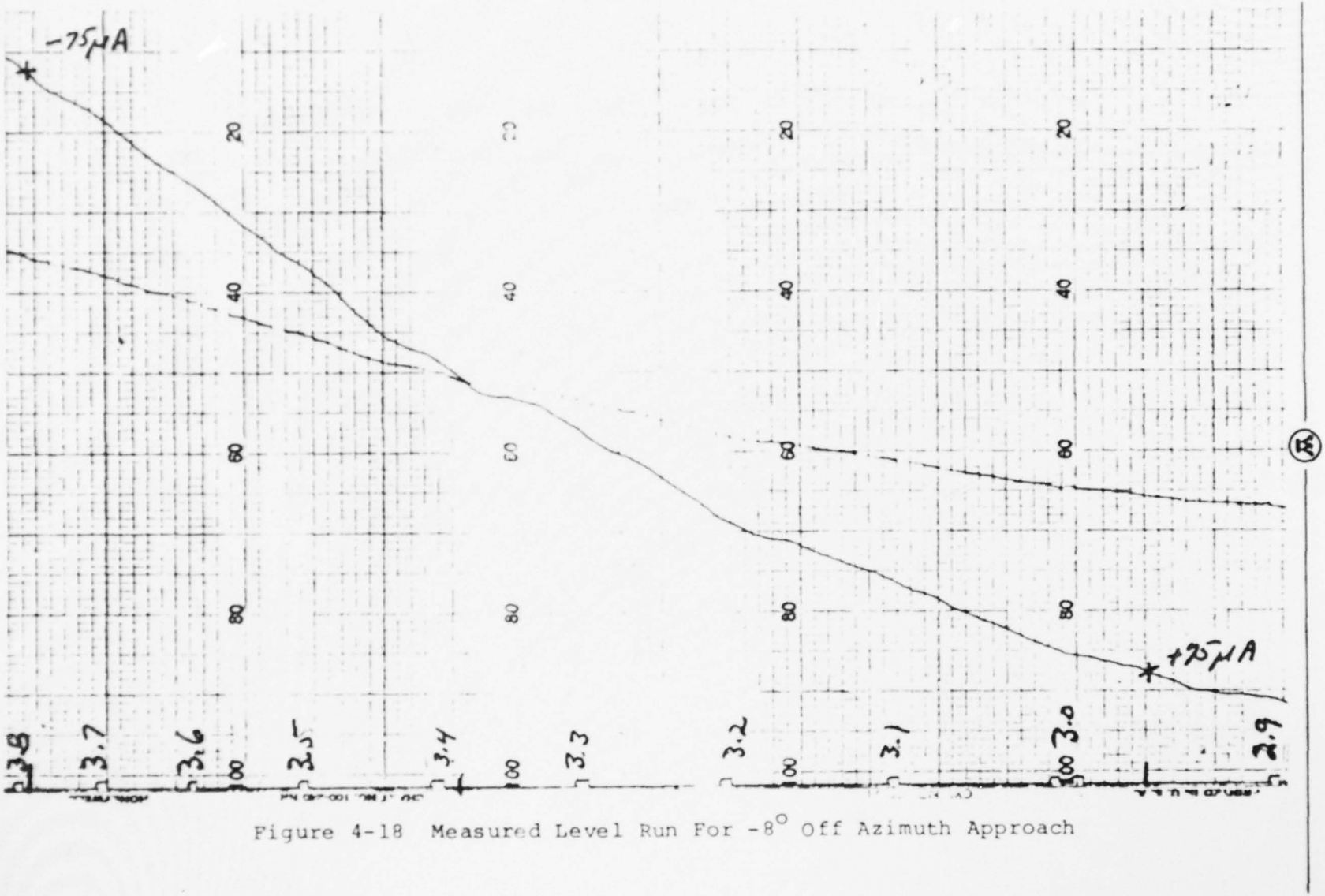

Figure 4-18 Measured Level Run For -8° Off Azimuth Approach

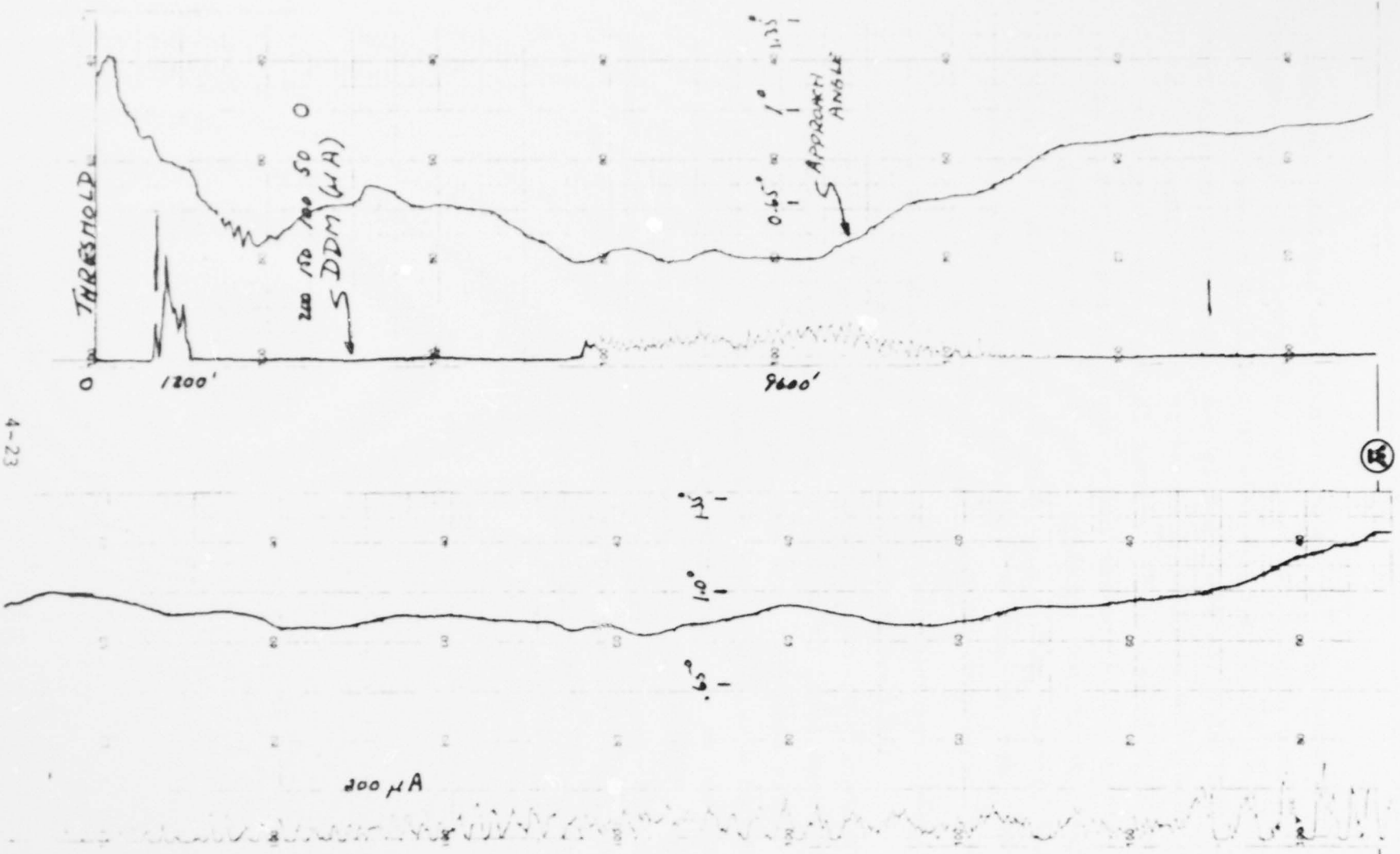

Figure 4-19 Measured Below Path Clearance

2000' from threshold. A computer simulation had been run which predicted this result, and is given in Figure 4-20. The loss of clearances is attributed entirely to the ditch between the antenna and the glide path, and is the only terrain modeled in Figure 4-20. The prediced decrease in clearance signal is not as large as that measured, and this is due to the fact that the computer simulation was for an approach angle of 0.5° while the test aircraft was actually at 0.9°. Had this been an operational site with a preliminary computer study, the antenna would have been located at a different position or some small amount of grading would have been recommended.

In summary, the antenna performed excellently at this site. Time and funding did not permit testing at more than one frequency. However, antenna pattern range data indicates that the same level of performance can be expected across the band. This same test site was used in 1972 to test the Compensated Waveguide Glide Slope Antenna, which has since been commissioned at six sites with two additional installations in progress. The dipole array substantially out performs the compensated waveguide in all regards. The structure is improved by about 12 dB average and the linearity of the level run transitions is significantly better.

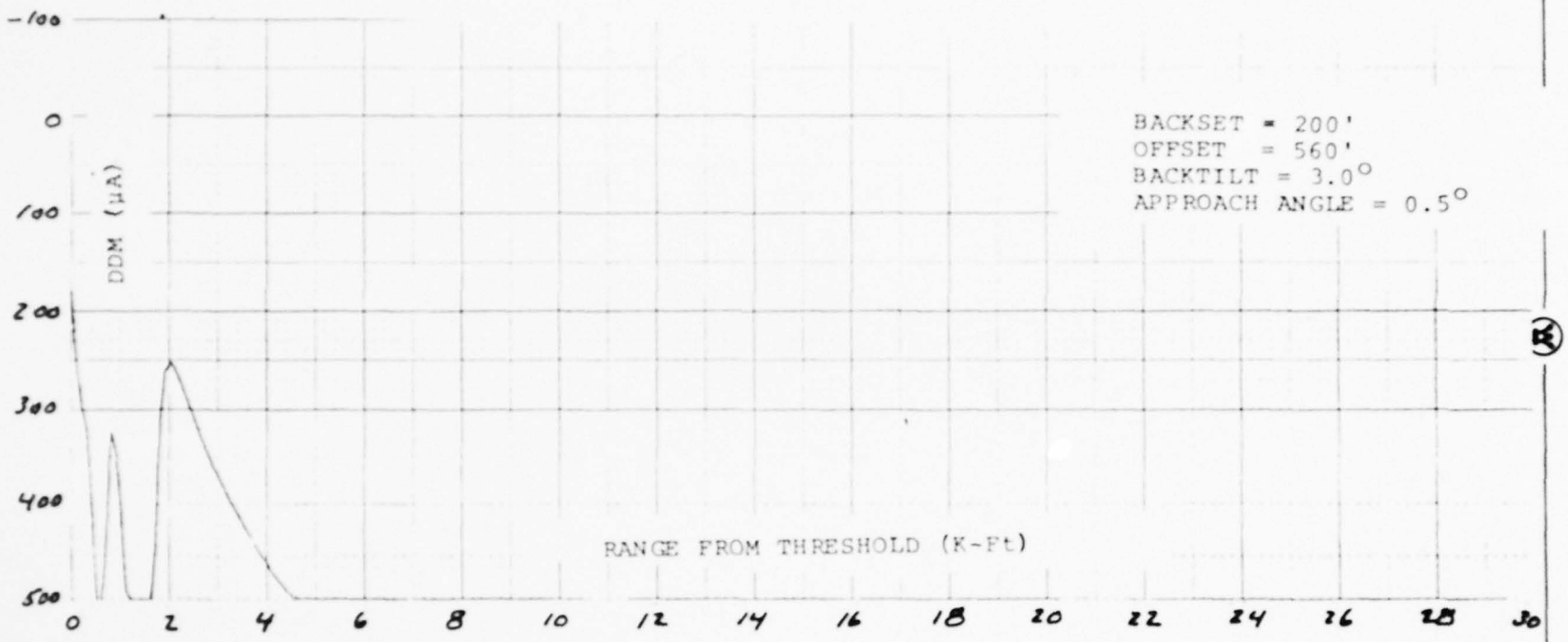

4-25/26

Figure 4-20 Computer Model Of Below Path Clearance

5.0 CONCLUSIONS AND RECOMMENDATIONS

An antenna has been designed which meets all the performance goals of the contract. It is broadband, and was shown to provide Category II performance over a wide range of severe terrain conditions. The antenna had a reliability problem which appears to have been solved, although no field tests have been performed since the modification.

Antenna tests were performed on both the antenna pattern range and flight checks in the field. These have shown an excellent antenna performance. In addition, an extensive program of computer modeling has indicated that the antenna can provide CAT II over a large class of problem terrain types.

The reliability problem which occurred during the field tests was entirely attributed to the failure of SMA connectors due to very long cable runs which were heavy and susceptible to thermally induced stress. In consultation with several cable manufacturers it was determined that the required reliability could be achieved by replacing all SMA connectors with phase stabilized cable with preformed bends and TNC connectors. This modification has been incorporated into the antenna but has not been field tested.

The antenna had been assembled and field tested prior to the final design of the monitor system. Hence, some rework had to be performed in order to incorporate the monitor sampling probes into the vicinity of the radiating elements. This required digging every dipole element out of the foam and replacing the element feed printed circuit with a board which, in addition to the dipole feed, contains a 20 dB coupled section for the monitor signal pick-up. It was felt that this could be done with little or no change to the effective aperture distribution. This is probably the case. However, in replacing the dipoles and re-foaming them in place, the single-cell foam construction

was destroyed. This allowed moisture to accumulate in the vicinity of the dipole, drastically altering the radiation characteristics. The normal radiation pattern was lost. While the foam was intact from the initial construction, the antenna had survived through several years of rain and snow. The problem only occurred after the foam had been removed, and replaced in the vicinity of the dipoles. Since it may be necessary to remove a dipole at some time, this points out a mechanical design problem. This must be corrected prior to an installation of this antenna system. It is recommended that all the foam be removed and that the structure housing the dipoles be strengthened to be self supporting without the need for foam. If this modification was incorporated, it is felt that the antenna reliability would be consistent with long term ILS requirements. A preliminary design modification has been completed, and the new type of construction would result in a small cost saving per unit.

The printed circuit distribution boards have been disassembled and tested after several years in an outside environment. They performed perfectly, with no sign of any deterioration. It is felt that this type of distribution system is a sound approach to low cost-high reliability ILS arrays.

In order to make the present antenna usable at a field site would require; (1) removing the foam and strengthening the mechanical structure, (2) re-measuring the radiation patterns in order to adjust for any small changes in excitation produced by the structure change, and (3) performing a field flight check in order to validate both the performance of the antenna and the monitor systems. Sufficient data has been accumulated on this program to indicate that this would provide an antenna system capable of providing an exceptional quality of CAT II performance at an extremely difficult site.

Aside from the present antenna, the monitor technique described in this report has a broad application to the monitoring of any system containing a large number of radiators and cables. For example, it can be directly applied to monitoring a localizer array. This could be accomplished using this monitor in its exact configuration, with the substitution of a reversed coupled directional coupler as a sampling device.

APPENDIX A

ANALYSIS OF RTT TRACKING ERROR

In the performance of a flight check it is necessary to know the exact position of the test aircraft at all points on the approach path in order to properly evaluate the performance of the glide slope system. This was accomplished by using Radio Theodelite Tracking (RTT), the system used on this contract. (The present system uses an inertial platform and computer analysis to provide this positional information.) The RTT has an inherent error which is a function of the geometry associated with the fact that the RTT cannot be located on the runway at the touch down point (TDP). (Note that the new inertial system also has an inherent error originating in the fact that it measures the angle from the aircraft to the antenna not to the touch-down point. This is not a significant error for image systems, which are located opposite touch-down, but is very significant for broadside arrays, which are considerably closer to threshold. The analysis to follow can be applied directly to this case if the antenna is assumed in place of the RTT.) An analysis was performed to determine the RTT error. This also resulted in defining a better mode of operation which produces a smaller RTT error.

The question of RTT error can best be understood by a simple example. The system is calibrated with the test aircraft at a large range. It is adjusted to provide $0\angle A$ for a 3° angle and $\pm 75\angle A$ for angles of $\mp 0.35^{\circ}$. Assume the aircraft flies in and never deviates from the 3° glide path. In the extreme case as the aircraft passes the RTT location, the RTT

operator must remove 3° from the theodolite in order to track the aircraft. This results in a very large signal in $\measuredangle$A being transmitted to the aircraft, when in actuality the signal should be 0$\measuredangle$A since the aircraft is in the 3° glide plane. This is the extreme error case. However, some error is present at all ranges, and increases as range decreases. This error is geometric in nature, and hence, some care is required in siting the RTT.

The geometry associated with this analysis is given in Figure A-1. It is desired to know the aircraft's true position. However, the RTT measures an angle, α', between the aircraft's location and the horizontal, at the RTT location. The terms used in the analysis are defined as:

- y = RTT offset
- b = RTT backset
- h = RTT height
- α' = RTT angle referenced to horizontal
- TCH = threshold crossing height at the desired glide path angle
- x = range from threshold to the aircraft
- $\bar{h}$ = height of desired glide path at the aircraft location
- $\bar{h}'$ = height of the aircraft referenced to the desired glide path

This analysis assumes that the aircraft remains over the runway center line extended, since there is no measurement made on azimuthal error. The measured angle, α', is only equal to the true glide path angle if the theodolite is located at the touchdown point. The next best case requires the theodolite to be located in the plane containing the desired glide path. Assuming flat ground between the RTT position and threshold, the RTT height which places it in the desired glide plane is given by,

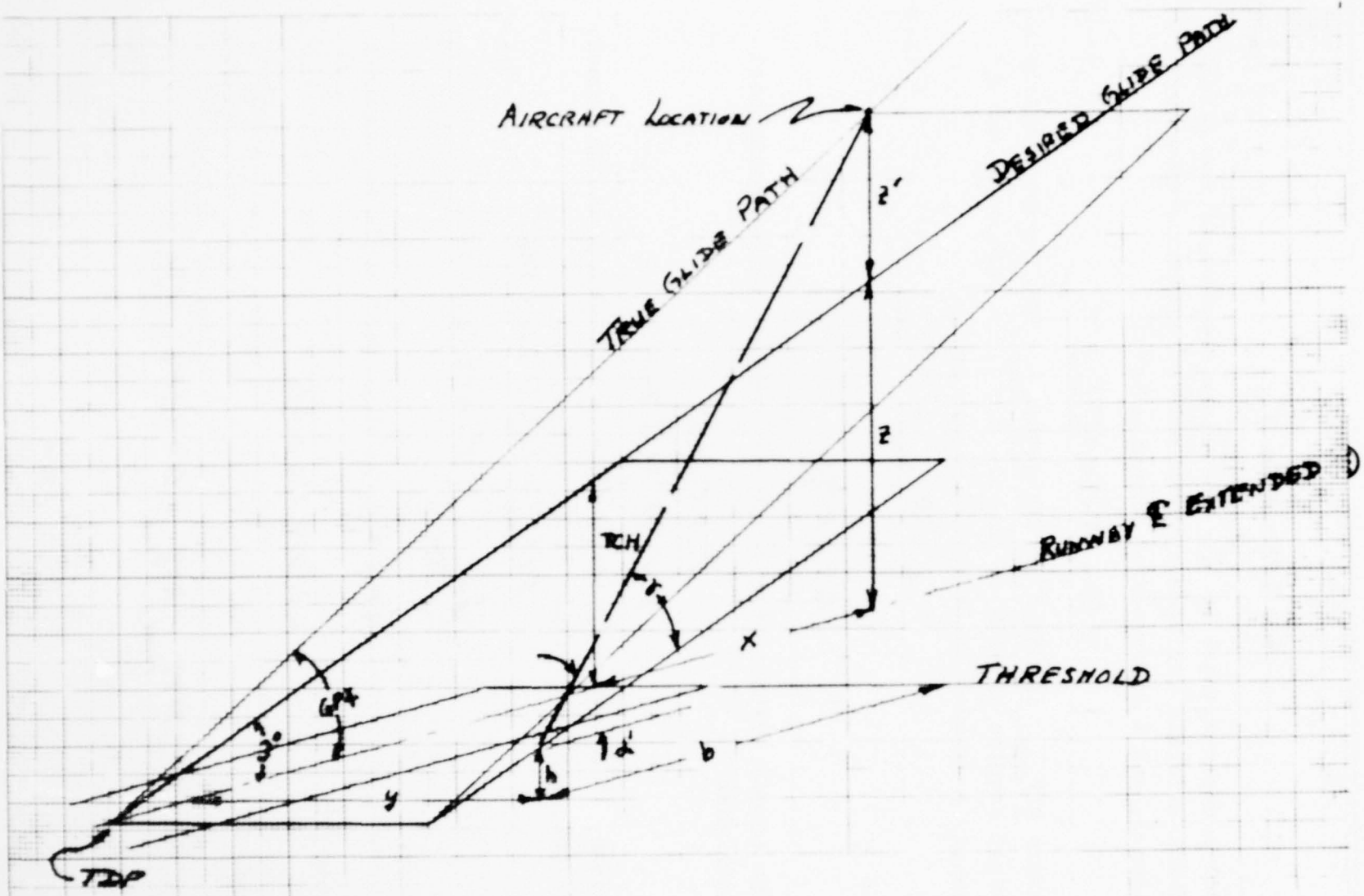

Figure A-1 Geometry For RTT Error Analysis

$$h = TCH - b \tan 3^\circ, \tag{A-1}$$

for a desired angle of 3°. The chart recorder on the flight check aircraft includes outputs for the antenna signal, RTT signal, and a differential output given by.

$$Diff = Ant - RTT_{Meas}, \tag{A-2}$$

where RTT_{meas} is based on the angle α'. The correct evaluation would require the RTT to measure the glide path angle not α'. Hence, a correction is needed, given by,

$$\Delta = RTT_{Meas} - RTT_{True} \tag{A-3}$$

or

$$Ant - RTT_{True} = Diff + \Delta \tag{A-4}$$

The normal RTT calibration is with respect to the horizontal, such that,

$$3^\circ = 0\ \mu A$$

$$3^\circ \pm 1.35^\circ = \mp 75\ \mu A$$

Hence, 1° of RTT displacement yields $214.286\ \mu$A of RTT signal, allowing the RTT signal to be written as,

$$RTT_{Meas} = (3^\circ - \alpha')\,214.286 \tag{A-5}$$

$$RTT_{True} = (3^\circ - GP\measuredangle)\,214.286 \tag{A-6}$$

where

$GP\measuredangle$ = true glide path angle to aircraft.

Let,

$$A = 214.286\ \mu A/^\circ,$$

then

$$RTT_{Meas} - RTT_{True} = \Delta = (GP\measuredangle - \alpha')A. \tag{A-7}$$

From the geometry of Figure A-1,

$$\text{Tan GP}\not\angle = \frac{z' + z}{\frac{TCH}{\text{Tan } 3^\circ} + x} \tag{A-8}$$

and

$$\text{Tan } \alpha' = \frac{z' + z - h}{\sqrt{(x+b)^2 + y^2}} \tag{A-9}$$

which for the case of equation A-1 is,

$$\text{Tan } \alpha' = \frac{z' + z + b \tan 3^\circ - TCH}{\sqrt{(x+b)^2 + y^2}} \tag{A-10}$$

Eliminate Z' + Z between equations A-8 and A-10,

$$GP\not\angle = \tan^{-1}\left\{\frac{\tan 3^\circ}{TCH + x \tan 3^\circ}\left[\sqrt{(x+b)^2+y^2}\,\tan\alpha' + TCH - b\tan 3^\circ\right]\right\}. \tag{A-11}$$

Since RTT_{meas} is a known quantity, available on the chart recorder output, rewrite equation A-5 as,

$$-\alpha' A = RTT_{Meas} - 3^\circ A. \tag{A-12}$$

Substituting equations A-11 and A-12 into equation A-7 gives,

$$\Delta = A \tan^{-1}\left\{\frac{\tan 3^\circ}{TCH + x\tan 3^\circ}\left[\sqrt{(x+b)^2+y^2}\,\tan\left(3^\circ - \frac{RTT_{Meas}}{A}\right)\right.\right.$$

$$\left.\left. + TCH - b\tan 3^\circ\right]\right\} - 3^\circ A + RTT_{Meas}, \tag{A-13}$$

where Δ is the correction to be added to the differential trace. Note that the correction is always smaller the closer the RTT is located to touch-down. Figure A-2 is a plot of the correction Δ for an RTT located at y = 100' and b = 822' for a TCH of 55'. This is very close to the touch-down point and yet the correction is substantial near threshold where Zone 3 data is critical for CAT II. (This correction would increase as y gets larger, as would be the case for a broadside array measured via the new inertial system. In practice, y may be as large as 820', as is the case at LaGuardia RW 22.)

Consider the example given prior to the analysis, in which it was shown that a very large RTT error exists as the aircraft passes the RTT location. This indicates that even when the aircraft is in the desired glide path, but not at extreme large ranges, there is an RTT error. Only at infinite range is this system absolutely correct. This type of geometric error could be immediately caused by a physical modification of the theodolite. If the theodolite base plate were inclined parallel to the desired glide path angle, an aircraft on path could be tracked at any range by only a rotation of the theodolete and no theodolite angle change. Hence, even in the extreme case of the aircraft flying past the RTT location, no signal would be transmitted from the RTT to the aircraft. This technique results in no required correction for aircraft on glide path at any range, whereas the system in use requires some correction everywhere except at infinite range.

An analysis was performed for this arrangement, in which the RTT measures an angle α with respect to the desired glide plane. The terms are the same as defined in Figure A-1 and the preceding analysis. With the RTT base plate elevated to an angle equal to the desired glide path angle (3°),

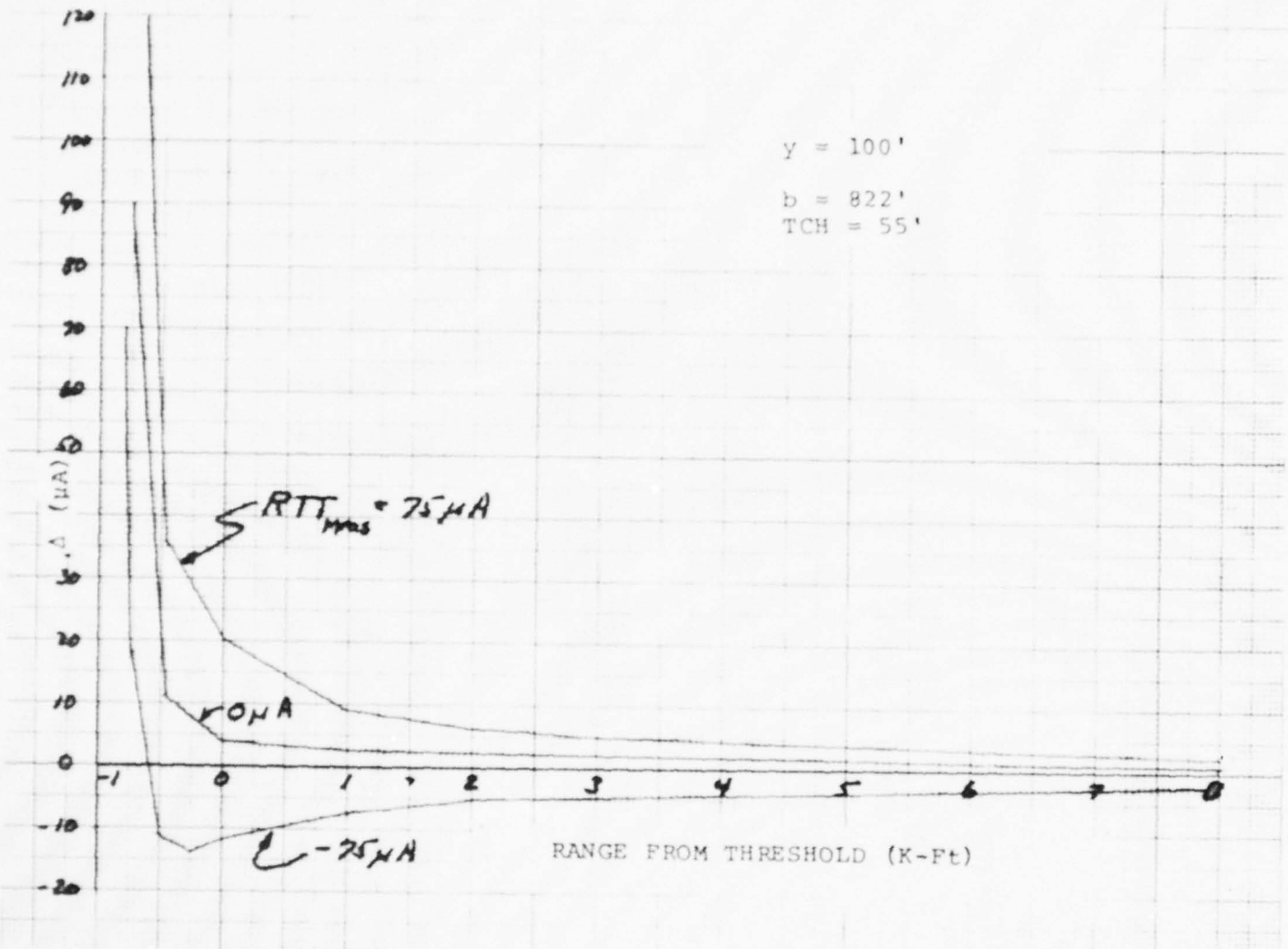

Figure A-2 Correction Curves For Normal RTT Operation

$$RTT_{Meas} = -\alpha A . \tag{A-14}$$

As previously given

$$RTT_{True} = (3^\circ - \Delta P\!\!\!/)A , \tag{A-6}$$

and therefore,

$$RTT_{Meas} - RTT_{True} = \Delta = (\Delta P\!\!\!/ - \alpha - 3^\circ)A . \tag{A-15}$$

Using the geometry of Figure A-1, one can show that,

$$\Delta = A \tan^{-1}\left\{ \tan 3^\circ + \frac{\tan 3^\circ \sqrt{(x+b)^2 + y^2}}{TCH + x \tan 3^\circ} \left[\tan\left(-\frac{RTT_{Meas}}{A} + \tan^{-1}\left(\frac{(x+b)\tan 3^\circ}{\sqrt{(x+b)^2 + y^2}} \right) \right) - \frac{(x+b)\tan 3^\circ}{\sqrt{(x+b)^2 + y^2}} \right] \right\} - 3^\circ A + RTT_{Meas} . \tag{A-16}$$

Again, Δ is a correction to be added to the differential trace. Note also that if $RTT_{meas} = 0$ then $\Delta = 0$ for all ranges and that the correction (Δ) has the same sign as RTT_{meas}. A solution of equation A-16 is given in Figure A-3 for the same theodolite location as used in Figure A-2. This improved technique would be more impressive if the y coordinate of the RTT had been larger.

AD-A077 042 WESTINGHOUSE DEFENSE AND ELECTRONIC SYSTEMS CENTER B--ETC F/G 9/5
DIPOLE BROADSIDE GLIDE SLOPE ARRAY.(U)
MAY 79 R S LITTLEPAGE , R RAJNIC DOT-FA74WA-3353
UNCLASSIFIED FAA-RD-79-69 NL

3 OF 3
AD-
A077042

END
DATE
FILMED
12-79
DDC

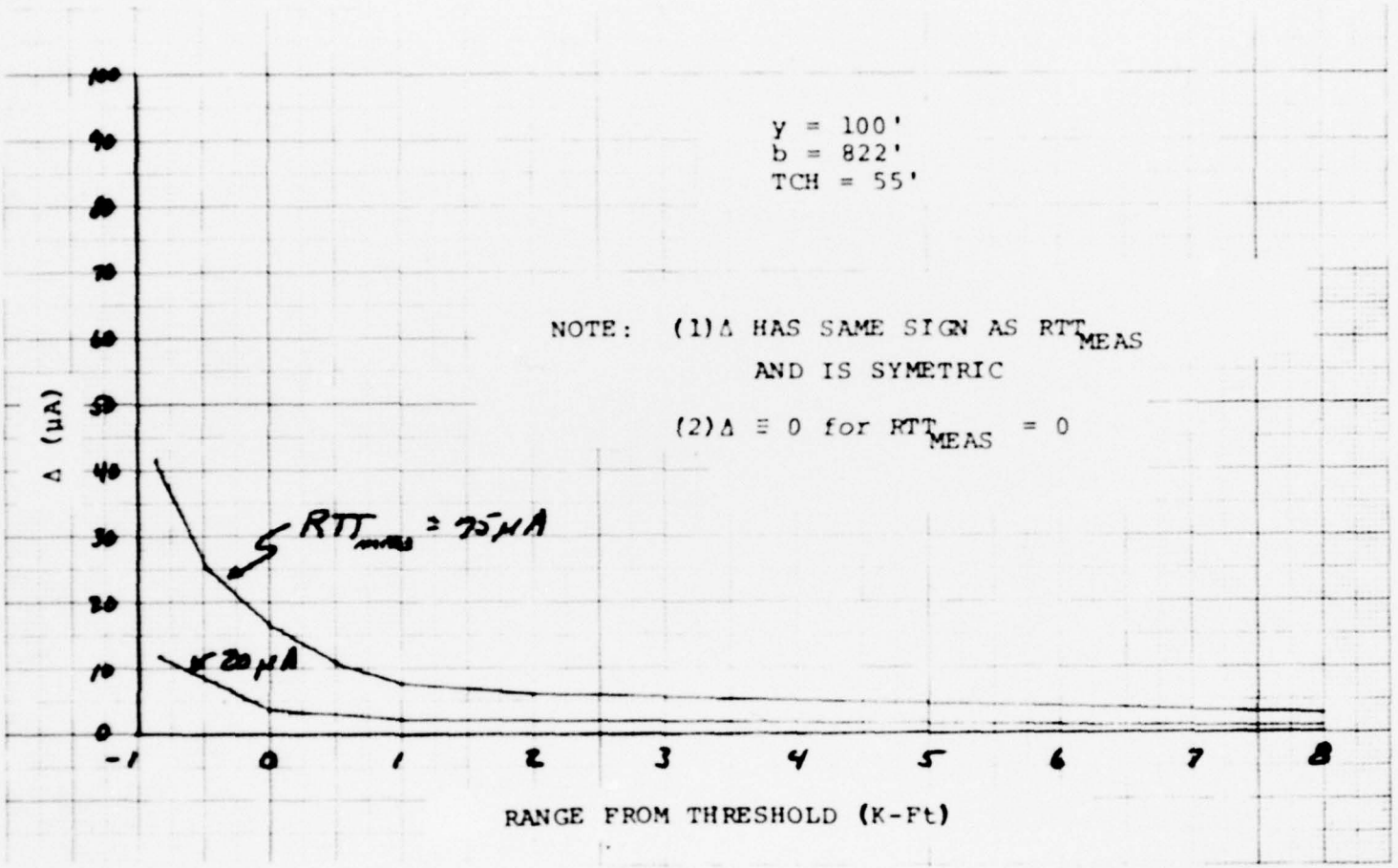

Figure A-3 Correction Curves For RTT With Base Plate In 3° Plane

APPENDIX B

ANTENNA PATTERN SYNTHESIS

Using mathematical synthesis, patterns meeting the requirements for glide slope antennas operating over rough ground have been generated. The method of analysis provides for in phase patterns (guidance phase components are zero), so that phasing problems encountered in certain earlier array work are avoided. This excludes using the Schelkunoff Polynominal method as a means of synthesis. The following is a summary of the synthesis technique.

A. Continuous Apertures

Let $\tilde{g}$ be an aperture function which is continuous across an aperture of length "a".

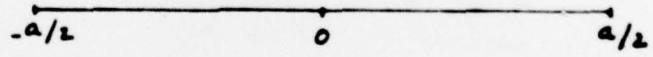

We define a new variable "p" that is dimensionless and related to the physical length "x" of the aperture by,

$$\rho = \frac{2\pi x}{a} \qquad \text{(B-1)}$$

Then the aperture is defined over the interval $[-\pi, \pi]$
The Fraunhhoffer (far field) diffraction pattern for the excitation $\tilde{g}$ is the Fourier transform of $\tilde{g}$ given by,

$$F(u) = \int_{-\pi}^{\pi} \tilde{g}(\rho)\, e^{j\rho u}\, d\rho, \quad \left(u = \frac{a}{\lambda}\cos\theta\right). \qquad \text{(B-2)}$$

The following prescription has been used to obtain an aperture corresponding to a particular far field pattern, under the condition of a continuous aperture.

I. For the desired far field F, it is approximated by an infinite product which characterizes it by its zeros.

II. Following Taylor, the continuous aperature corresponding to F is approximated by,

$$\tilde{g}(\rho) = \sum_{m=-N}^{N} \frac{F(m)}{2\pi} e^{-im\rho} , \qquad \text{(B-3)}$$

where the limit N is sought (by trial and error, so far) that gives the best approximation.

III. The validity of equation (B-3) is checked by transforming that expression back to the far field. This gives,

$$F_A(u) = \int_{-\pi}^{\pi} \tilde{g}(\rho) e^{i\rho u} du = \sum_{m=-N}^{N} \frac{F(m)}{2\pi} \int_{-\pi}^{\pi} e^{i(u-m)\rho} d\rho$$

$$= \sum_{m=-N}^{N} F(m) \frac{\sin\pi(u-m)}{\pi(u-m)} . \qquad \text{(B-4)}$$

Equation (B-4) indicates that one need not evaluate $\tilde{g}$ to test its validity, for F_A depends only on knowing F at the integers.

B. Discrete Radiators Equivalent to a Synthesis for a Continuous Aperture.

A discrete aperture can be characterized by,

$$\tilde{g}(\rho) = \sum_{k=-K}^{K}{}' g_k \delta(\rho - \rho_k) , \qquad \text{(B-5)}$$

(Σ' serves to remind us that $k \neq 0$),

where g_k is complex and contains the progressive as well as the individual radiating phases. The delta function serves to localize the oscillator strengths at p_k, V_k. The corresponding far field is equation (B-2),

$$F(u) = \int_{-\pi}^{\pi} \tilde{g}(p)\, e^{ipu}\, dp = \sum_{k=-K}^{K} g_k\, e^{ip_k u} . \qquad \text{(B-6)}$$

Adopting Taylor's synthesis analysis,

$$F_A(u) = \int_{-\pi}^{\pi} \hat{g}(p)\, e^{ipu}\, du = \sum_{m=-M}^{M} \frac{F(m)}{2\pi} \int_{-\pi}^{\pi} e^{i(u-m)p}\, dp , \qquad \text{(B-7)}$$

where, instead of performing the obvious integration in equation (B-7), we express it approximately by a K_g - point Gauss integration (K_g is an even integer) where the change of variable $y = \pi p$ is used. Thus,

$$\begin{aligned} F_A(u) &= \sum_{m=-M}^{M} \frac{F(m)}{2} \int_{-1}^{1} e^{i\pi(u-m)y}\, dy \\ &\doteq \sum_{m=-M}^{M} \frac{F(m)}{2} \sum_{k=1}^{K_g} w_k\, e^{i\pi(u-m)y_k} \\ &= \sum_{k=1}^{K_g} \left(\sum_{m=-M}^{M} \frac{F(m)}{2} w_k\, e^{-i\pi m y_k} \right) e^{ip_k u} , \quad (p_k = \pi y_k) \\ &= \sum_{k=-\frac{K_g}{2}}^{K_g/2} \left(\sum_{m=-M}^{M} \frac{F(m)}{2} w_k\, e^{-i\pi m y_k} \right) e^{ip_k u} , \end{aligned} \qquad \text{(B-8)}$$

where the weights, w_k, for the Gauss integral satisfy $w_k = w_{-k}$ and the zeros of the K_g th degree Legendre polynominal, y_k, $\exists\ y_k = -y_{-k}$.

Thus, equation (B-8) tells us that

$$F_A(u) = \sum_{k=-\frac{K_3}{2}}^{K_3/2}{}' \tilde{g}_k e^{i p_k u} , \qquad \text{(B-9)}$$

as is already given in equation (B-6), where the position of the $k^{\underline{th}}$ radiator is $p_k = \pi y_k$ and its excitation is

$$\tilde{g}_k = \sum_{m=-M}^{M} \frac{F(m)}{2} w_k e^{i \pi m y_k} . \qquad \text{(B-10)}$$

This technique has been used, with reasonable success, for an asymmetric far field pattern.